

THE UNIVERSITY OF HULL

**Development of an *insitu* quantitative measurement system  
for stress hormones; towards open microfluidic system**

being a thesis submitted for the Degree of

Doctor of Philosophy (Chemistry)

in the University of Hull

by

**Jwan Oday Abdulsattar**

BSc (Al-Mustansiriyah University, Iraq)

MSc (Al-Mustansiriyah University, Iraq)

August 2017

## Certificate

This is to certify that the thesis entitled “**Development of an *insitu* quantitative measurement system for stress hormones; towards open microfluidic system**” has been prepared under my supervision by Jwan Oday Abdulsattar for the award of the Degree of Philosophy in Chemistry in the school of Mathematics and Physical Science, the University of Hull.

Professor Gillian M. Greenway  
Head of School  
School of Mathematics and Physical Sciences  
University of Hull  
Hull, HU6 7RX, UK  
[www.hull.ac.uk](http://www.hull.ac.uk)  
[G.M.Greenway@hull.ac.uk](mailto:G.M.Greenway@hull.ac.uk)  
01482 466355

## Declaration of Authorship

I declare that the work presented in this thesis entitled “**Development of an *insitu* quantitative measurement system for stress hormones; towards open microfluidic system**” is original and is my own work to fulfil the requirements of the University of Hull Ph.D. degree in Chemistry. I certify that any passage(s) or diagram(s) have been copied from academic papers, books, the internet or any other sources these are clearly identified by the use of quotation marks and the reference(s) is fully cited.

Jwan Oday Abdulsattar

## **Abstract**

Personalized health diagnostic and monitoring has gained serious attention in recent years and one area of interest is the analysis of hormones which indicate increased stress levels. Cortisol (known also as hydrocortisone) and cortisone are steroid hormone (also known as stress hormones) that plays an important role in the regulation of many physiological processes such as glucose levels, blood pressure, and carbohydrate metabolism and they are considered as a potent biomarker for post-traumatic stress. The determination of stress hormones represents a challenge because their secretion follows a circadian rhythm (all day cycle) and their secretion are dependent on environmental and behavioral triggers. As a result, there is a need to develop a system for cheaply and rapidly monitoring their levels using approaches such as lab-on-a-chip (LOC) which combine high selectivity and sensitivity to provide valuable health informatics, not just in human but in animals such as fish being bred in a fish farm.

Selectivity in these devices can be achieved utilising an immunoassay approach taking advantage of the lock and key mechanism that is related to the antibody-antigen interaction. In this work, a new immunoassay method was developed to measure the stress hormones which involved the reproducible immobilization of cortisol and cortisone antibodies onto a tin-doped indium oxide (ITO) electrode. This was achieved by modifying the electrode in a two process step; the deposition of a nitro group onto the ITO electrode followed by the reduction of the nitro group to amino group using cyclic voltammetry. This approach enables a good orientation of the antibody on the surface. The antibodies were then immobilized using an EDC/Sulfo-NHS linkage. To enable electrochemical detection the antibodies were tagged with ferrocene to give a redox tag. When square wave voltammetry was utilised the method gave good limits of detection (LOD) of  $1.03 \text{ pg ml}^{-1}$  for cortisol and  $0.68 \text{ pg ml}^{-1}$  for cortisone.

The methodology was carried out using biological sample including Zebrafish whole- body sample and artificial saliva and reliable results were obtained without the need for complex extraction procedure.

The results of the analysis suggest that the proposed method has promise for the routine detection of stress hormones, which gives a good reason to detect cortisol and cortisone based on a chemiluminescence immunoassay. The antibodies were immobilised using the electrochemical method but then chemiluminescence detection was selected due to its high sensitivity and the simple instrumentation required. A static system was first constructed using a micropipette to add the chemiluminescence reagents with the use of a CCD camera and image J software to capture the chemiluminescence. To achieve chemiluminescence detection the ferrocene tag on the antibodies was first oxidised and then this acted as a catalyst for luminol and hydrogen peroxide chemiluminescence reaction. Optimum conditions were investigated and 20 mM luminol and 10 mM hydrogen peroxide were used with a 200 seconds exposure to the camera and an incubation time of 30 minutes. Using this approach limits of detection were obtained of  $0.47 \text{ pg ml}^{-1}$  and  $0.34 \text{ pg ml}^{-1}$  also  $R^2$  0.9912 and 0.9902 for cortisol and cortisone respectively. The method was also applied to Zebrafish and artificial saliva without analyte extraction and good results were obtained.

Once the successful chemiluminescence immunoassays had been developed it could be incorporated into *in situ* measurement devices. In this work, an open microfluidic approach was investigated to overcome the problems of blockages, high back pressure and air bubbles seen in closed microfluidic systems. A superhydrophobic ITO electrode substrate was prepared depending on the lotus leaf effect of extreme water repellence by the deposition of dichlorodimethylsilane (DCDMS) onto the substrate, followed by dip coating the hydrophobised ITO electrode into fumed silica nanoparticle suspensions

to increase the hydrophobicity. Superhydrophilic patterns were then produced using a mask and a UV/ozone lamp. The wetting properties were investigated in detail using a drop shape analysis system. Optimum conditions for the formation of a homogeneous coating were established giving the following results; fumed silica suspension concentration 4%, dip coating velocity  $3.18 \text{ cm min}^{-1}$ , and sonication time of 10 minutes. The results obtained from fluorescence microscopy showed the capability of fluid to flow along the superhydrophilic pattern acting as an open microfluidic channel. Finally, the open microfluidic approach was combined with the immobilisation procedure. Although further work will be needed to optimise the system, chemiluminescence detection was achieved when the chemiluminescence reagents were passed through the open microfluidic channels over the immobilised antibodies.

To conclude an electrochemical immobilization platform has been exploited to reproducibly immobilize the antibodies and develop a quantitative novel chemiluminescence assay for stress hormone analysis in combination with an open microfluidic device.

## **Dedication**

This thesis is dedicated to my parents, my brother Mohammed, my sisters Ban and Hanan. This work is also dedicated to all the people who stood by me during my difficult times when I stopped dreaming of completing my Ph.D. journey after two brain hemorrhage surgeries in the first and second Ph.D. years. Thank you to all the doctors, nurses, colleagues, supervisors, and academic staff who touched my heart with their endless love, encouragement, and support. I am really thankful for having you all in my life and I hope I can make you all proud with my achievement.

## **Acknowledgments**

Firstly, I would like to express my sincere gratitude to my supervisor Prof Gillian M. Greenway and Dr Tommy S. Horozov for their constant support, advice and useful scientific discussions. Their guidance helped me in all the time of research and writing of this thesis. I could not have imagined having a better advisor and mentor for my Ph.D. study.

I would also like to thank all the staff in Chemistry department for their kindness and help.

A very special thanks go to Emmanuel E. Ubuo, Kevin J. Wright and Zaid O. Oiaidha for the assistance they provided at all levels of the research project.

My sincere gratitude goes to my sponsor the Iraqi Ministry of Higher Education and Scientific Research, the Iraqi attaché in London and Ireland and Al-Mustansiriyah University in Iraq; I recognize that this research would not have been possible without their financial support and help.

Finally, I would like to thank my family, they were always supporting me and encouraging me with their best wishes. Your prayer for me was what sustained me thus far.



# Table of contents

<b>Certificate</b> .....	<b>i</b>
<b>Declaration of Authorship</b> .....	<b>ii</b>
<b>Abstract</b> .....	<b>iii</b>
<b>Dedication</b> .....	<b>vi</b>
<b>Acknowledgments</b> .....	<b>vii</b>
<b>List of tables</b> .....	<b>xii</b>
<b>List of Figures</b> .....	<b>xiii</b>
<b>Abbreviations</b> .....	<b>xxv</b>
<b>CHAPTER 1 INTRODUCTION</b> .....	<b>1</b>
1.1 Sensors .....	1
1.1.1 Biosensors.....	3
1.2 Glucocorticoids .....	4
1.2.1 Glucocorticoids effects.....	5
1.2.2 Cortisol .....	8
1.2.3 Cortisone .....	9
1.2.4 Selection of samples for analysis .....	10
1.2.5 Glucocorticoids detection.....	17
1.2.6 Immunoassay classification .....	23
1.2.7 Immunoassay immobilization.....	26
1.2.8 Detection .....	33
1.3 Chemiluminescence (CL) .....	41
1.3.1 Chemiluminescence reagents .....	42
1.3.2 Chemiluminescence detection .....	44
1.4 Microfluidics .....	46
1.4.1 The prospects of microfluidic immunosensing device .....	47
1.4.2 Classification .....	50
1.5 Open microfluidics .....	51
1.5.1 Basic principles of open microfluidics.....	54
1.5.2 Open microfluidic application .....	60
1.6 Cortisol and Cortisone detection in lab-on-chip (LOC) and point-of-care (POC) devices.....	62

1.7	Aims and objectives of the study	63
<b>CHAPTER 2 EXPERIMENTAL</b>		<b>64</b>
2.1	Chemicals and reagents used	64
2.2	Materials and instrumentation	66
2.2.1	Immunoassay electrochemical instrumentation	66
2.2.2	Chemiluminescence instrumentation	67
2.2.3	Preparation of superhydrophobic surfaces	68
2.2.4	Contact angle measurement	71
2.2.5	Coated substrates stability	72
2.2.6	Preparation of superhydrophilic patterns on the superhydrophobic surface	72
2.3	Construction of open fluid lab-on-a-chip device	75
2.3.1	Microfluidic device design	75
2.3.2	Integrated open microfluidic device	79
<b>CHAPTER 3 ANTI-CORTISOL AND ANTI-CORTISONE ELECTROCHEMICAL IMMOBILISATION AND STRESS HORMONES DETECTION USING ELECTROCHEMICAL TECHNIQUES</b>		<b>81</b>
3.1	Introduction	81
3.2	Experimental procedures	84
3.2.1	Determination of cortisol and cortisone using electrochemical assay	84
3.3	Results and discussion	90
3.3.1	Tin-doped indium oxide (ITO) electrode modification	90
3.3.2	Ferrocene tagged antibody immobilization onto ITO electrode	94
3.3.3	Characterization of ferrocene tagged anti-cortisol immobilized onto ITO electrode surface	95
3.3.4	Optimization of incubation time	97
3.3.5	Electrochemical immunoassay using cyclic voltammetry (CV) and square wave (SWV) techniques	98
3.3.6	Electrochemical calibration for cortisol and cortisone	100
3.3.7	Determination of biological samples using electrochemical immunoassay	102
3.4	Conclusions	106
<b>CHAPTER 4 DETERMINATION OF CORTISOL AND CORTISONE USING CHEMILUMINESCENCE (CL) ASSAY</b>		<b>108</b>
4.1	Introduction	108
4.2	Experimental Procedures	110
4.2.1	Preliminary investigations for signal change	110
4.2.2	Stability	111

4.2.3	Optimization of Chemiluminescence variables-----	111
4.2.4	Chemiluminescence immunoassay protocol -----	112
4.2.5	Stress hormones determination in real sample-----	112
4.2.6	Interferences -----	112
4.2.7	Comparison study with standard Enzyme-Linked Immunosorbent Assay (ELISA).....	113
4.3	Results and discussion -----	114
4.3.1	Oxidation of Ab-Fc on the surface -----	114
4.3.2	Investigation of Chemiluminescence Signal -----	115
4.3.3	The stability of ferrocenium cation-----	117
4.3.4	Optimization of operating variables-----	119
4.3.5	Calibration curve-----	123
4.3.6	Determination of target analyte in Zebrafish whole-body and artificial saliva samples .....	125
4.3.7	Interferences -----	130
4.3.8	Commercial ELISA kit-----	133
4.4	Conclusion-----	135

## **CHAPTER 5 FABRICATION OF OPEN MICROFLUIDIC CHIP USING WETTABILITY----- 137**

5.1	Introduction-----	137
5.2	Experimental procedures -----	140
5.2.1	Fumed silica suspension preparation-----	140
5.2.2	Investigation of ITO electrode wettability -----	140
5.2.3	Optimisation of superhydrophobic coating quality -----	140
5.2.4	Stability of the coatings -----	141
5.2.5	Fabrication of superhydrophilic patterns on the superhydrophobic coatings .....	141
5.2.6	Absorption capacity of the cotton waste collector -----	141
5.2.7	Water flow in the fabricated open microfluidic chip -----	141
5.2.8	Investigation of fluid flow using fluorescence microscopy-----	142
5.3	Results and discussion -----	143
5.3.1	Preparation of ITO electrodes with superhydrophobic surfaces -----	143
5.3.2	Factors affecting the preparation of superhydrophobic ITO electrode surfaces using the dip coating method -----	147
5.3.3	Stability of superhydrophobic surface coating-----	149
5.4	Fabrication of superhydrophilic patterns on superhydrophobic substrates by UV/ozone burning-----	150
5.4.1	Investigation of the fluid flow over superhydrophilic patterns-----	154
5.4.2	Construction of a lab-on-a-chip device -----	156
5.4.3	Absorption capacity of the cotton waste water collector-----	157

5.4.4	Investigation of steady state times for water flowing at different rates -----	158
5.4.5	Investigation of fluorescence particle movement along a hydrophilic channel..... -----	163
5.4.6	Effect of evaporation -----	165
5.5	Conclusions-----	166
<b>CHAPTER 6 OPEN MICROFLUIDIC APPLICATIONS IN QUANTITATIVE MEASUREMENT SYSTEM FOR STRESS HORMONES -----</b>		<b>167</b>
6.1	Introduction-----	167
6.2	Experimental -----	168
6.2.1	Ab –Fc immobilization procedures-----	168
6.2.2	Determination of cortisol by chemiluminescence detection integrated on an open microfluidic system-----	168
6.3	Results and discussion -----	169
6.3.1	Immobilization of Ab-Fc onto the open microfluidic chip -----	169
6.3.2	Cyclic voltammetry measurement-----	171
6.3.3	Chemiluminescence detection of Stress hormones -----	173
6.4	Conclusion-----	177
<b>CHAPTER 7 CONCLUSION -----</b>		<b>179</b>
7.1	Stress hormones antibodies electrochemical immobilization -----	179
7.2	Detection of stress hormones in real sample and off-chip-----	180
7.3	Wetting properties investigations towards open microfluidic platform-----	182
7.4	Combination of immunoassay methodology with open microfluidic system-	183
7.5	Future work-----	185
<b>REFERENCES.....</b>		<b>187</b>

## List of tables

<b>Table 2.1.</b> Shows the chemicals and reagents that have been used.....	64
<b>Table 3.1.</b> The Recovery and RSD values of cortisol and cortisone standard solution spiked in the Zebrafish whole-body sample (n = 3). .....	103
<b>Table 3.2.</b> The recovery and RSD values of cortisol and cortisone standard solution spiked in the artificial saliva sample for three different electrodes. ....	105
<b>Table 4.1.</b> The precision of immobilisation ferrocene tagged antibody on the ITO electrode surface. ....	117
<b>Table 4.2.</b> Analytical figures of merit for cortisol and cortisone using chemiluminescence immunoassay. ....	125
<b>Table 4.3.</b> The Recovery and RSD values of cortisol and cortisone standard solution spiked in the Zebrafish whole-body sample (n = 3). ....	128
<b>Table 4.4.</b> The Recovery and RSD values of cortisol and cortisone standard solution spiked in the artificial saliva sample for three different electrodes. ....	129
<b>Table 4.5.</b> Compounds have a similar structure to the cortisol and cortisone.....	131
<b>Table 5.1.</b> The measured and expected mass of water absorbed by the cotton collector attached to the outlet of the open microfluidic system after continuous pumping of water at different flow rates for 900 seconds.....	158
<b>Table 6.1.</b> Shows the reproducibility of the chemiluminescence signal using pipetting and pumping procedures of luminol and hydrogen peroxide mixture. ....	176

## List of Figures

- Figure 1.1.** Schematic of a sensor device consisting of the target analyte, bioreceptor (antibody, DNA, enzyme, whole cell, etc.), transducers (electrical, mass-based and optical), microprocessor, and a display screen that is accessible to any part of the world. ....2
- Figure 1.2.** Diagram illustrating the adrenal gland secretion with the ending products including epinephrine, norepinephrine, aldosterone, cortisol & cortisone. ....5
- Figure 1.3.** The anti-inflammatory process includes the liberation of mediators and cells to fight inventor substances aiming to prevent infection <sup>8</sup>. ....6
- Figure 1.4.** The hypothalamic-pituitary-adrenal (HPA) axis biosynthesis of stress hormones in the “fight or flight” response <sup>12</sup>. ....8
- Figure 1.5.** Conversion of cortisol and cortisone and vice versa in the presence of 11- $\beta$ -HSD1 isoenzyme (located mainly in the liver) and 11- $\beta$ -HSD2 isoenzyme (located mainly in kidney) by the oxidation of hydroxyl group in cortisol to ketone group to form cortisone or by the reduction of keto- group to hydroxyl group to form cortisol. .... 10
- Figure 1.6.** Illustration of the integration of cortisol into hair samples by means of (A) blood, (B) sebum, and (C) sweat <sup>30</sup>. .... 13
- Figure 1.7.** Zebrafish life cycle<sup>40</sup>. .... 15
- Figure 1.8.** Structure of an antibody. The basic structure of an antibody, indicating where the Fab (fragment antigen binding) and Fc (Fragment crystallization) regions are which chains are heavy and light with the disulphide bond linkages, amine groups, and carbohydrates. The variable region represents where the antigen can bind to the antibody, whereas the constant region is constant for all different antibodies <sup>88</sup>. ....22
- Figure 1.9.** Shows competitive immunoassay where antibodies are immobilized on the solid surface and a competition between antigens (found in the sample) and added tagged antigen on limited binding sites available on the immobilized antibodies. The high sample concentration resulted in a lower signal due to the less tagged antigen

binding to the antibodies. Therefore, an inversely proportional relationship between signal and antigen in the sample is found. ....	24
<b>Figure 1.10.</b> Shows a non-competitive immunoassay where the antibodies are immobilised on a solid surface and antigens are added to form the antibody-antigen complex. Afterwards, a second labelled antibody is added and bind to the complex for a period of time well known as incubation time. The signal produced is proportional to the concentration of the antigen, which means the more antigen in the sample results in the larger signal.....	24
<b>Figure 1.11.</b> Represent a schematic of an ELISA procedure <sup>96</sup> . ....	25
<b>Figure 1.12.</b> Illustrate generic antibodies immobilization methods <sup>99</sup> . ....	27
<b>Figure 1.13.</b> EDC coupling reaction <sup>101</sup> . ....	29
<b>Figure 1.14.</b> A typical cyclic voltammogram, where $E_{pc}$ = peak cathodic potential; $i_{pc}$ =peak cathodic current; $E_{pa}$ =peak anodic potential, and $i_{pa}$ =peak anodic current <sup>116</sup> . ....	35
<b>Figure 1.15.</b> The diagram shows an overview of SWV parameters <sup>118</sup> . ....	36
<b>Figure 1.16.</b> Jablonski diagram shows the luminescence process, where $S_0$ represents the ground state, $S_1$ first excited state, $S_2$ second excited state and $T_1$ triple state <sup>142</sup> . ....	39
<b>1.17.</b> Mechanism for the chemiluminescent reaction of luminol with hydrogen peroxide in a basic aqueous environment which emits light at $\lambda_{max}$ = 425 nm <sup>154</sup> . ....	43
<b>Figure 1.18.</b> Mechanism of Photomultiplier tubes detector <sup>164</sup> .....	44
<b>Figure 1.19.</b> Represent the steps for charge-coupled device (CCD) operation <sup>152</sup> .....	45
<b>Figure 1.20.</b> Lab-on-chip handheld microfluidic chip device as an example controller with smartphone app <sup>179</sup> . ....	47
<b>Figure 1.21.</b> A schematic of laminar flow where the smooth flow of fluid occurs in parallel layers with no breakage between them and turbulent flow where rough and random flow occurs.....	50
<b>Figure 1.22.</b> Two droplet open microfluidic configurations (A) continuous flow emulsion-based droplet (from T-junction and flow focusing) (B) electrowetting-based droplet <sup>198</sup> . ....	52

<b>Figure 1.23.</b> Wetting conduct of a droplet on various solid surfaces. (a) superhydrophobic surfaces, (b) hydrophobic surfaces, (c) hydrophilic surfaces, and (d) superhydrophilic surfaces.....	56
<b>Figure 1.24.</b> Diagram showing the forces in the three phases (solid, fluid, vapour) contact lines of a fluid drop on a perfect solid surface in the air. ....	57
<b>Figure 1.25.</b> The Wenzel and Cassie-Baxter type of wetting of a rough solid surface. In the Wenzel model, the fluid fully wets the grooves of the rough surface. In the Cassie-Baxter model, the droplets sit on the solid surface without penetrating the solid surface grooves.....	58
<b>Figure 1.26.</b> Examples of plants and animal kingdoms of superhydrophobic surfaces with SEM images which inspired researchers to fabricate artificial superhydrophobic surfaces in many commercial and scientific applications <sup>213</sup> .....	59
<b>Figure 2.1.</b> A schematic of an electrochemical cycle used for immunoassay procedures, with an Ag/AgCl electrode as a reference electrode, nickel wire as a counter electrode and the ITO electrode as a working electrode connected to Palm-sens potentiostat with the PStTrace 4.3 software designed by Auto Lab to measure the current. ....	67
<b>Figure 2.2.</b> Chemiluminescence instrumentation shows an ITO electrode alignment under the CCD camera, the box is closed and images were recorded using Image J software and a laptop connected to the camera. ....	68
<b>Figure 2.3.</b> Schematic of the setup used for the hydrophobization of different substrates in the vapour phase. O <sub>2</sub> is removed by flushing N <sub>2</sub> gas through the inlet. The silane agent is introduced through the outlet to the bottom of the vessel after flashing with N <sub>2</sub> to modify the substrates. ....	69
<b>Figure 2.4.</b> Schematic of the self-constructed dip-coater used to coat different substrates with fumed silica suspension using different withdrawal velocity and varying the concentration of fumed silica suspension. ....	70
<b>Figure 2.5.</b> Schematic explain the syringe pump flow rate conversion to dip coating speed. This can be calculated by the inner radius of the syringe (r) and distance of fluid flow (d).....	70



**Figure 2.6.** Schematic of the experimental setup used for coating substrate stability. The coated substrate attached to holder was immersed in a beaker filled with water and by the use of a magnetic bar and magnetic stirrer, a harsh circumstance was provided for the coated substrate. ....72

**Figure 2.7.** Self-constructed UV/ozone lamp box. The above schematic is the experimental arrangement used to fabricate superhydrophilic patterns on superhydrophobic surfaces by applying UV/ozone burning technique. The second image is an actual side view of burning setup. ....74

**Figure 2.8.** Experimental setup for investigating the tolerance of different masks to the heat introduced by the UV/ozone lamp during the burning process.....75

**Figure 2.9.** The top schematic shows the experimental setup used for pumping fluid to the device consisting of top platform (open microfluidic chip), bottom glass platform (holder) and the bottom platform was attached to the syringe pump by PTFE microbore tubing (i.d 0.81 mm, o.d. 1.42 mm and gauge size 21). Hamilton glass syringe was used to pump fluid to the device. The bottom photograph is an image of the setup showing the aggregation of fluid after pumping.....76

**Figure 2.10.** Shows the open microfluidic chip where the tube was attached to a needle vertically align to the coated ITO electrode, this tube was attached to a mechanical syringe pump to pump fluid. The setup was built on a plastic platform (17 mm×7 mm length and width, 0.3 mm thick). Another advantage of this design is there was no need for an outlet, a stopper filled with cotton is placed on the end of the electrode to suck all waste fluid.....77

**Figure 2.11.** Steady state flow setup using a pre-weighted cotton cover on the top of the reservoir located on one edge of the chip and the other edge is positioned under a needle glued to a syringe attached to a syringe pump. ....78

**Figure 2.12.** Shows the chemiluminescence immunoassay microfluidic setup.....80

**Figure 3.1.** A schematic of the electrochemical process for the immobilization of the ferrocene tagged antibody onto the modified electrode via an amide linkage. ....82

**Figure 3.2.** The inclusion of different antibodies orientations (A) randomized with some side-on, (B) end-on, on a solid surface, where the side-on orientation leads to

poor-to-moderated sensitivity and on the other hand the end-on orientation results in high sensitivity that can be attributed to well-controlled modified surface that can specifically capture the antigen.....83

**Figure 3.3.** Diagram of an ITO working electrode, attached with a copper tape placed on one edge of the conductive ITO electrode surface to work as a connection point. Three circles were placed on the ITO surface with 1.2 cm spacer from each center circle. ....85

**Figure 3.4.** A schematic of the nitrobenzene group immobilization involving a one electron reduction where the nitrobenzene diazonium tetrafluoroborate cation is cleaved off to give nitrogen gas and leaves free radical in the para position on the benzene ring which covalently bonds to the electrode surface <sup>227</sup> .....90

**Figure 3.5.** Cyclic voltammogram of the deposition of nitrobenzene on the ITO electrode using a solution of 2 mM 4-nitrobenzene diazonium tetrafluoroborate and 0.1 M tetrabutylammonium perchlorate in acetonitrile. The cyclic voltammetry run started at + 0.7 V scanning down to - 0.5 V and with a return sweep to + 0.7 V performed over four scans with a scan rate of 0.1 V s<sup>-1</sup> at room temperature. The reduction peak of + 0.19 V refers to nitrobenzene deposition onto the electrode. ....91

**Figure 3.6.** Schematic displaying the formation of nitrobenzene mono and multilayer. ....92

**Figure 3.7.** The proposed mechanism of the reduction of the nitro group to the amine group. Nitrobenzene undergoes an irreversible two electron, two proton reduction to give nitrosobenzene, two electrons, two proton reduction to give hydroxylamine group and two electrons, two proton reduction to give phenyl amine group <sup>228</sup> .....93

**Figure 3.8.** Voltammogram of the reduction of nitrobenzene to aniline. The cyclic voltammetry was run starting at + 0.4 V scanning down to - 1.25 V and with a return sweep to + 0.4 V performed over three oxidation-reduction voltammetry cycle scans with a scan rate of 0.1 V s<sup>-1</sup> at room temperature. The reduction peak at - 0.87 V represents the conversion of nitrobenzene to aniline onto the ITO electrode surface in 90:10 0.1M KCl: ethanol solution <sup>228</sup>. ....94

<b>Figure 3.9.</b> Cyclic voltammogram of the modified ITO electrode surface with and without the tagged ferrocene antibody. Scan rate 100 mV s <sup>-1</sup> . 10 mM PBS was the solution used to conduct all the experiments. ....	95
<b>Figure 3.10.</b> Cyclic voltammogram of ferrocene labelled anti-cortisol on the ITO electrode surface with various scan rates ranging from 10 mV s <sup>-1</sup> to 1000 mV s <sup>-1</sup> . ....	96
<b>Figure 3.11.</b> The graph indicates the change in current for 10, 15, 20, 30, 45 and 60 minutes incubation time for cortisol of 50 ng ml <sup>-1</sup> respectively from cyclic voltammetry measurements. Scan rate 100 mV s <sup>-1</sup> . ....	97
<b>Figure 3.12.</b> Cyclic voltammograms of the cortisol standard solutions ranging from (0.001 to 50 ng ml <sup>-1</sup> ) on the ferrocene tagged anti-cortisol antibody modified ITO electrode for an incubation time of 30 minutes, with the orange line correspond to the blank. Scan rate 100 mV s <sup>-1</sup> and the measurements were conducted in 10 mM PBS. ....	98
<b>Figure 3.13.</b> Square wave voltammograms presenting the effect of cortisol standard solutions with concentrations ranging from (0.001 to 50 ng ml <sup>-1</sup> ) on the current signal after the addition to the ferrocene tagged anti-cortisol antibody attached to the modified ITO electrode. These waves represent the current signal before subtracting from the blank. Measurements were carried out in 10 mM PBS. The orange line represents the blank prior to the addition of cortisol, frequency 25 Hz, amplitude 1 mV. ....	99
<b>Figure 3.14.</b> Calibration curve of cortisol standard solutions with $\Delta I_p$ current peak plotted against their concentrations. The error bar indicates standard deviation. (n = 3). The measurements were done using the square wave technique. The frequency of 25 Hz and amplitude of 1 mV. ....	100
<b>Figure 3.15.</b> Calibration curve of cortisone standard solutions with $\Delta I_p$ current peak plotted against their concentrations. The error bar indicates standard deviation (n = 3). The measurements were done using square wave technique. The frequency of 25 Hz and amplitude of 1 mV. ....	101
<b>Figure 3.16.</b> Square wave voltammogram showing the difference in current between Zebrafish whole-body sample before and after extraction with diethyl ether. ....	102
<b>Figure 3.17.</b> Shows square wave voltammogram for the artificial saliva spiked with 10 ng ml <sup>-1</sup> cortisol standard solution and compared it with 10 ng ml <sup>-1</sup> cortisol standard	

prepared in PBS. The comparison shows the shift in the peak from + 0.22 V to + 0.33 V. ....	104
<b>Figure 4.1.</b> Schematic of redox reaction for ferrocene that can be oxidised to ferrocenium ion and thereby catalyze the luminol: hydrogen peroxide chemiluminescence reaction. ....	109
<b>Figure 4.2.</b> Cyclic voltammogram for the oxidation of ferrocene tagged antibody to ferrocenium cation that catalyses luminol/hydrogen peroxide showing an oxidation peak at + 0.25 V. Scan rate 10 mV s <sup>-1</sup> . ....	114
<b>Figure 4.3.</b> (a) Image of an ITO electrode taken by digital camera showing the three separated circle containing immobilized ferrocene tagged anti-cortisol antibody, (b) chemiluminescence images of blank (immobilized ferrocene tagged antibody) after the addition of luminol/hydrogen peroxide mixture, (c) chemiluminescence image of the blank after the incubation of 50 ng ml <sup>-1</sup> cortisol hormone. Scale bar for image A is 5 cm, B and C are 0.5 cm. ....	115
<b>Figure 4.4.</b> Images of chemiluminescence signal related to ferrocene tagged antibody,(a) characterise the ferrocene tagged antibody before ferrocene oxidation, (b) immediately after the oxidation using the mixture of luminol/hydrogen peroxide, (c) characterise the ferrocene tagged antibody after one day of ferrocene tagged antibody oxidase, (d) after one week of ferrocene oxidation. The scale bar is 0.5 cm. ....	118
<b>Figure 4.5.</b> Reaction scheme for the catalytic effect of ferrocene on the luminol/hydrogen peroxide reaction. ....	118
<b>Figure 4.6.</b> A calibration curve showing the influence of luminol concentrations while keeping the concentration of hydrogen peroxide constant (10 mM) on the chemiluminescence emission signal. ....	120
<b>Figure 4.7.</b> Graph showing the influence of hydrogen peroxide concentration while keeping the concentration of luminol constant (20 mM) on the chemiluminescence emission signal. ....	121

**Figure 4.8.** The graph shows the effect of different incubation time on the chemiluminescence signal after the addition of 30  $\mu\text{l}$  of 50  $\text{ng ml}^{-1}$  of cortisol standard solution..... 122

**Figure 4.9.** The graph for exposure time optimisation after the addition of luminol (20 mM) and hydrogen peroxide (10 mM) mixture over the time interval from (50- 700 seconds) showing the highest chemiluminescence signal at 200 seconds, therefore, it was adopted for chemiluminescence experiments. .... 123

**Figure 4.10.** Calibration curve of cortisol standard solutions with concentrations from (0 - 50  $\text{ng ml}^{-1}$ ). Standards plotted against the  $\Delta\text{RLU}$  emission response, insert in the figure chemiluminescence image of each standard cortisol solution..... 124

**Figure 4.11.** Calibration curve of cortisone standard solutions with concentrations from (0 - 50  $\text{ng ml}^{-1}$ ). The standards RLU signal was plotted against the concentrations of the cortisone standard solutions..... 124

**Figure 4.12.** Chemiluminescence image of Zebrafish whole-body sample spiked standard cortisol solution (50  $\text{ng ml}^{-1}$ ) added to ferrocene anti-cortisol antibody immobilized onto modified ITO electrode (a) without extraction, (b) with extraction and (c) fish sample without the addition of standard and without extraction. Scale bar is 0.5 cm. .... 127

**Figure 4.13.** Represent the signal after the addition of artificial saliva spiked with cortisol standard solution 10  $\text{ng ml}^{-1}$ . The signal was decreased due to the reaction between the antibody and antigen that restrict the Fc moiety from its role as an oxidising agent for luminol and hydrogen peroxide reaction. The scale bar is 0.5 cm. .... 129

**Figure 4.14.** A column chart specifies the similar structure compounds potential interference with (a) ferrocene tagged anti-cortisol antibody and (b) ferrocene tagged anti-cortisone antibody after the addition of 50  $\text{ng ml}^{-1}$  of these compounds (cortisol, cortisone, prednisolone, 11-deoxycortisol, corticosterone, progesterone, and testosterone), the incubation time was 30 minutes and the luminol and hydrogen peroxide concentrations were 20 and 10 mM respectively to mimic the cortisol and cortisone optimum conditions..... 132

**Figure 4.15.** Calibration curves showing (a) the change in the optical density with the increase of cortisol concentration where the red points indicate the cortisol

concentrations and the green points are the error bar for each concentration, (b) the increase in optical density with a linear trend after subtracting the blank signal from the sample signal..... 134

**Figure 5.1.** Diagram illustrating (a) the principle of the hydrophobisation of the ITO electrode surface using dichlorodimethylsilane (hydrophobic surface), (b) and the fabrication of hydrophilic patterns on the surface of ITO electrode coated with a hydrophobic fumed silica layer (superhydrophobic surface) using a UV/ozone lamp. .... 139

**Figure 5.2.** Side image of a water droplet on an ITO electrode surface in air. The average contact angle $\theta$ , was found to be  $42.0 \pm 0.7^\circ$ . The scale bar is 1 mm..... 143

**Figure 5.3.** Side image of a water drop on the ITO electrode surface after its hydrophobisation with DCDMS. The average contact angle of  $101.4 \pm 0.5^\circ$  confirms the hydrophobicity of the surface has increased after treating it with DCDMS. The scale bar is 1 mm..... 144

**Figure 5.4.** A SEM image of a fumed silica coating showing that its surface is rough at micro-and nanoscopic level. Scale bar is 1 $\mu$ m. .... 145

**Figure 5.5.** Images (a-e) show the process of a water droplet rolling over a superhydrophobic surface which is coated with fumed silica. The water droplet easily rolls off the surface even on a horizontal substrate thus confirming its superhydrophobicity. The scale bar is 0.5 mm for all images. .... 146

**Figure 5.6.** Optical microscopy images of fumed silica coatings produced by dip coating at a withdrawal speed of 3.18 cm min<sup>-1</sup>. At three different concentrations of fumed silica suspensions (2, 4, and 5 wt.%) in ethanol prepared at 10 minutes sonication time. Cracks and defects are seen on the coating obtained at 5% silica suspension. The decrease of the silica concentration to 4% improves the coating quality by reducing the size and number of cracks. Partial inhomogeneous coatings are obtained at an even lower concentration of 2 %. The scale bar on all images is 200  $\mu$ m. .... 148

**Figure 5.7.** Images of a superhydrophobic coating deposited on an ITO electrode surface from 4 wt% fumed silica suspension by dip coating at a withdrawal speed of 3.18 cm min<sup>-1</sup> and sonication time 10 minutes, taken by a digital camera (a, b) and an optical microscope (c, d) before (a, c) and after (b, d) stirring in water for 5 min (see

section 2.2.5). The coating was stable and not damaged by the water flow during the stirring..... 149

**Figure 5.8.** Left sketch of a mask prepared by laser ablation with a channel in the middle of the coverslip. The right sketch is the shape and size of this laser prepared channel with a dimension of 1mm for D1 and D2, 0.5 mm for b and 7 mm of L. .... 150

**Figure 5.9.** Images of superhydrophilic patterns fabricated using a UV/ozone light irradiation through a coverslip mask with the following specifications: a dimension of 1 mm diameter for sides, 7 mm length and 0.5 mm width (see Figure 5.8) on the superhydrophobic substrate obtained by dip coating method from a 4 wt% fumed silica suspension, withdrawal speed  $3.18 \text{ cm min}^{-1}$  and sonication time 10 minutes..... 151

**Figure 5.10.** Shows the fabrication of superhydrophilic patterns on a glass substrate covered with fumed silica 4% wt, withdrawal speed  $3.18 \text{ cm min}^{-1}$ , and sonication time 10 minutes using dip coating method and using UV/ozone lamp. The channel fabrication can be seen as the edges would appear in microscope images at the cross point of superhydrophilic and superhydrophobic layers. Scale bar is  $200\mu\text{m}$ ..... 152

**Figure 5.11.** The temperature of the PMMA mask surface subjected to continuous irradiation from the UV/ozone lamp versus time. .... 153

**Figure 5.12.** Shows the hydrophobisation process: image (a) shows the ITO electrode before coating. Image (b) shows the plastic mask that is used for the fabrication of a superhydrophilic channel. Image (c) shows ITO electrode covered with 4% wt concentration of fumed silica suspension withdrawal speed  $3.18 \text{ cm min}^{-1}$  and sonication time of 10 minutes after the fabrication of a superhydrophilic channel using UV/ozone lamp. Scale bar for image 1 and 3 are 0.5 cm. The scale bar for image 2 is 1 cm..... 154

**Figure 5.13.** Series of images (a - f) showing the possibility of fluid flow through the superhydrophilic open microfluidic ‘channels’ fabricated onto an ITO electrode with superhydrophobic fumed silica coating. The scale bar for all images is 0.5 cm. .... 155

**Figure 5.14.** Shows the image of the design 2 of the set up where the fluid is delivered from a plastic tube attached to the syringe. While the exit is covered with cotton placed in a plastic cap as a waste container..... 157

**Figure 5.15.** Consecutive images showing the growth of water droplet at different times (a) 0 seconds insert in (a) a top view of the ITO electrode width of (0.5 cm) with a superhydrophilic pattern, (b) 20 seconds, (c) 60 seconds, (d) 120 seconds, (e) 240 seconds and (f) 300 seconds during pumping at a flow rate of  $30 \mu\text{l min}^{-1}$ . The scale bar is 1mm..... 160

**Figure 5.16.** Droplet height versus time during pumping water in an open microfluidic channel at flow rates of (10, 20, 30, 40 and  $50 \mu\text{l min}^{-1}$ )..... 162

**Figure 5.17.** Consecutive microscope images showing the movement of fluorescence particles starting from the inlet (a), moving through the ‘channel’ (b) to the reaction circle (c) towards the outlet with the cotton waste water collector (f). (b), (d) and (e) represents the path between the inlet, reaction circle, and outlet. This was done using a syringe pump at  $30 \mu\text{l min}^{-1}$  flow rate. The scale bar is 1 mm. .... 164

**Figure 5.18.** Shows the contact angle measured using DSA 10, Krüss instrument for superhydrophilic circle surrounded by a superhydrophobic surface after the coverage of the box attached to the DSA 10, Krüss instrument to reduce or prevent evaporation of the solvent and the there was a slight decrease in the contact angle after the immediate addition of solvent until one hour after the addition of the solvent. .... 165

**Figure 6.1.** A serial addition (a-e) of deposition solution (0.1 M tetrabutylammonium perchloride (TBAP) and 2mM 4-nitrobenzene diazonium tetrafluoroborate) dissolved in acetonitrile onto the superhydrophobic surface showing fumed silica surface damage. .... 169

**Figure 6.2.** Shows the change in the acetonitrile ratio to dissolve the deposition chemical components (tetrabutylammonium perchloride (TBAP) and 4-nitrobenzene diazonium tetrafluoroborate) where (a) represent 0.5 ACN: 4.5 DI, (b) 1.5 ACN: 3.5 DI, and (c) 2.5 ACN: 2.5 DI..... 170

**Figure 6.3.** Voltammogram of the deposition of nitrobenzene on the ITO electrode using a solution of 0.1 M tetrabutylammonium perchlorate and 2 mM 4-nitrobenzene diazonium tetrafluoroborate in 50:50% acetonitrile and deionized water. The cyclic voltammetry was run starting at + 0.7 V scanning down to - 0.6 V and with a return sweep to + 0.7 V performed over four scans with a scan rate of  $0.1 \text{ V s}^{-1}$  at room



temperature. The reduction peak of - 0.17 V refers to partially blocked electrodes because the electrode is covered with fumed silica layer<sup>249</sup>. ..... 172

**Figure 6.4.** Cyclic voltammetry of deposition solution dissolved by 50:50 ratio of acetonitrile and deionized water on the ITO electrode using 0.1 M KCl in aqueous ethanol solutio (90:10, v: v) as a reduction solution. Scan rate 0.1 V s<sup>-1</sup>. ..... 173

**Figure 6.5.** Shows the chemiluminescence signal of anti-cortisol antibody immobilized onto an ITO electrode, where the immobilization of the Ab-Fc onto the reaction circle was done and afterwards the circle was covered. The fabrication of the open microfluidic was done by depositing DCDMS on it and then the electrode was immersed in fumed silica suspension to fabricate superhydrophobic surface. Then superhydrophilic channel was made using UV/ozone lamp. The chip was placed in the chemiluminescence box under the CCD camera, and the mixture of luminol and hydrogen peroxide was pipetted using Eppendorf micropipette. The scale bar is 0.5 cm. .... 174

**Figure 6.6.** Shows the chemiluminescence signal of anti-cortisol antibody immobilized onto an ITO electrode, where a mixture of luminol and hydrogen peroxide is pumped for 200 seconds at flow rate of 30 µl min<sup>-1</sup> using a hydrodynamic syringe pump to fill the reaction circle that had been done by immobilizing the Ab-Fc and then it was covered by an adhesive tape to be immersed into fumed silica, this was done after depositing DCDMS and fumed silica suspension to yield a superhydrophobic surface. The chemiluminescence signal was captured using CCD camera. The scale bar is 0.5 cm..... 175

**Figure 7.1.** An actual image for the improved cover that omitted the use of adhesive tap..... 185

**Figure 7.2.** Preliminary design that enables multi-determination of stress hormones on the same chip..... 186

## Abbreviations

LOC	lab-on-a-chip
POC	point -of -care
PTSD	post-traumatic stress disorder
IUPAC	international union of pure and applied chemistry
$\mu$ TAS	micro total analysis system
DDS	drug delivery system
GCs	glucocorticoids
GR	glucocorticoid receptor
SNS	sympathetic nervous system
HPA	hypothalamic-pituitary-adrenal
CRH	corticotropin releasing hormone
ACTH	adrenocorticotrophic hormone
11 $\beta$ -HSD	11beta-hydroxysteroid dehydrogenase isoenzyme
ISF	interstitial fluid
CBG	corticosteroid-binding globulin
CFI	cortisol free index
UFC	urinary free cortisol
HPI	hypothalamic-pituitary-interrenal
MS	mass spectrometry
MS/Ms or M <sup>2</sup>	tandem mass spectrometry
APCI	atmospheric pressure chemical ionization
APPI	atmospheric pressure photoionization
ESI	electrospray ionization
TLC	thin layer chromatography
GC-MS	gas chromatography-mass spectrometry
LC	liquid chromatography
LC-MS/MS	liquid chromatography-tandem mass spectrometry
GC	gas chromatography

SPE	solid-phase extraction
LLE	liquid-liquid extraction
PPT	protein precipitation
UHPLC	ultra high-performance liquid chromatography
IA	immunoassay
Ab	antibody
Ig	immunoglobulin
Ag	antigen
Fab	fragment antigen binding
Fc	fragment crystallization
pAbs	polyclonal antibody
mAbs	monoclonal antibody
rAbs	recombinant antibody
ELISA	enzyme-linked immunosorbent assay
SPR	surface plasmon resonance
TLM	thermal lens microscope
WIOS	wavelength-interrogated optical sensing
WE	working electrode
RE	reference electrode
CE	counter electrode
SWV	square wave voltammetry
CV	cyclic voltammetry
RIA	radioimmunoassay
CL	chemiluminescence
AP	alkaline phosphatase
HPR	horseradish peroxidase
CCD	charge coupled device
MF	microfluidics
EWOD	electrowetting-on-dielectric

PMMA	polymethylmethacrylate
PS	polystyrene
DSA	drop shape analysis
ITO	tin-doped indium oxide
PBEs	partially blocked electrode

## **Chapter 1 Introduction**

With recent scientific developments and medical requirements, there has been a rapid increase in the demand for healthcare monitoring systems to monitor specific biomarkers. As a result, there is a need for construction of a portable, disposable, automated and miniaturized systems to easily monitor a range of biochemical markers, such as lab-on-a-chip (LOC) devices and point-of-care (POC) systems etc., which can provide valuable health informatics.

In this thesis, the biomarkers of interest are stress hormones, including cortisol and cortisone, which are secreted depending on environmental and behavioral triggers, and follow a circadian rhythm (all day cycle)<sup>1</sup>. For example, these systems can be used for understanding human day-night stress hormones cycle secretion by developing wearable/cloth mountable and easy to use analytical detection devices. Application of these devices could be for monitoring post-traumatic stress disorder (PTSD), stress levels of soldiers during battles, investigating the effect on firefighters bodies, and the effect of pesticide on farmers. Environmental applications would include the effect of pollutants on fish<sup>2</sup>.

The objective of the research presented in this dissertation is to provide a system that can combine the high selectivity and sensitivity of immunoassay biosensors and the rapid measurement of microfluidic platforms. This can provide a solid base for the identification and monitoring cortisol and cortisone levels in Zebrafish whole-body sample and human artificial saliva samples.

### **1.1 Sensors**

Sensors can be defined as devices that consist of an active detecting element incorporated with a signal transducer. These two components in the sensors can play a

major role in transmitting either electrical, mass-based or optical signal to digital signal for selective compound analysis<sup>3</sup>. Figure 1.1.

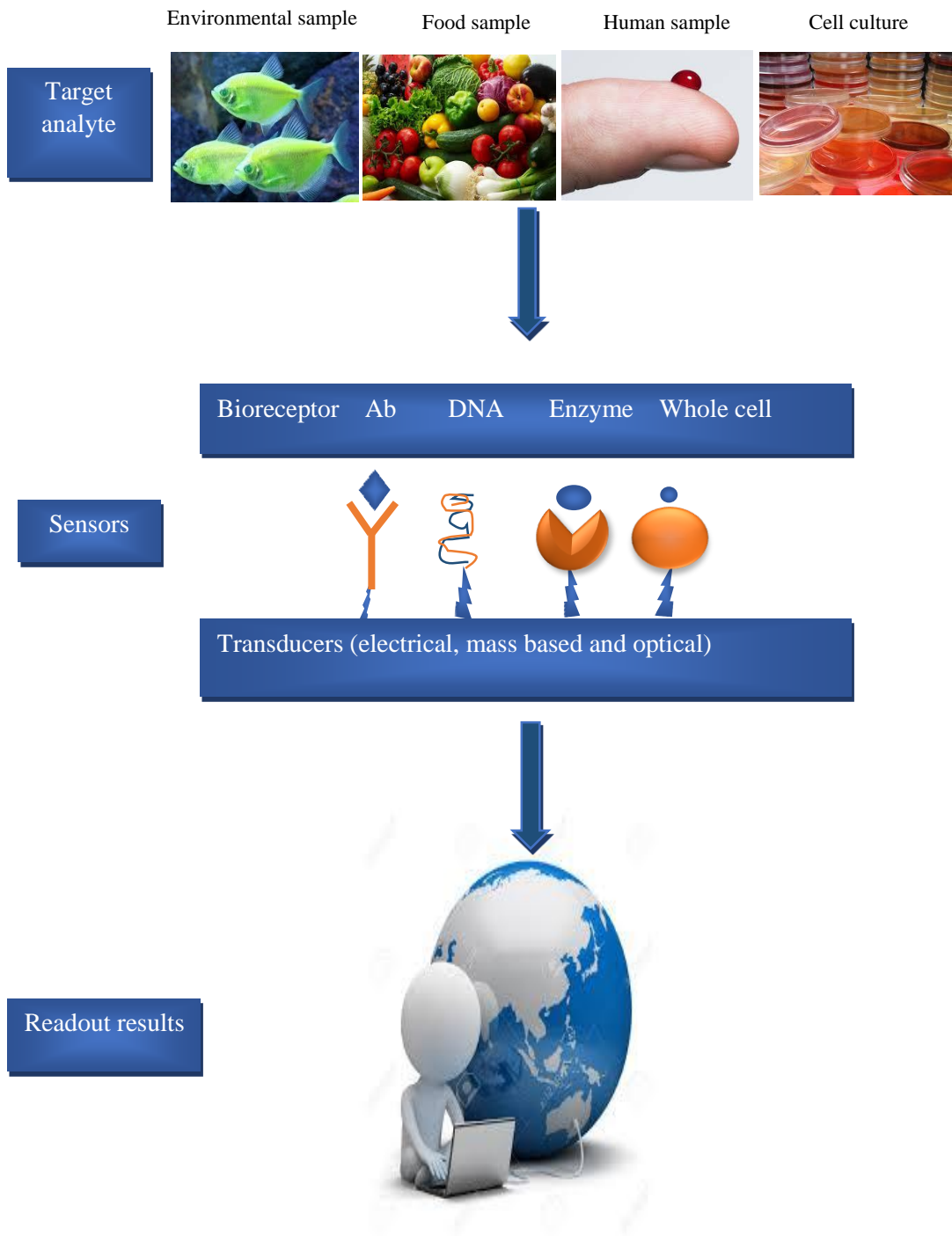


**Figure 1.1.** Schematic of a sensor device consisting of the target analyte, bioreceptor (antibody, DNA, enzyme, whole cell, etc.), transducers (electrical, mass-based and optical), microprocessor, and a display screen that is accessible to any part of the world.

Sensors can be classified into two categories: chemical sensors and biosensors. According to the international union of pure and applied chemistry (IUPAC), “a chemical sensor transforms chemical information ranging from the concentration of a specific sample component to total composition analysis, into an analytically useful signal”<sup>4</sup>. On the other hand, biosensors are composed of a biological sensing material well known as bioreceptor and a physical transducer<sup>5</sup>.

### **1.1.1 Biosensors**

Combining a biosensors ability to interact with an analyte at an extremely low concentration with extremely high selectivity, enables their application in a variety of applications using lab-on-a-chip (LOC), micro total analysis systems ( $\mu$ TAS), drug delivery system (DDS) and point-of-care systems (POC). Biosensors devices can be divided into bioreceptor that can be aptamers, protein receptors, DNA, enzyme, tissue, and antibodies; which transform biochemical information (substrate) into a form of energy to provide readable data<sup>4,5</sup>.

The second part is the transducers converts the biological response to a detectable analytical signal. Depending on the output signal, transducers can classify into electrochemical transducers (amperometric, potentiometric, impedimetric, and conductometric), mass-based transducers (piezoelectric, surface acoustic wave and magnetoelastic) and optical transducers (absorbance, luminescence, fluorescence, and reflective index)<sup>5</sup>. The transducers will be discussed in more details in section 1.2.8.

The analogue signal is correlated to concentration unit and is transferred to a digital signal *via* a microprocessor and display on a computer or mobile phone screen for analysis. The combination of a biosensor, transducer, microprocessor and display screen

have given a rise to the construction of industrial, forensics, environmental, healthcare and medical biosensors platforms <sup>6</sup>.

The specific bioreceptor/transducer constituent is determined by the bioanalyte chosen to be identified, detect and monitor. In this work glucocorticoids (GCs) including cortisol and cortisone hormones have been investigated as biomarkers for stress and will be detailed in the next section.

## **1.2 Glucocorticoids**

Glucocorticoids (GCs) belongs to corticosteroids class, which are cholesterol-derived hormones produced by the adrenal gland (cortex) located above the kidney <sup>7</sup>. The adrenal gland is divided into two regions: an inner adrenal gland (medulla), which is responsible for the epinephrine (adrenaline) and norepinephrine (noradrenaline) hormones secretion <sup>8</sup> as can be seen in figure 1.2.

The second region is the outer adrenal gland (cortex) which is involved in the secretion of the corticosteroids. These can be subdivided into two types: mineral corticoids such as aldosterone which involve in the regulation of electrolyte and water balance in the human body, the other type are glucocorticoids including cortisol and cortisone; they have the metabolic, anti-inflammatory, and stress effects <sup>9</sup>.(Figure 1.2).



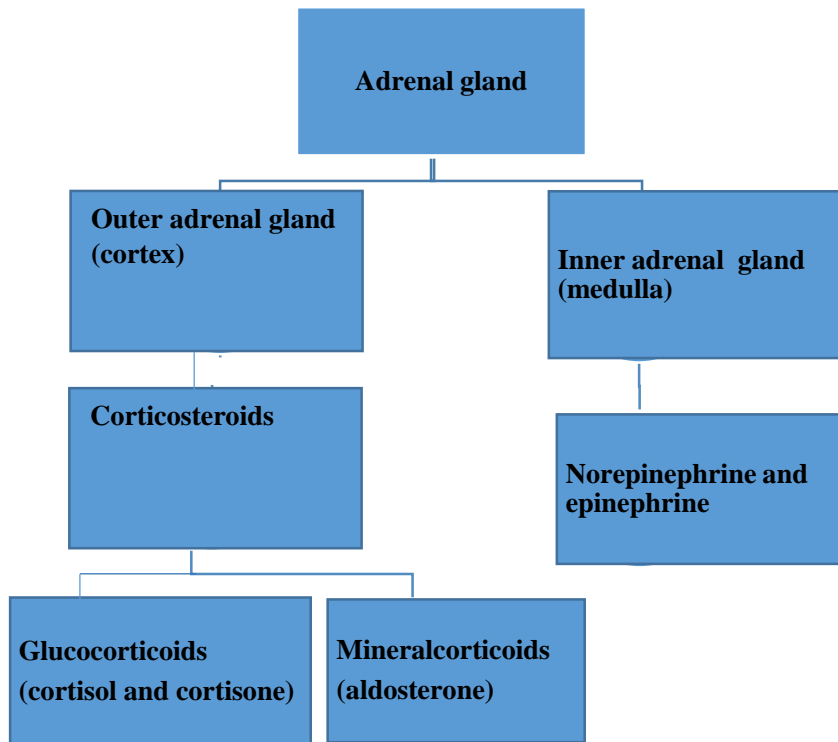


**Figure 1.2.** Diagram illustrating the adrenal gland secretion with the ending products including epinephrine, norepinephrine, aldosterone, cortisol & cortisone.

## **1.2.1 *Glucocorticoids effects***

### **1.2.1.1 *Metabolic effect***

The name glucocorticoids relate to (glucose + cortex + steroid), and their metabolic effect on glucose, glucocorticosteroids is the less common name. During fasting, glucocorticoids hormones stimulate the production of glucose in the cells (especially in the liver), stimulate the fat breakage in adipose (fat) tissues, and inhibits the storage of glucose and fat in cells to maintain normal levels of glucose in the blood <sup>8</sup>.

### **1.2.1.2 *Anti-inflammatory effect***

GCs have the ability to inhibit all levels of inflammatory response from injury or diseases. For that reason, they are considered to be effective anti-inflammatory compounds. The defensive role of the GCs mechanism can be understood as follows.

The primary step is the GCs diffusion across the cells membrane and the interaction with a glucocorticoid receptor (GR) to form a complex in the cytoplasm. The formed complex then accesses the nucleus (probably DNA), and a series of processes in the nucleus called a transcription occur. The final results are the production of protein molecules controlling the suppression of protein production involved in inflammation <sup>10, 11</sup>. This process is shown in figure 1.3.

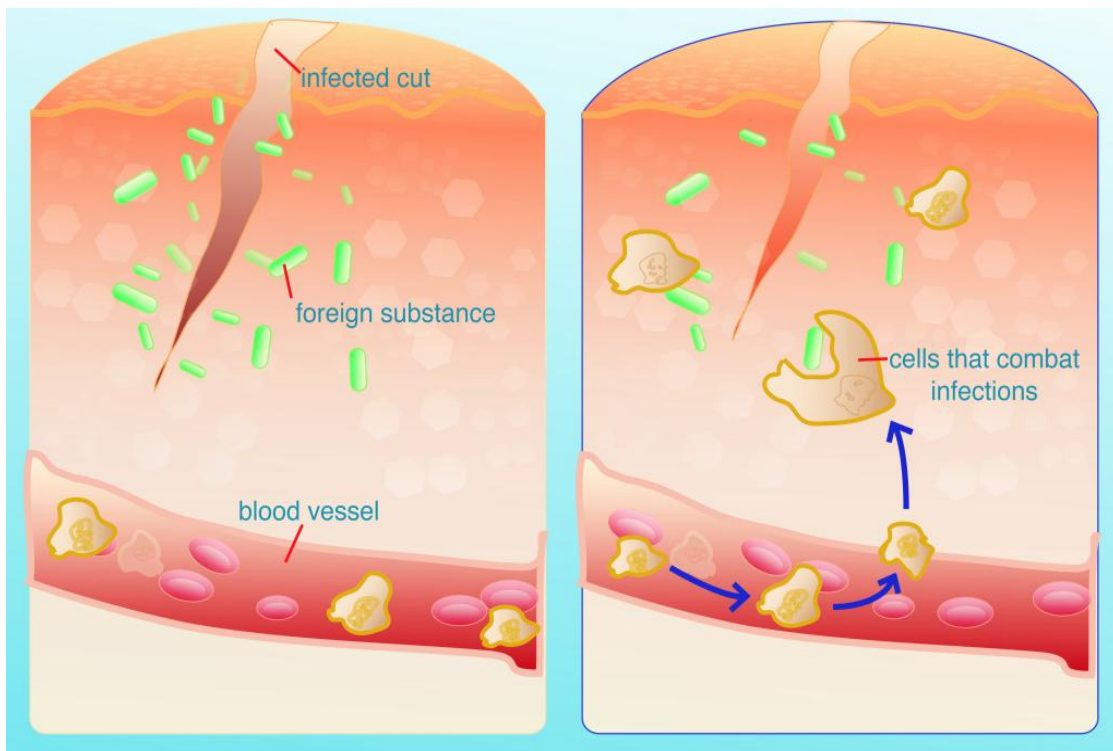


**Figure 1.3.** The anti-inflammatory process includes the liberation of mediators and cells to fight inventor substances aiming to prevent infection <sup>8</sup>.

### *1.2.1.3 Effect of stress*

Stress is defined as homeostasis state alteration due to intrinsic and extrinsic events, whether actual or perceived. This threatens is then counteracted by a cascade of physiologic responses to re-establish and maintain homeostasis. Stress is triggered in human by different events such as fear, grief, anxiety, sleep fragmentation, insomnia,

depression, excitement, guilt, embarrassment also, performance evaluations, clinical appointments, public speaking, and skydiving (to name but a few) <sup>12</sup>.

The significant characteristic of the stress response is that it should finish when the stressor has ended. Chronic stress can be fatal on the body by causing hypertrophy of the adrenal gland, atrophy of the lymphatic organs, ulcers in the stomach, fertility problems, insulin resistance, hyperlipidemia, cardiovascular disease, hypertension and chronic inflammation. Management of unavoidable sources of stress is key for preventing hypothalamic-pituitary-adrenal (HPA) dysfunction. The patient participation in treatment and understanding is necessary to improve health and prevent substantial for early mortality <sup>12</sup>.

The primary step of stressor termination for an individual's survival is the activation of the sympathetic nervous system (SNS) and the hypothalamic-pituitary-adrenal (HPA) axis as the brain detects a disruption in homeostasis. The release of catecholamines (epinephrine and norepinephrine) within seconds of the onset of the stressor attack relies on the SNS, as an example release of epinephrine maximizes blood flow as a result of heart racing and high blood pressure but heart failure and arteriosclerosis can result if there is persistent racing of the heart and high blood pressure. The HPA axis depends on the release of cortisol in humans and corticosterone in rodents after several minutes of stressor onset. This aims to supply an immediate energy source (glucose) via gluconeogenesis. The cortisol hormone is considered as the most potent biomarker for stress in humans and receives the most attention in clinical and scientific research <sup>13</sup>.

The relationship between cortisol levels and chronic stress is detected as cortisol aims to transfer cellular processes from metabolic functions to functions that are necessary for immediate survival (i.e., in the "fight or flight" response). However, the long-term

elevation of GCs starves some tissues of necessary resources and inhibit immune action, increasing the tendency to disease<sup>14</sup>. Figure 1.4.

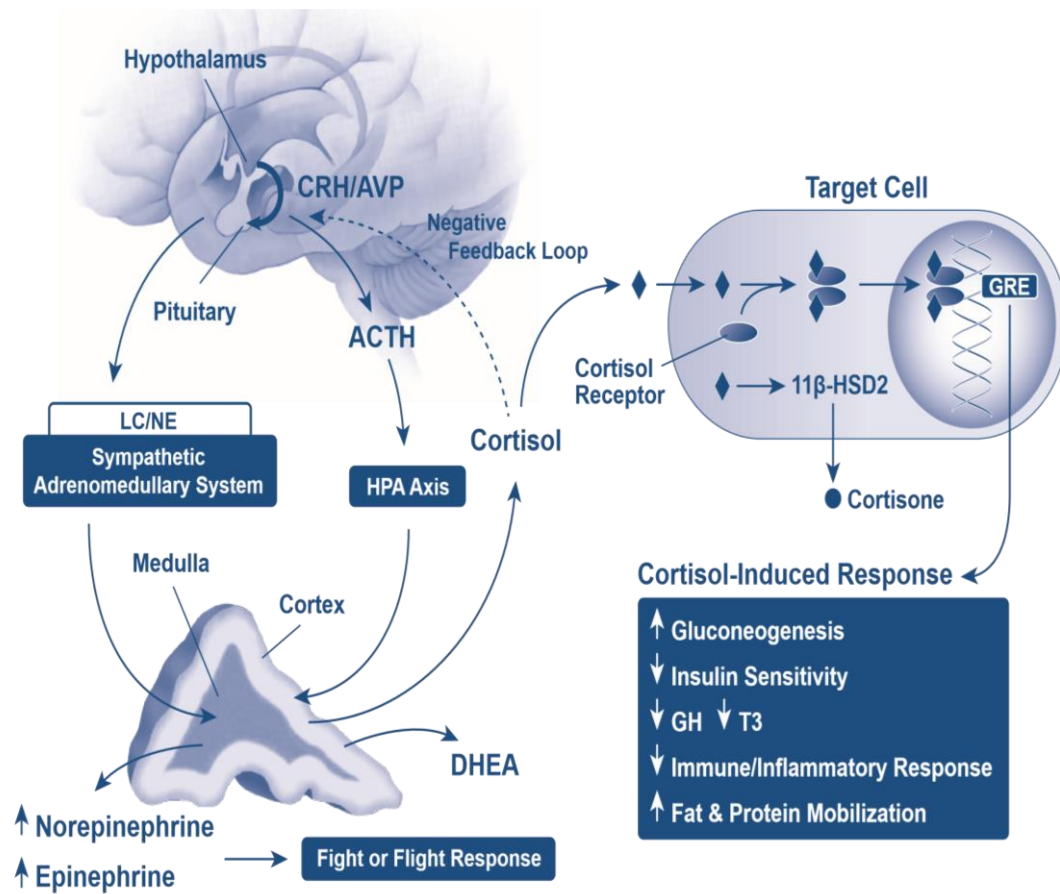


**Figure 1.4.** The hypothalamic-pituitary-adrenal (HPA) axis biosynthesis of stress hormones in the “fight or flight” response<sup>12</sup>.

The focal point of this research will be on detection and measurement of GCs hormones including cortisol and cortisone as an indication of stress.

### 1.2.2 Cortisol

Cortisol 11β,17α,21-trihydroxypreg-4-ene-3,20-dione; as shown in figure 1.5, is a major steroid hormone that belongs to the family of glucocorticoids. It is secreted initially at the hypothalamic-pituitary-adrenal (HPA) axis that releases corticotropin-

releasing hormone (CRH), this travels to the pituitary glands, and with the help of specialised cells leads to the release of the adrenocorticotrophic hormone (ACTH) into the bloodstream that reaches the adrenal cortex. The response of the adrenal cortex is to increase the production of cortisol. As mention previously cortisol participates in the regulation of many physiological processes such as glucose, protein, fat and carbohydrate metabolism, blood pressure and anti-inflammatory action <sup>15</sup>.

Hypocortisolism (insufficient production of cortisol) is well known in Addison's disease, associated with weight loss, fatigue, hypotension and coma in severe cases <sup>16</sup>, whereas hypercortisolism (excessive production of cortisol ) may lead to obesity and bone fragility symptoms which contributed to Cushing's diseases, also brain aging, immune dysfunction or increased fatty and amino acid concentration in blood which are the most common symptoms for high cortisol concentration <sup>17</sup>.

### **1.2.3 Cortisone**

Noble prize winner Edward C. Kendall was first to identify cortisone as a steroid hormone that is released in response to stress by the adrenal gland. Cortisone (17 $\alpha$ ,21-dihydroxypregn-4-ene-3,11,20-trione) chemical structure is closely related to cortisol <sup>18</sup>, as can see in figure 1.5.

The production of cortisone is by the steroidogenesis process. In the adrenal gland steroidogenesis begins with cholesterol synthesis, then a series of modifications occur leading to the synthesis of cortisol <sup>19</sup>. Cortisone can originate from cortisol by interconversion of cortisol to cortisone and vice versa by the 11beta-hydroxysteroid dehydrogenase isoenzyme (11 $\beta$ -HSD). The 11 $\beta$ -HSD 2 isoenzyme is located in mineralocorticoid targets tissues such as the placenta, kidney, and colon which is responsible for the cortisol conversion to cortisone by oxidation. On the other hand,

11 $\beta$ -HSD 1 is mainly present in the liver, adipose tissue, and lung. It is responsible for cortisone conversion to cortisol, thus cortisone is considered as a precursor molecular for cortisol. The cortisol/cortisone shuttle regulates the intracellular access of glucocorticoids to the receptors. The importance of determining both hormones relies on understanding the complication presented from their effect <sup>20</sup>. As seen in figure 1.5.

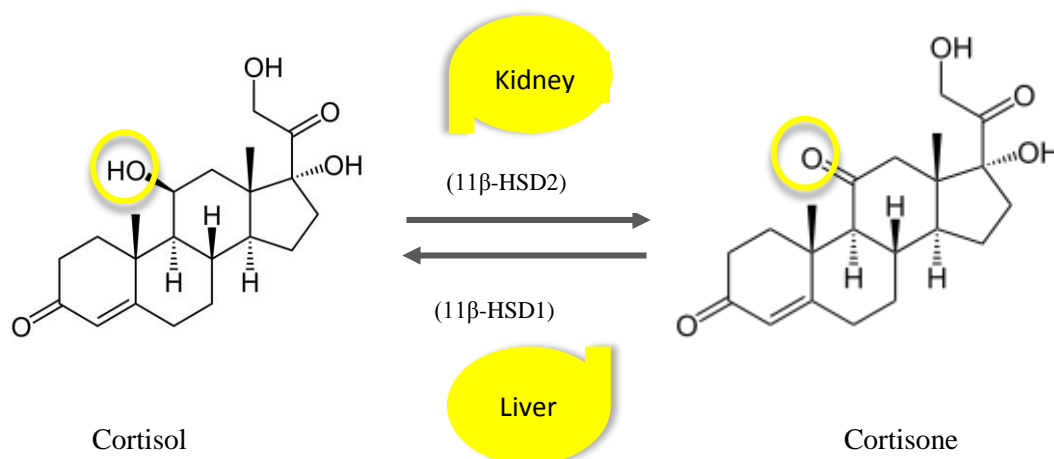


**Figure 1.5.** Conversion of cortisol and cortisone and vice versa in the presence of 11- $\beta$ -HSD1 isoenzyme (located mainly in the liver) and 11- $\beta$ -HSD2 isoenzyme (located mainly in kidney) by the oxidation of hydroxyl group in cortisol to ketone group to form cortisone or by the reduction of keto- group to hydroxyl group to form cortisol.

Cortisone has been considered as an inactive metabolite of cortisol but it has been pointed out that it can be used as another stress biomarker to evaluate the effect of inactive and active glucocorticoids. In addition, cortisone concentrations have been found to be higher than those of cortisol in the hair, thus cortisone might be more reliably detected than cortisol <sup>21</sup>.

#### 1.2.4 Selection of samples for analysis

Measuring cortisol and cortisone by analytical methods in various biofluid can be challenging due to the presence of interferences in the sample matrix. In this section, an

overview of the pros and cons of utilising different biofluids like blood, urine, hair, interstitial fluid (ISF), saliva, whole-body (Zebrafish), nail, faeces, sweat and wastewater samples will be presented.

#### ***1.2.4.1 Blood sample***

Blood samples have long been used to give information on cortisol and cortisone circadian rhythms. Approximately 90% of the cortisol in the blood is bonded to corticosteroid-binding globulin (CBG) and in the inactive state; around 7% is bounded to serum albumin. This leaves (1-3 %) unbound and biologically active<sup>22</sup>. The ratio of serum total cortisol/CBG (free cortisol index (FCI)) is correlated to serum-free cortisol, which is considered to be the biologically active component<sup>23</sup>.

Cortisol blood levels fluctuate from 25  $\mu\text{g dl}^{-1}$  (9 am) to 2 $\mu\text{g dl}^{-1}$  (midnight). Problems with using blood as a sample include the need to collect the sample by puncture of the vein to collect blood which can be a painful procedure as experienced by the patient which may cause an increase in cortisol and cortisone values. Furthermore, blood is a biohazard and specialised medical staff are required to handle and store the sample and sterile equipment increasing the cost of the blood assay. For all these reasons the blood is not the preferred sample which to determine cortisol and cortisone levels<sup>2, 24</sup>.

#### ***1.2.4.2 Urine samples***

Urinary free cortisol (UFC) is the optimal test for Cushing disease diagnosis<sup>25</sup>. 10 - 100  $\mu\text{g 24h}^{-1}$  is the normal value for cortisol in urine which is the only active form presented in urine. Urine assay indicates the cortisol production over an interval of time extended to 24 hours. This makes the sample collection a complicated procedure<sup>26</sup>.

Also, this procedure requires the patient to carry a specific container to collect the urine all day, restricting patient movement. Contamination must be avoided and the collection

container must keep in a refrigerator over the period of collection. Another problem with the urine assay is interferences from other endogenous steroids metabolites and synthetic glucocorticoids such as prednisolone <sup>2</sup>.

#### ***1.2.4.3 Hair sample***

In the recent years, hair analysis has become popular especially for toxicology, forensic science, clinical diagnostic and for stress-related researchers <sup>27</sup>. The main mechanism for incorporation of drugs, hormones, agents, or toxic in hair is explained below. Externally, substances can accumulate onto hair surface from surrounding environment by means of pollution, smoke, and use of creams or ointment containing cortisol. Internally, hair follicles lie inside the skin and receive substances by a diffusion process from blood capillaries, as well as through sweat and sebum secretion <sup>28</sup>.

Hair analysis is considered to give a "windows to the past" providing a calendar of substance production or intake, (see figure1.6). The concentration of cortisol and cortisone in hair was first cited by Raul *et al.* and was found to range from (5 to 91 pg mg<sup>-1</sup>) and (12 to 163 pg mg<sup>-1</sup>) for cortisol and cortisone respectively <sup>29</sup>.



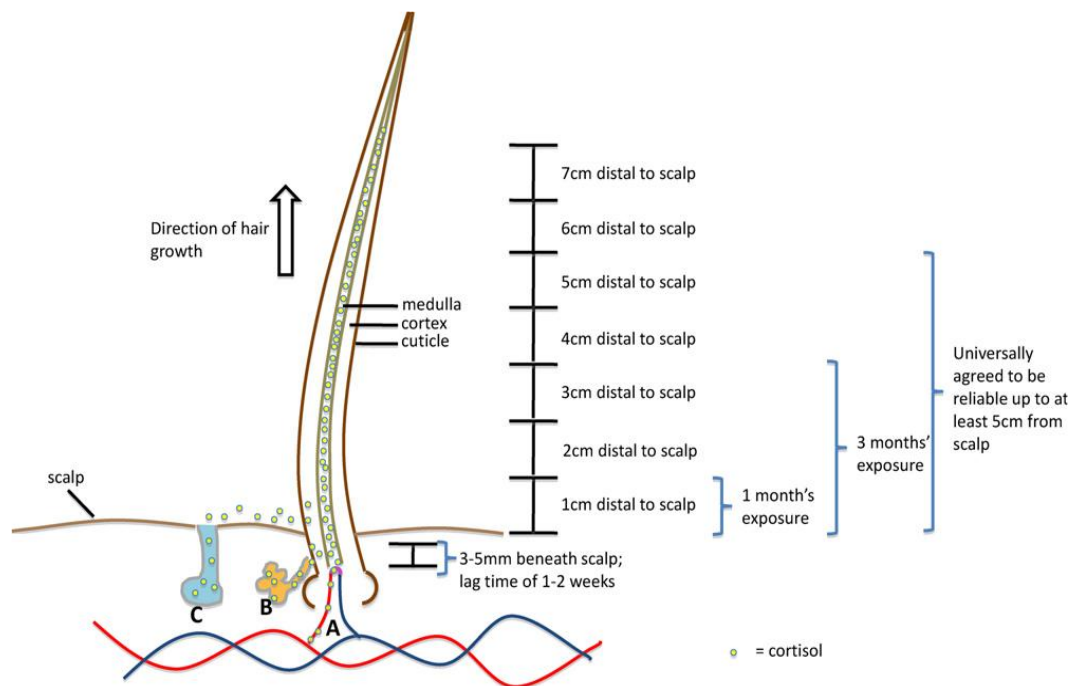


**Figure 1.6.** Illustration of the integration of cortisol into hair samples by means of (A) blood, (B) sebum, and (C) sweat <sup>30</sup>.

Analytical assay for stress hormones analyses in hair has received little attention compared with the increased use of hair as a biomarker of stress hormones, this may be attributed to a large amount of hair matrix needed, also it is quite a long method for sample preparation <sup>31</sup>.

#### **1.2.4.4 Interstitial Fluid (ISF)**

For non-clinical setting and with the need for continuous sample measurements, interstitial fluid (ISF) or tissue fluid is considered as an attractive sample. Interstitial fluid is an extracellular fluid that bathes and surround the human body's cell. Interstitial fluid resembles blood plasma in composition. Proteins and metabolites concentration in ISF is related to their concentration in capillaries as they move in a similar approach from capillaries to cell <sup>32</sup>.

The ISF content consists of sugars (glucose), salts, fatty acids, amino acids, coenzymes, hormones, neurotransmitters, minerals such as calcium, magnesium, and potassium as well as waste products from the cell result from metabolism. These nutrients are continuously exchanged between plasma and interstitial fluid across the walls of blood capillaries<sup>33</sup>.

ISF sampling is rarely mentioned and new, the collection can be non-invasive using wearable ISF device attached to the patient. This can provide 2-3 days harvesting ISF sample in painless techniques<sup>34</sup>. An ISF harvesting device has been reported by Venugopal *et al.* this device utilizes a laser to create micropores in the upper layer of the skin (stratum corneum) and ISF fluid which is found below the skin is collected continuously by applying a small amount of vacuum<sup>32</sup>. However, biocompatibility, biodegradation and sterility issues due to the usage of microneedles will affect the application.

#### ***1.2.4.5 Saliva sample***

Saliva is a preferred sampling option to monitor cortisol and cortisone for diagnostic tests for characterising of disorders related to the hypothalamic-pituitary-adrenal (HPA) axis and recommended by endocrinologists for Addison's disease, Cushing's syndrome, circadian rhythm, stress-related disorders and adrenal abnormalities<sup>2,35</sup>.

A list of advantages associated with saliva will be reviewed. For one, the simplicity of salivary sample collection reduces the rate of positive false test results; as seen with venepuncture that leads to artificial alteration to stress biomarker values. Patients have the ability to collect their sample without the need of healthcare professionals. In addition, saliva does not clot and is produced continuously, which makes it easy to repeat at short intervals<sup>36,37</sup>.

Another advantage is the presence of cortisol in its active biological form only in saliva, this can be explained due to filtration of CBG and albumin-bound cortisol during the capillary exchange and different intracellular mechanisms at the salivary duct. Low concentration of cortisol in saliva ( $0.05 - 0.5 \mu\text{g dl}^{-1}$ ) however demand an assay with high sensitivity and low detection limit <sup>2</sup>.

#### ***1.2.4.6 Whole-body sample (Zebrafish sample)***

Over the years, fish have been favoured as a research model where goldfish was used in aquatic toxicology since the mid eighteenth century. Zebrafish (*Danio rerio*) a small tropical freshwater fish have been selected as a model organism in many research fields including biomedical research (development and genetic studies), toxicology, pathology, stress, and immunology. The species are easy to breed, have a short life cycle and small size as can be seen in figure 1.7 that shows the short life cycle of the Zebrafish <sup>38, 39</sup>.

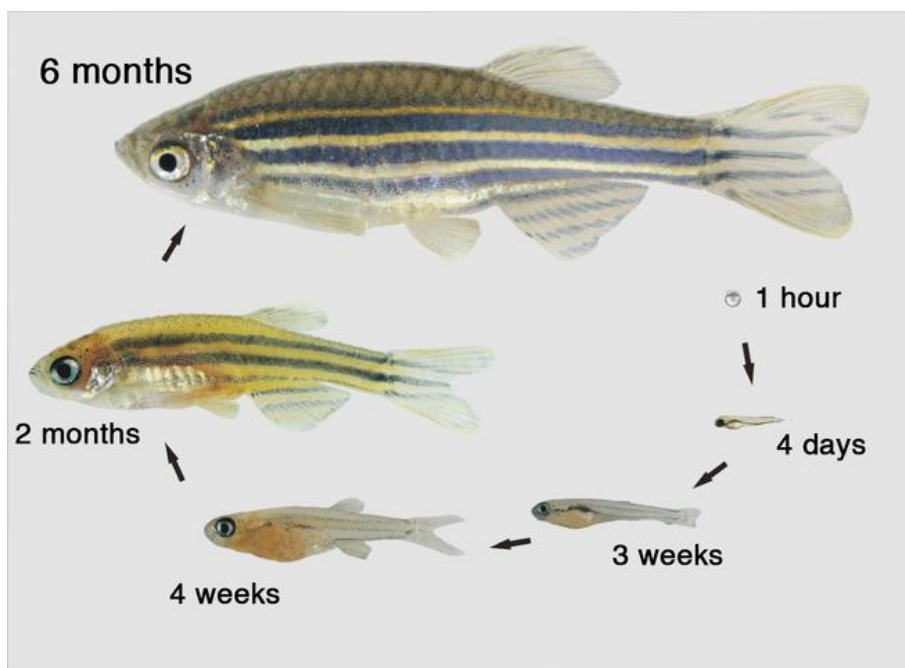


**Figure 1.7.** Zebrafish life cycle<sup>40</sup>.

The Zebrafish belongs to the Cyprinide family which was called *Brachydaniorerio* until 1981, and then it was changed to *Danio rerio* as its scientific name <sup>39</sup>. As a simple vertebrate species, the Zebrafish is physiologically homologous to humans and other mammalian species, permitting scientists to obtain new insights into the pathways and mechanisms relevant to human clinical treatments and pathogenesis at the same time keeping cost and maintenance at a minimum <sup>41</sup>.

The key point of Zebrafish is the similarities of functional and anatomical between hypothalamic-pituitary-interrenal (HPI) axis and human hypothalamic-pituitary-adrenal (HPA) axis in the human neuroendocrine system due to similar classical vertebrate neurotransmitters and neuroendocrine system that gives a robust physiological response to stress <sup>42</sup>. Zebrafish mimic humans in the secretion of cortisol as result of a variety of stressor: shaking, cold or trauma<sup>43</sup>, crowding, capturing, handling and transporting <sup>44</sup>. On the other hand for rodents, amphibians, reptiles, and birds the main secretion is corticosterone <sup>45</sup>. To date, Zebrafish have been extensively used for laboratory stress models and research has been published using either blood samples <sup>46</sup> or preferably whole-body sample due to its small size and inadequate blood volume <sup>47-49</sup>.

#### ***1.2.4.7 Nail, faeces, sweat and wastewater samples***

Stress hormones are usually determined using the above samples in addition to other samples including nail <sup>50, 51</sup>, faeces <sup>52-55</sup>, sweat <sup>56</sup> and wastewater <sup>57-59</sup>. However, the usability of these samples may be restricted for several reasons, including ethical barriers for invasive sampling, tedious sample preparation and expensive chemicals used, etc. The techniques used to determine cortisol and cortisone is presented in the next section.

## **1.2.5 Glucocorticoids detection**

There are diverse techniques for stress hormone detection in a biological sample. These use instrumental techniques such as mass spectrometry, chromatography techniques and bioanalytical techniques such as an immunoassay.

### **1.2.5.1 Instrumental techniques**

Mass spectrometry (MS) and Tandem mass spectrometry, also known as MS/MS or MS<sup>2</sup> have received attention as a quantitative technique for steroids hormones analysis<sup>60, 61</sup>. The well-known strategy for the assessment of analysis specificity involves the conversion of the sample to an ionized state usually by the loss of electrons, then the ions are analyzed and monitor according to the mass to charge ratio (m/z) for each analyte<sup>62</sup>.

The widely recognized advantage of ionization techniques for mass spectrometry which include atmospheric pressure chemical ionization (APCI)<sup>63</sup>, atmospheric pressure photoionization (APPI)<sup>64</sup> and electrospray ionization (ESI)<sup>65</sup> is an enhancement in the sensitivity and increase in selective ionization. On the other hand, mass spectrometry-based instruments are complex requiring sample preparation, technical expertise, and additional standardization methods to assure the diagnostic utility of the methods leading to a substantial disadvantage in applying mass spectrometry to routine high throughput testing in laboratories<sup>66</sup>.

Chromatography techniques are the most commonly used in laboratories for quantitative bioanalysis. This is attributed to their high sensitivity and selectivity. Previously reported analytical procedures for stress hormones analysis, have utilized a variety of chromatography techniques such as thin layer chromatography (TLC). This technique enhances the possibility of analysing complex sample simultaneously, the availability and requires a low cost in instrumentation and allows an easy change of

solvent<sup>67</sup>. Kartsova *et al.* conducted an experiment for the separation of exogenous and endogenous steroids hormones. This was carried out using a micellar mobile phase to improve the selectivity of the TLC technique. As a result,  $R^2$  for both cortisol and cortisone were 0.9852 and 0.9954 respectively<sup>67</sup>. Despite the simplicity and availability of TLC technique, it suffers from the application of only non-volatile compounds and non-automated system which limits its use<sup>68</sup>.

The introduction of gas chromatography coupled with mass spectrometry improved stress hormones measurements. Shibasaki *et al.* used GC-MS in the determination of cortisol and cortisone in plasma with a correction coefficient for cortisol 0.999 and cortisone 0.999<sup>69</sup> and Wood *et al.* compared gas chromatography and liquid chromatography-tandem mass spectrometry techniques to analyse urinary free cortisol, the results showed that there was an agreement between the two methods ( $R^2 = 0.9937$ )<sup>70</sup>. Although the high separation resolution acquired from chromatography and the additional detection specificity provided by the mass spectrometry, GC/MS is unsuited for routine laboratory methods for measuring steroids. The reason for this is GC-MS procedures employ multiple derivatization steps that are not suited for routine laboratory procedures, which is disadvantageous as it is time-consuming with labor-intensive sample preparation<sup>71,72</sup>.

Liquid chromatography (LC) and liquid chromatography-mass spectrometry (LC-MS/MS) overcomes problematic issues related with GC and GC-MS/MS, thus it has become the method of choice for analytical stress hormone measurements in laboratories. Advantages include simultaneously multiple analyte measurements, the need for less sample volume and preparation, shorter period of time for analyzing steroid hormones, and a potential for automation. This is in addition to high analytical specificity and sensitivity<sup>73</sup>.

The quantitative determination of multiple steroid hormones including estradiol, cortisol, cortisone, corticosterone, testosterone, progesterone, dehydroepiandrosterone (DHEA) in human saliva was reported by Gao *et al.* achieving fast throughput time of 5.20 minutes <sup>74</sup>. In clinical diagnosis, LC-MS/MS is widely used to monitor drugs and measure biomarkers of diseases including endogenous steroids. Cushing's syndrome was diagnosed using LC-MS/MS technique, by measuring levels of urinary free cortisol (UFF), urinary free cortisone (UFE) and the UFF: UFE ratio <sup>75</sup>.

Although liquid chromatography is one of the best-known techniques for steroids hormone analysis, it suffers from contamination and interferences. Contamination affects the mass analyzer which can cause potential ion suppression, increase the need for instrument maintenance and give high background signals. Impurities are introduced with reagents and solvents that lead to loss of sensitivity, change in ionization efficiency and analyte degradation. To eliminate potential interferences from mass transitions used by LC-MS/MS and to assure that the analyte only is measured, tests for evaluation of potential interference must include analysis of structurally similar compound and sample constituents which add more steps for the analysis of steroids <sup>76</sup>.

Another disadvantage of LC technique related to the biological matrices which are not amenable to direct analysis with LC-MS/MS so extraction, clean-up and concentration steps are required for sample preparation. Common techniques involve solid-phase extraction (SPE) <sup>77</sup>, liquid-liquid extraction (LLE) <sup>78</sup>, protein precipitation (PPT) <sup>79</sup> and dilution have been used in laboratories for sample preparation to reduce sample matrix effect, sample complexity and give more sensitivity to the method. In the same time, it raises time and cost consumption.

Saracino *et al.* improved the time required for simultaneous analysis of cortisol, cortisone and corticosterone levels in saliva, plasma, blood and urine samples. The achieved time was less than 10 minutes using a reversed phase column, the method gave linear results over a range of (5 – 100 ng ml<sup>-1</sup>) using diode array as a detector <sup>80</sup>. Sanchez-Guijo *et al.* constructed an HPLC-MS/MS coupled to semi-automated sample work-up step with minimal human involvement. This was achieved by applying turbulent flow technique for direct sample injection reducing the required total time for sample preparation, the resulted limit of detection and limit of quantification were 0.5 and 1.0 ng ml<sup>-1</sup> for cortisone and 1.0 and 2.0 ng ml<sup>-1</sup> for cortisol <sup>81</sup>. Ultra high-performance liquid chromatography (UHPLC) is a technique that can increase separation efficiency and improve resolution. It does this by using HPLC columns with mean particles size less than 2 µm along with new commercial instrumentation capable of driving the eluent through the column at higher pressure, this allows optimum linear velocity to be reached for smaller particles size columns <sup>76</sup>. McWhinney *et al.* reported this advantage to measure cortisol, cortisone, prednisolone, dexamethasone, and 11-deoxycortisol in a routine laboratory, this was done by comparison with HPLC the cortisol method yielded a regression equation of  $UHPLC = 1.06 \times HPLC + 9.82$ ,  $R^2 = 0.992$  <sup>82</sup>.

To conclude chromatography-based assays for stress hormones are highly sensitive and selective, however, the sophisticated instrumentations and high expenditure of time limits the practical applicability of this technique.



### ***1.2.5.2 Immunoassay biosensor***

As mentioned previously biosensors are constructed from a bioreceptor (antibodies were chosen for this work and further details will be discussed later) and a measurement transducers (electrochemical and chemiluminescence techniques were chosen). Immunoassay is an analytical technique that employs the specific recognition between an antibody and antigen to measure the concentration or the presence of an analyte<sup>83</sup>. This is a fundamental assay that is globally used for stress hormone detection and monitoring. Antibodies (Ab) (or immunoglobulins (Ig)) are heavy (~150 kDa) proteins. They are secreted in human and animals by plasma cell as an immunological response to the presence of foreign substances (usually called antigens (Ag)) such as bacteria and viruses to neutralize the Ag as a body self-defense. This benefits from the unique Ab structure which can be only recognized by a specific part of the foreign target (Ag) in a lock and key mechanism. The interaction between the antigen and the antibody depends on van der Waals forces, electrostatic forces, hydrogen bond and hydrophobic interactions<sup>84, 85</sup>.

The basic unit is a monomer which is a Y shape molecule that includes four polypeptide chains: two identical heavy chains ( $\alpha$ ,  $\gamma$ ,  $\epsilon$ ,  $\mu$  and  $\delta$ ) and two identical light chains ( $\kappa$  and  $\lambda$ ) connected by disulfide bonds. Each chain consists of structural domains called an Ig domains of 100 amino acids. Heavy and light chains consist of two regions. The variable region Fab (fragment antigen binding) is responsible for antibody specificity due to the presence of Fab fragments (paratope) which are located at the top of both heavy and light chains (analogue to a lock), which is specific for one epitope (similarly analogue to a key) on the antigen. The second region is a constant region Fc (Fragment crystallization) which binds to a certain receptor to initiate antibody dependent cell cytotoxicity also being transported to a variety of places, such as tears<sup>86, 87</sup>. Figure 1.8.

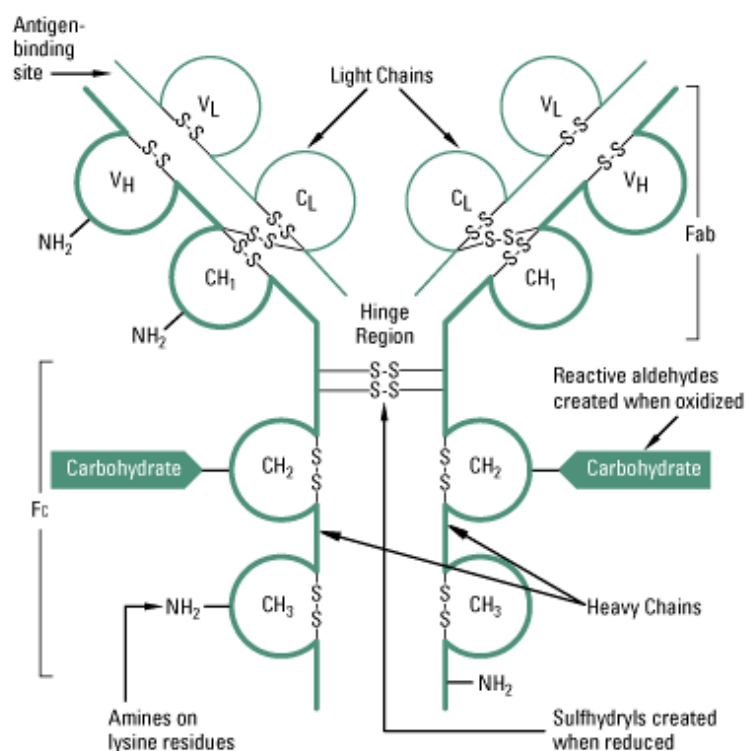


**Figure 1.8.** Structure of an antibody. The basic structure of an antibody, indicating where the Fab (fragment antigen binding) and Fc (Fragment crystallization) regions are which chains are heavy and light with the disulphide bond linkages, amine groups, and carbohydrates. The variable region represents where the antigen can bind to the antibody, whereas the constant region is constant for all different antibodies <sup>88</sup>.

There are three ways that an antibody contributes to immunity. The first way is by coating the pathogen, the antibody stimulates removal of the pathogen by macrophages and other cells; in the second way they trigger destruction of pathogens by stimulating other immune response such as the complement pathway; and in the third way the antibodies bind to pathogens preventing them from entering or damaging cells <sup>89</sup>.

Antibodies can be obtained from hyper-immunized animals or hybridoma cells. Polyclonal antibodies (pAbs), are produced by animals (e.g. rabbits, chicken, etc.). The production of pAbs are inexpensive but may suffer from the cross-reactivity with

structurally similar compounds. While monoclonal antibodies (mAbs) are produced from mice; this antibody is more sensitive but more expensive. Recently, recombinant antibodies (rAbs) were produced from various animals by amplifying Ab gene using polymerase chain reaction and expressed in different formats such as fragment antigen binding and variable domain fragment, etc. In addition, plants have the potential for antibody production <sup>90</sup>.

### **1.2.6 *Immunoassay classification***

Immunoassays can be categorized into four basic configurations, depending on the phase where the immunoreaction takes place (homogeneous and heterogeneous) and on the antibody-antigen measuring scheme (competitive and non-competitive). “Mix and measure” techniques is a popular term for homogeneous assay where no filtration, multiple washing, and incubation steps are required. Homogeneous assay usually takes place in the solution and the detection of the analyte is obtained by chemical or physical changes resulted from Ab-Ag complex formation. Despite the homogenous immunoassay mentioned advantages, it suffers from disadvantages such as reduction in sensitivity and specificity due to the presence of sample matrix <sup>85,91</sup>.

On the other hand, heterogeneous immunoassay relies on the immobilization of the antibodies on a solid surface, the interaction of the Ab-Ag then occurs and the analyte is measured. A washing step is introduced to remove unused antigen or any contamination. A heterogeneous assay advantage is an increase in target sensitivity and specificity compared with the homogeneous assay <sup>84,92</sup>.

Homogeneous and heterogeneous can further subdivide into competitive and non-competitive formats (figure 1.9 and 1.10). In this category, the classification is based on the order of reagents added and the effect of interaction between the reagents after addition. In the competitive format; there is a competition between unlabelled antigen and labeled antigen for a limited number of antibody binding sites. Whereas in non-competitive format antigen forms a complex with an excessive amount of labelled antibody

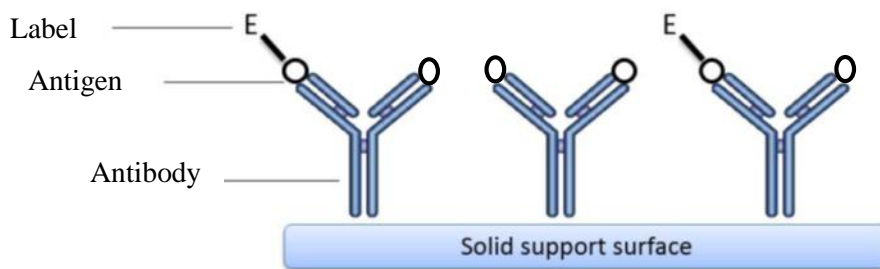


**Figure 1.9.** Shows competitive immunoassay where antibodies are immobilized on the solid surface and a competition between antigens (found in the sample) and added tagged antigen on limited binding sites available on the immobilized antibodies. The high sample concentration resulted in a lower signal due to the less tagged antigen binding to the antibodies. Therefore, an inversely proportional relationship between signal and antigen in the sample is found.

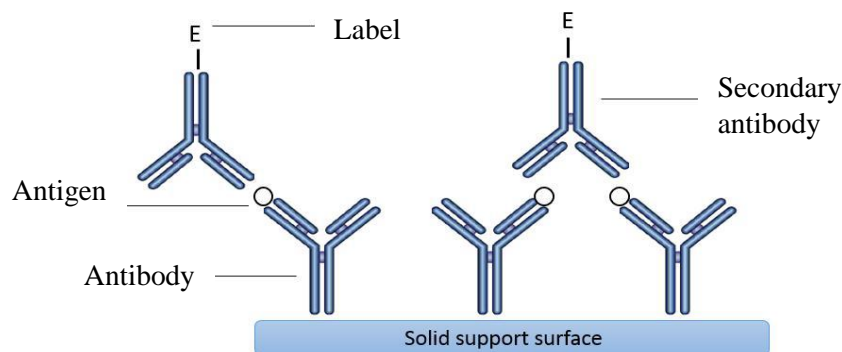


**Figure 1.10.** Shows a non-competitive immunoassay where the antibodies are immobilised on a solid surface and antigens are added to form the antibody-antigen complex. Afterwards, a second labelled antibody is added and bind to the complex for a period of time well known as incubation time. The signal produced is proportional to the concentration of the antigen, which means the more antigen in the sample results in the larger signal.

The essential assay that is used in the health system and laboratories for measuring stress hormone levels is the enzyme-linked immunosorbent assay (ELISA). Typical methodology depends on the use of enzyme labelled antigen and antibody to observe the biological molecules such as protein, hormones, and peptides. Major enzymes used are alkaline phosphatase, horseradish peroxidase and glucose oxidase. In 96-well microliter plates, the antigen (in the liquid phase) is allowed to bind to the specific primary antibody. This can be detected by a secondary enzyme-coupled antibody. The chromogenic substrate for the enzyme produces a color change to qualitatively detect the antigen <sup>95</sup> (figure 1.11).

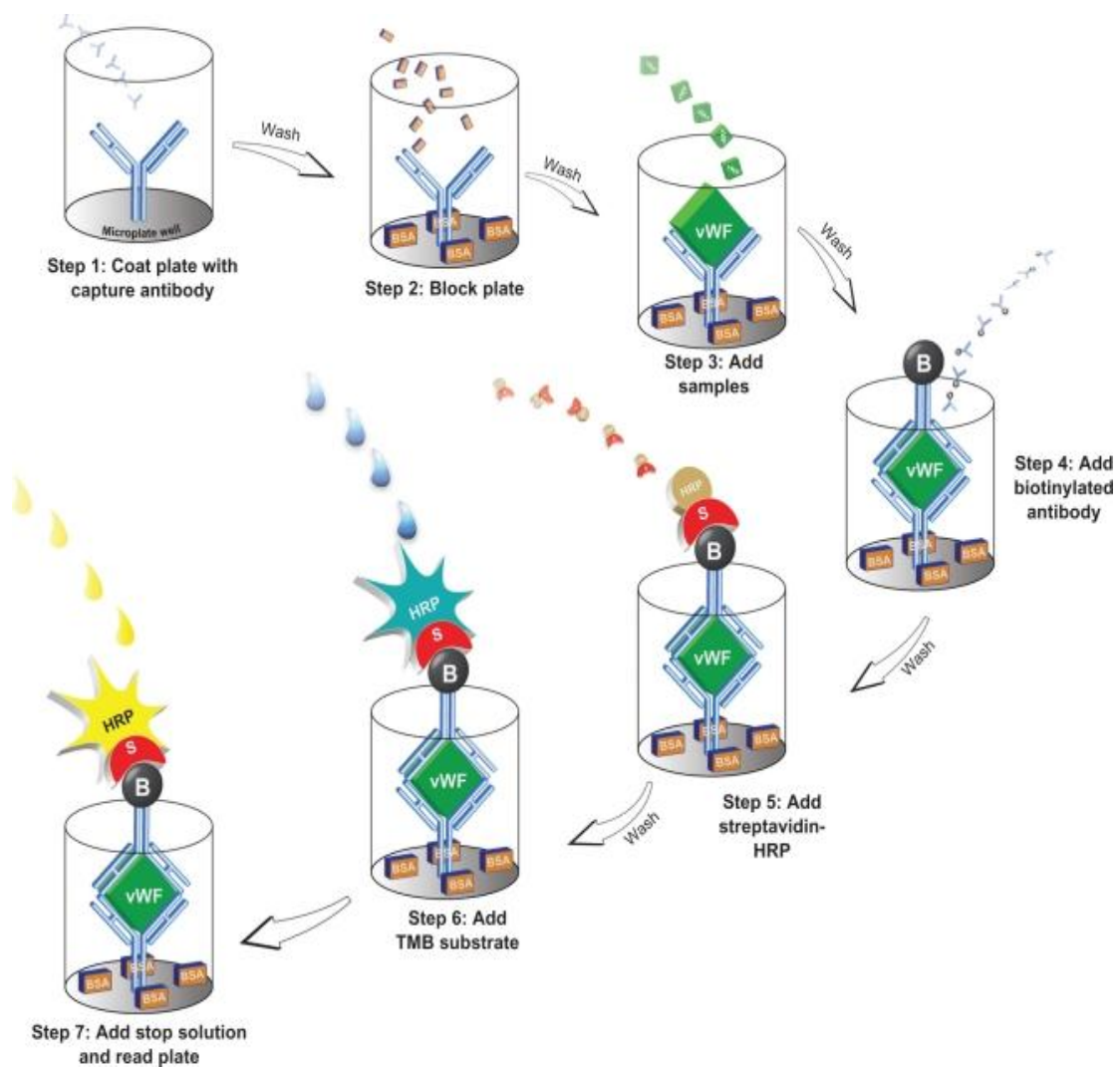


**Figure 1.11.** Represent a schematic of an ELISA procedure <sup>96</sup>.

Sesay *et al.* reported an approach for the determination of cortisol in human saliva based on (direct and indirect) competitive reaction. To achieve this goal, ovalbumin was conjugated to cortisol and used for developing an indirect competitive ELISA, while The linear range for both methods was (0.5 –70 ng ml<sup>-1</sup>) and (2 – 330 ng ml<sup>-1</sup>) and detection limits of 0.5 and 1.2 ng ml<sup>-1</sup>, respectively. Although ELISA is sensitive it is labor and time-consuming <sup>97</sup>.

### **1.2.7      *Immunoassay immobilization***

The aim of this work is to develop a sensitive detection system (biosensor), thus heterogeneous immunoassay will be used as it delivers more sensitivity than homogeneous immunoassay. Immobilization of functional molecules (biosensing elements) on the solid surface (transducers) to detect the analyte (cortisol and cortisone) is a fundamental point in heterogeneous immunoassay due to the influence of specificity and sensitivity that the immobilization step offers.

The success of any immobilization methods is provided by the correct orientation (also known as site-specific immobilization) of the biomolecules (antibodies, DNA, etc) on the sensor surface, which allows their bioactivity and functionalities to be ideal for a definite binding of the analyte. To ensure the high reproducibility, reliability, low cost, and better sensitivity the reactive groups of the biomolecules have to be facing the analyte and must retain their biological functionality because this reduces the interferences caused by non-specific binding.

There are two approaches for immobilization; these include covalent and non-covalent (entrapment, cross-linking, biological binding, and adsorption) as can be seen in figure 1.12. A covalent bond is preferable due to specificity while non-covalent offers the

simplicity but lack of specificity<sup>98</sup>. A short review on each immobilization approaches will be described in the next section.

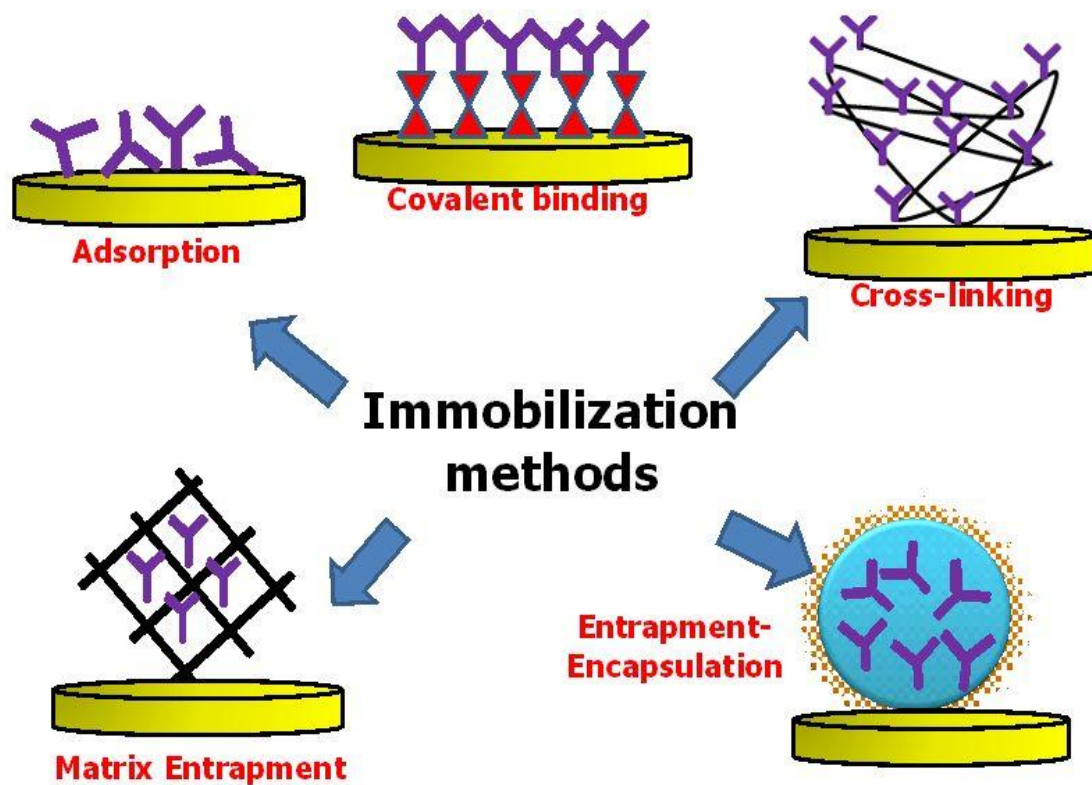


**Figure 1.12.** Illustrate generic antibodies immobilization methods<sup>99</sup>.

### ***1.2.7.1 Covalent bond***

The covalent bond between the functional group of both surface and antibodies is a chemical bond and resulted in a non-reversible process and this gives the advantage of ultimate biomolecules orientation.

A full comprehension of the antibody and surface functional groups are the substantial key for choosing the best method for immobilization. The targets functional groups on the antibody are an amine, hydroxyl, carboxylic acid and a thiol group. These functional

groups include : (i) amino group of N-terminal amino-acid and free amino group of lysines, (ii) sulfhydryl group of cysteine, (iii) thio ether group of methionine, (iv) carboxylate group of C-terminal amino acid and p and y-carboxylate group of aspartic acid and glutamic acid respectively, (v) phenolic group of tyrosine, (vi) imidazolyl group of histidine, (vii) guanidinyl group of arginine and (viii) indolyl group of tryptophan <sup>100</sup>.

A widely used form of covalent immobilization uses the amine group because of the easy access to these group. EDC (1-ethyl-3-(3-dimethyl aminopropyl)-carbodiimide) – NHS (N-hydroxysuccinimide) is a preferred method for immobilization through the coupling reaction between amino and carboxylic groups. Initially, carboxyl groups on the solid surface on which the antibody is to be immobilized are chemically activated with the EDC-NHS group to enable the linkage of the amino group forming stable amide linkages. The mechanism involves EDC binding to the carboxyl groups to form unstable O-acylisourea ester intermediate which stabilizes by the addition of sulfo-NHS by converting it to amine-reactive NHS-ester intermediate. This step allows the efficient conjugation to a primary amine <sup>101</sup>.

The main advantage of EDC coupling is water solubility, this permits direct bioconjugation without previous organic solvent dissolution. Another advantage is the excess of reagents and by-product can be easily removed by dialysis or gel filtration. Therefore, this protocol was used for diverse molecules such as enzyme, antibodies, peptides, DNA, etc. attachment to surfaces <sup>101</sup>. The reaction scheme is presented in figure 1.13.



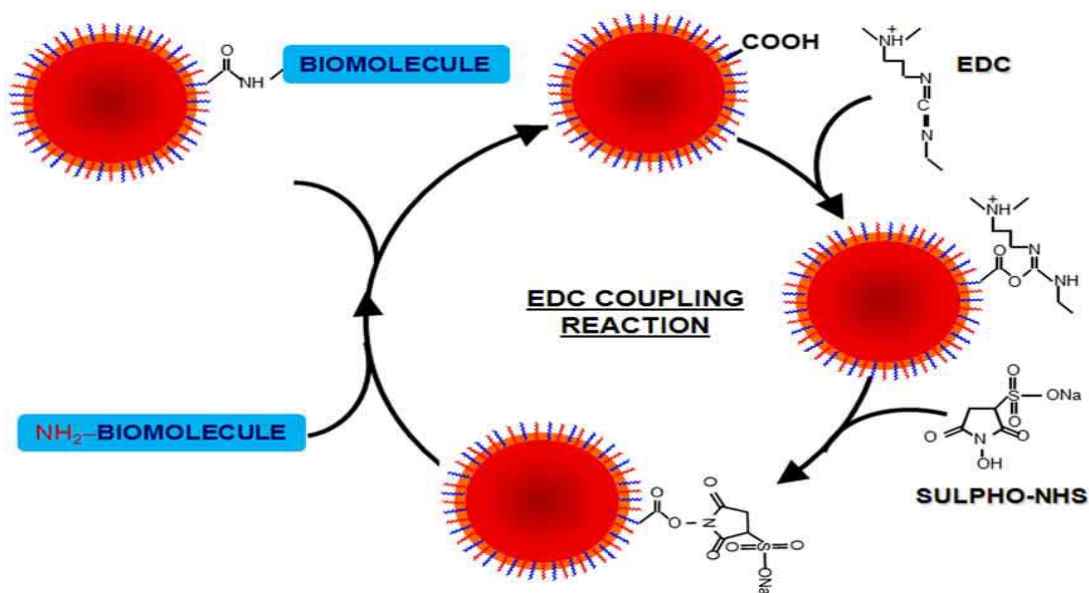


**Figure 1.13.** EDC coupling reaction <sup>101</sup>.

Another example of an immobilization method using the linkage between carboxylic acid and amine groups was published by Yamaguchi *et al.* A dry-chemistry based on the fabrication of electrochemical biosensor to permit point-of-care assessment of salivary cortisol as stress biomarker was achieved. The synthesis of cortisol (CORT)-glucose oxidase (GOD) conjugation was carried out using adipic acid dihydrazide (ADH) as a linker. Initially, GOD was modified to an aldehyde and formed a GOD-ADH complex through a hydrazone bond. This complex was reacted with cortisol to form the GOD-(ADH)-CORT employing the reaction of the amine group of COD-ADH conjugated with the carboxylic group of CORT <sup>102</sup>.

Schiff's base reactions are also used for linkage through the amino group reaction with an aldehyde group. This reactions attraction is it occurs efficiently at high and low pH and it proceeds in mild conditions. The chemistry behind Schiff's base is the formation of unstable Schiff's base, followed by a reduction to be stabilized resulting in the

formation of a stable secondary amine linkage. The most used reagents for this reaction are sodium borohydride and sodium cyanoborohydride <sup>98</sup>.

Aldehyde groups are generated by oxidation of hydroxyl group of carbohydrates presented in the antibody using potassium or sodium periodates. The activated diol group resulted can be covalently coupled the antibody to the amino-functionalized surface <sup>103</sup>. Glutamic and Aspartic acids contain carboxyl groups which can be activated by carbodiimide (CDI), this enables the covalent coupling with the surface through the amines groups <sup>104</sup>.

The application of thiol chemistry ensures the stability in the three-dimensional fold due to its ability to form disulphide bridges. The traditional coupling approaches involving thiol side groups of proteins are maleimides, disulphide- or vinyl sulphone-derivatized surfaces. Another type of antibody immobilization using thiol group is chemisorption (thiol-adsorption) which can be defined as the strong interaction between thiolated molecules and a metal surface. With thiols, the reaction is assumed to occur as an oxidative addition to gold with the release of hydrogen, whereas in the case of disulphides, a cleavage of the S-S bond takes place <sup>105</sup>.

#### **1.2.7.2        *Non-covalent approaches to immobilisation***

##### **❖ *Entrapment (encapsulation)***

The principle of this approach is based on the entrapment of the active component physically into a coating or film. Silicone rubber, starch, sol-gel, polyvinyl chloride, polyvinyl alcohol, and polyacrylamide are examples of films/matrices <sup>98</sup>.

Fang *et al.* were able to present a protocol for the contribution of sol-gel sensing and immunoassay to detect cortisol in human serum based on sol-gel encapsulation. Competitive immunoassay experiments were carried out using sol-gel thin films

prepared by combining tetramethyl orthosilicate (TMOS), DI water, HCl, and methanol. Afterwards, a mixture of monoclonal antibody to cortisol and sodium phosphate buffer solution was added to sol/methanol mixture. Clean glass coverslips were dip coated with the prepared thin films. Fluorescence was detected from the labeled cortisol and could be correlated with the concentration of unlabeled cortisol from serum <sup>106</sup>.

The benefit of entrapment immobilization is its suitability for labile molecules that may degrade or lose activity under harsh immobilization conditions. However, it is not popular in biosensor industry and restricted to research field only due to weak bonding between biomolecule and the transducer or matrix which means the biomolecule can be easily leached out leading to restriction of regeneration opportunity <sup>98</sup>.

#### ❖ *Cross-linking*

Cross-linking reagents including difluorodinitrobenzene, hexamethylene, bismaleimido-hexane, disuccinylsuccinate, dimethyl suberimidate, diisocyanate, and glutaraldehyde are used for cross-linking immobilization. This approach is considered as a combination of entrapment and covalent bonding. The role of cross-linkers is to polymerise the surface and consequently to attach the entrapped biomolecules to the surface as a result of the formation of intermolecular <sup>98</sup>. Shrivasta was able to introduce different bridge length linkers incorporated with horseradish peroxidase (HPR) enzyme, this was coupled to a carboxylic derivative of cortisol for immunoassay <sup>107</sup>.

#### ❖ *Adsorption*

Another useful active biomolecule immobilization method on the sensor surface is adsorption. This method depends on intermolecular forces including van der Waals, hydrophobic, hydrogen bond and ionic bonds that allow protein adsorption to various surfaces. Merits of this method lie in its simplicity, while the demerits include its

dependence on a variety of environmental conditions including temperature, ionic strength, and pH which makes the method unreproducible<sup>108</sup>. Leung *et al.* measured cortisol in plasma sample by applying adsorption technique to construct a quantitative plasma lateral flow assay, the linearity of the calibration curve was up to 1280 ng ml<sup>-1</sup> with  $R^2 = 0.9807$ <sup>109</sup>.

#### ❖ **Biological Binding (Matrix entrapment)**

Immobilization of biomolecules on sensor surface can be achieved by biological binding (bioaffinity) which offer an advantage in term of bond strength, flexibility, and specificity. One of the most widespread examples of this method is the use of the avidin-biotin complexes, which depends on attachments of the avidin-biotin complex on the surface *via* a strong non-covalent bond, this overcomes the harsh conditions required for many biological assays<sup>98</sup>. Although this system has the advantage of simplicity, it does suffer from certain limitations. Avidin is positively charged at neutral pH due to the high isoelectric point, therefore, nonspecifically binding to negatively charged molecules may occur. In addition, avidin is a glycoprotein and reacts via the carbohydrate moiety with molecules such as lectins<sup>110</sup>.

As mentioned previously, the antibody/antigen interaction with sensor surface is achieved in different ways; the covalent, cross-linked and affinity attachment are recommended for biomolecules orientation because of surface high resistance to temperature, pH, and ionic strength, also in terms of high stability and reproducibility. The entrapment and adsorption attachment mostly lead to unfavorable orientation and reduction or loss of the biomolecules mobility.

### **1.2.8 Detection**

Biosensors have been successfully used with wide range of transducers to recognize a physicochemical change caused by binding the complex with the biomolecules immobilized on the transducer. Coupling a detector to the biosensors is a crucial step, where most clinical diagnostic and environment monitoring require low power consumption, automation, high sensitivity and specificity of the target analyte. A range of transducers have been used to detect cortisol and cortisone in a variety of samples; these include electrochemical transducers which include current (amperometric) and potential (potentiometric). The second category is optical transducers which can be subdivided into label-free (surface plasmon resonance (SPR), thermal lens microscope (TLM), and wavelength-interrogated optical sensing (WIOS)) and labelled (absorbance, fluorescence, radioactive and chemiluminescence) <sup>111</sup>. Chemiluminescence and voltammetry are the transducers used in the current project due to their simplicity and sensitivity, a detailed description will be described in this section. The other types will be given a short review.

#### **1.2.8.1 Electrochemical detection**

Quantitative analysis is evaluated using the electrochemical detection which relies on the interaction between the electrode (probes) and chemical species that result in a change in electrical signals such as potential or current.

The electrochemical process began with a potential applied to an electrode surface immersed in a solution. The electrolytes are attracted towards the electrode surface forming an “electrical double layer”. As a result of this movement, a potential difference will occur (when two different phases or materials come in contact with each other a potential gradient is formed at the interfacial region). This means there will be electrons passing out through the external circuit seen as current <sup>112</sup>.

There are two types of process in electrochemical phenomenon: 1) electrolytic process where chemical reactions occur on the passage of an electrical current, 2) galvanic or voltaic process where electrical current is produced due to chemical reactions. The electron transfer between the electrodes and the electrolyte (sample) are based on the oxidation/reduction reaction occurring at the electrode surface. Normal electrochemical cells consist of a three electrodes configuration, a working electrode (WE) which gives the electrons to the sample and where the reaction occurs to determine the analyte concentration. The reference electrode (RE) with a known potential enables the working electrode potential to be detected. In order to complete the cycle, a counter electrode (CE) is minimizing the electrical current flowing through the reference <sup>111, 113</sup>.

Voltammetry has attracted attention as a technique to study the chemical reaction from a kinetic data point of view, especially cyclic voltammetry, which is the ideal method to get a rapid system informatics. In cyclic voltammetry (CV); oxidation (scanning up) and reduction (scanning down) reactions which take place at the working electrode surface on varying the applied potential can be monitored as a measurable current. The current change on applying potential can be plotted with current (vertical axis) versus potential (horizontal axis) to give a voltammogram <sup>114, 115</sup>, as shown in figure 1.14.

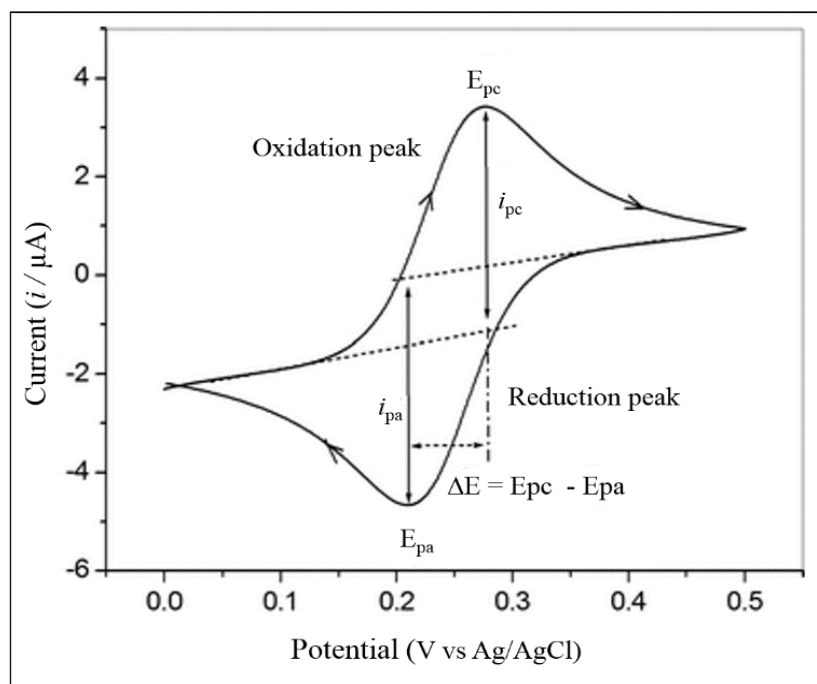


**Figure 1.14.** A typical cyclic voltammogram, where  $E_{pc}$  = peak cathodic potential;  $i_{pc}$  = peak cathodic current;  $E_{pa}$  = peak anodic potential, and  $i_{pa}$  = peak anodic current <sup>116</sup>.

Cyclic voltammetry is rarely used for quantitative determination because it lacks the ability to distinguish between faradic current (related to electron transfer) and capacitance current (related to charging and discharging of the electrochemical double layer). Therefore, another technique has attracted much attention which is square wave voltammetry analysis (SWV). This method gives increased sensitivity which can be explained by the capability of faradic current and capacitance current differentiation. The current obtained in SWV is the result of the capacitance current being subtracted from the overall current measured, including the faradic current from the redox reaction, this leads to improved sensitivity. Another reason for preferring SWV on CV is the oxygen effect where SWV is unaffected due to the pulsing of the technique. Whereas, CV measurement is effected by the oxygen which has an effect on the analysis. An additional advantage of the SWV is the speed (just a few milliseconds) which allows experiments to be performed in milliseconds <sup>116, 117</sup>.

The SWV technique involves the addition of a pulse of constant amplitude at the end of each potential step. The current is measured twice, at a point just before the pulse and at the end of the pulse, the difference is recorded as a net current. According to the followed equation:

$$\Delta i = I_F - I_R \dots\dots\dots \text{Equation 1.1}$$

Where  $I_F$  is the forward current and  $I_R$  is the reversed current.

Since the differential current is measured during this type of experiments, regular waves are not observed and instead peaks superimposed on a staircase waveform will be obtained to form square wave voltammetry <sup>112</sup> as can be seen in figure 1.15.

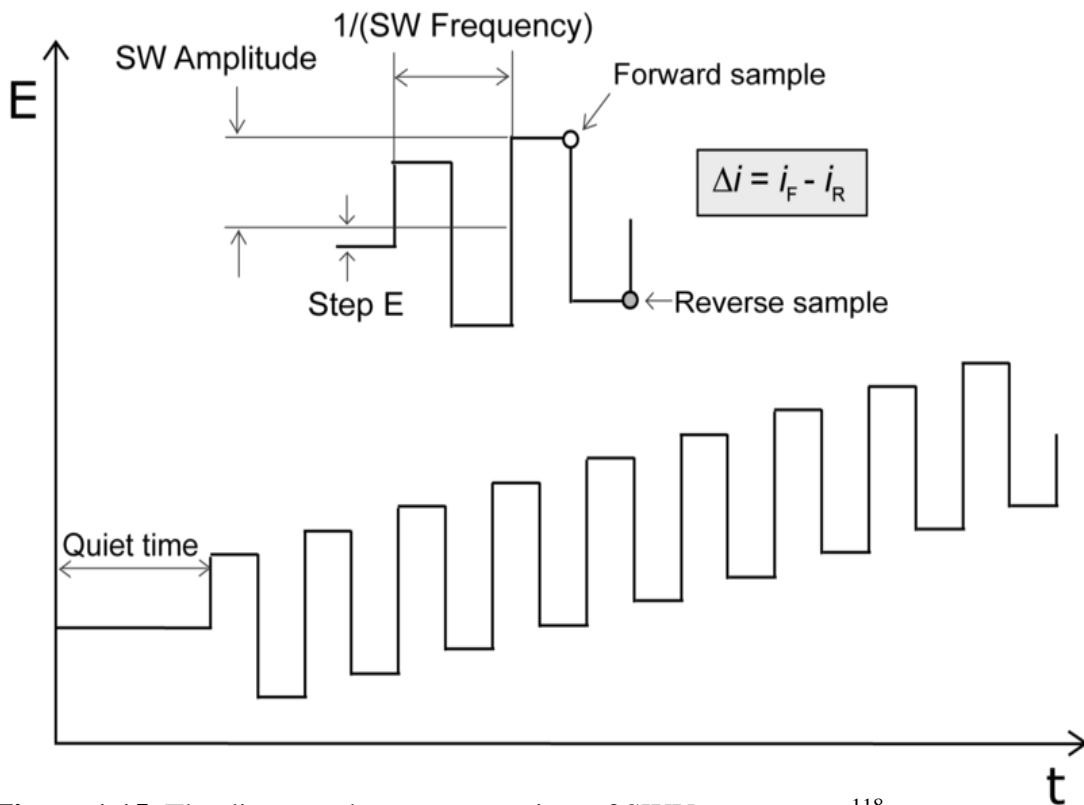


**Figure 1.15.** The diagram shows an overview of SWV parameters <sup>118</sup>.

Extensive academic proof-of-concept studies have demonstrated the use of electrochemical detection in cortisol and cortisone immunoassay biosensors <sup>119-129</sup>, in



principle it is based on the measuring the alteration in the electrical merits of a conductive substrate as a result of analyte adsorption on a surface functionalized with antibody sensitive to the analyte. At the electrode, the electrical change is assigned to the concentration variation of the electro active redox species <sup>130</sup>.

In general, electrochemical method capital cost of batch fabrication is low, and owns the ability for miniaturization without loss of performance has elevated this method up to speed with diverse immunosensing. However, inherited limitation of sensitivity and selectivity figures incorporated with electrochemical detection has slightly restricted their use <sup>113, 131</sup>.

#### **1.2.8.2 Optical detection**

##### **❖ Label-free optical biosensor**

Due to the ubiquity of optical instruments in the laboratories, optical techniques provided a solid base for cortisol and cortisone detection. Both label-free and labelled optical sensors are used. The label-free biosensors include surface plasmon resonance (SPR) technology depends on the measurement of the refractive index (RI) changes near the biosensor surface as a response to biomolecules interactions <sup>132</sup>. Stevens *et al.* described a portable SPR biosensor for cortisol estimation in saliva. A competition assay generated from cortisol-specific monoclonal antibodies were tested with a 6-channel SPR biosensor. A detection limit of 0.36 ng ml<sup>-1</sup> was obtained which is sufficiently sensitive for clinical tests, but because the SPR chip is expensive, it is not favourable as a commercial concept <sup>133</sup>. Thermal lens microscope (TLM), is highly recommended for quantization of ultra-low trace amount of the analyte in small sample volumes. In this method, refractive index change due to heat released from sample molecules interaction is measured <sup>134</sup>. In wavelength interrogated optical sensing

(WIOS) refractive index changes are measured by scanning the resonance conditions <sup>135</sup>.

Spectrophotometric techniques involve the detection of analyte concentrations by measuring the absorbance of a specific wavelength of incident light. A Conventional UV–visible spectrophotometer coupled with microfluidic chip suffers from the reduction in sample volumes which decrease the optical path length through the sample and impact on the sensitivity according to Beer-Lambert law. This is one of the disadvantages of this technique. In addition, the need for an external light source raises the cost <sup>111</sup>. Despite these disadvantages, spectroscopic detectors incorporated with different techniques were used for stress hormone detection due to their availability <sup>136, 137</sup>.

The simplicity driving from label-free detection methods enables real-time monitoring of reactions. At the same time, the instrumentation associated with the label-free detection is expensive and prone to interference including nonspecific binding of biomolecules to the sensor surface and changes in measurement conditions <sup>138</sup>.

#### ❖ *Labelled optical biosensors*

Labelled optical sensors are introduced to overcome the drawbacks of the low sensitivity in addition to expensive label-free detection methods; these methods include radiolabels, fluorescence, and chemiluminescence labels. The latter will be addressed in more details.

#### **1. Radioactive**

Stress hormone was determined using radioimmunoassay (RIA) as a detection method <sup>139, 140</sup>. Usually, in this method, an antigen is labelled with gamma-radioactive isotopes such as <sup>125</sup>I, attached to tyrosine and a competitive immunoassay is then used.

The radioactivity of the antigen-antibody complex can then be measured using gamma counter to determine the amount of radiolabelled antigen bound to the antibody and subsequently the concentration of antigen in sample <sup>90, 141</sup>.

This method is considered fast, sensitive and specific. The method is not popular due to the radio label, which requires specially trained persons, special instruments, and labs need to have a license to handle these materials. Also, another issue is related to storage and disposal of radioactive material where special arrangements are needed that raises the cost <sup>90, 141</sup>.

## 2. Fluorescence

Fluorescence is a form of luminescence that emitted light after light absorbance or other electromagnetic radiation by a substrate. This can be explained using Jablonski diagram as shown in figure 1.16.

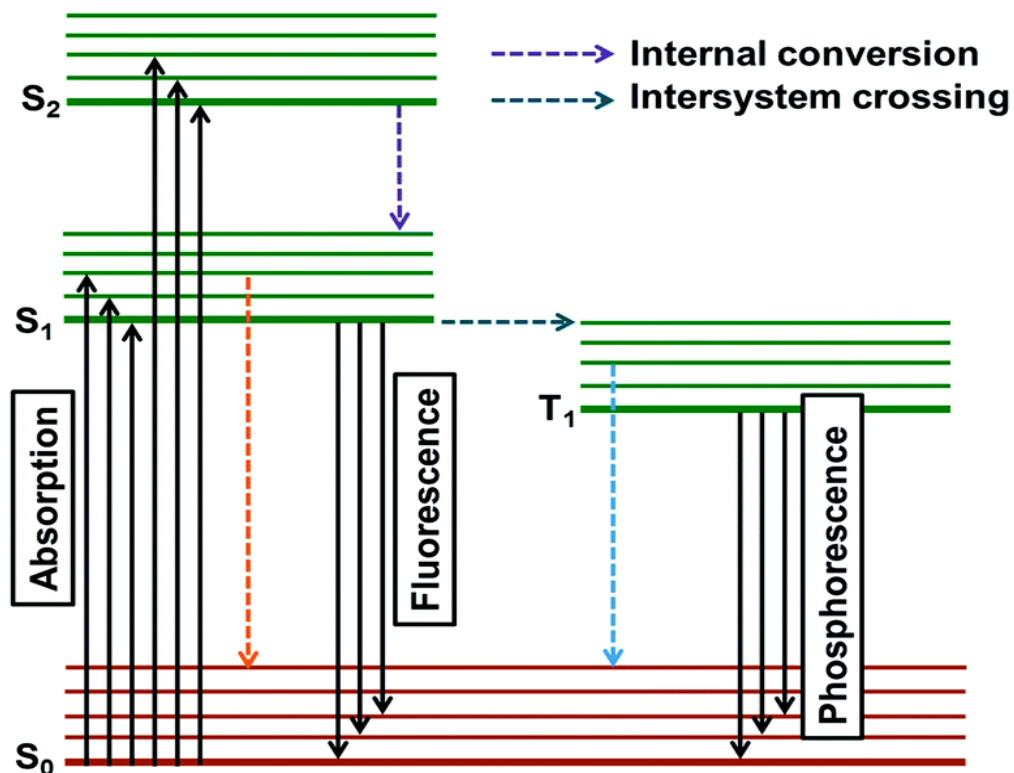


**Figure 1.16.** Jablonski diagram shows the luminescence process, where  $S_0$  represents the ground state,  $S_1$  first excited state,  $S_2$  second excited state and  $T_1$  triple state <sup>142</sup>.

As can be seen from figure 1.16 the absorption of ultraviolet or visible light (photon) by species results in an electron excitation from the ground state to excited single state. At that point, the electron can return to the ground state ( $S_0$ ) either from the single excited state ( $S_1$ ) emitting light through fluorescence or by undergoing intersystem crossing to a triple excited state ( $T_1$ ). At that point, the electron relaxes back to the ground state in a process called phosphorescence with light emission.

Fluorescence is used in immunoassays where fluorophores or fluorescent dye are used to label the antibody or antigen. For example, the sandwich fluorescence immunoassay includes the following steps: the sample containing the target protein initially binds to captured protein immobilised on the solid surface. The next step is washing the unspecifically bound molecules by using a wash buffer. This was followed by the exposure of the captured target protein to a labelled antibody with a washing step to flush out the excess of labelled antibody. The complex is illuminated by specific wavelength to produce fluorescence intensity related to the target molecules in sample <sup>143</sup>.

Van Lenten *et al.* studied daily cortisol variations in relation to sleep duration in humans using solid phase time-resolved fluorescence immunoassay to measure cortisol samples <sup>144</sup>. Due to the high sensitivity and high selectivity of fluorescence detection for immunoassays, it is widely used. Despite this advantage, fluorescence suffers from background signal resulting from autofluorescence (biological structures naturally absorb light and emitted light) of sample constituents such as protein containing aromatic acids, flavins, NAD(P)H and lipopigments <sup>145</sup>. The other disadvantage is related to expensive fluorescent dye accompanied by limited shelf life <sup>111</sup>.

### 1.3 Chemiluminescence (CL)

There have been numerous investigations of chemiluminescence as an analytical tool for immunoassay detection for pharmaceutical analysis<sup>146</sup>, forensic identification<sup>147</sup>, environmental monitoring<sup>148</sup>, food safety application<sup>149</sup> and clinical diagnosis<sup>150</sup>. In chemiluminescence immunoassays, the light used to determine the presence or concentration of an analyte is generated from a chemical reaction without the need for an external light source which can be an advantage. Furthermore, problems with photoluminescence such as source instability and light scattering are omitted as the excitation is not required for sample radiation. A high background resulting from unselective photoexcitation is omitted which has the advantage of high sensitivity due to the low background noise. Additional advantages of chemiluminescence include low reagent consumption, high stability of several reagents, the use of non-toxic reagents, light fast emission, short incubation time due to high sensitivity, and a large linear response (up to six digit magnitude)<sup>151</sup>.

A chemical reaction which produces a sufficient amount of energy (300 KJ mole<sup>-1</sup> for blue light and 150 KJ mole<sup>-1</sup> for red light emission) is needed for the promotion of an electron to an excited state since the excitation occurs from the chemiluminescence reaction itself not from light as in fluorescence. Therefore, the reaction must be sufficiently exothermic for this to happen<sup>151, 152</sup>.

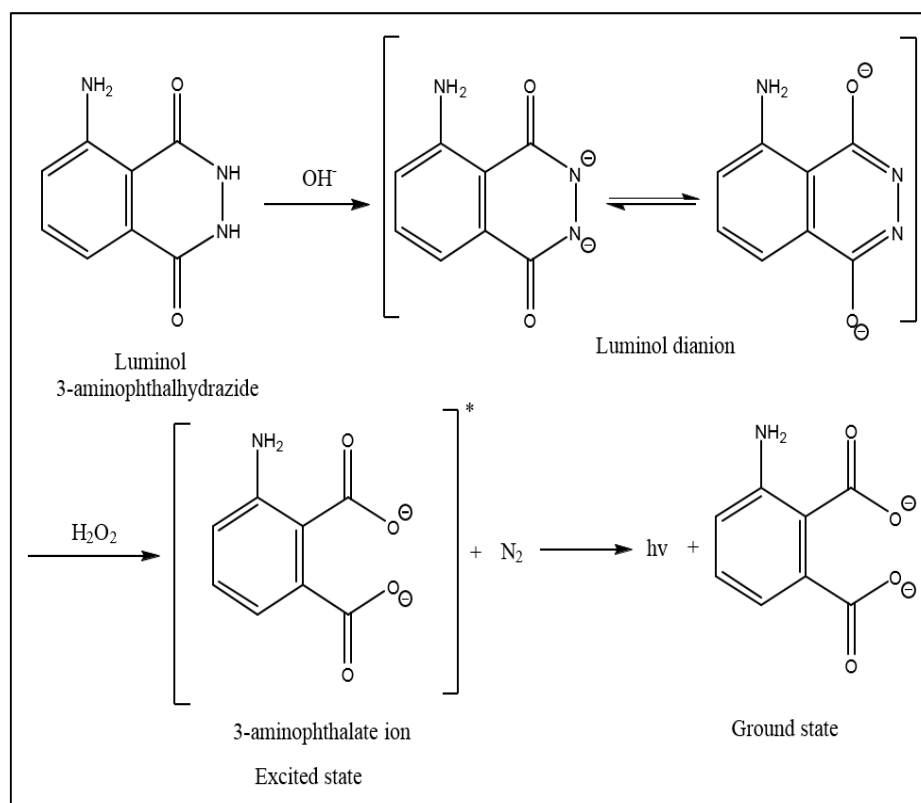
The quantum efficiency (quantum yield  $\phi_{cl}$ ) is well characterist for chemiluminescence reactions and represents the fraction of molecules that emit light intensity on return to the ground state, it is obtained from three ratios as given in the equation below:

$$\phi_{cl} = \phi_c \times \phi_e \times \phi_f \dots\dots\dots \text{Equation 1.2}$$

Where  $\phi_c$  is the fraction of reacting molecules giving excitable molecules and accounts for the yield of the chemical reaction,  $\phi_e$  reflects the fraction of these molecules that enter the excited state and  $\phi_f$  is the fraction of these molecules that return to the ground state by emitting a photon <sup>151</sup>.

### 1.3.1 *Chemiluminescence reagents*

For the development of a chemiluminescence immunoassay, reagents such as luminol, isoluminol (and its derivatives), hydrogen peroxide and acridinium dyes are required for chemiluminescence reaction. Luminol (3-aminophthalhydrazide) as seen in figure 1.17, is well documented as a chemiluminescent compound since its discovery in 1928 by Albrecht. The most common oxidizing reagent used with luminol is hydrogen peroxide which increases the luminescent intensity of luminol, it exhibits chemiluminescence at  $\lambda_{max}$  425 nm in alkaline solution. Proteins denature in strong alkaline conditions, therefore, peroxidases are chosen because luminol can be oxidized in mild condition. Luminol is usually used as it is widely available, is cost-effective and accepted to study biological systems <sup>153</sup>. Figure 1.17 explains the mechanism for the luminol-H<sub>2</sub>O<sub>2</sub> reaction in alkaline solution.



**1.17.** Mechanism for the chemiluminescent reaction of luminol with hydrogen peroxide in a basic aqueous environment which emits light at  $\lambda_{\text{max}} = 425 \text{ nm}^{154}$ .

Under basic conditions, luminol loses protons from the nitrogen to form the resonance luminol dianion where the negative charge moves onto the carbonyl oxygen. Hydrogen peroxide in the presence of cooxidant such as HPR oxidase the luminol dianion into a 3-aminophthalate ion with the loss of nitrogen in the excited state. As a final step, the 3-aminophthalate return to the ground state and emitting the extra energy as a photon of light <sup>155</sup>.

The chemiluminescence reaction can be enhanced in the presence of a catalyst, such as enzymes i.e alkaline phosphatase <sup>156</sup>,  $\beta$ -D-galactosidase <sup>157</sup> and horseradish peroxidase (HRP) <sup>158</sup>. Also metals such as cobalt <sup>159</sup>, copper <sup>160</sup>, iron <sup>161</sup>, and manganese <sup>162</sup>. The intensity of light emitted is greater compared to that from traditional luminol-hydrogen peroxide reaction <sup>163</sup>.

### 1.3.2 Chemiluminescence detection

Chemiluminescence signals can be analysed and detected by different methods; photomultiplier tubes and charge – coupled devices (CCD) are the main methods used.

#### ❖ *Photomultiplier tubes*

Photomultiplier tubes are extensively used in chemiluminescence detection due to their high sensitivity, in terms of detecting a small number of photons. The photon interacts with the photocathode, then a photoelectron is released due to the photoelectric effect. The photoelectrons are accelerated and amplified through a series of dynodes where they are multiplied by means of secondary electron emission. This process is repeated at each dynode until it reaches finally to the anode to be collected. The generated current through the system is measured at the end. If more than one label is to be detected the photomultiplier tubes need to be coupled with a monochromator and individual analyses for each photon emitted by analyte at different wavelengths must be carried out which complicates the detection system <sup>152</sup> (figure 1.18).

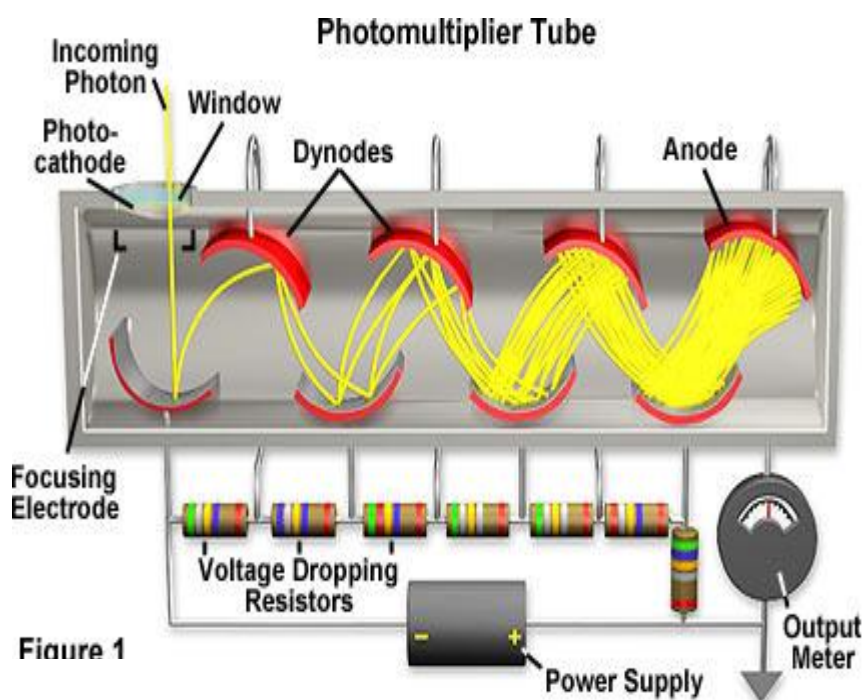


**Figure 1.18.** Mechanism of Photomultiplier tubes detector <sup>164</sup>.



❖ *Charge-coupled device (CCD)*

The CCD device overcomes the limitation of multiple analyte analysis that the photomultiplier device suffers from; by the integration of the device into a camera to analyse the images that are detected. This allows for spatial detection of immobilized antibodies. Figure 1.19 shows the schematic of CCD operation, a rectangular array of individual pixels, which is built into a camera absorb photons to create photoelectrons, these are stored and integrated into the pixel. Afterward, the charge is transferred from each row to the lowest row then to the readout area. The charge is then converted into a voltage using the charge to voltage convertor (CVC) to give an image which can then be analyzed. In the end, the pixel is reset for the next image. The CCD address the potential understanding of specific antibody by detecting the light signal even with the presences of different antibodies in multiple application which cannot be achieved with photomultiplier device <sup>152</sup>.

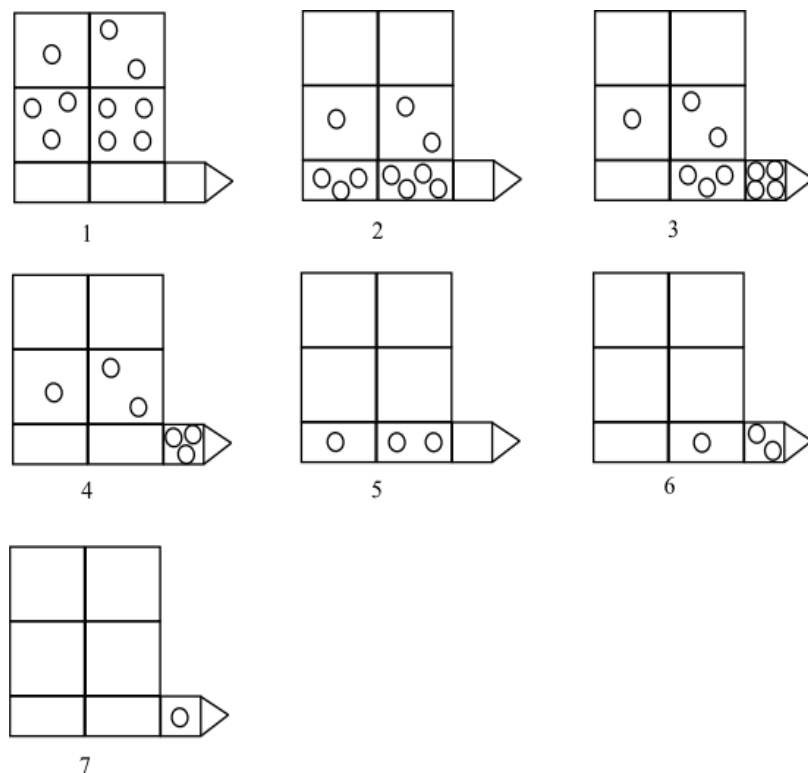


**Figure 1.19.** Represent the steps for charge-coupled device (CCD) operation <sup>152</sup>.

According to the chemiluminescence advantages from simplicity and sensitivity mentioned earlier in this section, chemiluminescence equipped with CCD device was selected to detect the concentration of cortisol and cortisone in Zebrafish and saliva samples in this thesis.

#### **1.4 Microfluidics**

Microfluidics can be best defined as "the science and technology of systems that process or manipulate small ( $10^{-9}$  to  $10^{-18}$  liters) amount of fluid, using channels with dimensions of tens to hundreds of micrometers". This method can be used to control the concentration of molecules in space and time <sup>165</sup>. The microfluidics concepts go back to 1950s, originating in the inkjet printer manufacturing. In 1970 a miniaturized gas chromatograph system was demonstrated and this has been followed by a huge rise in the number of publications in this field <sup>97</sup>. Microfluidic systems have been successfully used in the diverse area including chemistry <sup>166</sup>, medicine <sup>167</sup>, engineering <sup>168</sup>, forensics <sup>169</sup> and bioanalytical researches <sup>170</sup>, for example for DNA separation and analysis<sup>171</sup>, cell separation<sup>172</sup> and manipulation<sup>173</sup>, enzyme kinetic studies <sup>174</sup>, drug discovery <sup>175</sup>, and immunoassay <sup>176</sup>, etc.

This diversity is related to major advantages of microfluidic systems: (i) the use of small sample and reagent volumes alongside the easier integration of multiple processes on a single device (ii) reduction of chemical waste and contamination (iii) construction of microfluidic device is relatively inexpensive and (v) improvement in sensitivity and resolution, such characteristics make this microfluidic system appropriate for dealing with limited or degraded samples. Finally, it can be said that due to its miniaturized design, microfluidic systems can be considered to be portable, compact and easy to use <sup>177, 178</sup> as shown in figure 1.20.

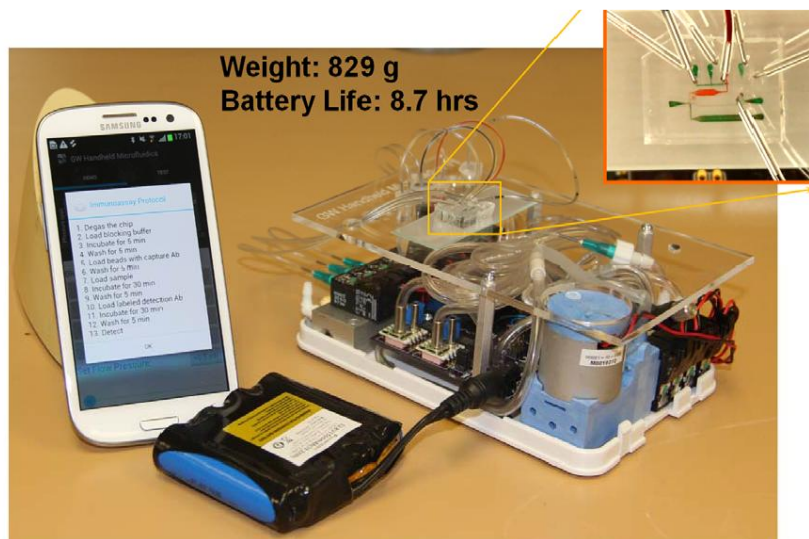


**Figure 1.20.** Lab-on-chip handheld microfluidic chip device as an example controller with smartphone app <sup>179</sup>.

#### **1.4.1 The prospects of microfluidic immunosensing device**

Due to the high selectivity and low sample consumption, immunoassays have been widely used in different applications. However, this technique suffers from some drawbacks involving multi-steps procedures (washing, mixing, and incubation), and the fact that they are time-consuming and relatively expensive. Therefore, researchers seek an analytical improvement, resulting in the automated and miniaturized microfluidic platform combination with the immunoassay to fulfil the important criteria of a simple, cheap, automated, and selective system <sup>84</sup>. The following section will provide the basic requirements and principles of this promising technology.

##### **1.4.1.1 Materials**

A key factor in microfluidic immunosensing chip fabrication is the material substrate that is used. Various substrate materials have been reported, such as silicon <sup>180</sup>, glass <sup>181</sup>, and polymers <sup>182</sup>. Silicon is the most common surface due to extensive surface chemistry studies plus its high-temperature resistance and good thermal conductivity. However, silicon suffers from some disadvantages such as it is not optically transparent,

electrically conductive and it is expensive compared to other materials. On the other hand, glass has good optical transparency, and is not electrically conductive and is chemically resistant, which makes glass substrate good for practical application in a commercial immunoassay. Nonetheless, handling with glass is slightly complicated due to the fact that glass is fragile which add extra attention and it is less expensive than silicon but more expensive than other materials <sup>183</sup>. Polymers are popular for bioanalysis with desirable characteristics such as simple fabrication, biocompatibility and reduced cost <sup>84</sup>. Suitable polymers include polymethylmethacrylate (PMMA) <sup>184</sup>, polydimethylsulfoxide (PDMS) <sup>185</sup> and polystyrene(PS) <sup>186</sup>, etc. Nevertheless, polymers have some disadvantages such as limited temperature range, and lower optical transparency compared to glass <sup>187</sup>.

Recently different modified electrodes have been used in microfluidic systems, including glassy carbon, gold (Au), carbon paste, screen-printed electrode and ITO electrode where they act as a support material for reagent immobilization, miniaturizing the microfluidic immunosensing device. The antibody or antigen localized immobilization on an electrode surface implementing an electrochemical method <sup>117</sup>.

The antibody-antigen interaction with the material surface is achieved by the modification of the surface or the antibody-antigen modification using the covalent and non-covalent binding as described in section 1.2.7.

#### ***1.4.1.2 Sample/ Reagent transport***

Microfluidic immunoassays are directly affected by the performance of the fluid transport system. Therefore the fluid transfer plays an important role inside a microchannel. This can be categorized into three main fluid handling forces:

1. Electric forces where the fluid transport system depends on flow generated by the electrophoretic and electroosmotic interaction of ionic species with the applied electrical field, whereas electrowetting force depends on the manipulation of the fluid drop in the presence of program voltage applied to an electrode array.
2. Pressure-driven flow, this can be achieved by the aid of a syringe pump or by applying vacuum at the outlet of the channel in order that the reagents can be delivered inside the microfluidic immunoassay system.
3. Passive forces, this force does not need an external power source that transport fluid. Mainly gravity and capillary forces have been employed to drive fluid within microchannel <sup>131</sup>.

#### ***1.4.1.3 Reagents mixing***

In microfluidic channels, the fluid flow through the channel must be considered. The flow of a fluid through a microfluidic channel is characterized by the Reynolds number ( $Re$ ), defined as

$$Re = \frac{\rho U_0 L_0}{\eta} \dots\dots\dots \text{Equation 1.3}$$

Where  $\rho$  is the density of the fluid ( $\text{kg m}^{-3}$ ),  $U_0$  is the velocity of the flow ( $\text{m s}^{-1}$ ),  $L_0$  is the diameter of channel (m), and  $\eta$  is the viscosity ( $\text{N S m}^{-2}$ ). Where there is a Reynolds number of  $< 2000$  the flow is seen as laminar where mixing then only occurs via viscous forces of the two fluid, if the Reynolds number is greater than 3000 then the flow is seen as turbulent flow where mixing relies on diffusion of the reagent across the channel, if the Reynolds number is between 2000 and 3000 it is termed to be a transition from laminar to turbulent flow <sup>117, 188</sup>. As shown in figure 1.21.

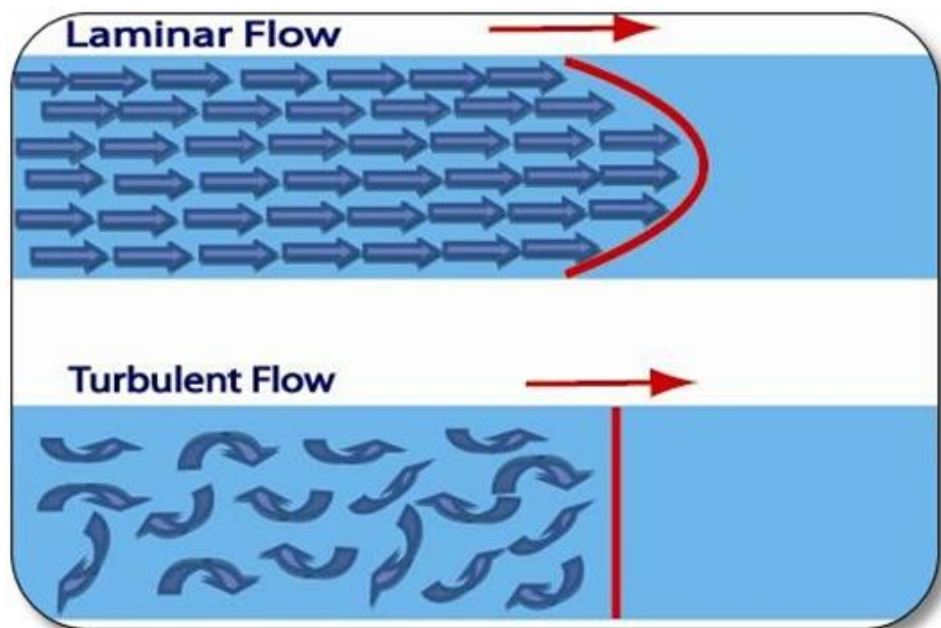


**Figure 1.21.** A schematic of laminar flow where the smooth flow of fluid occurs in parallel layers with no breakage between them and turbulent flow where rough and random flow occurs.

Coupling a detector to microfluidic immunosensing devices system is an important step, where it is required low power consumption, automation, and high sensitivity and specificity to the target analyte detection. A variety of detection technologies has been demonstrated, including optical and electrochemical technologies. This was described in details in section 1.2.8.

## **1.4.2 Classification**

### **1.4.2.1 Closed microfluidics**

Over the past two-decades, the closed microfluidic concept has been growing due to minimization and integration of chemical and physical processes such as fluid transport, mixing, valving, separation, and detection. In order to perform the previous process, the closed microfluidic device consists of microfluidic unit operations including valves, pumps, actuators, switches, sensors, dispensers, mixers, filters, separators, heaters, etc.

A closed microfluidic system composed of glass, silicon or polymer-based material consists of tiny microchannels as networks, allowing fluid to flow <sup>189, 190</sup>.

Despite the advantages offered by the closed microfluidic system, the device development is hindered by the need of mechanical components which add complexity to the device. In addition, the fabrication process using a material such as silicon and glass requires a complex process such as chemical etching and thermal bonding which takes time and cost, while the polymer fabrication using hot embossing suffer from the bubbles trapped between the stamp and the substrate which requires a specialized vacuum and this can reduce the reproducibility <sup>191, 192</sup>. Air bubble impacts significantly on the fluid flow behaviour within the microfluidic system which poses a challenge for the microfluidic platform operation <sup>193</sup>. Handling biological samples such as blood through the microfluidic system adds more complexity to the system compared to pure water handling due to blockage issues <sup>194</sup>. For these reasons closed microfluidic devices are not favoured from a commercial manufacturing perspective.

## **1.5 Open microfluidics**

Since closed microfluidic systems were developed research into a related but distinct technology, open microfluidic systems have been carried out, primarily to overcome the inherited problems related to the closed microfluidic system. Open microfluidic system, have open boundaries where the biological, environmental, forensic samples, etc. should be able to interact with microfluidics in the open space. The fluid moves mainly due to capillary forces <sup>195</sup>.

The advantage of this system lies in the simplicity of open microfluidic chip architecture design, resulting in lower fabrication costs, and this approach overcomes bubble trapping. Also, the easy accessibility of reagents and samples addition and optical

observations are facilitated. All these aspects have emerged open microfluidic system as a versatile approach for the development of an integrated microfluidic device for the lab-on-chip application<sup>196, 197</sup>. Open microfluidic include droplet, and continuous open microfluidic systems that will be explained in the following section:

❖ *Droplet microfluidics*

Droplet microfluidic system includes both electrowetting-based droplet (well known as a digital droplet or discrete droplet) and continuous-flow emulsion-based droplet microfluidics. In digital microfluidics, the discrete droplet for both reagents and sample are manipulated by applying an electrical potential to an array of the electrode on an open surface. This technique is driven by surface tension or so-called electrowetting or electrowetting-on-dielectric (EWOD). While for the other technique droplet is formed as a result of an emulsion created using two immiscible liquids including gas/liquid and liquid/liquid systems. For the droplet generation control, various techniques are used such as dielectrophoresis and channel geometry (T-junction)<sup>167, 198</sup>. As shown in figure1.22.

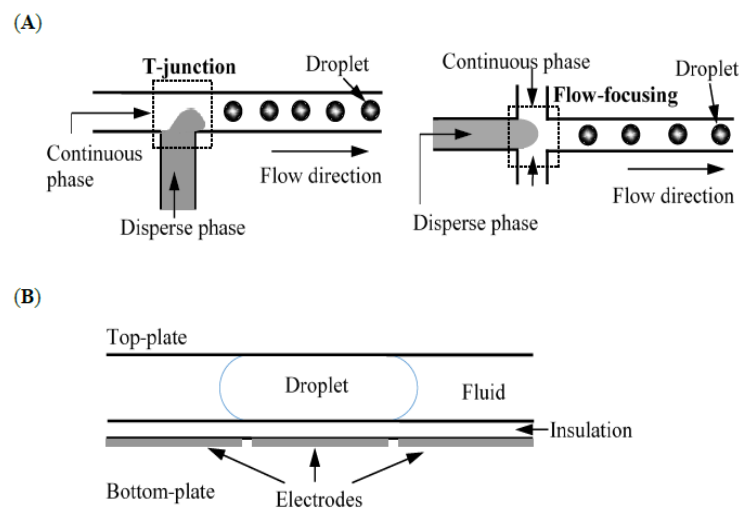


**Figure 1.22.** Two droplet open microfluidic configurations (A) continuous flow emulsion-based droplet (from T-junction and flow focusing) (B) electrowetting-based droplet<sup>198</sup>.



Despite this field has been a prosperous research field for biomarkers analysis, but has many challenges to overcome, reaching to an easy-to-use and cost-effective devices that can be commercially and routinely used by the scientist as well as the doctors, farmers, etc., such as analyse of droplets content; where the dominant approach for the analysis is fluorescence technique because it is able to detect a few molecules in each droplet in a high-throughput manner. This restricts making benefit from other techniques that offer more chemical information and comparable sensitivity as fluorescence. Additionally, the generation of droplets is mainly driven by steady state methods which cannot adjust to make droplet streams with various contents <sup>199</sup>.

#### ❖ *Continuous flow open microfluidics*

A new promising generation of microfluidics has recently been investigated. The continuous open microfluidic technique includes devices that are designed using wettability pattern consisting of hydrophilic patterns on a hydrophobic substrate or conversely, by applying a hydrophobic pattern on a hydrophilic substrate. Once the surface is patterned, the aqueous sample flow will be along the hydrophilic channel fabricated on a hydrophobic substrate by capillary forces, provided the pressure is maintained below a critical value (thus this is called surface-directed fluid flow), since the fluid (aqueous solution) will only wet the hydrophilic patterns as the hydrophobic region acts as “curbs” <sup>200</sup>.

Several parameters are involved in fluid flow on surface-patterned channels: the critical pressure that the virtual walls can withstand; the critical width of the hydrophilic pathways that can support spontaneous fluid flow; the smallest width of fluid streams required under external pressure without entering the hydrophobic regions; the critical radius of curvature of turns that can be introduced into hydrophilic pathway without

fluid crossing the hydrophilic-hydrophobic boundary and the minimum distance for two fluid streams to remain separated under the maximum pressure <sup>201</sup>.

One of the most famous examples of hydrophobic/hydrophilic surfaces used for building the microfluidic device is paper as so-called “paper-based microfluidic” or “lab on paper”. The fundamental principle that paper microfluidics lies on is the paper basic material which is cellulose, it is considered naturally hydrophilic and allows penetration of fluid within its fiber matrix <sup>202</sup>. Patterns are fabricated on the paper sheet aiming to create micron-scale capillary channels on paper which enable fluid to be confined inside the patterns and therefore fluid flow can be guided in a controlled manner.

The ubiquitous and cheap material of paper, comparability with a wide range of chemical/medical/biochemical applications and the omitting of external forces to enable fluid flow and depending on capillary forces, made paper becomes an attractive substrate for building microfluidic devices. However, this material has its limitation related to sample retention. Once the fluid is transport through the patterns there is a risk of low efficiency of sample delivery due to evaporation, where the total volume which reaches the detection zone is less than 50% of the delivered sample. Also, the limit of detection is high for colorimetric method incorporated into the paper device, this limit the detection of very low concentration <sup>203</sup>. Therefore, different materials have been investigated to construct microfluidic devices as will be explained in section 1.5.3.

### **1.5.1 Basic principles of open microfluidics**

To understand the fluid flow in all microfluidic devices, it is important to explain the parameters and principles of the substrate surface from a physics point of view. This is particularly important in open microfluidics.

### ***1.5.1.1 Surface wettability***

Wetting is the ability of fluid droplet to maintain contact with a surface<sup>204</sup>. The balance between adhesive and cohesive forces can be used to determine the degree of wetting (wettability). The fluid drop spreading across the surface is driven by the adhesive forces between the fluid and solid. Whereas, the cohesive forces within the fluid act to preserve the spherical shape of the drops thus reducing its contact with the solid surface. This phenomenon is applied in many areas as an example in self-cleaning textile, anti-icing / anti-fogging glass, corrosion control, coatings/painting, printing ink, dyeing, microfluidics, cosmetics/healthcare, agrochemicals, petrochemicals and medical devices, etc<sup>205</sup>. To understand the surface wetting properties, two crucial factors: surface chemistry and topography (roughness and smoothness) of the surface will be discussed in detailed.

Molecules in solid have balanced interactions in all directions, as a result, it remains in equilibrium. This is because of being closely packed to achieve minimum repulsion and maximum attraction. In a fluid, molecules at the surface are attracted inwards due to the lack of neighbouring molecules above them. This leads to surface tension development. As a result, fluid drops tend to have a sphere shape to minimize its surface free energy (sphere consider as the smallest surface area)<sup>206, 207</sup>.

To determine the fluid footprint on a solid surface and whether the fluid droplets rest on the solid surface or pull out into a film, three interfacial fluid-solid-vapour forces must be considered. The balance between these three interfacial forces can be measured by the contact angle ( $\theta$ ). The contact angle of fluid droplet at a three phase point is used to measure the degree of wetting. The droplet angle between the solid-fluid interface and a tangent to the fluid surface drawn to the boundary of the three phase where the fluid, solid and vapour meet is the contact angle of a fluid droplet on the solid surface.

If the contact angle of the water drop is less than 90 °, the surface is classified as hydrophilic. If the contact angle is 0°, the surface is called a super hydrophilic surface. Surfaces on which a water droplet has a contact angle bigger than 90°, but lower than 150°, are called hydrophobic. The superhydrophobic surface is extremely water repellent; a water droplet shows an apparent contact angle higher than 150° and can easily move around on such surfaces even if very small forces are applied<sup>206</sup>. Wetting of different types of surfaces is illustrated in figure 1.23.

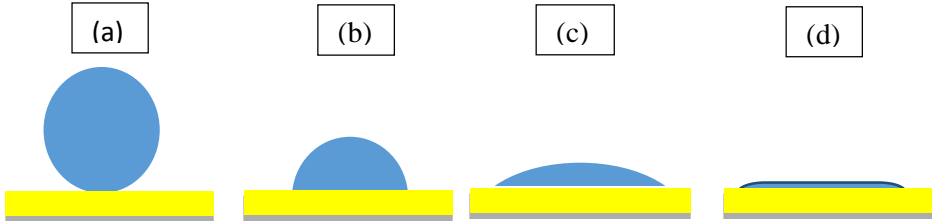


**Figure 1.23.** Wetting conduct of a droplet on various solid surfaces. (a) superhydrophobic surfaces, (b) hydrophobic surfaces, (c) hydrophilic surfaces, and (d) superhydrophilic surfaces.

The Young’s equation shown below describes the force balance at the contact line between the three interfaces (fluid-solid-vapour) in an ideal flat surface as in figure 1.24.

$$\gamma_{LV} \cos\theta = \gamma_{sv} - \gamma_{sl} \dots\dots\dots \text{Equation 1.4}$$

Where  $\gamma_{LV}$  is the surface tension between the fluid and vapour,  $\theta$  is the contact angle (CA),  $\gamma_{sv}$  is the surface tension between the solid and vapour and  $\gamma_{sl}$  is the surface tension between the solid and fluid. This equation is applied for flat and smooth surfaces<sup>208</sup>.

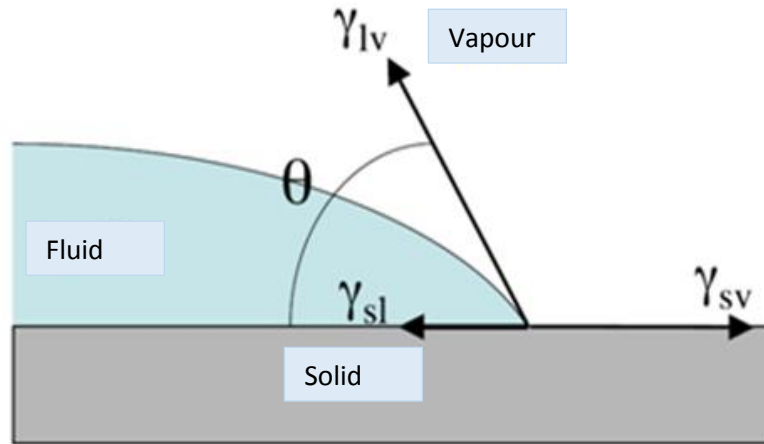


**Figure 1.24.** Diagram showing the forces in the three phases (solid, fluid, vapour) contact lines of a fluid drop on a perfect solid surface in the air.

For rough surfaces, the Wenzel and Cassie-Baxter equations are used for describing the contact angle. The Wenzel model is used when the fluid is in contact with the rough solid surface at every point of the wet area, the Cassie-Baxter is only valid when the air is trapped at some points between the surface and the fluid. Figure 1.25 illustrates both Wenzel and Cassie-Baxter models while equation 1.5 and 1.6 give the contact angle for both models <sup>204, 209</sup>.

$$\cos\theta_e = r \cos\theta_s \dots\dots\dots \text{Equation 1.5}$$

Where  $r$  is the roughness factor,  $\theta_e$  is the effective contact angle,  $\theta_s$  is the static contact angle.

$$\cos\theta_e = \lambda \cos\theta_{s1} + (1-\lambda) \cos\theta_{s2} \dots\dots\dots \text{Equation 1.6}$$

Where  $\theta_{s1}$ ,  $\theta_{s2}$  are the static contact angles and surface fraction  $\lambda$ ,  $1-\lambda$  of the component surface.

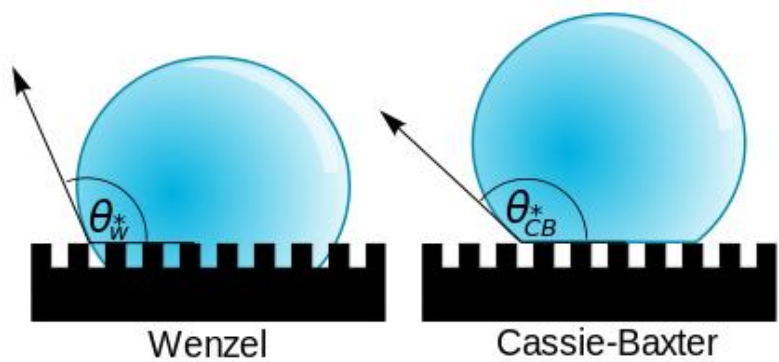


**Figure 1.25.** The Wenzel and Cassie-Baxter type of wetting of a rough solid surface. In the Wenzel model, the fluid fully wets the grooves of the rough surface. In the Cassie-Baxter model, the droplets sit on the solid surface without penetrating the solid surface grooves.

#### ***1.5.1.2 Superhydrophobic surface***

Superhydrophobic surfaces have numerous profitable applications as these surfaces can be transferred to commercial products because of their self-cleaning, anti-sticking and anti-contamination properties. This remarkable phenomenon was first observed from natural plants self-cleaning after a simple rain shower as the natural environment get contaminated or polluted, also it is a self-defense against pathogenic organisms <sup>210</sup>. A famous example of natural superhydrophobic surfaces is lotus leaf which has a water contact angle of  $161 \pm 2.7^\circ$ , this is attributed to epicuticular wax secreted by the lotus leaf itself forming a hierarchical micro- and nano-structure, the combination of roughness and wax contributed to the superhydrophobicity of this surface <sup>211</sup>. In addition to a lotus leaf, there are various natural surfaces that present the superhydrophobic surfaces from the plant kingdom including red rose petal, scallion, and garlic, etc. <sup>206</sup>. Examples of superhydrophobic surfaces are presented also in animals such as water strider legs, cicada orin's wings and butterflies wings which are water repellent where water droplet roll-off their surfaces <sup>212</sup>. Figure 1.26.

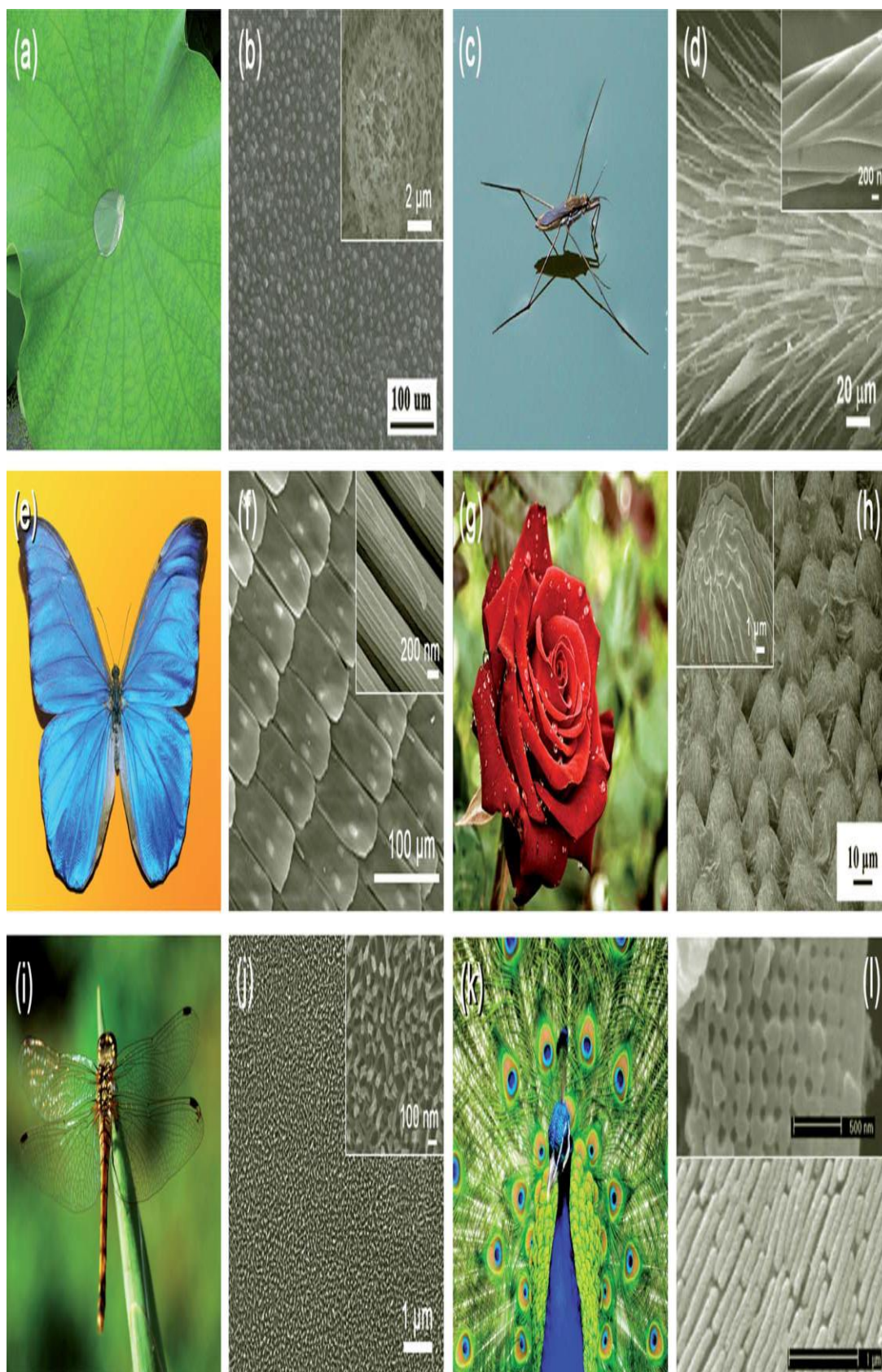


**Figure 1.26.** Examples of plants and animal kingdoms of superhydrophobic surfaces with SEM images which inspired researchers to fabricate artificial superhydrophobic surfaces in many commercial and scientific applications <sup>213</sup>.



The knowledge from biomimetic (learning from the nature) inspired researchers to mimic superhydrophobic surfaces by producing artificial surfaces taking in consideration the principle connections related to water repellency and surface roughness using different techniques including lithography, etching, plasma treatment, electro-spinning, templating, layer by layer deposition, chemical vapour deposition and use of nanoparticles <sup>212</sup>.

### **1.5.2 *Open microfluidic application***

There have been several papers published in this area, Zhao *et al.* studied the principles of fluid flow inside surface-patterned channels using ultraviolet (UV) photolithography for surface patterning for 2.5 hours. This was done using glass and cover glass masks at  $\lambda_{\max}=320$  nm to fabricate hydrophilic channels on the self-assembled monolayers of the organotrichlorosilanes <sup>201</sup>. West *et al.* used glass surface initially silanised with a monolayer of dichlorodimethylsilane (DCDMS) to offer a hydrophobic layer and consequently, hydrophilic patterns were created using dielectric barrier discharge (DBD) micro plasma jet. Samples of unilamellar lipid vesicles (as virus mimic) were decorated with biotin to give an antigen proxy, while the antibody was decorated with the avidin to provide antibody proxy for bio recognition. The virus mimics were directed through the hydrophilic path over the avidin sensor side to be captured by the avidin probs. This procedure had a disadvantage of non-specifically antibody deposition on the surface which limits the use of this procedure. In addition, the patterns fabricated by microplasma writing suffer from the ability to resist surface energy changes <sup>214</sup>. Casavant *et al.* demonstrated an open and suspended microfluidic channels that use surface tension to fill and maintain a fluid in a microscale structures. The microsystem was used to extract cortisol secreted by cells in culture into an organic solvent (pentanol) to perform metabolic studies. Although microchannels were fabricated using cheap and



available PDMS coated with parylene C and plasma-treated to provide a contact angle ranging from 20° to 30°, the detection method using an integrated HPLC system coupled to a quadrupole-linear ion trap mass spectrometer restrict the portability and cost effective related to this method <sup>197</sup>.

Sousa *et al.* used commercially cartridge paper. It was soaked in poly (hydroxybutyrate) (PHB) to modify the surface. Inkjet printer was used to fabricate curved open lines. Pumping fluid for flow rate starting from 0.6 ml min<sup>-1</sup> and up to 1.6 ml min<sup>-1</sup> witness a confined flow in the wettable path, while for 2.5 ml min<sup>-1</sup> there was no longer good spatial control on the fluid flow <sup>196</sup>. Oliverira *et al.* Imprinted two-dimensional superhydrophilic channels on polystyrene (PS) surface using masks made of polymeric sheets. This surface was exposed to UV/ozone or plasma radiation where only the exposed channel-shaped features of the mask are exposed to the radiation <sup>215</sup>. Small and large volumes of fluid transportation through hydrophilic patterns were investigated by Ghosh *et al.* The superhydrophobic surface was generated by mixing fluoroacrylic polymer matrix (serves as the primary constituent of the superhydrophobic surface) with a suspension of TiO<sub>2</sub> nanoparticles and ethanol (to increase the roughness), the prepared solution was sprayed using airbrush to form intrinsically superhydrophobic surface on three different surfaces including mirror-finished aluminium, polyethylene terephthalate (PET) films and paper. These samples were dried in a preheated oven at 60 °C for four hours which consider a time and cost consuming. Superhydrophilic patterns were fabricated upon exposure to UV light (390 nm) using a transparency film printed with black negative patterns by the use of a commercial laser <sup>216</sup>. The open microfluidic technique is relatively new and has space for development.

## 1.6 Cortisol and Cortisone detection in lab-on-chip (LOC) and point-of-care (POC) devices

Owing to its merits of small samples and reagent consumption, a high degree of automation that eliminates error usually accompanying human handling, leading to false positive results percentage reduction, low-cost fabrication, the performance of multiplexed analyte detection, selectivity and sensitivity lab on a chip can have large advantages. Laboratory methods offer an accurate and sensitive protocol for the detection of hormones, pathogenic organisms, and another medical analyte, however, these protocols suffer from laborious sample preparation and expensive instrumentation. Lab-on-chip technology offers this advantage by integrating many laboratory functions on a single chip and developing a low-cost point of care system, that express the ideal diagnostic test according to the world human organization (WHO) definition which is ASSURED term This acronym is an abbreviation of “affordable, sensitive, specific, user-friendly, rapid, and equipment-free and deliverable”<sup>138</sup>.

Vasudev *et al* presented an automated low temperature co-fired ceramic (LTCC) based microfluidic system integrated with an electrochemical immuno-sensor platform for cortisol detection. The sensor showed a linear range of 10 pM- 100 nM at a sensitivity of  $0.2 \mu\text{A M}^{-1}$  using cyclic voltammetry. The authors designed a system that established the basis for the development of a POC cortisol sensor where the reaction chamber is designed for a volume of 10  $\mu\text{l}$ , therefore the 3D microfluidic architecture required three layers of the bottom layer to provide the specific volume<sup>217</sup>.

Chemiluminescent (CL)-Lateral flow immunoassay (LFIA) method integrated into a smartphone was developed by Zangheri *et al* to detect cortisol. The detection limit was  $0.3 \text{ ng ml}^{-1}$  and the quantitative analysis range was  $(0.3-60 \text{ ng ml}^{-1})$ . This method is based on competitive immunoassay using peroxidase-cortisol conjugate, illuminate by

luminol/enhancer/hydrogen peroxide<sup>218</sup>. A home-self-diagnostic device technology for biomarkers monitoring is a growing area that is able to compete for conventional technologies achieving the same sensitivity and selectivity.

### **1.7 Aims and objectives of the study**

The aim of this work was to develop a low-cost portable method for the selective and sensitive detection of cortisol and cortisone. Two applications were investigated, firstly the quantitative determination of cortisol and cortisone in Zebrafish for low cost, rapid, environmental analysis. Secondly the detection of cortisol and cortisone in artificial saliva as an example of a point of care detection method. The specific objectives of the work were:

1. Development of a selective and specific method for the quantitative detection of cortisol and cortisone using an immunoassay with square wave voltammetry.
2. Development of a selective and specific analytical method for the quantitative detection of cortisol and cortisone using chemiluminescence immunoassay.
3. Fabrication of superhydrophobic surfaces using chemical deposition method and further enhancement of superhydrophobicity by dip coating into fumed silica suspension to be applied to an open microfluidic platform.
4. The preparation of superhydrophilic channels on the superhydrophobic surfaces using UV/Ozone lamp with masks made of different materials including coverslip, thick glass, and plastic.
5. Control of fluid flow. Open microfluidic channels.
6. Employment of an immunoassay procedure onto the open microfluidic platforms to construct a lab-on-chip (LOC) devices.

## Chapter 2 Experimental

Within this chapter, the basic reagents, materials, instruments, and procedures for the development of the open microfluidic device are described for the work reported in this thesis. In subsequent chapters, specific and detailed experimental procedures are reported for the development of the immunoassays and sample preparation.

### 2.1 Chemicals and reagents used

**Table 2.1.** Shows the chemicals and reagents that have been used.

Chemicals and reagents	Supplier	Purity/Grade
<b>Cortisol &amp; Cortisone Immunoassay detection</b>		
Anti-cortisol antibody	Abcam biochemicals, UK	-
Anti-cortisone antibody	Abcam biochemicals, UK	-
Cortisol (hydrocortisone)	Abcam biochemicals, UK	-
Cortisone	Sigma-Aldrich, UK	≥98%
Phosphate buffer saline tablet (PBS)	Sigma-Aldrich, UK	-
Luminol	Sigma-Aldrich, UK	97%
Hydrogen peroxide (H <sub>2</sub> O <sub>2</sub> )	Sigma-Aldrich, UK	Analytical grade
Ferrocenecarboxylaldehyde (FcCHO)	Sigma-Aldrich, UK	98%
Potassium carbonate (K <sub>2</sub> CO <sub>3</sub> )	Sigma-Aldrich, UK	≥99%
Sodium borohydride (NaBH <sub>4</sub> )	Sigma-Aldrich, UK	98%
Hydrochloric acid (HCl)	Sigma-Aldrich, UK	Analytical grade
Tertrabutylammonium perchlorate (TBAP)	Fluka, UK	≥99%
4-Nitrobenzene diazonium tetra-fluoroborate	Sigma-Aldrich, UK	97%

Potassium chloride (KCl)	Sigma-Aldrich, UK	≥99%
Sodium hydroxide (NaOH)	Fisher scientific, UK	Analytical grade
<i>N</i> -(3-Dimethylaminopropyl)- <i>N</i> '-ethylcarbodiimide hydrochloride (EDC)	Fluka, UK	≥98%
<i>N</i> -Hydroxysulfosuccinimide sodium salt (Sulfo-NHS)	Sigma-Aldrich, UK	≥98%
Tween 20	Sigma-Aldrich, UK	-
Bovine serum albumin (BSA)	Sigma-Aldrich, UK	≥96%
Ethanol (EtOH)	Fisher scientific, UK	HPLC grade
Acetonitrile (ACN)	Fisher scientific, UK	HPLC grade
<i>N,N</i> -dimethylformamide (DMF)	Sigma-Aldrich, UK	≥99%
Artificial saliva recipe and Zebrafish sample		
Ammonium nitrate	Sigma-Aldrich, UK	97%
Potassium phosphate	Sigma-Aldrich, UK	99%
Potassium citrate	Sigma-Aldrich, UK	99%
Uric acid sodium salt	Sigma-Aldrich, UK	99%
Urea	Sigma-Aldrich, UK	99%
Lactic acid sodium salt	Sigma-Aldrich, UK	-
Bovine submaxillary gland mucin Type I-S	Sigma-Aldrich, UK	-
tricaine methane sulfonate (500 mg ml <sup>-1</sup> MS-222)	Sigma-Aldrich, UK	97.5%
Interferences		
Prednisolone	Sigma-Aldrich	≥99%
Progesterone	Sigma-Aldrich	≥99%
Corticosterone	Sigma-Aldrich	≥92%
11-Deoxy cortisol	Sigma-Aldrich	-
Testosterone	Sigma-Aldrich	≥98%
Fabrication of superhydrophobic/hydrophilic surfaces		
Fumed silica particles	Evonik	-
Dichlorodimethylsilane (DCDMS)	Sigma-Aldrich, UK	99.5%

## **2.2 Materials and instrumentation**

### **2.2.1 *Immunoassay electrochemical instrumentation***

Electrochemical measurements took place with a standard three-electrode system using a Palm-sens Potentiostat (Palm Instruments, Netherlands) connected to the PSTrace 4.3 software. The electrochemical cell comprised of a tin-doped indium oxide (ITO) coated glass electrode (Delta Technologies Limited, USA) which was the working electrode, a nickel wire as the counter electrode, as this enables more versatility with respect to the experimental setup and silver/silver chloride (Ag/AgCl) (3M NaCl)(ALVATEK) as the reference electrode (BSA, UK). All potentials were reported versus the Ag/AgCl reference electrode at room temperature. When making the measurement the scan rate was  $100 \text{ mV s}^{-1}$ . Figure 2.1.

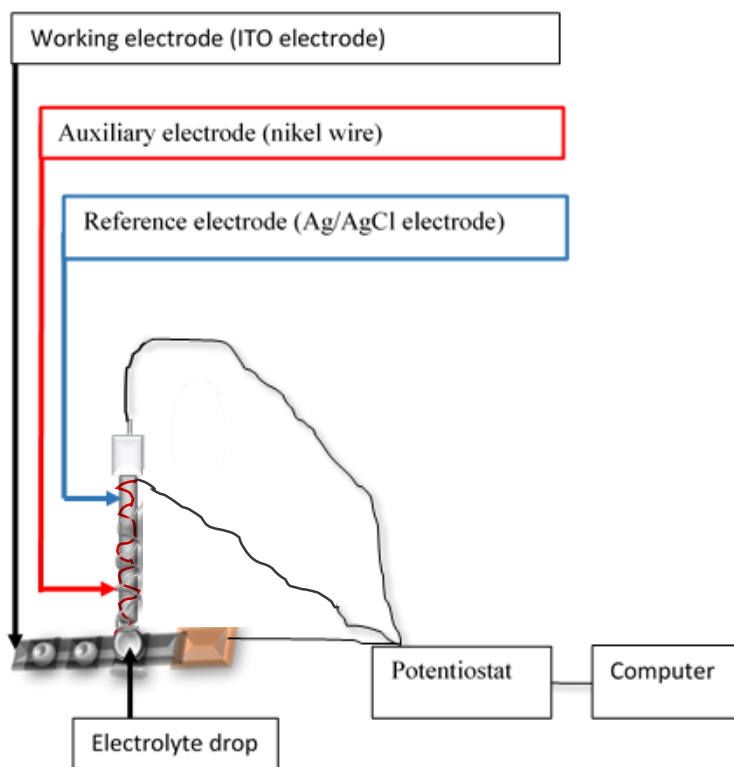


**Figure 2.1.** A schematic of an electrochemical cycle used for immunoassay procedures, with an Ag/AgCl electrode as a reference electrode, nickel wire as a counter electrode and the ITO electrode as a working electrode connected to Palm-sens potentiostat with the PStTrace 4.3 software designed by Auto Lab to measure the current.

### 2.2.2 Chemiluminescence instrumentation

Studies of the analyte (cortisol and cortisone) optimization and determination in standards and samples (Zebrafish whole-body and artificial saliva samples) were made using chemiluminescence instrument figure 2.2. Chemiluminescence results were obtained using a charge-coupled device (QHY6CCD) camera fitted with a high-resolution pixel lens (Radox Toxicology Headquarters, Crumlin, Co. Antrim, UK). Image J software was employed for analysis.

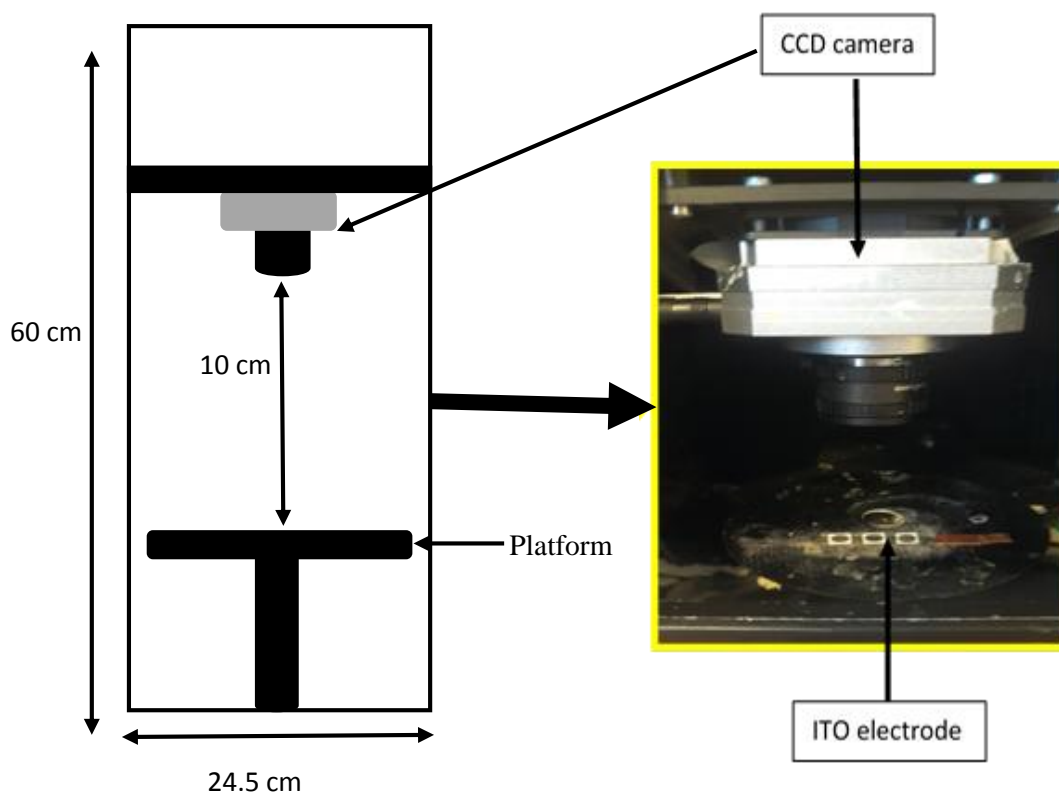


**Figure 2.2.** Chemiluminescence instrumentation shows an ITO electrode alignment under the CCD camera, the box is closed and images were recorded using Image J software and a laptop connected to the camera.

### **2.2.3 Preparation of superhydrophobic surfaces**

This can be done in two process steps:

#### **2.2.3.1 Hydrophobization of surfaces using dichlorodimethylsilane (DCDMS)**

Different substrates (glass and plastic slides) were fixed into a Teflon holder before their transfer into an airtight vessel as shown in figure 2.3. The vessel was fitted with gas inlet and outlet and was first flushed with nitrogen (Energas Ltd., High purity) to ensure negligible humidity, then dichlorodimethylsilane (DCDMS) (approximately 300 $\mu$ l) was injected into the bottom of the sealed container without touching the substrate surface using a micropipette to prepare homogeneous layer of hydrophobic surface onto the substrate. The airtight vessel was then left for one hour in a fume cupboard for



silanization. After silanization, substrates were removed from the container and left in a fume cupboard for 10 minutes to remove the excess DCDMS agent (ventilation).

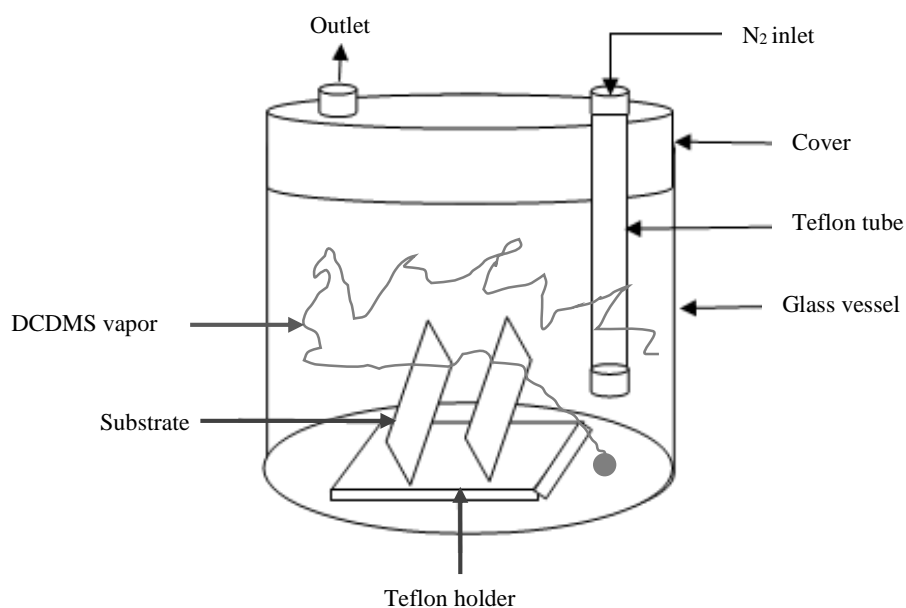


**Figure 2.3.** Schematic of the setup used for the hydrophobization of different substrates in the vapour phase. O<sub>2</sub> is removed by flushing N<sub>2</sub> gas through the inlet. The silane agent is introduced through the outlet to the bottom of the vessel after flushing with N<sub>2</sub> to modify the substrates.

#### ***2.2.3.2 Fabrication of porous silica substrate layer by dip-coating method***

The porous silica suspension was deposited on the substrate by a dip coating method using a mechanical pump syringe (model NE-1000 New Era Pump System Inc. USA). The substrate was first introduced into the fumed silica suspensions (Aerosil R2O2 hydrophobic fumed silica, Evonic), this was done by fixing the substrate into a clip attached to the plunger of the pump. Operating the pump allows the slides to immerse vertically into a vessel containing the fumed silica dispersion, these slides remain in the suspension for one minute before being pulled out at a constant speed. Figure 2.4.

Following this procedure, the fumed silica dispersion adhered onto the substrate, while some of the adhered dispersion was drained by gravity to form a thin coated film. This occurred when the substrate is being withdrawn. Subsequently, these substrates were left in the natural air to ensure evaporation of the solvent<sup>219</sup>. Different suspension concentrations and withdrawal speeds were investigated for the ideal coating.

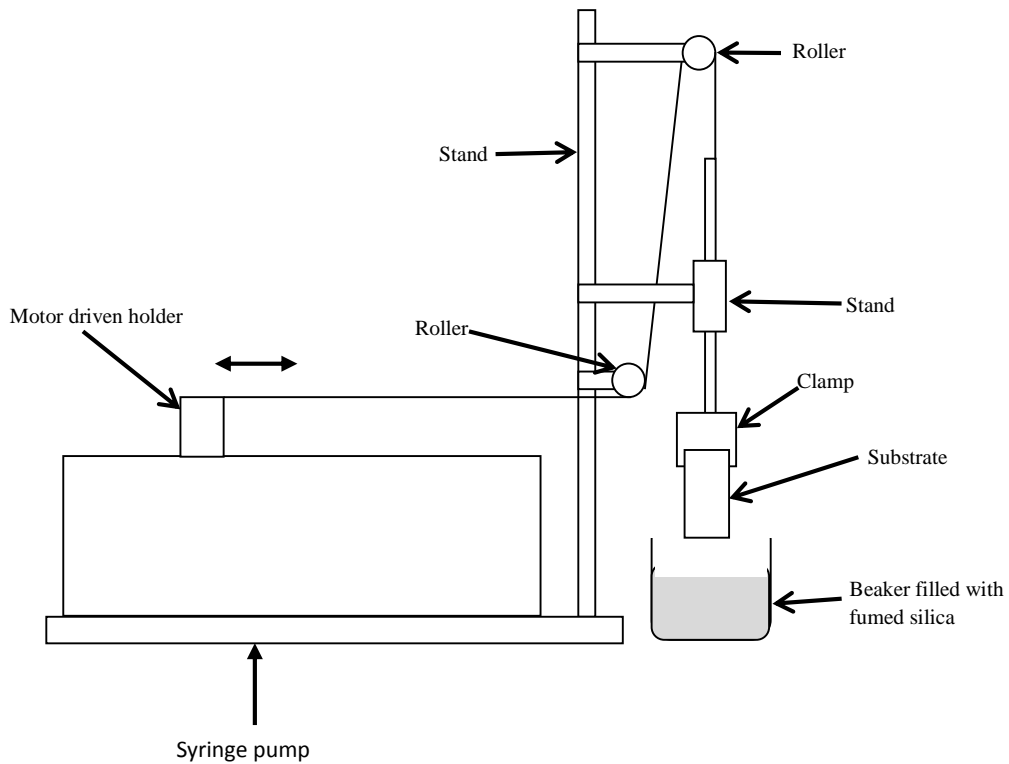


**Figure 2.4.** Schematic of the self-constructed dip-coater used to coat different substrates with fumed silica suspension using different withdrawal velocity and varying the concentration of fumed silica suspension.

The self-constructed dip-coater was programmed to measure flow rate through a cylindrical syringe for a fluid as shown in figure 2.5.

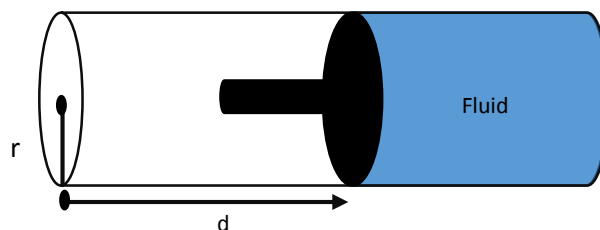


**Figure 2.5.** Schematic explain the syringe pump flow rate conversion to dip coating speed. This can be calculated by the inner radius of the syringe ( $r$ ) and distance of fluid flow ( $d$ ).

To overcome this problem, a conversion from flow rate (ml min<sup>-1</sup>) to speed (cm min<sup>-1</sup>) was achieved using the following calculation to measure the speed instead of flow rate.

$$\text{Flow rate} = \frac{\text{Volume}}{\text{Time}} = \frac{\text{Area} \times \text{Distance}}{\text{Time}} = \text{Area} \times \text{Speed} \dots \dots \dots \text{Equation 2.1}$$

$$\begin{aligned} \text{Speed (S)} &= \frac{\text{Flow rate(FR)}}{\text{Area(A)}} \\ &= \frac{\text{Flow rate}}{\pi r^2} \dots \dots \dots \text{Equation 2.2} \end{aligned}$$

S represents speed (cm min<sup>-1</sup>), FR is the flow rate (ml min<sup>-1</sup>) and r is the inner radius syringe used (cm).

#### **2.2.4 Contact angle measurement**

To investigate the wetting properties of the surfaces that were fabricated, contact angles of sessile water drops on different substrates at the different position were measured before and after hydrophobization of the substrates, also after coating with fumed silica suspension using drop shape analysis system (DSA10, Krüss) (sessile drop method). Droplets were initially dispensed on the sample surfaces and placed on the DSA instrument stage using a glass needle (Hamilton glass syringe) and the chamber was closed to prevent sample fluid evaporation, the stage was illuminated from the side and images of the droplets were captured using the camera fitted on the other side. It was difficult to image droplets on superhydrophobic surfaces by the above procedure due to the ease in which the droplets slide off the surfaces, therefore films were recorded to show the superhydrophobic surfaces characterization. All the measurements were an average of at least three different droplets made on three replicated samples.

### 2.2.5 Coated substrates stability

The stability of the coated layer and the patterns were investigated by dipping the coated slides into a beaker filled with water, stirred by a magnetic stirrer for five minutes, as shown in figure 2.6. Finally, images were taken using an optical microscope and digital camera.

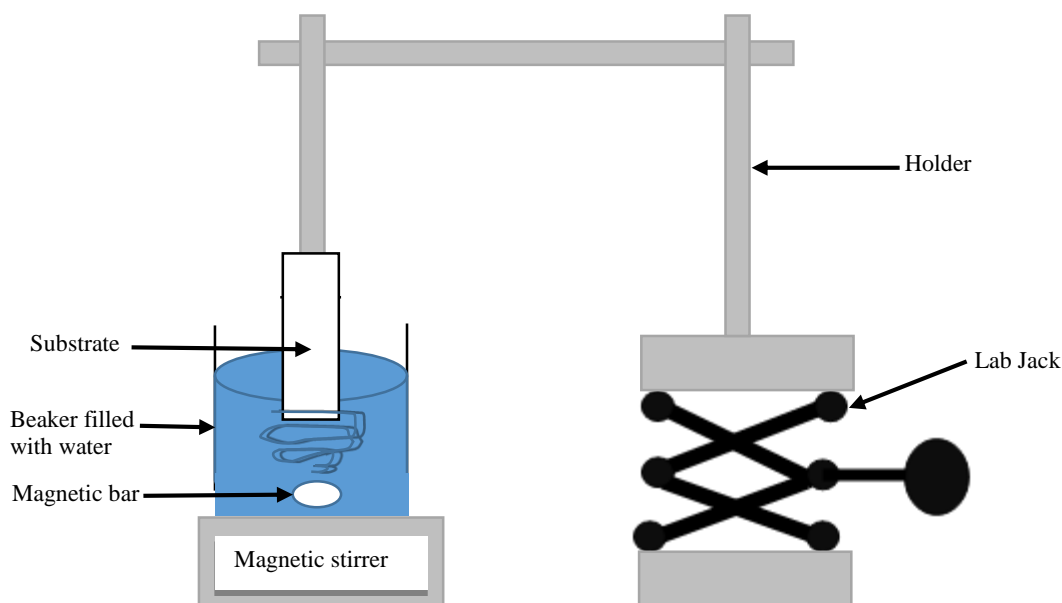


**Figure 2.6.** Schematic of the experimental setup used for coating substrate stability. The coated substrate attached to holder was immersed in a beaker filled with water and by the use of a magnetic bar and magnetic stirrer, a harsh circumstance was provided for the coated substrate.

### 2.2.6 Preparation of superhydrophilic patterns on the superhydrophobic surface

Superhydrophilic patterns on different substrates surfaces were fabricated by irradiating the superhydrophobic surfaces with UV/ozone pen ray lamp through different types of masks. The experimental setup is shown in Figure 2.7 coated superhydrophobic substrates were placed on a clean stepped like glass holder, and selected masks were placed on top of the superhydrophobic substrates. Then the glass holder was placed on the clean adjustable stainless steel platform in a clean UV/ozone lamp box, and the

position of this stage was adjusted and fixed to ensure the distance between the UV/ozone lamp and the coated substrate was approximately 0.5 mm. Once everything was set, the UV/ozone lamp box was closed and switched on for 30 minutes. Finally, the UV/ozone lamp was switched off after this burning process was finished, and the UV/ozone lamp box was kept open inside the fume cupboard for 10 minutes to ensure all reactive ozone and oxygen atoms were fully evacuated. Complex superhydrophilic patterns were obtained by repeating this burning technique with a suitably chosen mask for a number of times as required.

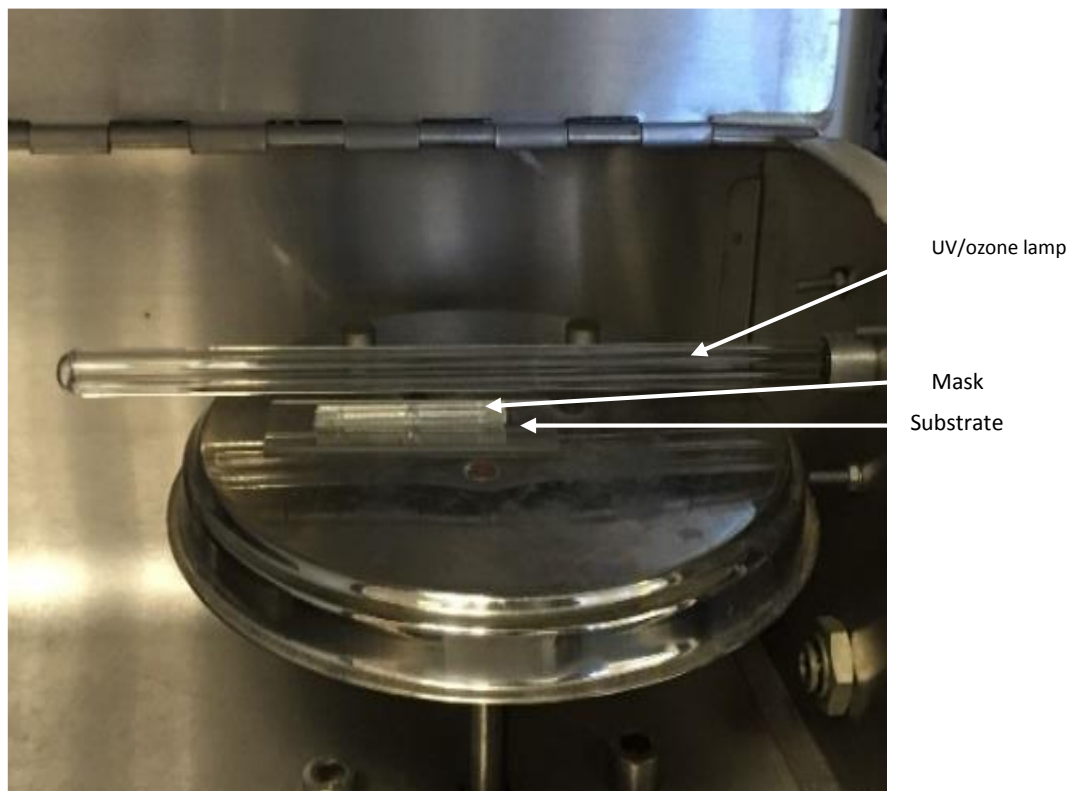
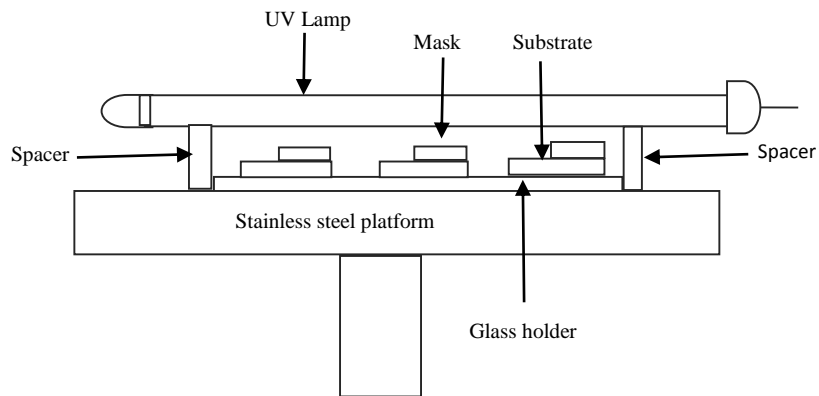


**Figure 2.7.** Self-constructed UV/ozone lamp box. The above schematic is the experimental arrangement used to fabricate superhydrophilic patterns on superhydrophobic surfaces by applying UV/ozone burning technique. The second image is an actual side view of burning setup.

### 2.2.6.1 Masks used to fabricate superhydrophilic patterns and heat tolerance

Different types of photomasks with a variety of geometrical patterns were used including glass coverslips 170  $\mu\text{m}$  thick glass slips (25  $\times$  25 mm, Chance Proper LTD, UK), glass slides 1 mm thick plates of glass (7  $\times$  50 mm Thermo Scientific, Menzel-Glaser, UK) and plastic slides 0.5 mm thick plates of plastic (7  $\times$  50 mm, Hurlbat company, UK). Different masks heat tolerances from exposure to the UV/ozone lamp was investigated using an HH 306A OMEGA (Data Logger Thermometer, UK) in a self-constructed setup shown in figure 2.8.

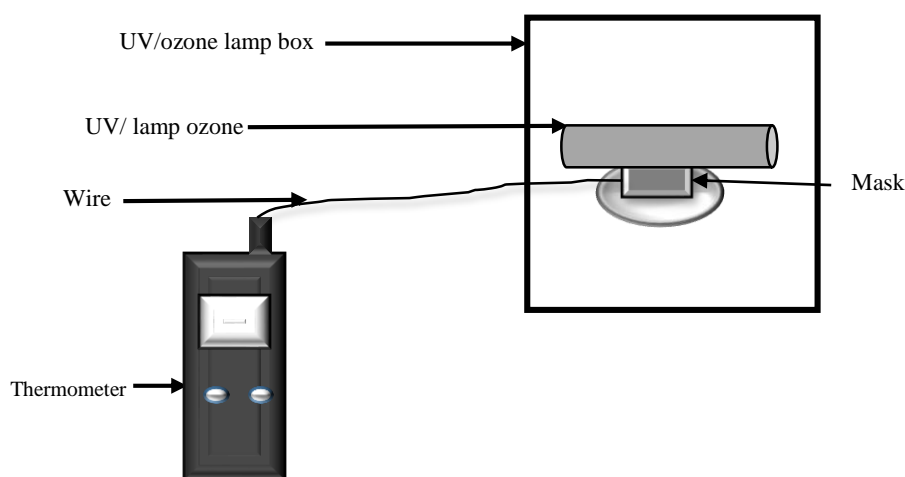


**Figure 2.8.** Experimental setup for investigating the tolerance of different masks to the heat introduced by the UV/ozone lamp during the burning process.

## 2.3 Construction of open fluid lab-on-a-chip device

### 2.3.1 Microfluidic device design

The lab-on-a-chip device design originated from a closed microfluidic design, but with the use of open microfluidic principles. Figure 2.9 illustrates the initial design on a glass platform (3.5 mm  $\times$  2.5 mm  $\times$  0.3 mm length, width and thick) with a hole drilled through it to enable the microfluidic device to be connected to a mechanical syringe pump and this was done using Teflon tubing (*PTFE microbore tubing (i.d 0.81 mm, o.d.*

1.42 mm and gauge size 21) attached to a syringe pump from one side and the other side was glued to pre-drilled hole on the bottom glass platform using epoxy resin. The detection chamber consists of the superhydrophobic coated substrates with superhydrophilic patterns fabricated using different masks, was adjacent on the top of the glass platform. These two platforms were bonded to each other using double sided sellotape. The superhydrophilic patterns were wetted by pumping fluid at a constant speed through the superhydrophilic pattern by the use of the syringe pump to investigate the possibility of fluid flow, the channel was observed by using the DSA 10, Krüss camera and videos were recorded.

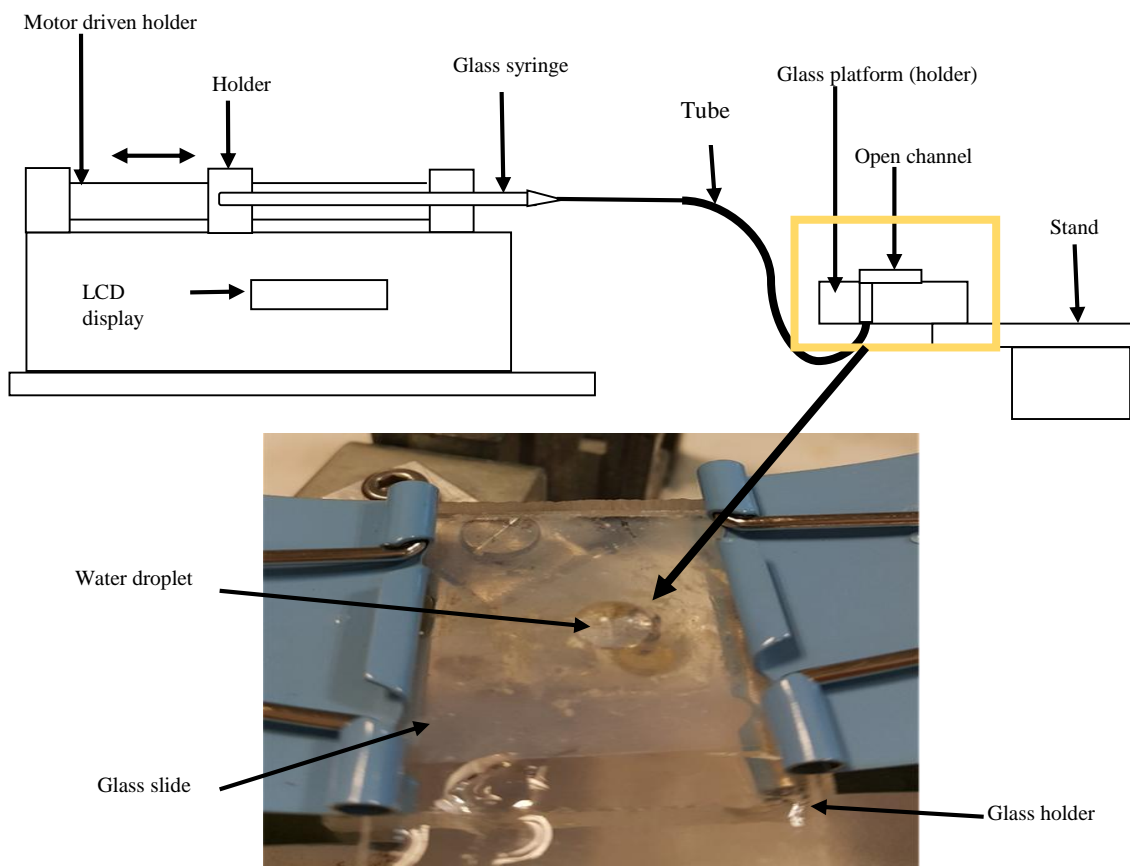


**Figure 2.9.** The top schematic shows the experimental setup used for pumping fluid to the device consisting of top platform (open microfluidic chip), bottom glass platform (holder) and the bottom platform was attached to the syringe pump by PTFE microbore tubing (i.d 0.81 mm, o.d. 1.42 mm and gauge size 21). Hamilton glass syringe was used to pump fluid to the device. The bottom photograph is an image of the setup showing the aggregation of fluid after pumping.



Another design of the chip did not require drilling circle as an outlet or inlet where the fluid is delivered from a tube attached to the end of the pump syringe. The other end of the tube was attached to a needle covered with a plastic tube. The needle ended approximately 1 mm above the ITO electrode. The outlet was a reservoir and on the top of it, there was a stopper filled with cotton (Webril Handi Pads) to act as a sucker to suck waste fluid. Figure 2.10.

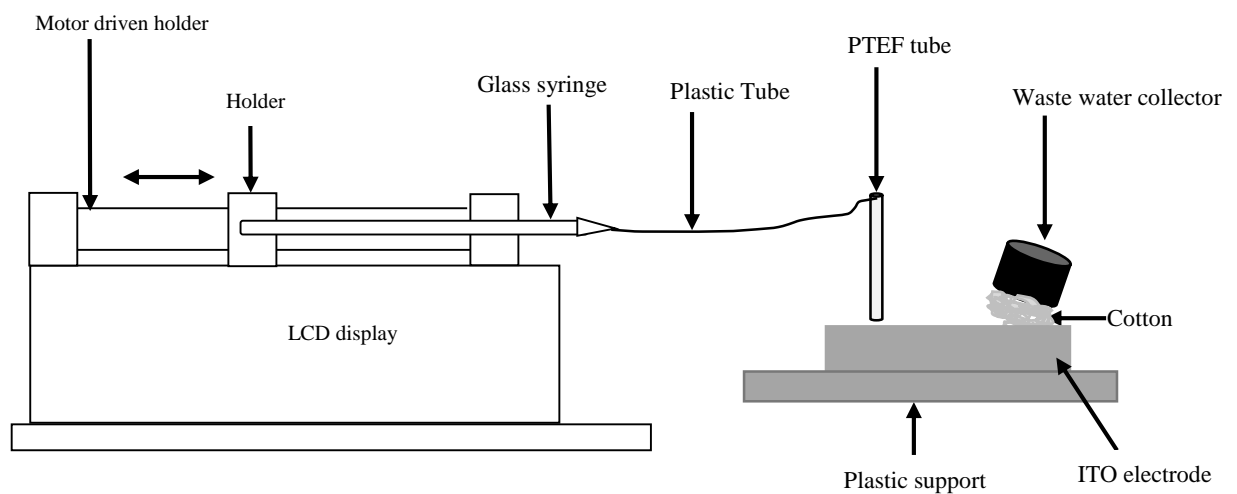


**Figure 2.10.** Shows the open microfluidic chip where the tube was attached to a needle vertically align to the coated ITO electrode, this tube was attached to a mechanical syringe pump to pump fluid. The setup was built on a plastic platform (17 mm×7 mm length and width, 0.3 mm thick). Another advantage of this design is there was no need for an outlet, a stopper filled with cotton is placed on the end of the electrode to suck all waste fluid.

### 2.3.1.1 Find the steady state flow

To simplify the design of the chip, a reservoir was fabricated onto the ITO surface and the steady state time of fluid flow was then investigated. The following setup (figure 2.11) was prepared where a chip was coated with fumed silica and the superhydrophilic pattern was fabricated using the outlined procedures in sections 2.2.3 and 2.2.6. The chip was placed on the DSA 10, Krüss instrument platform and on end, a needle was

attached to a syringe pump and was fitted on the top of this end. While the other end of this chip which contained the fabricated reservoir, cover filled with cotton was positioned on the top of the reservoir. Different flow rates were investigated (10, 20, 30, 40, and 50  $\mu\text{l min}^{-1}$ ) and videos were recorded.

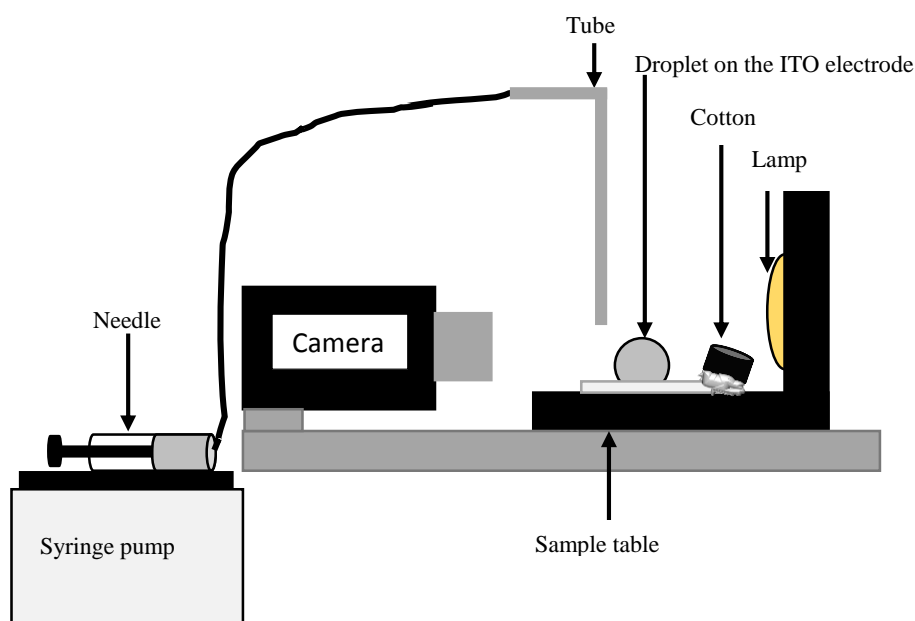


**Figure 2.11.** Steady state flow setup using a pre-weighted cotton cover on the top of the reservoir located on one edge of the chip and the other edge is positioned under a needle glued to a syringe attached to a syringe pump.

### **2.3.1.2 Fluid flow visualization using a fluorescence microscope**

Moving forward to automated the procedure, a setup consisting of the microfluidic chip as described in figure 2.10 was placed on the fluorescence microscope stage which had a CCD camera (Nikon ECLIPSE TE2000-U) fixed on the top of the chip to capture images and videos of the fluorescence particles, those were recorded using image pro software. At the beginning, deionized water was filled into a syringe (Hamilton, Reno,

Nevada – 500  $\mu$ l) which was attached to a mechanical syringe pump and deionized water was pumped through the open channels adopting a fixed needle above the inlet hole of the channel to ensure the wetting of the channel. Afterward, the microscope was covered with a black sheet and approximately 900  $\mu$ l of fluorescence particles solution was withdrawn to fill the tube of the syringe pump followed by pumping fluorescence particles solution to the channel.

The open channel was visualized and consequently, the microscope lamp was turned off and a blue-light filter cube with an excitation filter wavelength of (510-560 nm), was turned on to capture the particles movement. Waste fluorescence particles solution was sucked out by cotton placed on the top of the outlet hole of the chip.

### ***2.3.2 Integrated open microfluidic device***

The major aim of the work was the fabrication a microfluidic chip with integrated antibodies to measure hormones. With this in mind, a device consists of mechanical syringe pump attached to a fixed setup needle placed on the top of the chip. The chip was designed where the modified ITO electrode previously immobilized with the antibody, coated with superhydrophobic layer and appropriate superhydrophilic channels patterns as mentioned in sections 2.2.3 and 2.2.6 was slotted into a hosting plastic slide and this was glued to the plastic platform (used as a stand) to ensure the stability of the electrode onto the stand platform. A cover containing cotton was placed on the top of an inlet reservoir of the ITO electrode fabricated using UV/ozone lamp and a specific mask to reduce fabrication steps instead of drilling holes and tubing. The latter setup was placed in a black box fitted with CCD camera which was connected to the computer where images were analyzed by Image J software. The chemiluminescence reagents (luminol and hydrogen peroxide) were mixed and filled into a syringe covered with aluminum foil, placed onto the mechanical syringe pump

and connected to the vertical needle attached to the platform by a tube across the black box, the mixture was ready to be pumped into the reaction circle. As seen in figure 2.12.

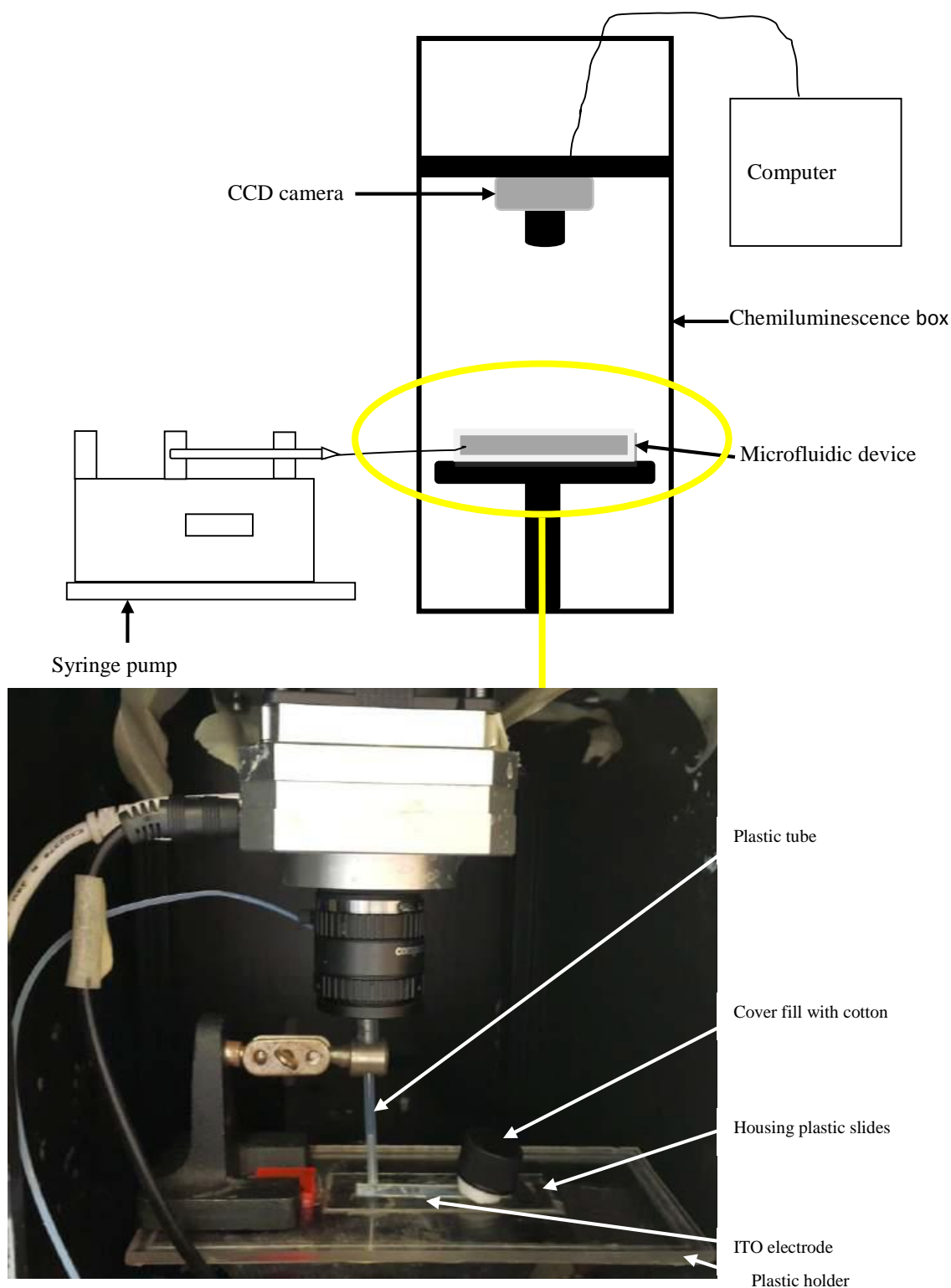


**Figure 2.12.** Shows the chemiluminescence immunoassay microfluidic setup.

## **Chapter 3 Anti-cortisol and anti-cortisone electrochemical immobilisation and stress hormones detection using electrochemical techniques**

The work described in this chapter concerns the immobilization procedure for anti-cortisol and anti-cortisone and their characterisation using cyclic voltammetry technique. An electrochemical-based assay was then developed and applied to real samples of Zebrafish whole-body and artificial saliva samples.

### **3.1 Introduction**

In an effort to develop a reproducible process for an antibody immobilization on a solid surface, Dou *et al.* introduced an electrochemical immunoassay strategy to immobilize an antibody on a modified gold electrode in order to determine the cardiac biomarker creatinine kinase. This method was based on the synthesis of an Ab-Fc bioconjugate to chemically tag the antibody, followed by the immobilization of the ferrocene tagged antibody onto an electrode. To achieve this; the electrode was modified by an electrochemical deposition of 4-nitrobenzene diazonium tetrafluoroborate, followed by an electrochemical reduction of the nitrobenzene group to an amine group using cyclic voltammetry technique<sup>220</sup>. Previous studies gave a mechanistic insights for diazonium salt coupling to different surfaces to improve the surface morphology knowledge. This was elucidated by different instruments such as time-of-flight secondary ion mass spectroscopy (ToFSIMS) that gave the length of time a potential which was applied during the electrografting, while atomic force microscopy (AFM) was used to analysis the depth of samples. The thickness of films on the surfaces was measured by ellipsometry and voltammograms acquired from cyclic voltammetry instrument confirmed sample electro grafting<sup>221</sup>. Figure 3.1 shows a scheme of the process.

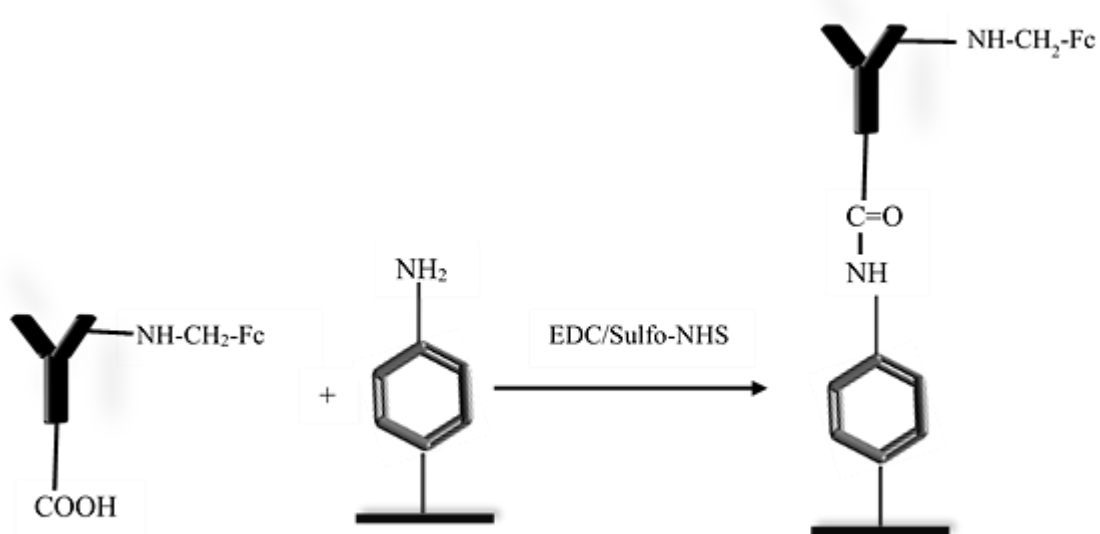


**Figure 3.1.** A schematic of the electrochemical process for the immobilization of the ferrocene tagged antibody onto the modified electrode via an amide linkage.

This was considered to provide “end-on” rather than “side-on” orientation of the antibodies as the antibody's carboxylic acid group exist at the base of the heavy chain and it is these that couple the amines groups of the modified surface. The specific antibody orientation is considered a crucial aspect because it determines the effectiveness of the biosensor as the Fab region must be available for binding with the antigen<sup>220, 222, 223</sup>. Figure 3.2 display the different antibodies orientation.

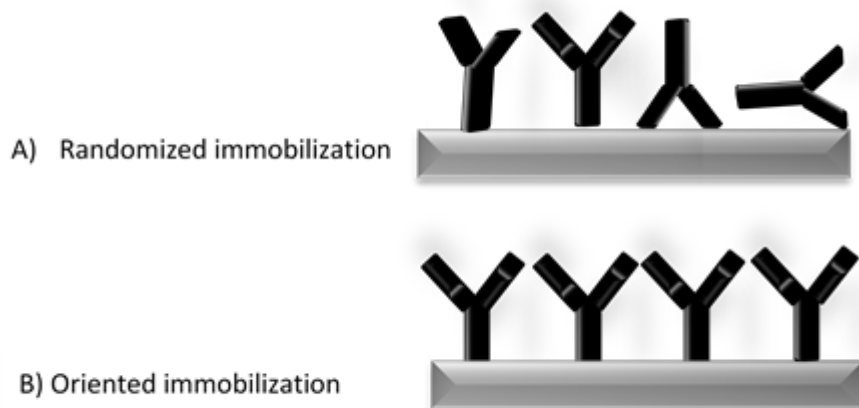


**Figure 3.2.** The inclusion of different antibodies orientations (A) randomized with some side-on, (B) end-on, on a solid surface, where the side-on orientation leads to poor-to-moderated sensitivity and on the other hand the end-on orientation results in high sensitivity that can be attributed to well-controlled modified surface that can specifically capture the antigen.

Within this project, the above method was adapted to immobilize anti-cortisol and anti-cortisone antibodies on the ITO electrode to determine cortisol and cortisone to carry out an electrochemical immunoassay to detect and monitor the analyte (Zebrafish whole- body and artificial saliva samples) by measuring the change in current using cyclic voltammetry and the more sensitive square wave techniques.

## **3.2 Experimental procedures**

This section includes the specific experimental procedures for immobilization of the antibodies, characterization of the antibodies, optimization, calibration studies and real samples determination.

### ***3.2.1 Determination of cortisol and cortisone using electrochemical assay***

#### ***3.2.1.1 Antibody immobilization via the electrochemical process***

##### ***❖ ITO electrode modification with $-NH_2$ group***

The monoclonal anti-cortisol antibody ( $2 \text{ mg ml}^{-1}$ ) was immobilized onto a modified ITO electrode. This step was achieved by the deposition of a nitro functional group onto the conductive surface of an ITO electrode and sequentially the reduction of the nitro group to amino group through an electrochemical reduction of the nitrobenzene, allowing the antibody binding to the modified electrode via an amine group on the ITO electrode surface. Therefore the electrode surface had to be modified electrochemically in advance using the following procedure:

For all the experiments conducted in this chapter a copper tape was placed on one end edge of the conductive side of an ITO electrode as a connection point to the standard three electrodes setup including the Ag/AgCl (reference electrode) and nickel wire (counter electrode) to complete the electrochemical cycle (mentioned in section 2.2.1). Then the surface of the electrode was divided into three circles by a self-adhesive circle with holes, this was carried out to facilitate the addition of the antibody in spatially separated positions onto the electrode surface, this would allow the measurement of multiple analytes as depicted in figure 3.3.



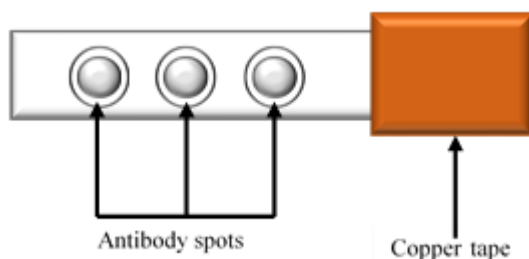


**Figure 3.3.** Diagram of an ITO working electrode, attached with a copper tape placed on one edge of the conductive ITO electrode surface to work as a connection point. Three circles were placed on the ITO surface with 1.2 cm spacer from each center circle.

For the electrode modification, an aliquot of 30  $\mu\text{l}$  of deposition solution consisting of 0.1 M tetrabutylammonium perchloride (TBAP) and 2mM 4-nitrobenzene diazonium tetrafluoroborate in acetonitrile was spotted onto the circle on the ITO electrode. The nickel wire and silver/silver chloride (Ag/AgCl) electrode were in touch with the circle. A cyclic voltammeter was then used to scan from + 0.7 V down to - 0.5 V and back to + 0.7 V at scan rate 100  $\text{mV s}^{-1}$ . Then the electrode was washed with acetonitrile and placed into aqueous ethanol solution (90:10, v/v) containing 0.1M potassium chloride, where the electro-formation of a phenyl amine was achieved during 3 reduction-oxidation scans using cyclic voltammetry, starting at + 0.4 V with a sweep to - 1.25 V returning to + 0.4 V again.

#### ❖ *Synthesis of antibody tagged with ferrocene*

Bare antibodies do not give a measurable electrochemical response on the addition of an antigen and therefore, the antibodies were chemically labelled with a redox tag, using the methodology outlined by Dou *et al.*<sup>220</sup>. This was achieved by the addition of a 10  $\mu\text{l}$  aliquot of (2  $\text{mg ml}^{-1}$ ) of anti-cortisol antibody to 190  $\mu\text{l}$  of phosphate buffer saline (PBS)(10 mM) and the pH was adjusted to ~ 9 using 5% aqueous potassium carbonate ( $\text{K}_2\text{CO}_3$ ) (5 % w/v). Then a solution of ferrocenecarboxaldehyde was dissolved in

dimethylformamide (DMF) (20 mg in 200 $\mu$ l) and added to the antibody solution. After an incubation of 30 minutes to permit the formation of an imine product Ab-N=CH-Fc; a reduction of the resulting imine to secondary amine was carried out by the addition of sodium borohydride (2 mg) to give Ab-NH-CH<sub>2</sub>-Fc. This solution was left for 10 minutes, afterward, the solution was readjusted to pH ~ 7 using hydrochloric acid (HCl) (0.1M). Whatman universal indicator paper (1-11) was used to confirm all pH changes.

The antibody was purified to remove any ferrocene excess; by centrifugation (12,000 rpm for 20 minutes), then the supernatant was transferred into a 2  $\times$  viva spin (500, GE Healthcare, Sweden); the solution was then re-centrifuged (12,000 rpm for 10 min) and the purified antibody on the top vial was topped up with 100 $\mu$ l PBS (10 mM) and centrifuge as a washing step. The final solution was stored in the fridge (4° C) until required.

#### ❖ *Immobilization of ferrocene labeled antibody onto the ITO electrode*

This was achieved by mixing a 10 $\mu$ l aliquot of the ferrocene tagged antibody (prepared as in previous section) with an equal volume of an activation buffer consisting of 2mM (*N*-(3-dimethylaminopropyl)-*N*'-ethylcarbodiimide hydrochloride) (EDC) and 5 mM (*N*-hydroxysulfosuccinimide sodium salt) (sulfo-NHS) in 2 ml PBS (10 mM) for 15 minutes to activate the –COOH on the antibody to facilitate the bonding to the electrode *via* an amide linkage. Subsequently, 30  $\mu$ l of this solution was added to the modified ITO electrode and left covered for 18 hours in the fridge at 4° C. The activation buffer was freshly prepared when required.

#### **3.2.1.2 Confirmation and characterization of antibody immobilisation**

The electrode with the immobilized anti-cortisol antibody was washed with 0.1% Tween 20 (0.1 v/v) in PBS (10 mM) solution. Afterwards, the electrode was

treated with bovine serum albumin (BSA) (1 %, w/v) in PBS (10 mM) for 30 minutes to block unoccupied sites on the ITO electrode. The electrode was then washed with 0.1% Tween 20 in PBS. Cyclic voltammetry was used to confirm the immobilization of the antibody by comparing voltammograms before and after immobilization onto the ITO electrode. Cyclic voltammetry was carried out using PBS (10 mM) and different scan rates were investigated, ranging from (10 – 1000 mV s<sup>-1</sup>).

### ***3.2.1.3 Optimization of the antigen incubation time***

To determine the optimum time for the antigen to be incubated with immobilized antibody, 50 ng ml<sup>-1</sup> of cortisol (hydrocortisone) standard solution was selected for the study with a range of incubation times (10, 15, 20, 30, 45 and 60 minutes). For the procedure, a 30 µl of the antigen was added to the immobilized antibody and incubated. The electrode was then washed with Tween 20 and cyclic voltammetry was carried out as previously.

### ***3.2.1.4 Electrochemical immunoassay***

A stock solution of cortisol was prepared by dissolving 5 mg of cortisol (cortisol) in ethanol and making the volume up to 50 ml in PBS (10 mM) to give a concentration of 100 ppm. Then increasing volumes of stock solution were transferred into a series of 5 ml volumetric flask and made up the mark with PBS (10 mM) to prepare set of working standard from (0.001-50 ng ml<sup>-1</sup>).

The electrodes with the immobilized antibody (section 3.2.1.1) were washed with PBS (10 mM) and the calibration standards (antigen) were added to each electrode individually starting from the lowest (0.001 ng ml<sup>-1</sup>) concentration to the highest concentration (50 ng ml<sup>-1</sup>). After an incubation period of 30 minutes the electrode with the spotted antigen was re-washed with PBS (10 mM) and a measurement was made

using cyclic voltammetry in PBS (10 mM) over 3 scans followed by square wave voltammetry also in PBS (10 mM) where the frequency was 25 Hz with an amplitude of 1 mV, the scan was between 0 V and + 0.5 V. This procedure was repeated for cortisone.

### ***3.2.1.5 Determination of cortisol and cortisone in Zebrafish whole-body sample and artificial saliva samples using electrochemical immunoassay***

Two biological samples were tested; Zebrafish whole-body and artificial saliva samples to investigate the concentration of cortisol and cortisone.

#### ***❖ Zebrafish whole-body sample***

All experiments in this study were ethically approved and followed the HO schedule 1 methods prepared by HO licence holders. Zebrafish were purchased from Ings lane Garden Centre, Dunswell, UK. The samples were maintained in an aquarium (in the Biological Sciences Department at the University of Hull) before the experiments. Fluctuations in cortisol occur due to the natural circadian rhythms and to overcome this all samples were taken at approximately the same time of the day. Zebrafish were captured, euthanized with tricaine methane sulfonate (500 mg ml<sup>-1</sup> MS-222) and to remove the excess of water the Zebrafish samples were blotted on paper towel. Whole-body cortisol extraction was performed according to Canavello *et al.* method <sup>42</sup>, where the samples were individually weighed, dissected into smaller parts and placed into a 10 ml screw top disposable test tube, then 1 ml of PBS and 5 ml diethyl ether were put into the test tube which was then vortexed for 1 minute before centrifugation for 5 minutes at 3500 rpm. To separate the aqueous and organic layer, the test tube was placed into liquid nitrogen and the unfrozen layer ( organic layer containing cortisol ) was poured into a new test tube and kept overnight in the fume hood to allow the diethyl ether evaporation.

The yellowish lipid extract obtained was reconstituted with 1 ml of cortisol standard dissolved in phosphate buffer saline (PBS) and stored at 4° C for 24 hours. An alternative method was tested by repeating all above processes except the extraction method was omitted.

#### ❖ *Artificial Saliva*

A recipe outlined by West *et al.* <sup>224</sup> was used to prepare an artificial human saliva sample which include sodium chloride (1.954 g L<sup>-1</sup>), ammonium nitrate (0.328 g L<sup>-1</sup>), potassium phosphate (0.639 g L<sup>-1</sup>), potassium chloride (0.202 g L<sup>-1</sup>), potassium citrate (0.308 g L<sup>-1</sup>), uric acid sodium salt (0.021 g L<sup>-1</sup>), urea (0.198 g L<sup>-1</sup>), lactic acid sodium salt (0.146 g L<sup>-1</sup>) and bovine submaxillary gland mucin Type I-S (30 g L<sup>-1</sup>), the solution was completed with deionised water. The stock solution of cortisol was prepared as in section 3.2.1.4, but for all standard, there was a slight difference where they were made up in artificial saliva instead of PBS (10 mM). The electrochemical immunoassay described in section 3.2.1.4 was repeated using the above biological sample. All the above procedure were repeated for cortisone.

### 3.3 Results and discussion

#### 3.3.1 Tin-doped indium oxide (ITO) electrode modification

The immobilization protocol was investigated and characterized using cyclic voltammetry. Tin-doped indium oxide (ITO) was selected as the electrode for various reasons including its high optical transmittance and the ease in which a thin layer can be deposited <sup>225</sup>. In addition to its electrical conductivity properties that occur due to the doping ions (i.e tin) that acts as cationic dopant in the  $\text{In}_2\text{O}_3$  lattice, where for the Sn atoms substitute the In atoms and the difference between both atoms valence resulted in the free electron donation to the lattice also the introduction of tin into the lattice facilitate the interstitial oxygen atoms migration within the anionic sub-lattice <sup>226</sup>.

##### 3.3.1.1 Nitrobenzene diazonium reduction

An electrochemical reduction was used to modify the ITO electrode surface. This was carried out in two steps using cyclic voltammetry, as mentioned in section 3.2.1.1. The first step included electrochemical deposition of a nitrobenzene group using 0.1 M tetrabutylammonium perchlorate (TBAP) and 2 mM of 4-nitrobenzene diazonium tetrafluoroborate solution dissolved in acetonitrile. This is explained by the attachment of nitrobenzene radical to the surface of the ITO electrode as illustrate in figure 3.4.

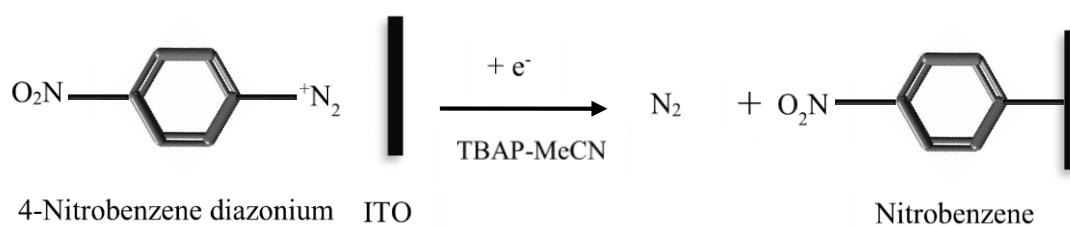


**Figure 3.4.** A schematic of the nitrobenzene group immobilization involving a one electron reduction where the nitrobenzene diazonium tetrafluoroborate cation is cleaved off to give nitrogen gas and leaves free radical in the para position on the benzene ring which covalently bonds to the electrode surface <sup>227</sup>.

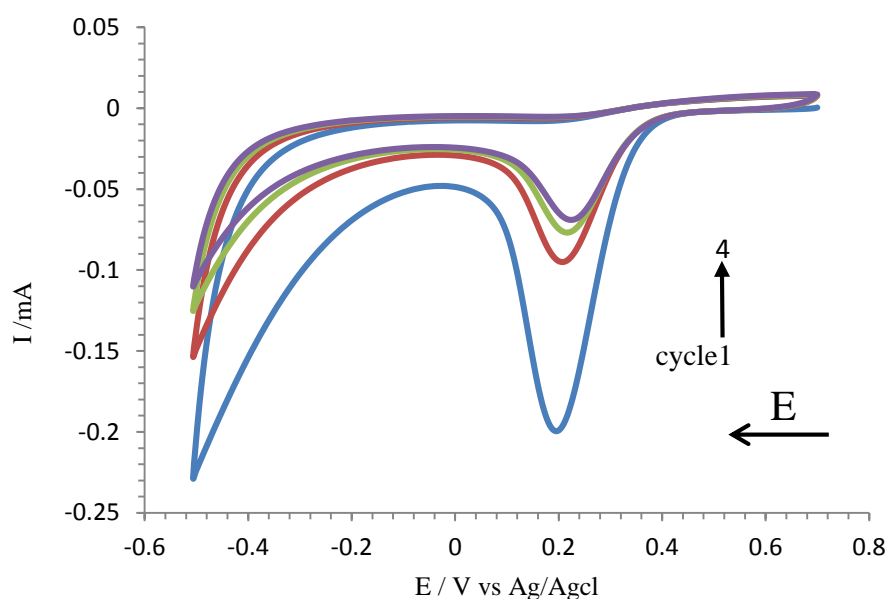


**Figure 3.5.** Cyclic voltammogram of the deposition of nitrobenzene on the ITO electrode using a solution of 2 mM 4-nitrobenzene diazonium tetrafluoroborate and 0.1 M tetrabutylammonium perchlorate in acetonitrile. The cyclic voltammetry run started at +0.7 V scanning down to -0.5 V and with a return sweep to +0.7 V performed over four scans with a scan rate of  $0.1 \text{ V s}^{-1}$  at room temperature. The reduction peak of +0.19 V refers to nitrobenzene deposition onto the electrode.

Figure 3.5 shows the cyclic voltammograms for reduction. It can be seen that the first cycle there is a peak relating to an irreversible reduction at +0.19 V. This can be attributed to the nitrobenzene deposition. It is assumed that after the first scan a monolayer is formed. The reduction of peaks after scan 2, 3 and 4 is due to the formation of a multilayer through the addition of nitrobenzene to the ortho position of the pre-deposited layer which blocks the electron transfer from the ITO electrode into the solution <sup>117</sup>. As can be seen in figure 3.6.

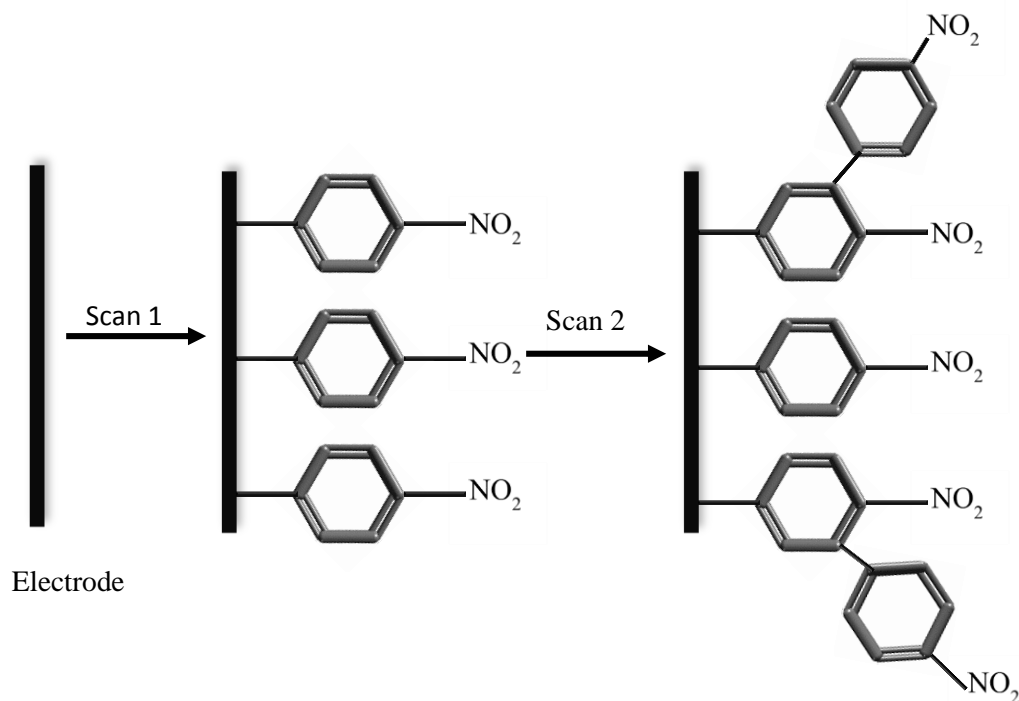


**Figure 3.6.** Schematic displaying the formation of nitrobenzene mono and multilayer.

The second step in the ITO electrode modification process consists of the reduction of nitrobenzene to aniline in protic solution using cyclic voltammetry. Ethanol was used to carry out the reduction process as a protons donor. This can be explained regarding the following mechanism mentioned in figure 3.7, which is a 6 proton and 6 electrons process. In the first step, a nitroso group is formed with a two proton and two electron reduction. Afterwards, this group forms a hydroxylamine with a two proton and two electron reduction, this reversely step where a nitroso group is formed. This causes the appearance of a peak at - 0.3 V. The final step includes another two protons, two-electron reduction to give the end product of this reaction which is aniline <sup>228</sup>.



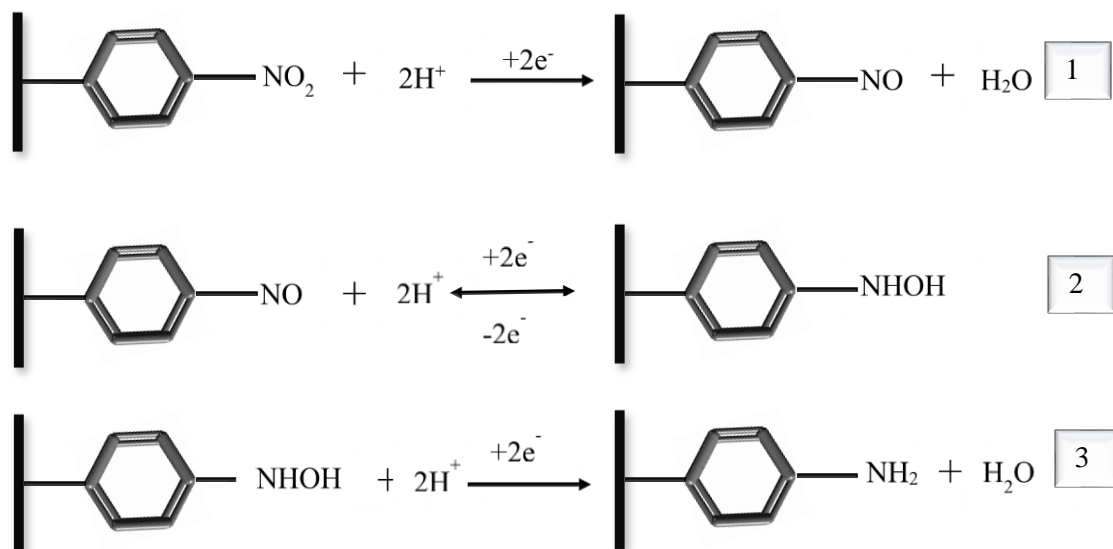


**Figure 3.7.** The proposed mechanism of the reduction of the nitro group to the amine group. Nitrobenzene undergoes an irreversible two electron, two proton reduction to give nitrosobenzene, two electrons, two proton reduction to give hydroxylamine group and two electrons, two proton reduction to give phenyl amine group<sup>228</sup>.

The voltammograms in figure 3.8 shows that for the first scan an irreversible reduction peak is obtained at - 0.87 V, which is attributed to the conversion of nitrobenzene to aniline after immersing the electrode into a solution of 0.1 M KCl: ethanol. Towards the completion of scan 1, there was an oxidation peak at - 0.3 V which can be attributed to the reverse step through a two electrons oxidation/reduction mechanism which is step 2 in figure 3.7<sup>228</sup>. For subsequent (2, 3, and 4) voltammograms there was a reduction due to self-inhibition through blockage of the electrode surface.

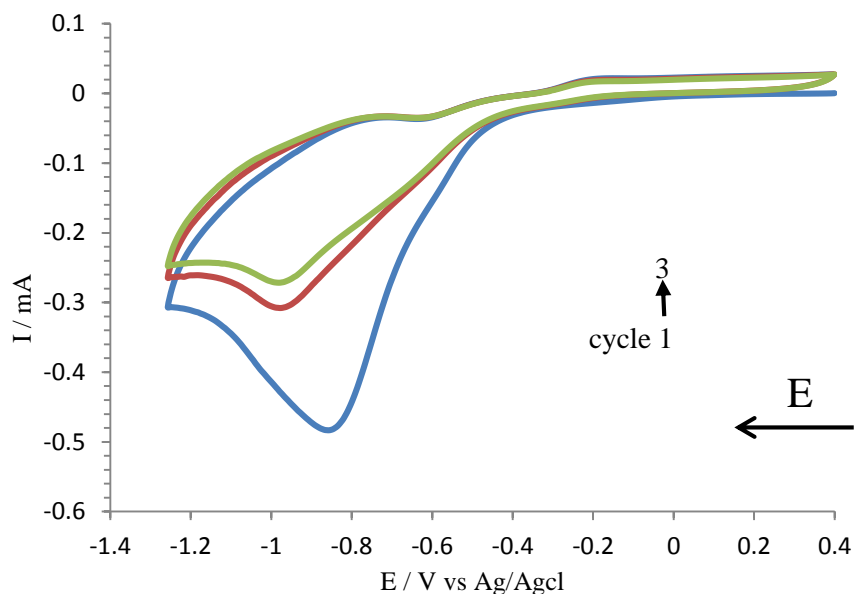


**Figure 3.8.** Voltammogram of the reduction of nitrobenzene to aniline. The cyclic voltammetry was run starting at + 0.4 V scanning down to - 1.25 V and with a return sweep to + 0.4 V performed over three oxidation-reduction voltammetry cycle scans with a scan rate of  $0.1 \text{ V s}^{-1}$  at room temperature. The reduction peak at - 0.87 V represents the conversion of nitrobenzene to aniline onto the ITO electrode surface in 90:10 0.1M KCl: ethanol solution <sup>228</sup>.

### 3.3.2 Ferrocene tagged antibody immobilization onto ITO electrode

As described previously for electrochemical detection the antibody had to be labelled with an electroactive tag. Ferrocenecarboxaldehyde (Fc-CHO) was utilized in a two stage process (see section 3.2.1.1.); the first stage (synthesis) involved the synthesis of Ab-Fc. This was achieved by the reaction between the Fc-CHO and the antibody free amino group to form an unstable Schiff base compound. This compound was further reduced by adding sodium borohydride to form a Schiff base <sup>229</sup>. The second stage (immobilization) involved the addition of activation solution consisting of EDC and

Sulfo-NHS prepared in PBS, which was used as a linker to bind the antibody to the ITO electrode surface *via* an amide linkage. The EDC compound activates the acid group by forming o-acylisourea, then by using the NHS-Sulfo, a fast transformation of the NHS-ester occurs, which interacts with the amino group on the electrode to form the amide linkage<sup>220</sup>, as shown in figure 3.1. This enables the acid groups residing at the base of the antibody heavy chain to bind to the electrode end up, i.e. in the desired position to interact with the antigen.

### 3.3.3 Characterization of ferrocene tagged anti-cortisol immobilized onto ITO electrode surface

To confirm the success of the immobilization process, cyclic voltammetry measurements were conducted for the modified ITO electrode surface without the antibody (blank) and with the tagged ferrocene antibody as described in section 3.2.1.2. Figure 3.9 shows the comparison between blank ITO electrode surface and modified ITO electrode surface with the tagged ferrocene antibody using cyclic voltammetry.

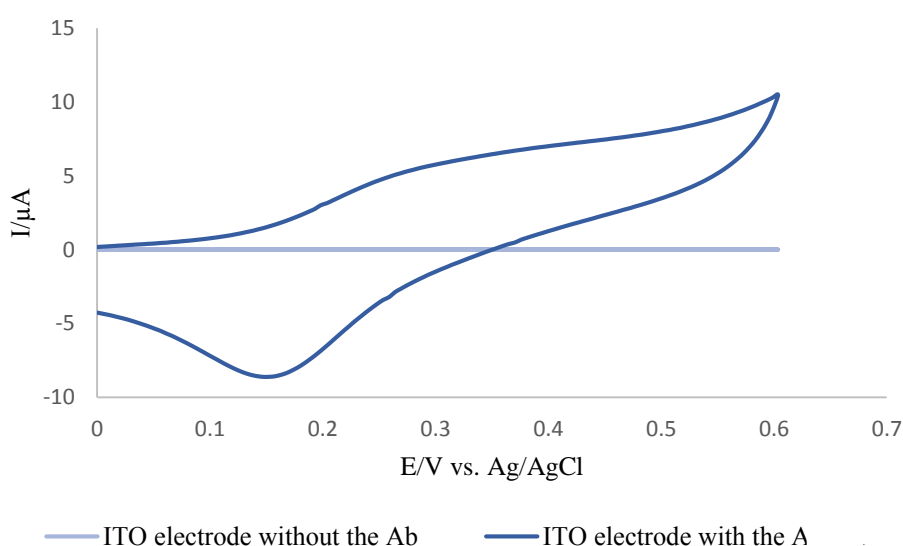


**Figure 3.9.** Cyclic voltammogram of the modified ITO electrode surface with and without the tagged ferrocene antibody. Scan rate  $100 \text{ mV s}^{-1}$ . 10 mM PBS was the solution used to conduct all the experiments.

An oxidation peak at + 0.25 V was seen for the ITO electrode with the tagged ferrocene antibody. This confirms the oxidation of the ferrocene to the ferrocenium cation on the ITO electrode surface with a reduction peak at + 0.15 V. As would expect no peak was seen for the blank ITO electrode.

In the next step, a range of different scan rates was investigated for the immobilization of the tagged antibody on the ITO electrode as shown in figure 3.10 from 10  $\text{mV s}^{-1}$  raising to 1000  $\text{mV s}^{-1}$ .

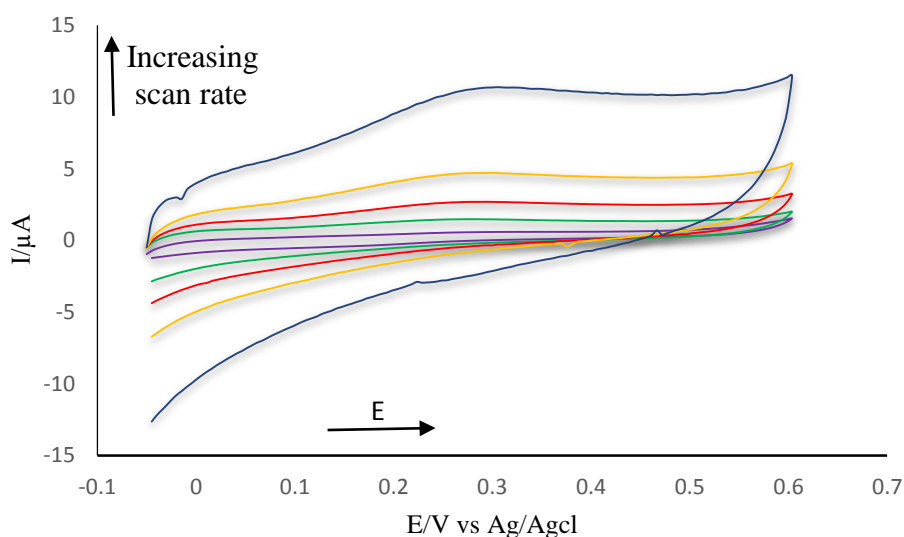


**Figure 3.10.** Cyclic voltammogram of ferrocene labelled anti-cortisol on the ITO electrode surface with various scan rates ranging from 10  $\text{mV s}^{-1}$  to 1000  $\text{mV s}^{-1}$ .

As can be seen from figure 3.10 an increase in the scan rate leads to an increase in current and an obvious oxidation peak at + 0.25 V confirm the ferrocenium cation oxidation from ferrocene on the ITO electrode with a reduction peak at + 0.15 V that is not clearly visible compared to the oxidation peak. Slower scan rate causes slower analysis time and small signals while faster scan rate effects the electrode kinetic where

ITO electrode resistance will contribute to the signal, therefore  $100 \text{ mV s}^{-1}$  was selected for all electrochemical immunoassay experiments.

### 3.3.4 Optimization of incubation time

To optimize the immunoassay protocol, the incubation time for the antigen needed to be studied (10, 15, 20, 30, 45 and 60 minutes) were chosen to keep a realistic time for lab-on-a-chip measurements, section 3.2.1.3.

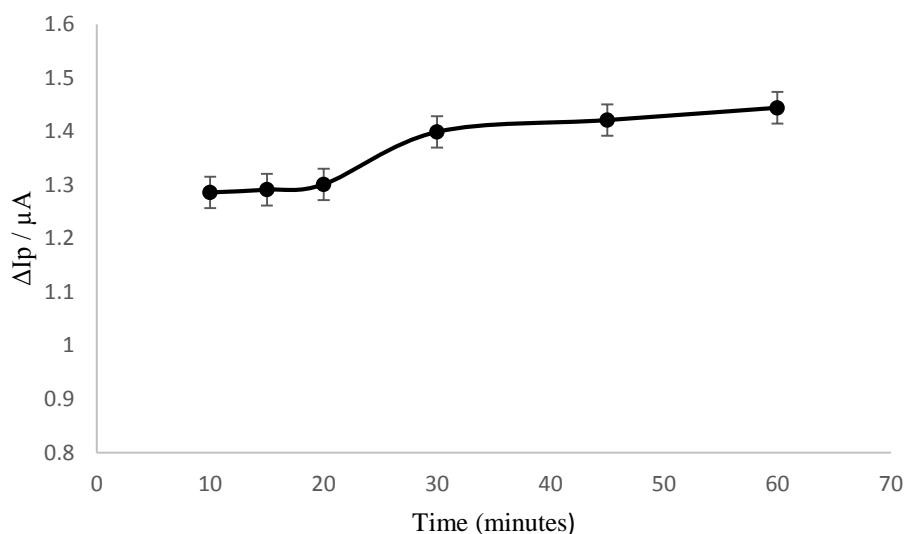
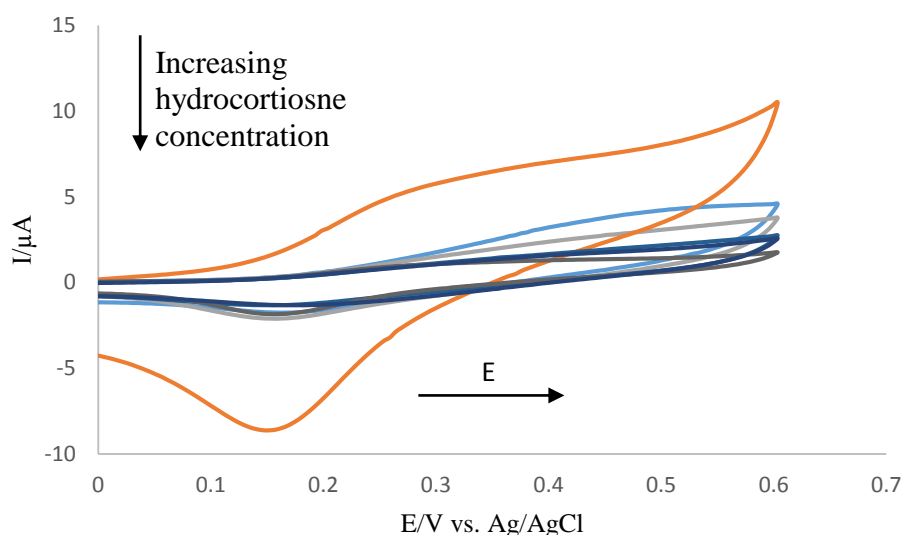


**Figure 3.11.** The graph indicates the change in current for 10, 15, 20, 30, 45 and 60 minutes incubation time for cortisol of  $50 \text{ ng ml}^{-1}$  respectively from cyclic voltammetry measurements. Scan rate  $100 \text{ mV s}^{-1}$ .

Figure 3.11 gives the effect of incubation time on the current signal by adding a fixed amount of cortisol  $50 \text{ ng ml}^{-1}$  to the ferrocene tagged cortisol immobilized onto the ITO electrode for the different time. It can be concluded that there was an increase in the current signal until 30 minutes after which the current signal began to plateau. Therefore 30 minutes was selected as the optimum incubation time to carry out the electrochemical immunoassay.

### 3.3.5 Electrochemical immunoassay using cyclic voltammetry (CV) and square wave (SWV) techniques

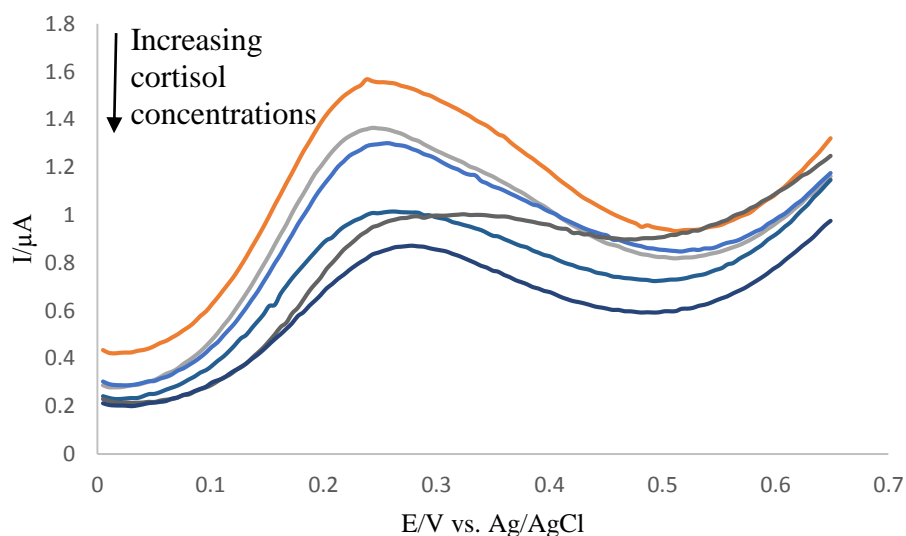
The addition of different concentrations of the antigens was then investigated to prepare calibrations using both CV and SWV techniques (mentioned in section 3.2.1.4.).



**Figure 3.12.** Cyclic voltammograms of the cortisol standard solutions ranging from (0.001 to 50 ng ml<sup>-1</sup>) on the ferrocene tagged anti-cortisol antibody modified ITO electrode for an incubation time of 30 minutes, with the orange line correspond to the blank. Scan rate 100 mV s<sup>-1</sup> and the measurements were conducted in 10 mM PBS.

Figure 3.12 represents the change in current for cyclic voltammetry which corresponds to the various addition of cortisol solutions to the ferrocene tagged anti-cortisol antibody immobilized on the modified ITO electrode. This figure shows the orange line representing the blank (without the addition of standard cortisol), which appears clearly to have an oxidation and reduction peaks at + 0.25 V and + 0.15 V respectively. A significant decrease in oxidation and reduction peaks were observed after the addition of cortisol and this continues as the cortisol concentrations increase. This is because of antibody paratop region bind to antigen epitope region with the association of primarily

electrostatic and hydrophobic interaction. In addition, van der Waals interaction and hydrogen bonding are involved in the antigen-antibody bound system. This lead to blocking out ferrocene moieties attached to the paratope where this causes an alteration in the ferrocene environment i.e. the ferrocene cannot further participate in potential voltammetry<sup>220</sup>.



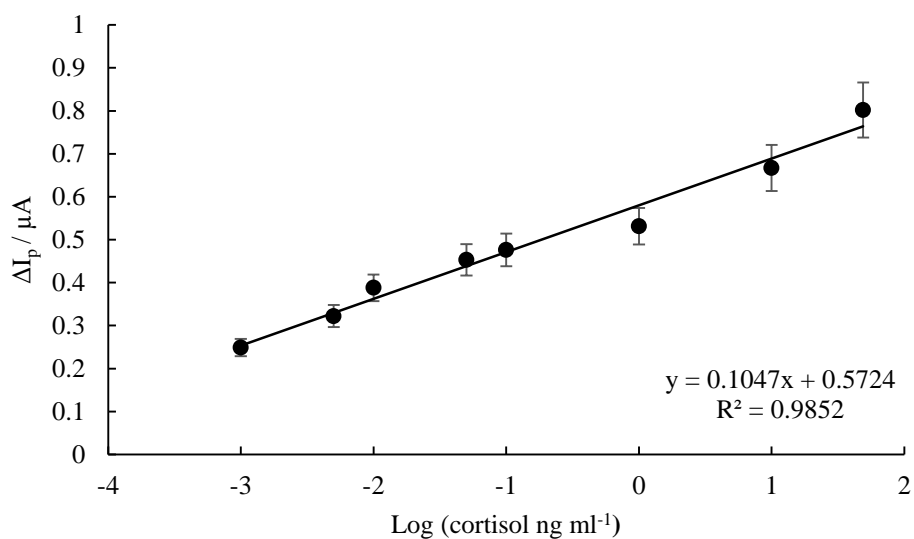
**Figure 3.13.** Square wave voltammograms presenting the effect of cortisol standard solutions with concentrations ranging from (0.001 to 50 ng ml<sup>-1</sup>) on the current signal after the addition to the ferrocene tagged anti-cortisol antibody attached to the modified ITO electrode. These waves represent the current signal before subtracting from the blank. Measurements were carried out in 10 mM PBS. The orange line represents the blank prior to the addition of cortisol, frequency 25 Hz, amplitude 1 mV.

Figure 3.13 shows the change in current for the standards using square wave voltammetry. It is noticeable that there is a clear peak at + 0.22 V with a drop in the current signal as the cortisol concentrations increase. The signal change was more noticeable with square wave voltammetry compared to cyclic voltammetry, and although the CV technique offers a full information about the system behavior the SWV

technique has the advantage of high sensitivity as described in section 1.2.8.1. Therefore SWV technique was chosen for the construction of the calibration curves.

### 3.3.6 Electrochemical calibration for cortisol and cortisone

In order to determine the concentration of cortisol and cortisone in biological samples (Zebrafish whole-body and artificial saliva samples), calibrations curves were constructed using the following concentrations (0.001, 0.005, 0.01, 0.1, 1, 10, 25, and 50 ng ml<sup>-1</sup>), using the procedure as described in section 3.2.1.4. The calibration was plotted using the signal change after the addition of antigen from the equation  $\Delta I_p = I_{Ab} - I_{Ag}$ , where  $I_{Ab}$  is the current before the addition of the antigen and  $I_{Ag}$  is the current after the addition of antigen.



**Figure 3.14.** Calibration curve of cortisol standard solutions with  $\Delta I_p$  current peak plotted against their concentrations. The error bar indicates standard deviation. ( $n = 3$ ). The measurements were done using the square wave technique. The frequency of 25 Hz and amplitude of 1 mV.

Figure 3.14 shows the standard cortisol calibration curve using square wave voltammetry, where the  $\Delta$  peak current ( $\Delta I_p$ ) is plotted against the log of concentrations



of cortisol The plot shows a linear correlation between (0.001-50 ng ml<sup>-1</sup>) which are within the standard range for cortisol and cortisone in both Zebrafish whole-body sample<sup>47</sup> and artificial saliva sample<sup>230</sup> with a correlation coefficient 0.9852. The limit of detection (LOD) was calculated and found to be 1.03 pg ml<sup>-1</sup>.

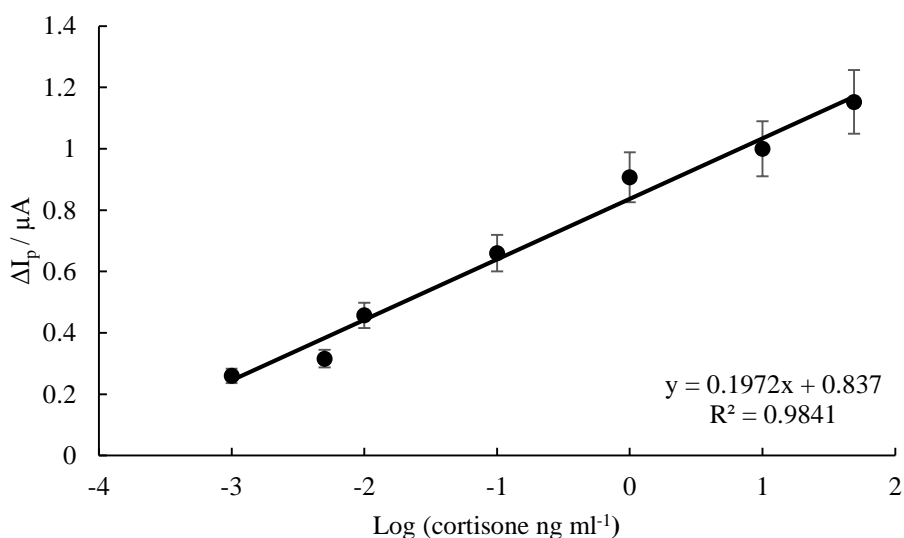


**Figure 3.15.** Calibration curve of cortisone standard solutions with  $\Delta I_p$  current peak plotted against their concentrations. The error bar indicates standard deviation ( $n = 3$ ). The measurements were done using square wave technique. The frequency of 25 Hz and amplitude of 1 mV.

A series of cortisone standards were prepared and measured as described in section 3.2.1.4 with figure 3.15 showing the calibration curve for cortisone. A linear trend was observed over the range that would be expected for cortisone levels in Zebrafish whole-body sample and artificial saliva sample. The  $R^2$  was slightly lower than for cortisol at 0.9841. The limit of detection was calculated and was found to be 0.68 pg ml<sup>-1</sup>.

### 3.3.7 Determination of biological samples using electrochemical immunoassay

Having established the system applicability to carry out an electrochemical immunoassay, the next step was to investigate this system in a biologically related matrix, the aim of this work was to determine the cortisol and cortisone in Zebrafish whole-body and artificial saliva samples as prepared in section 3.2.1.5.

#### ❖ Zebrafish whole-body sample

The level of Zebrafish in the whole-body sample was investigated to determine stress hormones. Researchers often use diethyl ether as an extraction solvent in preparation for detection by HPLC, GC, and LC to overcome the problems related to matrix interference. A comparison was made between measurements with and without the extraction procedure (see section 3.2.1.5). The results obtained are shown in figure 3.16.

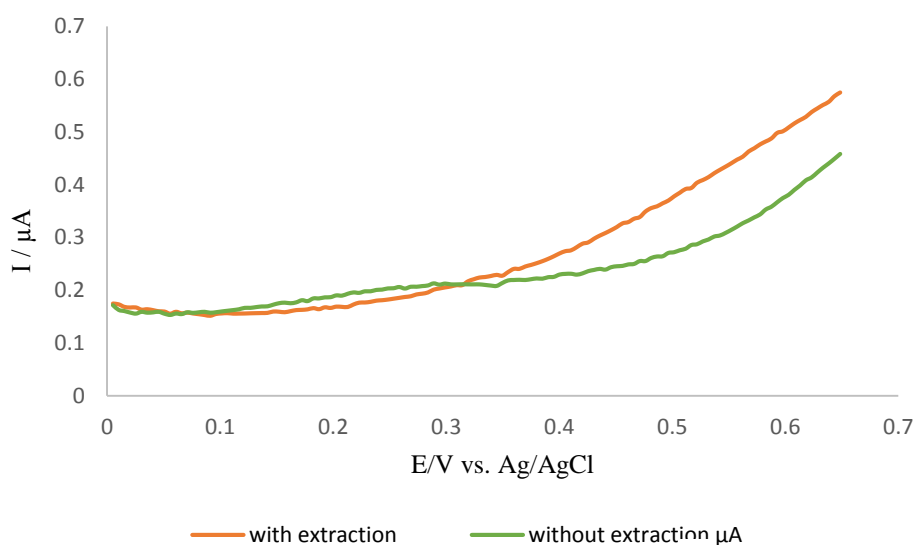


**Figure 3.16.** Square wave voltammogram showing the difference in current between Zebrafish whole-body sample before and after extraction with diethyl ether.

As can be seen from the above figure the two square wave voltammograms differ from each other, however, at the peak potential + 0.26 V there is a negligible difference for

both square wave voltammograms which shows the sensitivity and selectivity of the used procedure and allows the uses of the sample without the extraction. Also, there was a shift in the peak current to + 0.26 V from the observed from the buffer voltammogram at + 0.22 V, this can be attributed to the matrix used but the same trend is observed by decreasing the signal. Therefore and to minimize the number of steps which is one of targets aim of this thesis, the following experiments were done without the extraction.

Recovery and RSD values were calculated and summarized in table 3.1 for both cortisol and cortisone using single point standard addition method.

**Table 3.1.** The Recovery and RSD values of cortisol and cortisone standard solution spiked in the Zebrafish whole-body sample (n = 3).

Analyte	Concentration added( $\text{ng ml}^{-1}$ )	Recovery %	RSD %
Cortisol	50 $\text{ng ml}^{-1}$	87.7 %	1.12 %
Cortisone	10 $\text{ng ml}^{-1}$	82.6 %	2.22 %

From table 3.1 cortisol recovery was 87.7 % and cortisone was 82.6 %. Also, the values of the RSD was 1.12 % for cortisol and 2.22 % for cortisone respectively. The data were obtained from figures 3.14, 3.15 and 3.16. These results show the applicability of the immunoassay protocol followed by square wave detection for the determination of stress hormones in Zebrafish whole-body sample.

#### ❖ *Artificial saliva*

The second biological sample to be investigated was artificial saliva. The artificial saliva recipe was prepared as described in section 3.2.1.5 and spiked with cortisol

(10 ng ml<sup>-1</sup>) and cortisone (25 ng ml<sup>-1</sup>) and incubated for 30 minutes. These concentrations were chosen as they represent the maximum clinical concentration in artificial saliva to analyze the resulting data clearly.

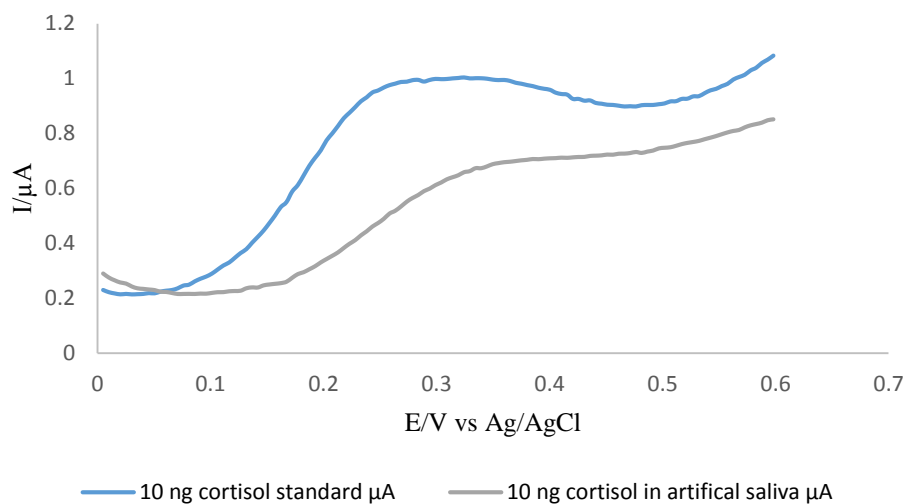


**Figure 3.17.** Shows square wave voltammogram for the artificial saliva spiked with 10 ng ml<sup>-1</sup> cortisol standard solution and compared it with 10 ng ml<sup>-1</sup> cortisol standard prepared in PBS. The comparison shows the shift in the peak from + 0.22 V to + 0.33 V.

A comparison was carried out between the standard cortisol solution 10 ng ml<sup>-1</sup> and artificial saliva spiked with 10 ng ml<sup>-1</sup> standard cortisol solution. It can be seen from figure 3.17 that there was a shift in the peak from + 0.22 V to + 0.33 V resulted from the matrix effect.

The possibility of stress hormones detection in a real sample using electrochemical immunoassay was achieved with the decrease in the current signal compared with the current related to the standard solution. A shift in the current voltammogram was observed which may attribute to the matrix effect. Table 3.2 summarize the data obtained from cortisol and cortisone.

**Table 3.2.** The recovery and RSD values of cortisol and cortisone standard solution spiked in the artificial saliva sample for three different electrodes.

Analyte	Concentration added( $\text{ng ml}^{-1}$ )	Recovery %	RSD %
Cortisol	$10 \text{ ng ml}^{-1}$	89.00 %	1.25 %
Cortisone	$25 \text{ ng ml}^{-1}$	88.49 %	1.70 %

Calculation for both recovery and RSD were done using data from figures 3.14, 3.15 and 3.17. The data gave a recovery of 89.00 % and 88.49 % for cortisol and cortisone respectively. For the RSD % values, it was 1.25 % for cortisol and more value for cortisone giving a value of 1.70 %.

For the comparison of the new method with the published method using electro-immunoassay, the new method offers a low-cost due to the anti-cortisol antibody immobilization process took place on the ITO electrode which considers less expensive from the gold electrode used in literature. In addition the newly developed biosensor was built on an ITO electrode while the published device was built on Whatman filter paper (which suffer from several disadvantages mentioned in section 1.5), this paper was coated with poly (styrene)-block-poly(acrylic acid) (PS67-b-PAA27) polymer and graphene nanoplatelets (GP) suspension to increase the sensitivity of the immune response while the proposed method gives the simplicity in building the device as same as sensitivity, with a LOD of  $1.03 \text{ pg ml}^{-1}$  showing that the proposed method is more sensitive from the published work where the obtained LOD was  $3 \text{ pg ml}^{-1}$  <sup>231</sup>.

Further studies were not carried out because of the complexity of incorporating of the electrochemical setup consisting of three electrodes (counter, reference, and working) with the open microfluidic setup.

### 3.4 Conclusions

Within this chapter, a successful new electrochemical immunoassay method was developed to detect and measure stress hormones (cortisol and cortisone) in two biological samples (Zebrafish whole-body and artificial saliva samples). This method depended on the reliable immobilization of the antibody onto an ITO electrode. The flat ITO electrode allows a uniform layer of nitro groups to be deposited leading to the antibodies being arranged in a uniform layer. In addition, the controllability of the antibody orientation by the attaching from the Fc region via an amide linkage resulted in high sensitivity.

The limit of detection (LOD) obtained for this procedure was  $1.03 \text{ pg ml}^{-1}$  for cortisol and  $0.68 \text{ pg ml}^{-1}$  for cortisone respectively. The correlation coefficient were 0.9852 and 0.9841 for cortisol and cortisone respectively with a linear concentration from ( $0\text{-}50 \text{ ng ml}^{-1}$ ) which covers the standard levels of stress hormones in both selected biological samples, Zebrafish whole-body and artificial saliva.

The incubation time was investigated and 30 minutes was found to be the optimum incubation time. This time would be acceptable for the LOC system as total process time can be determined within 35 minutes.

Although a sensitive and selective electrochemical assay has been developed, the incorporation of this assay with an open LOC system (which is the aim of this research) would be challenging. This can be explained from two point-of-view aspects. The first aspect is the open architectural design of the chip where the working electrode (ITO electrode) is used as the chip platform and the dichlorodimethylsilane and fumed silica suspension is deposited onto the electrode to fabricate the superhydrophobic surface with superhydrophilic patterns. This needs the elimination of reference and counter

electrodes which are connected to Potentiostat from the chip to facilitate the construction of an open microfluidic chip.

The second aspect is related to the reproducibility and accuracy of the assay incorporated onto an open chip where the coverage of the surface with superhydrophobic layer will significantly affect the electron transfer (as it will be explained in chapter 6).

Therefore an alternative protocol was investigated using chemiluminescence which is well known for its simplicity and sensitivity. Nevertheless, the electrochemical protocol could be used off-chip to determine the stress hormones without the need for complex sample preparation.

## **Chapter 4 Determination of cortisol and cortisone using chemiluminescence (CL) assay**

In this chapter, the electrochemically based antibody immobilization was used to perform environmentally and clinically relevant immunoassays for stress hormones biomarkers (cortisol and cortisone) using chemiluminescence detection.

### **4.1 Introduction**

The antibody electrochemical immobilization on the ITO electrode was found to provide reproducible and reliable results, hence this procedure was amended for chemiluminescence detection to meet the requirements of the lab-on-a-chip system.

Chemiluminescence is widely used in different fields due to its simplicity, sensitivity and low-cost optical requirements. A conventional chemiluminescence reaction is a luminol: hydrogen peroxide system, that can promote to give higher light emission by the use of catalysts which include either enzymes such as horseradish peroxidase<sup>232</sup> or metal catalysts such as ferrocenecarboxaldehyde<sup>233</sup> that contain iron (figure 4.1).

The higher signal is obtained as a result of the possibility of amplifying the analyte signal via analyte regeneration at the electrode, such that many photons are generated per analyte species. This strategy should yield an enhancement in the signal without increasing the background, thereby yield an improvement in detection limits<sup>233</sup>.



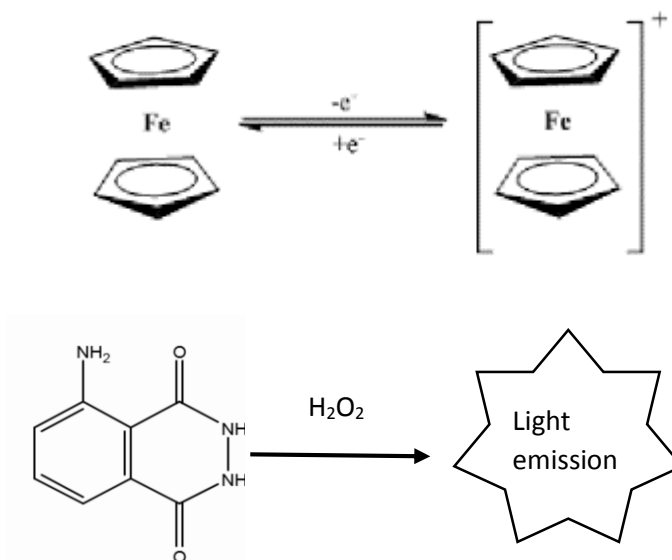


**Figure 4.1.** Schematic of redox reaction for ferrocene that can be oxidised to ferrocenium ion and thereby catalyze the luminol: hydrogen peroxide chemiluminescence reaction.

The mechanism include electrocatalysis of the luminol:hydrogen peroxide chemiluminescence reaction via ferrocene moiety at the ITO electrode where luminol oxidation was inhibited due to the coating onto the electrode that acts as barrier layers on electrodes, such that redox reactions that are inherently slow and/or that need close interaction of a redox molecule with an electrode surface are selectively inhibited (e.g. direct luminol electrooxidation reaction). In contrast, the electrochemical oxidation of ferrocene is allowed owing to ferrocene group hydrophobicity nature, which promotes interaction with a hydrophobic surface, also the overall rapid kinetics of the ferrocene-ferrocenium redox reaction<sup>233</sup>. In this way, it was possible to generate chemiluminescence emission via the ferrocene catalyst.

## 4.2 Experimental Procedures

### 4.2.1 *Preliminary investigations for signal change*

The first experiment was conducted by using the modified ITO electrode prepared in section 3.2.1.1 and immobilized anti-cortisol antibody was determined following the same protocol mentioned in section 3.2.1.2. The difference in the procedure for chemiluminescence was the need to convert the ferrocene attached to the antibody immobilized onto the modified ITO electrode to the ferrocenium cation. This was achieved in an electrochemical oxidation process, in which a cyclic voltammetry scan was carried out using PBS (10 mM) spotted onto the immobilized antibody circles (isolated by the adhesive stickers as described previously in chapter 2) starting from - 0.05 V up to + 0.6 V at scan rate  $10 \text{ mV s}^{-1}$ , this involved one scan.

A mixture of luminol (20 mM) and hydrogen peroxide (10 mM) was spotted onto the electrode (30  $\mu\text{l}$ ) and images were taken at selected times using the CCD camera, and an image of a blank ITO electrode (immobilized anti-cortisol antibody without the antigen) was also taken to subtract the blank from the sample. To investigate the antibody-antigen interaction, 30  $\mu\text{l}$  of 50  $\text{ng ml}^{-1}$  of antigen was added to the circle containing ferrocenium cation attached to the antibody immobilized onto the modified ITO electrode for one hour incubation time this was to provide the chance for the antibody and antigen interaction to occur in which any extent of signal change would be observed. Then it was washed with 0.1% Tween 20 (0.1 v/v) in PBS (10 mM) solution to effectively remove excess material from the electrode, the electrode was treated with bovine serum albumin (BSA) (1 %, w/v) in PBS (10 mM) for 30 minutes as it is considered sufficient time for blocking unoccupied sites on the ITO electrode. Then it was washed with 0.1% Tween 20 in PBS, afterwards a mixture of 30  $\mu\text{l}$  of 20 mM luminol and 10 mM hydrogen peroxide is added. Light intensity was calculated using

Image J software after the image was taken by a CCD camera and subtract from the blank.

#### **4.2.2 Stability**

The stability of the modified ITO electrode tagged with ferrocene was tested. Chemiluminescence measurements were taken immediately, after one day and after one week after oxidation to compare the results. The ITO electrodes were stored in the PBS until it was needed at 4° C.

#### **4.2.3 Optimization of Chemiluminescence variables**

Chemiluminescence experiments were conducted to evaluate the influence of luminol concentration, hydrogen peroxide concentration, incubation time and exposure time in order to achieve the maximum chemiluminescence immunoassay emission signal. Various concentrations (1, 5, 10, 20, 30 and 40 mM) of luminol were added to a fixed concentration 10 mM of hydrogen peroxide and the mixture was spotted onto the circle on the ITO electrode to determine the highest signal. After fixing the luminol concentration that gives the maximum signal, an alteration in hydrogen peroxide concentrations (1, 5, 10, 20, 30, and 40 mM) was tested with the optimum concentration of luminol. The incubation time for the antigen was done varying incubation times (5, 10, 15, 20, 30, 45, and 60 minutes) and the chemiluminescence signal was taken after the addition of the luminol and hydrogen peroxide mixture to the circles to choose the optimum. The optimization of exposure time was done by mixing the optimum concentrations of luminol and hydrogen peroxide for a time interval from (50-700 seconds). The luminol and hydrogen peroxide mixture volume for all conducted experiments was 30 µl.

#### **4.2.4 Chemiluminescence immunoassay protocol**

Cortisol stock solution was prepared as in section 3.2.1.4 to give a solution of 100 ppm, from which the standards were prepared in PBS (10 mM) to give working standards (0.001-50 ng ml<sup>-1</sup>). For the chemiluminescence immunoassay protocol, the procedure mentioned in 4.2.1 was done to each concentration. The same above procedure was used but with the addition of sequence standards (0.001-50 ng ml<sup>-1</sup>) for cortisone.

#### **4.2.5 Stress hormones determination in real sample**

In order to determine stress hormones in a real sample including Zebrafish whole-body and artificial saliva samples prepared in section 3.2.1.5, the procedure in section 4.2.1 was repeated for both samples individually and for both hormones (cortisol and cortisone).

#### **4.2.6 Interferences**

The samples selected for analysis were Zebrafish whole-body and artificial saliva samples, these have complex matrices which despite the high selectivity of the antibody-antigen reaction may have constituents that would interfere with the results. The species selected to investigate were cortisol, cortisone, prednisolone, 11-deoxycortisol, progesterone, corticosterone, and testosterone with a standard concentration of 50 ng ml<sup>-1</sup> which was chosen to be greater than the higher concentration of each compound expected to exist naturally within these samples<sup>47, 230</sup> and the procedure outlined in section 4.2.1 was done with the addition of different antigen.

Each compound stock solution was prepared by dissolving 5 mg in ethanol and making the volume up to 50 ml in PBS (10 mM) to give a concentration of 100 ppm, then serial dilutions were made to prepare 50 ng ml<sup>-1</sup> working solution using volumetric flasks (5 ml).

#### ***4.2.7 Comparison study with standard Enzyme-Linked Immunosorbent Assay (ELISA)***

To evaluate the new method, an ELISA standard method was performed using a human salivary cortisol assay kit (ab 154996- cortisol ELISA kit, Abcam, UK). The ELISA assay was carried out as per the instructions provided within the ELISA kit supplied by the company, where 25 µl of the standards and samples were added to the wells, then 200 µl of 1X cortisol-HRP was added and incubated for one hour at 37° C. After the incubation, the wells were washed three times with 300 µl of deionized water and then a 100 µl of 3,3',5,5'-tetramethylbenzidine (TMB) substrate was added and left for exactly 15 minutes at room temperature in the dark in order to be catalysed by HRP to produce blue coloration. The final addition was 100 µl of stop solution to terminate the color development and produces a color change from blue to yellow. The absorbance of the sample was measured at 450 nm within 30 minutes of stop solution addition using a labtech international plate reader and the manufacturer's software supplied with the instrument was used to analysis the data. A non-competitive immunoassay was carried out to determine the analyte (see section 1.2.6).

## 4.3 Results and discussion

### 4.3.1 Oxidation of Ab-Fc on the surface

The first step to carry the chemiluminescence procedure was the oxidation of the ferrocene to ferrocenium cation using cyclic voltammetry. This was carried out as described in section 4.2.1, the scan started at - 0.05 V with a sweep to + 0.7 V without a return sweep to cover one scan using 10 mM PBS solution as can be seen in figure 4.2. The scan rate was 10 mV s<sup>-1</sup> to enable more time at a set potential which would kinetically favour the ferrocene oxidation.

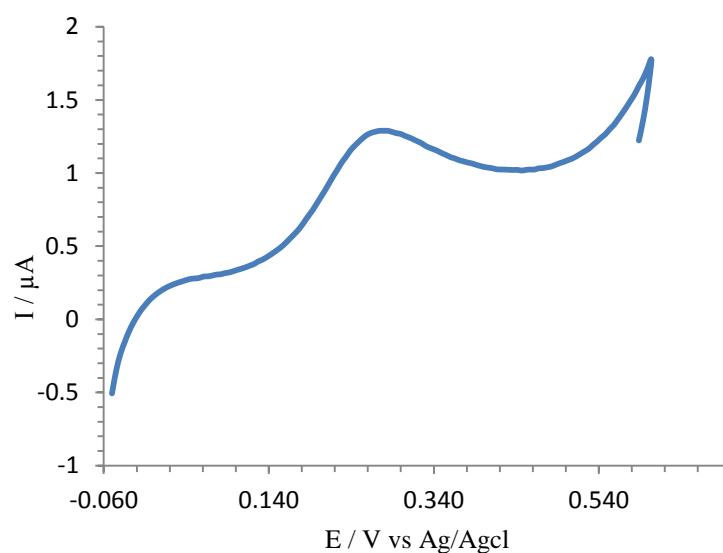


**Figure 4.2.** Cyclic voltammogram for the oxidation of ferrocene tagged antibody to ferrocenium cation that catalyses luminol/hydrogen peroxide showing an oxidation peak at + 0.25 V. Scan rate 10 mV s<sup>-1</sup>.

The oxidation peak at + 0.25 V shown in figure 4.2 represents the ferrocene oxidation to ferrocenium cation. This which is essential for the chemiluminescence reaction to occur with the iron located in the ferrocenecarboxaldehyde acting as a catalyst for luminol/hydrogen peroxide<sup>234</sup>.

### 4.3.2 Investigation of Chemiluminescence Signal

In this work, the chemiluminescence signal was measured using charge coupled device (CCD) camera fitted with an 8 mm high-resolution pixel lens and image J was used for analysis of the data. The entire experimental setup can be seen in figure 4.3. To investigate the chemiluminescence signal effect before and after the addition of an antigen, a preliminary experiment was conducted by adding 30  $\mu\text{l}$  of luminol and hydrogen peroxide mixture to the ferrocene tagged antibody before and after the incubation of 50  $\text{ng ml}^{-1}$  cortisol hormone which was chosen because it is the highest concentration it will give a clear chemiluminescence signal.

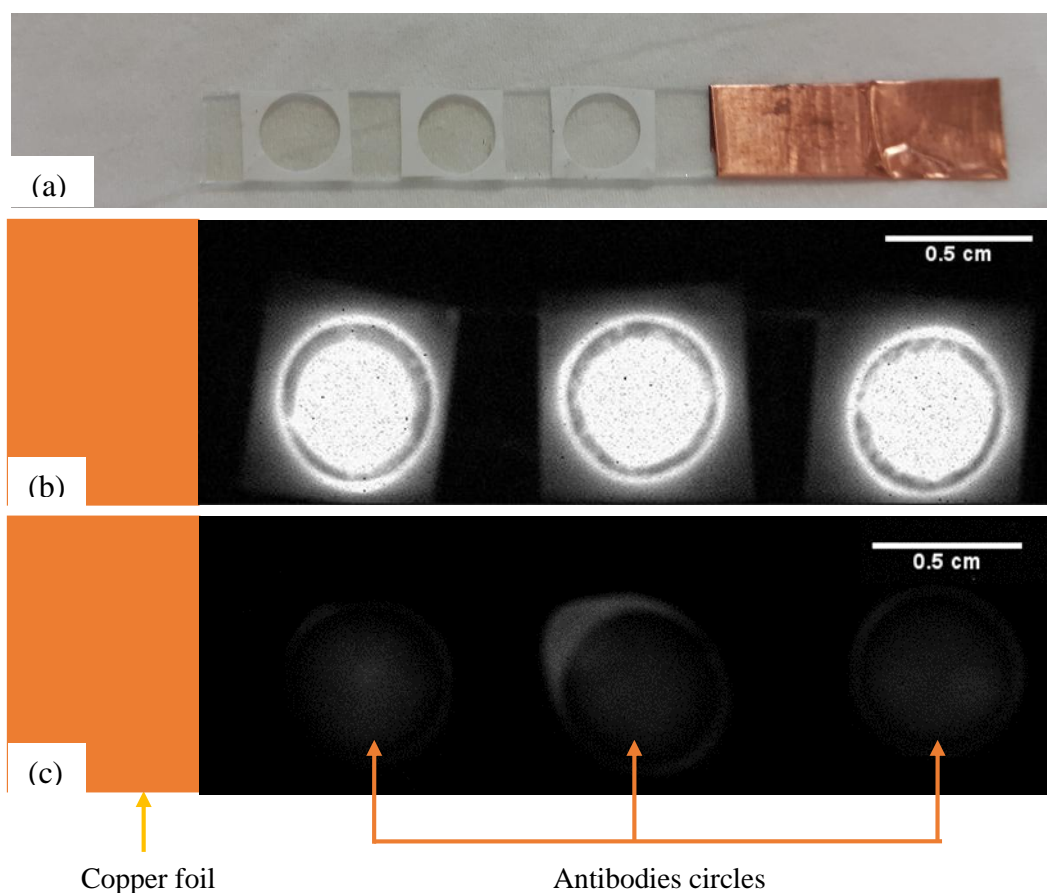


**Figure 4.3.** (a) Image of an ITO electrode taken by digital camera showing the three separated circle containing immobilized ferrocene tagged anti-cortisol antibody, (b) chemiluminescence images of blank (immobilized ferrocene tagged antibody) after the addition of luminol/hydrogen peroxide mixture, (c) chemiluminescence image of the blank after the incubation of 50  $\text{ng ml}^{-1}$  cortisol hormone. Scale bar for image A is 5 cm, B and C are 0.5 cm.

Figure 4.3 demonstrated the applicability of ferrocene to be used as catalyst in the luminol/hydrogen peroxide reaction, where figure 4.3 (a) is a photograph of the ITO electrode with the immobilised antibody, (b) shows the chemiluminescence image taken by CCD camera for the oxidised ferrocene tagged anti-cortisol antibody after the addition of luminol/hydrogen peroxide mixture and before the addition of antigen, (c) shows the chemiluminescence image taken by CCD camera for oxidised ferrocene tagged antibody after the addition of antigen ( $50 \text{ ng ml}^{-1}$ ). As can be seen, a decrease in the chemiluminescence signal from 227.3 RLU for the blank to 21.5 RLU after the addition of the antigen ( $50 \text{ ng ml}^{-1}$  cortisol standard solution) was observed. The analyte chemiluminescence signal was obtained from subtracting the blank chemiluminescence signal from the analyte chemiluminescence signal to enable the detection of an analyte using this method.

The chemiluminescence emission signal is highest without the addition of the antigen as the oxidized ferrocene is reduced and luminol is oxidized emitting the chemiluminescence light. The signal will then decrease when the antigen binds to the antibody by affecting the electron transfer at the surface (blocking effect) that reduces the efficiency of the ferrocenium catalyst<sup>220</sup> yielding a lower chemiluminescence signal.

Experiments were carried out to investigate the reproducibility and effectiveness of the ferrocene tagged antibody immobilization on the ITO electrode surface. The previously described experiment was repeated on three circles within the same electrode (intra-assay) and different circles on different electrodes (inter-assay) individually for four electrodes. The results are summarized in Table 4.1.



**Table 4.1.** The precision of immobilisation ferrocene tagged antibody on the ITO electrode surface.

Within electrode	Circle 1 RLU	Circle 2 RLU	Circle 3 RLU	Average $\pm$ STD	RSD%
Electrode 1	253.04	252.97	249.69	251.90 $\pm$ 1.91	0.75
Electrode 2	237.33	218.81	233.49	237.30 $\pm$ 3.79	1.61
Electrode 3	213.02	199.19	191.11	200.13 $\pm$ 9.52	4.76
Electrode 4	225.69	219.34	215.08	220.03 $\pm$ 5.33	2.42
Final results				227.34 $\pm$ 5.14	2.38

The data shown in table 4.1 for the RSD % for three circles within the same electrode was between 0.75 - 4.76 %, whereas the RSD% between different circles of different electrodes was 2.38 %. This shows that there is no significant difference in chemiluminescence signal between circles on the same electrode and circles on different electrodes.

### ***4.3.3 The stability of ferrocenium cation***

One key factor needs to be tested in order to apply this procedure to lab-on-a-chip system, is the stability of the ferrocene oxidation which was tested by capturing images for the three circles containing the ferrocene tagged anti-cortisol antibody before oxidation, directly after the ferrocene oxidation by luminol/hydrogen peroxide mixture, one day and one week after the ferrocene oxidation and it was kept in 10 mM PBS solution during for the whole period of experiment at 4° C.

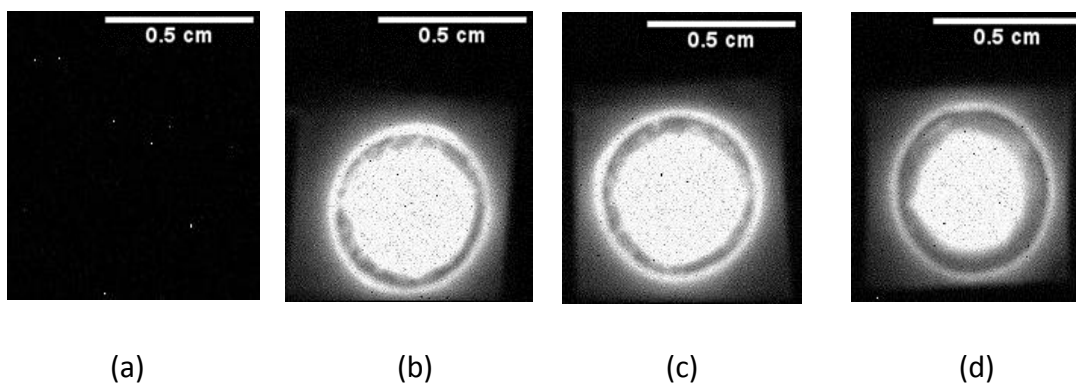


**Figure 4.4.** Images of chemiluminescence signal related to ferrocene tagged antibody, (a) characterise the ferrocene tagged antibody before ferrocene oxidation, (b) immediately after the oxidation using the mixture of luminol/hydrogen peroxide, (c) characterise the ferrocene tagged antibody after one day of ferrocene tagged antibody oxidase, (d) after one week of ferrocene oxidation. The scale bar is 0.5 cm.

Simplicity is the key point in constructing a lab-on-a-chip system, therefore, the stability of ferrocene tagged antibody after oxidation for the long term of time is necessary to ensure the applicability of the ITO electrode containing the ferrocene without the need of oxidising the ferrocene before every chemiluminescence measurements. Figure 4.4 shows good and promising results for ferrocene stability, where (a) no light emission was observed because the ferrocene in its neutral form does not catalyse the luminol/hydrogen peroxide reaction (b) immediately after oxidation which shows an increase in the signal up to 224.01 RLU as expected because of ferrocenium cation action as a catalyst following the below reaction scheme (figure 4.5)<sup>235</sup>.

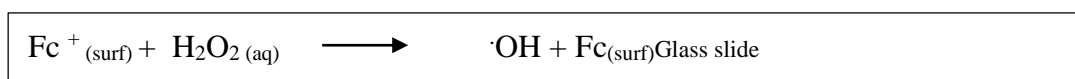


**Figure 4.5.** Reaction scheme for the catalytic effect of ferrocene on the luminol/hydrogen peroxide reaction.

Where the ferrocenium cation breaks down the hydrogen peroxide creating hydrogen radical which reacts with luminol and emitting the chemiluminescence signal, (c) and (d) shows a minor decrease in the chemiluminescence measurement giving an RLU of 220.12 and 196.65 for the ferrocene tagged antibody after oxidation and storage in 10 mM PBS for one day and one week respectively which does not impact the analysis.

#### ***4.3.4 Optimization of operating variables***

The effect of different operating conditions (luminol concentration, hydrogen peroxide concentration, incubation time and exposure time) on the chemiluminescence emission signal were investigated to achieve the maximum chemiluminescence signal. The latter variables optimization studies were illustrated graphically in figures 4.6, 4.7, 4.8 and 4.9 which showed their chemiluminescence signals were strongly affected by these different operating conditions.

##### ***❖ Influence of luminol concentration***

Experiments were conducted by the procedure outlined in section 4.2.3 and were carried out to evaluate the influence of different luminol concentrations ranging from (1 - 40 mM) on the chemiluminescence signal. The amount of chemiluminescence emission signal during the series of investigations were determined by subtracting the blank (the oxidised ferrocene tagged anti-cortisol antibody immobilized onto the modified ITO without the addition of luminol/hydrogen peroxide mixture) from the samples (the ferrocene tagged anti-cortisol antibody immobilized onto the modified ITO electrode after the addition of luminol/hydrogen peroxide mixture).

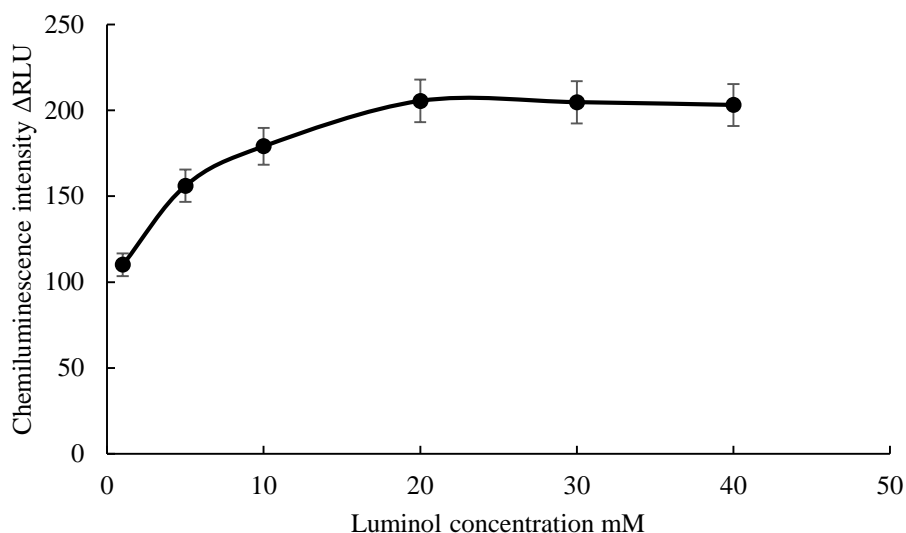


**Figure 4.6.** A calibration curve showing the influence of luminol concentrations while keeping the concentration of hydrogen peroxide constant (10 mM) on the chemiluminescence emission signal.

Chemiluminescence experiments were carried out at different luminol concentrations ranging from (1- 40 mM) as cited in figure 4.6, where increasing the concentration of luminol lead to the increase of chemiluminescence signal between (1- 20 mM) where 20 mM luminol concentration reaches the optimum signal of 205.4 RLU. Subsequent reading shows a decrease in the curve to 203.7 RLU for 30 mM reaching 202.1 RLU for 40 mM because luminol produced self-absorption of the emitted radiation<sup>236</sup>. Therefore 20 mM luminol was conducted for all experiments within this chapter.

#### ❖ *Influence of hydrogen peroxide concentration*

To study the effect of hydrogen peroxide concentrations on chemiluminescence emission signal different concentrations in the range of (1- 40 mM) were tested.

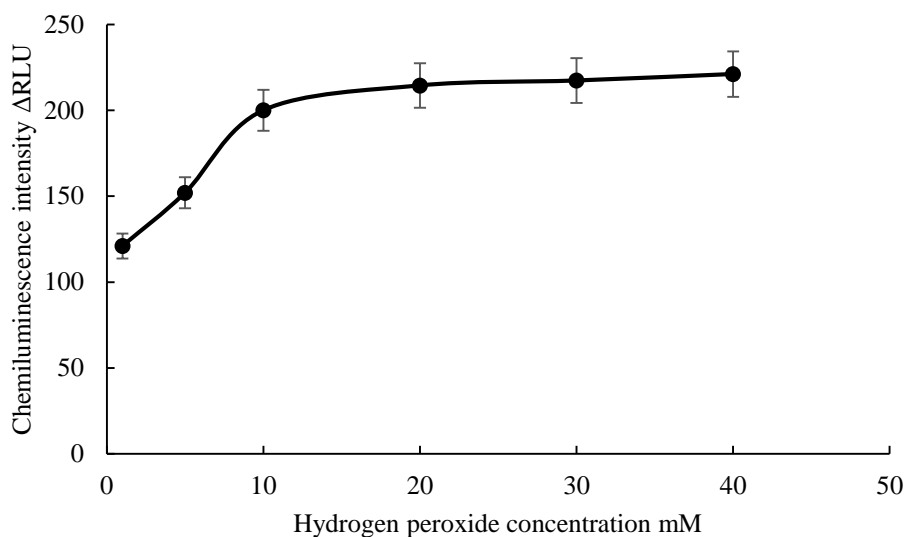


**Figure 4.7.** Graph showing the influence of hydrogen peroxide concentration while keeping the concentration of luminol constant (20 mM) on the chemiluminescence emission signal.

A similar trend to luminol changing concentrations was observed for hydrogen peroxide changing concentrations (as shown in figure 4.7). It was observed as a general trend that there was an increase in chemiluminescence emission signal with the increase in concentrations up to 10 mM. Above that concentration the chemiluminescence emission signal was seen to stabilise up to 40 mM, therefore 10 mM hydrogen peroxide was chosen as an optimum concentration.

#### ❖ *Influence of incubation time*

The incubation time of antibody-antigen interaction was tested according to the procedure mentioned in section 3.2.1.3 with chemiluminescence as a detector following the procedure of chemiluminescence detection outlined in section 4.2.1.

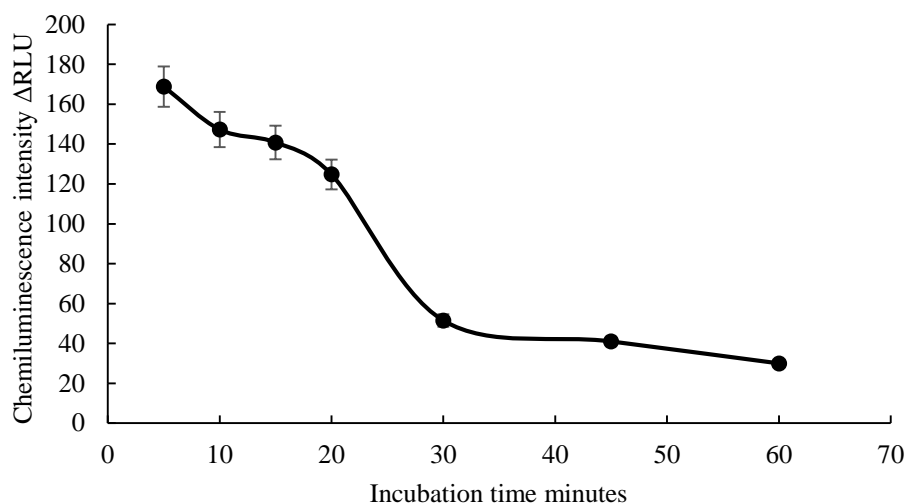


**Figure 4.8.** The graph shows the effect of different incubation time on the chemiluminescence signal after the addition of 30  $\mu$ l of 50 ng ml<sup>-1</sup> of cortisol standard solution.

As expected the incubation time of antibody-antigen interaction was 30 minutes as same as for electrochemical immunoassay as shown in figure 4.8 where the chemiluminescence RLU increased to 168 RLU at 5 minutes, this may be due to insufficient time to complete the interaction between the antibody and the antigen. Then the signal reached the lowest signal between 30 and 60 minutes with no significant difference, therefore 30 minutes was chosen for further experiments.

#### ❖ *Influence of exposure time*

Exposure time is a fundamental parameter for an economical lab-on-a-chip system. It can be defined as the length of time that an image required to be exposed to the CCD camera to acquire the highest chemiluminescence signal. Consequently, it is important to study its influence on the chemiluminescence signal of over time intervals from (50 to 700 seconds).

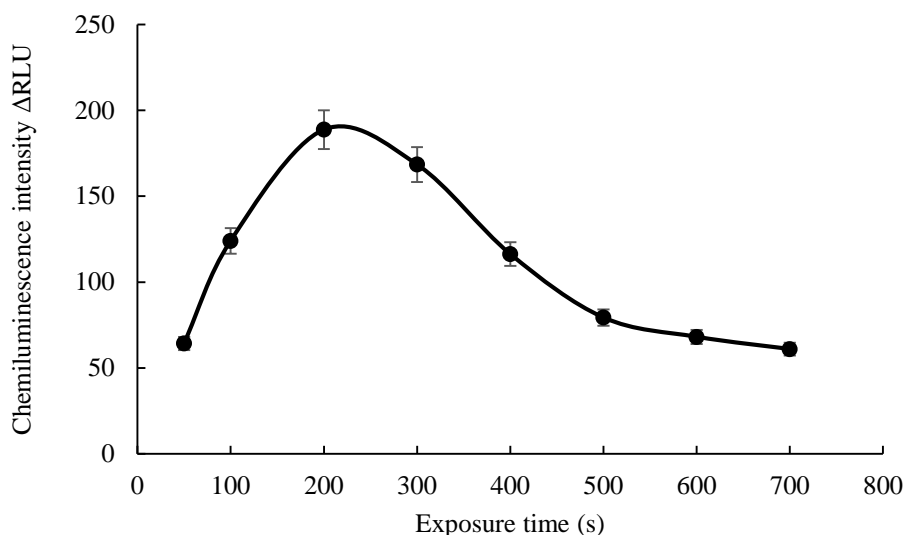


**Figure 4.9.** The graph for exposure time optimisation after the addition of luminol (20 mM) and hydrogen peroxide (10 mM) mixture over the time interval from (50- 700 seconds) showing the highest chemiluminescence signal at 200 seconds, therefore, it was adopted for chemiluminescence experiments.

Figure 4.9 shows that the chemiluminescence emission signal initially increased with exposure time up to 200 seconds and after this time the chemiluminescence signal decreases this is because while the image is still taken, the chemical reaction is established at the same time. Therefore, 200 seconds was deemed more than sufficient to establish the optimum chemiluminescence signal and used in all subsequent studies.

#### **4.3.5 Calibration curve**

To determine cortisol and cortisone calibration curves were obtained by preparing a set of standards solutions at concentrations ranging from (0 - 50 ng ml<sup>-1</sup>) and the chemiluminescence immunoassay was performed as described in section 4.2.4.

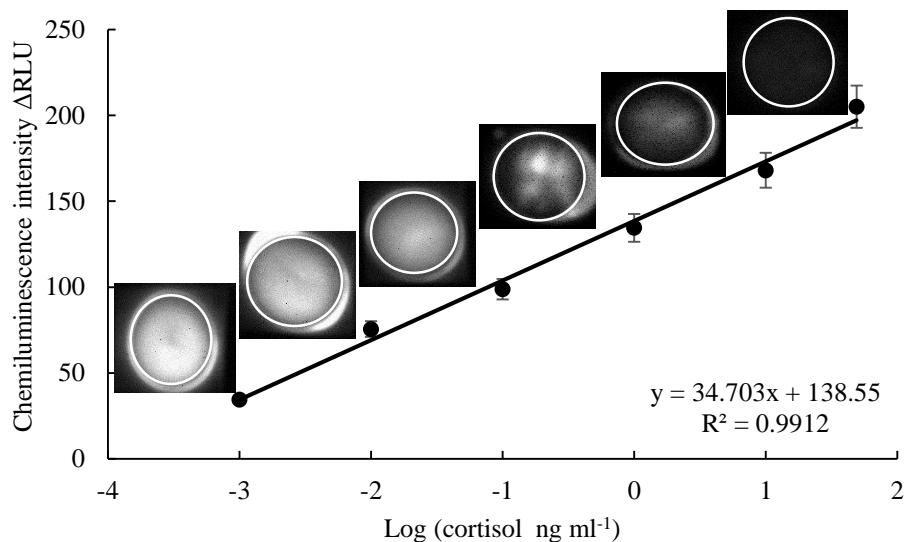


**Figure 4.10.** Calibration curve of cortisol standard solutions with concentrations from (0 - 50 ng ml<sup>-1</sup>). Standards plotted against the ΔRLU emission response, insert in the figure chemiluminescence image of each standard cortisol solution.

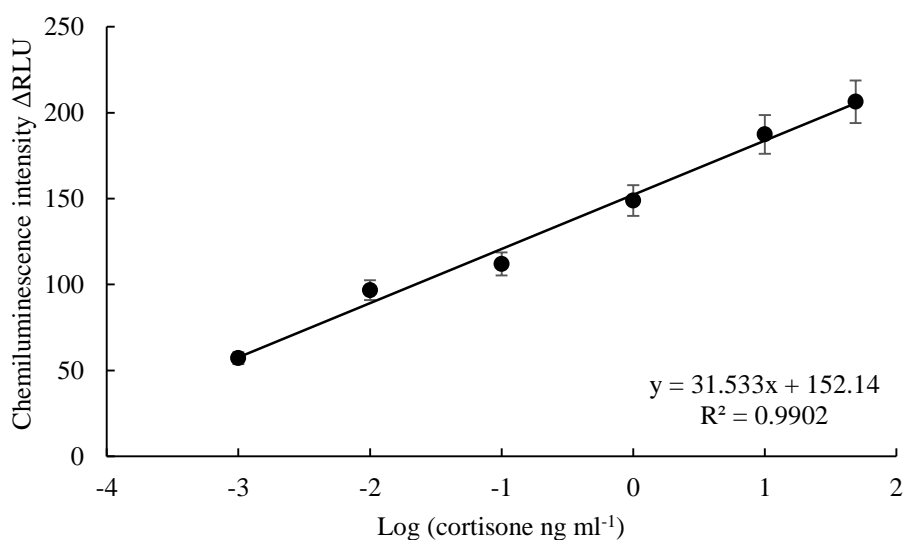


**Figure 4.11.** Calibration curve of cortisone standard solutions with concentrations from (0 - 50 ng ml<sup>-1</sup>). The standards RLU signal was plotted against the concentrations of the cortisone standard solutions.



As expected the  $\Delta$  RLU (resulted from subtract the RLU values of the blank without the addition of the antigen from the RLU values after the addition of an antigen) increased with the increase of standard solutions concentrations (figure 4.10 and 4.11) giving a linearity over the range required to analyse the target analyte in real sample and with correlation coefficient of 0.9912 and 0.9902 for cortisol and cortisone respectively. Table 4.2 present the figure of merit calculated for both cortisol and cortisone.

**Table 4.2.** Analytical figures of merit for cortisol and cortisone using chemiluminescence immunoassay.

Analyte	Correlation coefficient	Linearity	LOD (pg ml <sup>-1</sup> )
Cortisol	0.9912	34.703 x + 138.55	0.47
Cortisone	0.9902	31.533 x + 152.14	0.34

The limit of detection for cortisol and cortisone were 0.47 and 0.34 pg ml<sup>-1</sup> and the results were found to better compared to that obtained from electrochemical immunoassay described in chapter 3 where a limit of detection of 1.03 pg ml<sup>-1</sup> and 0.68 pg ml<sup>-1</sup> were obtained for cortisol and cortisone respectively.

#### ***4.3.6 Determination of target analyte in Zebrafish whole-body and artificial saliva samples***

Further experiments were carried out to determine the concentration of stress hormones in a real sample including Zebrafish whole-body and artificial saliva samples, this was done by the addition of 1 ml of cortisol standard solution (50 ng ml<sup>-1</sup>) to both samples individually.

#### ❖ *Zebrafish whole-body sample*

Zebrafish whole-body sample was prepared according to the procedure mentioned in section 3.2.1.5 taking in consideration the extraction method. Measurements were done with and without the extraction procedure as shown in figure 4.12 that shows chemiluminescence emission of (a) real sample spiked with 1 ml of 50 ng ml<sup>-1</sup> of cortisol standard solution and the extraction method was done giving an RLU of 22.4, (b) real sample spiked with 1 ml of 50 ng ml<sup>-1</sup> without extraction with RLU of 29.0. A clear observation is that was a decrease in the light intensity for real sample with extraction and without extraction compared with the standard solution of cortisol that gave an RLU of 21.5. As was shown from chapter 3 that the use of the sample without the extraction is acceptable due to the minor change in the chemiluminescence signal as in the electrochemical signal decrease.

An observation of white round edge for the reaction cycle which can be explained by “coffee ring effect” because of solution evaporate more quickly at the edges than at the center. Therefore the remaining solution at the center will move outward in an attempt to fill the caps, this movement creates concentrated layers forming a dense ring<sup>237</sup>.

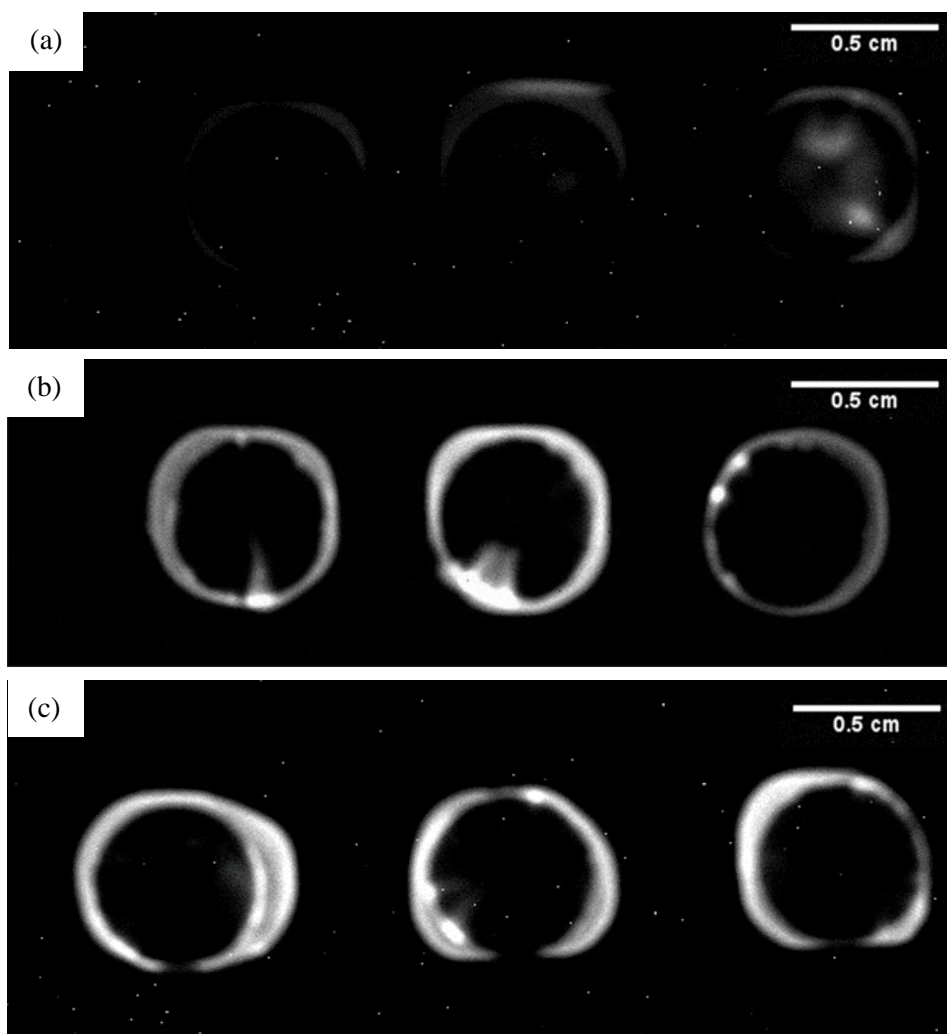


**Figure 4.12.** Chemiluminescence image of Zebrafish whole-body sample spiked standard cortisol solution ( $50 \text{ ng ml}^{-1}$ ) added to ferrocene anti-cortisol antibody immobilized onto modified ITO electrode (a) without extraction, (b) with extraction and (c) fish sample without the addition of standard and without extraction. Scale bar is 0.5 cm.

As a result, the single point standard addition method was done using two samples; one spiked with  $50 \text{ ng ml}^{-1}$  standard solution (without extraction) (figure 4.12 (b)) and the other was the real sample without the addition of a standard solution (without extraction) (figure 4.12 (c)), the data obtained was used to calculate the recovery and RSD for both cortisol and cortisone as summarized in table 4.3.

**Table 4.3.** The Recovery and RSD values of cortisol and cortisone standard solution spiked in the Zebrafish whole-body sample (n = 3).

Analyte	Concentration added( $\text{ng ml}^{-1}$ )	Recovery %	RSD %
Cortisol	50	91.0 %	1.25
Cortisone	10	90.0 %	2.00

The data obtained from table 4.3 indicates the good recovery for both hormones where cortisol recovery was 91.0 % and cortisone was 90.0 %. Also the values of the RSD ranging between 1.25 % and 2.0 % for cortisol and cortisone respectively. These results show the applicability of the immunoassay protocol followed by chemiluminescence detection for the determination of stress hormones in Zebrafish whole-body sample. Comparing and interpreting Zebrafish whole-body sample cortisol values from diverse researches should be done considering different environmental conditions and procedures that can easily effect on the cortisol values. The new procedure was compared with ELISA technique obtaining an LOD of  $0.27 \text{ ng ml}^{-1}$  and  $R^2 = 0.99^{47}$ , while using the capillary electrophoresis and UV-visible absorbance with plasma Zebrafish sample the obtained LOD was ( $0.2 - 2 \text{ ng ml}^{-1}$ ) and the recovery was (81 – 109 %) <sup>238</sup>. As mentioned in chapter one, both methods provide high sensitivity but high cost materials and sophisticated instruments restrict their use in biosensor fabrication compared with the new method which require a portable CCD camera and black box for measurements and an ITO electrode to perform the immunoassay which simplify the method and reduce cost to approximately 9 or 10 pounds for the immunoassay and approximately (100-120 pounds) for the entire chemiluminescence device including the CCD camera, black box and image J requirements for the detection and analysis.

❖ *Artificial saliva*

Artificial saliva recipe preparation mentioned in 3.2.1.5 was used to prepare the saliva which was spiked with  $10 \text{ ng ml}^{-1}$  cortisol and  $25 \text{ ng ml}^{-1}$  cortisone standard solutions and the resulted solutions were incubated for 30 minutes to be measured using chemiluminescence as a detector. Figure 4.13.



**Figure 4.13.** Represent the signal after the addition of artificial saliva spiked with cortisol standard solution  $10 \text{ ng ml}^{-1}$ . The signal was decreased due to the reaction between the antibody and antigen that restrict the Fc moiety from its role as an oxidising agent for luminol and hydrogen peroxide reaction. The scale bar is 0.5 cm.

The data obtained from cortisol and cortisone were summarized in table 4.4.

**Table 4.4.** The Recovery and RSD values of cortisol and cortisone standard solution spiked in the artificial saliva sample for three different electrodes.

Analyte	Concentration added( $\text{ng ml}^{-1}$ )	Recovery %	RSD %
Cortisol	10	92.59 %	2.04 %
Cortisone	25	90.73%	1.98%

From figure 4.13 and table 4.4 the recovery was calculated giving a recovery of 92.59 % and 90.73 % for cortisol and cortisone respectively. Another statistical parameter was calculated which was the RSD % which was 2.04 % of cortisol and less

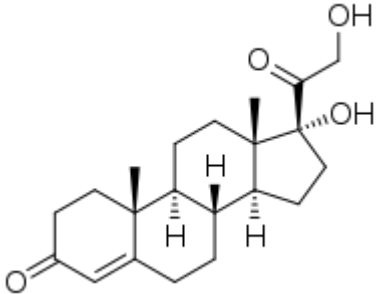
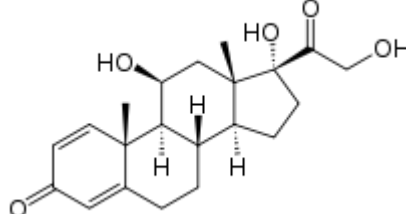
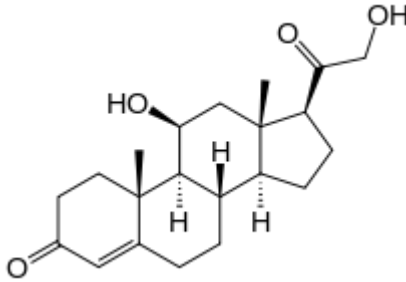
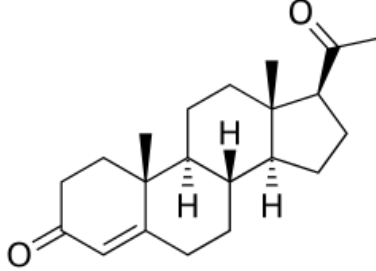
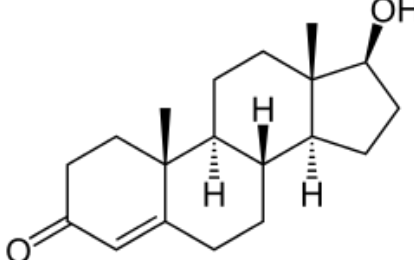
value for cortisone giving a value of 1.98 %. The obtained results from the immunoassay using as a chemiluminescence detector present a good applicability to be used in open microfluidic system. To be compared with other literature researchers which show an  $R^2 = 0.92$  (compared with the new method which gave an  $R^2$  of 0.9912) and a range between (0.4 - 11.3 ng ml<sup>-1</sup>). The proposed method in this thesis shows a reduction in cost and time compared to literature method which uses alkaline phosphatase-labeled anti-cortisol antibody (ALP-labeled antibody) by using a special kit (alkaline phosphatase labelling kit) while for the new method the attached ferrocene which is cheaper than ALP catalyze the luminol/hydrogen peroxide reaction to give the chemiluminescence signal<sup>37</sup>.

#### **4.3.7 Interferences**

To investigate the effect of any compounds in the Zebrafish whole-body sample and human saliva sample on the chemiluminescence measurements, interference experiments were conducted. As the antibody-antigen interaction is very selective the main interferences are likely to have similar structures (table 4.5) which could interact with the anti-cortisol and anti-cortisone antibodies immobilized onto the modified ITO electrode resulting in false results. 50 ng ml<sup>-1</sup> of cortisol, cortisone, 11- deoxycortisol, prednisolone, corticosterone, progesterone, and testosterone standard solutions were prepared as mentioned in section 4.2.6.

Three ITO modified electrode were prepared as previously and were spotted with 30  $\mu$ l of each compound with incubation time of 15 minutes and the chemiluminescence signal was measured after the addition of a mixture of 20 mM luminol and 10 mM hydrogen peroxide and kept for 200 seconds as for the analysis of the species of interest using optimum conditions to acquire the chemiluminescence images as these are the optimum conditions for cortisol and cortisone chemiluminescence measurements.

**Table 4.5.** Compounds have a similar structure to the cortisol and cortisone.

Compound	Structure
11-Deoxycortisol	 <p>The structure of 11-Deoxycortisol is a steroid nucleus with a ketone group at C3, a double bond between C4 and C5, and a hydroxyl group at C17. It lacks the hydroxyl group at C11 and the side chain at C17 found in cortisol.</p>
Prednisolone	 <p>The structure of Prednisolone is a steroid nucleus with a ketone group at C3, a double bond between C4 and C5, a hydroxyl group at C11, and a side chain at C17 consisting of a hydroxyl group, a ketone group, and a hydroxymethyl group.</p>
Corticosterone	 <p>The structure of Corticosterone is a steroid nucleus with a ketone group at C3, a double bond between C4 and C5, a hydroxyl group at C11, and a side chain at C17 consisting of a ketone group and a hydroxymethyl group.</p>
Progesterone	 <p>The structure of Progesterone is a steroid nucleus with a ketone group at C3, a double bond between C4 and C5, and an acetyl group at C17.</p>
Testosterone	 <p>The structure of Testosterone is a steroid nucleus with a ketone group at C3, a double bond between C4 and C5, and a hydroxyl group at C17.</p>

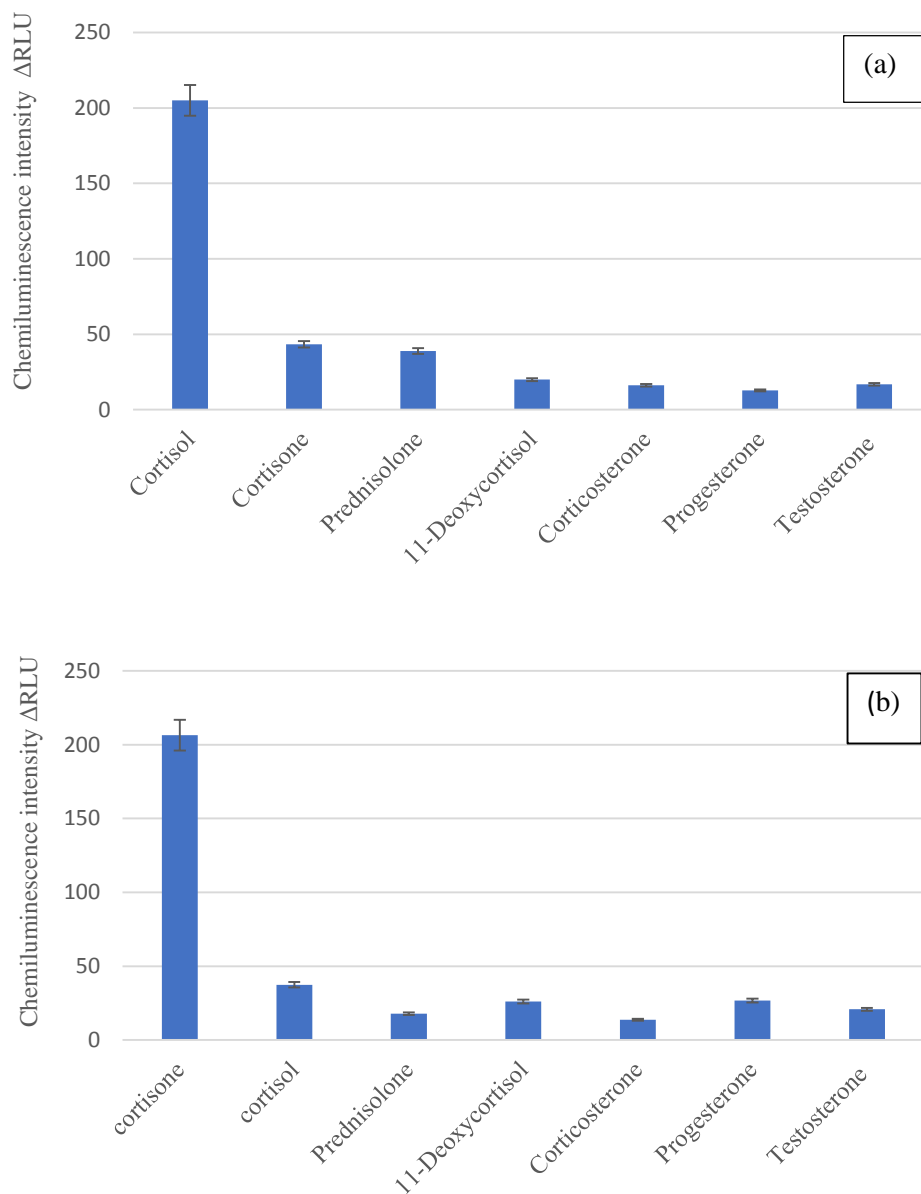


**Figure 4.14.** A column chart specifies the similar structure compounds potential interference with (a) ferrocene tagged anti-cortisol antibody and (b) ferrocene tagged anti-cortisone antibody after the addition of  $50 \text{ ng ml}^{-1}$  of these compounds (cortisol, cortisone, prednisolone, 11-deoxycortisol, corticosterone, progesterone, and testosterone), the incubation time was 30 minutes and the luminol and hydrogen peroxide concentrations were 20 and 10 mM respectively to mimic the cortisol and cortisone optimum conditions.



As can be seen from figure 4.14 (a) cortisone, prednisolone, 11-deoxycortisol, corticosterone, progesterone, and testosterone have very little inference with the anti-cortisol antibody where the RLU for these compounds ranging from (12 - 38) except for cortisone the RLU was 43 but with the consideration to cortisol RLU which was 205. It can be said that the presence of these compounds does not impact on the adopted immunoassay in this thesis. Figure 4.14 (b) shows also the effect of the similar compounds on the ferrocene tagged anti-cortisone and as expected there was a minor interference effect from these compounds with slightly more effect from cortisol with 37 but this inference can be considered negotiable compared to cortisone RLU of 206.42. These experiments were done according to 50 ng ml<sup>-1</sup> for each compound which exceeds normal levels found in Zebrafish whole-body and saliva samples.

The results obtained show good selectivity respecting the idea of the interaction of cortisol and cortisone to the anti-cortisol and anti-cortisone antibodies respectively without the possibility of incorrect results from the compounds that exist in the samples and may interfere.

#### **4.3.8 Commercial ELISA kit**

To evaluate the immunoassay protocol used in this thesis, a comparison with a reference method must be done. Stress hormone is usually tested with a traditional ELISA assay which is performed in the majority of hospital service laboratories. Therefore, it was decided to test the stress hormones using a commercial ELISA and compare the results with the immunoassay protocol using the procedure mentioned in the section 4.2.7.

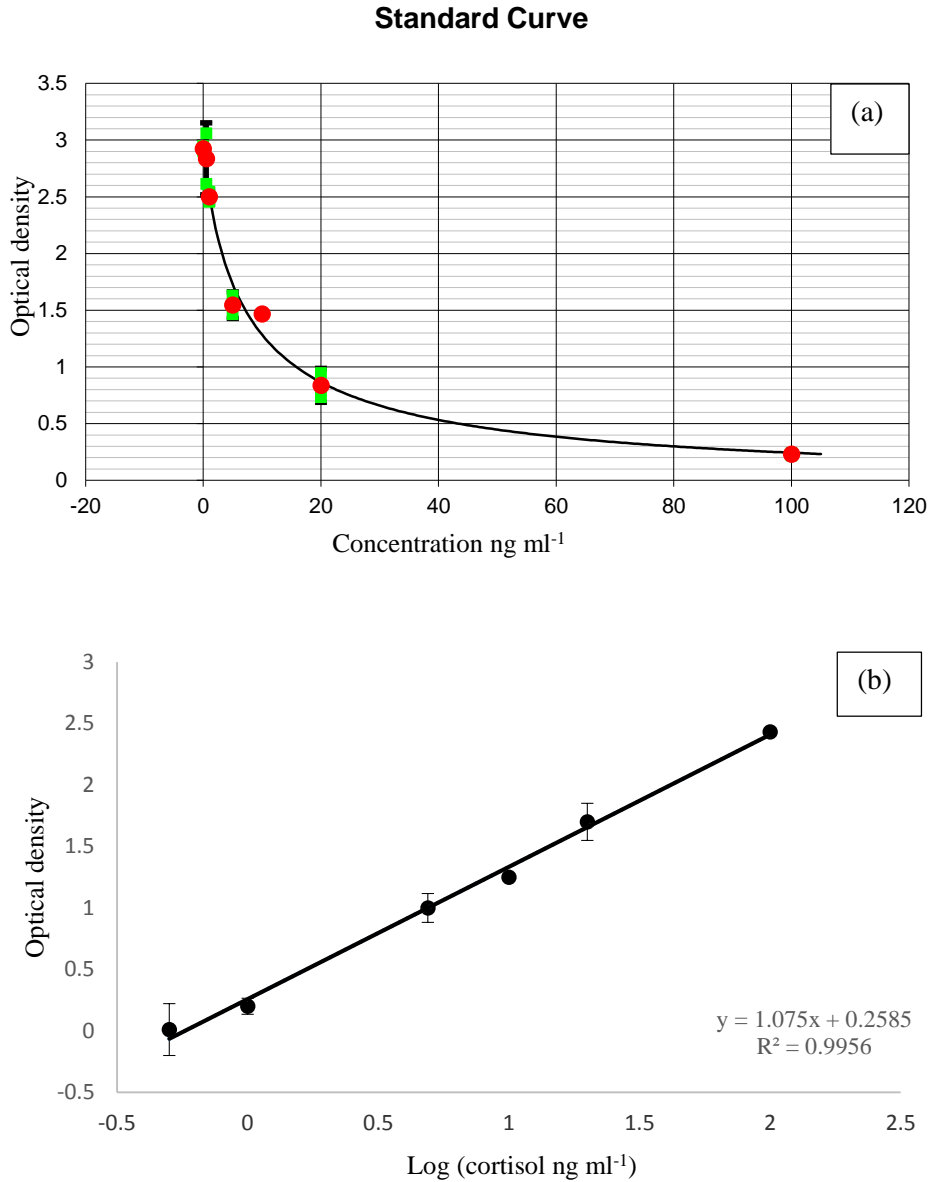


**Figure 4.15.** Calibration curves showing (a) the change in the optical density with the increase of cortisol concentration where the red points indicate the cortisol concentrations and the green points are the error bar for each concentration, (b) the increase in optical density with a linear trend after subtracting the blank signal from the sample signal.

Figure 4.15 (a) and (b) gives the relationship between the optical intensity signal and the standardized concentrations of cortisol. It can be observed that the optical intensity signal increase with the increase of the concentration of the cortisol to give a linear

calibration curve with  $R^2$  of 0.995. The Zebrafish whole-body sample was tested giving a concentration of  $44.56 \text{ ng ml}^{-1}$  (with extraction) and  $46.78 \text{ ng ml}^{-1}$  (without extraction) which confirm the results obtained by electrochemical immunoassay and chemiluminescence immunoassay to omit the extraction procedure and the use of sample only without any additional steps.

There was a good agreement with the proposed method where  $R^2$  for cortisol was 0.991 compared with  $R^2$  for cortisol using ELISA kit was 0.995 with an LOD of  $0.12 \text{ ng ml}^{-1}$  ( from the data sheet provided by the Abcam company). This applied also for the concentration obtained by the standard method (ELISA) mentioned above compared with the chemiluminescence immunoassay concentration ( $47.86 \text{ ng ml}^{-1}$ ). As a result, it can be concluded from the results obtained from the conventional tests that the development of a sensitive chemiluminescence immunoassay for stress hormone was achieved.

#### **4.4 Conclusion**

A new inexpensive rapid chemiluminescence method has been developed by the applicability of the ferrocene to be used as a catalyst through a chemiluminescence approach, where the ferrocene converts to ferrocenium cation immobilized onto the modified ITO electrode using cyclic voltammetry technique. The stability of the oxidase antibody on the electrode was investigated and the results showed high stability after oxidation over one week which simplify the proposed protocol. Also, optimum conditions including luminol concentration, hydrogen peroxide concentration, incubation time and exposure time were found to be 20 mM, 10 mM, 30 minutes and 200 seconds respectively.

Calibration curves for both cortisol and cortisol were constructed and give LOD at 0.47 and 0.34  $\text{pg ml}^{-1}$  for cortisol and cortisone with 0.9912 and 0.9902 correlation coefficient which indicates a high sensitivity of this method compared with the square wave used a detection which gave a LOD at 1.03 and 0.68  $\text{pg ml}^{-1}$  with correlation coefficient of 0.9869 and 0.9841 for cortisol and cortisone respectively. The device constructed during this research has shown to outstanding the ELISA test for detection of cortisol by more than two order of magnitude. These figures can be compared to the LOD for ELISA of 0.12  $\text{ng ml}^{-1}$ .

Potential interferences were examined and the obtained results confirmed the selectivity of this protocol. A comparison with commercial ELISA kit was performed to make a clear assessment of the chemiluminescence immunoassay where the limit of detection was lower than the ELISA kit, in addition, the chemiluminescence instrumentation decreased the cost for the determination of stress hormones.

The promising results obtained from the chemiluminescence immunoassay protocol encourage the construction of a device that combines between sensitivity, simplicity, and selectivity of chemiluminescence immunoassay with the automated, cost and time reduction advantages of microfluidics. Open microfluidics using wettability properties was chosen due to the advantages that this technique provide over the closed microfluidics. This includes the easy delivery and optical observation of reagents and samples added to the chip. Omission the need of mechanical components such as mixers, valves, etc because fluid flow is mainly due to capillary or gravity forces. Also, reduction in device fabrication is achieved by applying the ITO electrode as an open microfluidic platform without the need for complex and cost consuming process for closed microfluidic fabrication as it will be detailed in next chapter.

## **Chapter 5 Fabrication of open microfluidic chip using wettability**

In this chapter, experiments into the application of an open microfluidic platform for the determination of stress hormones were performed. ITO glass solid substrates were made superhydrophobic by depositing hydrophobic fumed silica particles on them using the dip coating method (see section 2.2.3). The wetting properties, quality, and stability of the coatings were investigated and the dip coating conditions optimised. Microfluidic chips of different designs were fabricated by making superhydrophilic patterns on superhydrophobic substrates by using UV/ozone lamp irradiation. Through the use of appropriate photo-masks water flow was confined in the superhydrophilic pattern and this was investigated by direct and fluorescent microscopy observations.

### **5.1 Introduction**

The different aspect of solid wetting and its importance for open microfluidics have already been discussed in chapter 1. The continuous open microfluidic approach adopted in the present study relies on the aqueous solution flow being confined in a superhydrophilic pattern on a superhydrophobic surface. In this work, superhydrophobic substrates were prepared by depositing hydrophobic fumed silica particles on smooth ITO glass electrodes.

Fumed silica, also known as pyrogenic silica as it produced from flame pyrolysis of silicon tetrachloride or quartz sand. The resulted compound have chainlike, branched, three-dimensional secondary particles which agglomerate into tertiary particles<sup>239</sup>. Fumed silica particles were selected because they have excellent mechanical and thermal stability and are commercially available. In addition, they are inexpensive and their wetting properties can be tuned by chemical or other means. The particles were deposited on the ITO electrode by dip coating to benefit from the simplicity of this

method which is capable of producing a uniform thin layer on solid surfaces<sup>240</sup>. The fabrication of superhydrophilic patterns was achieved using different photo-masks with the aid of a UV/ozone lamp (figure 5.1) in an attempt to construct an open microfluidic chip for lab-on-a-chip analysis.

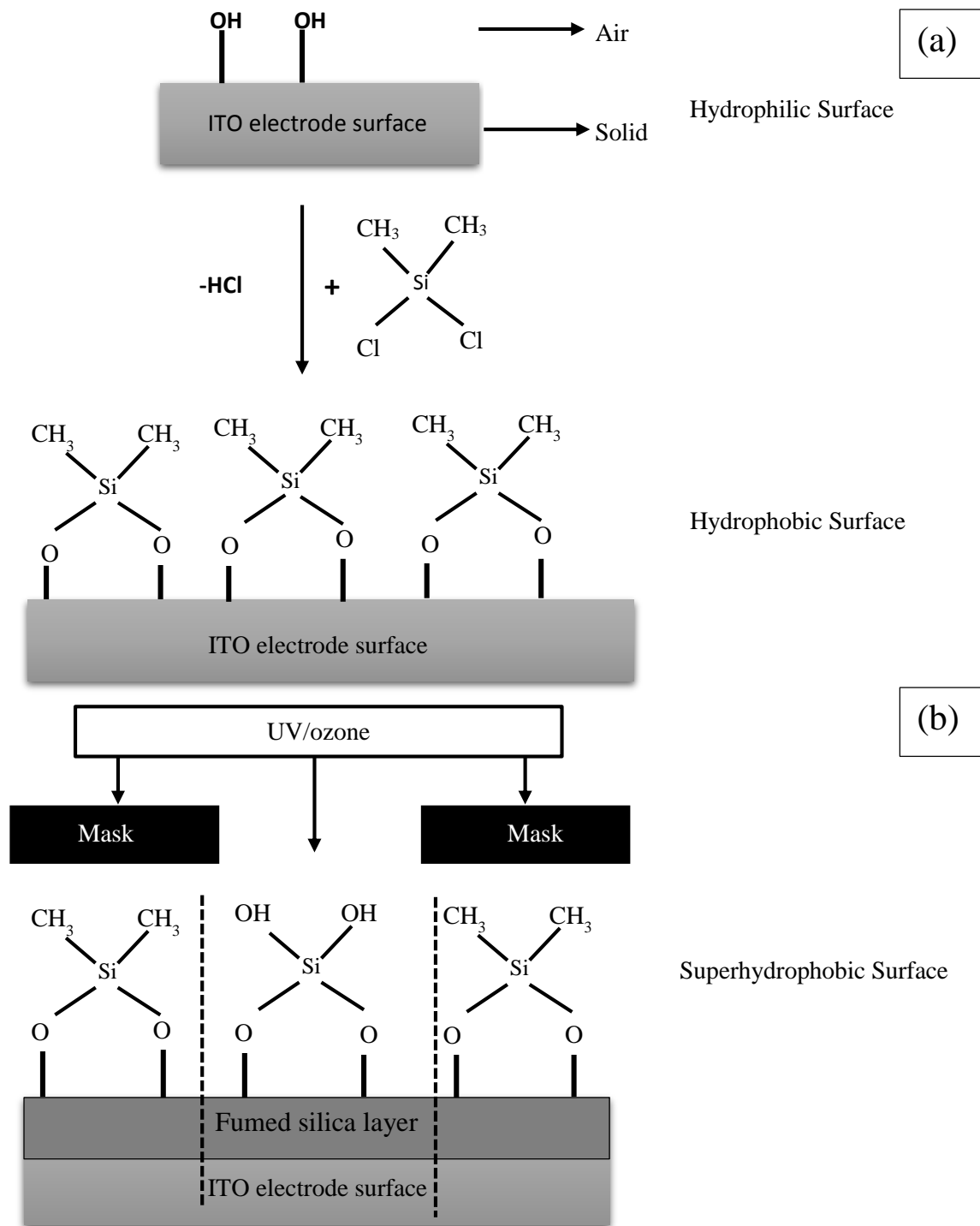


**Figure 5.1.** Diagram illustrating (a) the principle of the hydrophobisation of the ITO electrode surface using dichlorodimethylsilane (hydrophobic surface), (b) and the fabrication of hydrophilic patterns on the surface of ITO electrode coated with a hydrophobic fumed silica layer (superhydrophobic surface) using a UV/ozone lamp.

## **5.2 Experimental procedures**

### ***5.2.1 Fumed silica suspension preparation***

Fumed silica suspensions were prepared by dispersing dry fumed silica particles powder in ethanol. This was achieved by weighing (2, 4, and 5 g) of the powder and dispersing it in 100 ml of ethanol in a volumetric flask to give (2, 4, and 5 wt. %) concentrations. The particles-ethanol mixture was sonicated by an ultrasonic vibracell processor (Sonics & Materials) at 60 W for 10 minutes. The vessel was placed in an ice-water bath during the sonication process to avoid the process overheating.

### ***5.2.2 Investigation of ITO electrode wettability***

Preliminary experiments were conducted to investigate the wettability of the ITO electrode before and after its hydrophobisation. Afterwards, the hydrophobised ITO electrode was coated with hydrophobic fumed silica suspensions using the method outlined in section 2.2.3. The suspensions that have been used in the dip coating method are described in section 5.2.1. The contact angles of the bare, hydrophobised, and coated ITO electrode were measured by using a drop shape analysis system (DSA 10, Krüss) to determine the changes in the electrode wettability due to its surface modification (see section 2.2.4).

### ***5.2.3 Optimisation of superhydrophobic coating quality***

The effect of the sonication time (5, 10, 15, and 20 minutes) of the particle suspension preparation and dip coating speed (0.159, 1.59, 3.18 and 4.77 cm min<sup>-1</sup>) on the coating quality at three different fumed silica suspension concentrations (2, 4 and 5 wt.%) were investigated and the conditions optimised to achieve a homogeneous coating. Optical microscope images of the coatings were used for assessing their quality.



#### ***5.2.4 Stability of the coatings***

The stability of the coating on the ITO electrode was assessed using a setup constructed in-house as described in section 2.2.5. In the stability tests, the electrode was dipped into a beaker filled with water and stirred on a magnetic stirrer at high speed for five minutes (figure 2.6). The images of the coating were taken by an optical microscope and a digital camera before and after stirring was compared.

#### ***5.2.5 Fabrication of superhydrophilic patterns on the superhydrophobic coatings***

A home built UV/ozone lamp setup was used to prepare superhydrophilic patterns as described in section 2.2.6. Different types of masks were fabricated at the University of Hull from glass coverslips, glass and plastic slides were tested in order to find a cost-efficient method for making open microfluidic system.

#### ***5.2.6 Absorption capacity of the cotton waste collector***

In the open microfluidic setup, a cotton collector was placed on the outlet port and was used to absorb the waste water flowing out of the system in the experimental procedure described in the previous section. The absorption capacity of the cotton collector was an important parameter in building the open microfluidic chip because it sets the upper limit of continuous water pumping. That was determined in a set of experiments by the change of the cotton weight before and after pumping the water at different flow rates (10, 30, 60, and 90  $\mu\text{l min}^{-1}$ ).

#### ***5.2.7 Water flow in the fabricated open microfluidic chip***

The flow of water confined in the hydrophilic pattern of the microfluidic chip was generated by using a syringe pump through a needle located at the inlet of the pattern. The water flowing out at the other end of the pattern was absorbed by a cotton collector. The distribution of water flowing in the hydrophilic pattern was monitored over time

by side imaging using the camera of the DSA 10, Krüss until a steady flow was reached at different flow rates in the range ( $10 - 50 \mu\text{l min}^{-1}$ ).

### ***5.2.8 Investigation of fluid flow using fluorescence microscopy***

To visualise the fluid movement across the superhydrophilic patterns on the superhydrophobic ITO electrode surface,  $10 \mu\text{m}$  Carboxylate YG fluorescent particles (Fluoresbrite TM) and a fluorescence microscope were used. A fluorescent particle suspension was used in the flow experiments, this was prepared by adding a  $50 \mu\text{l}$  aliquot of a concentrated particle suspension ( $2.38 \times 10^5 \text{ particles ml}^{-1}$ ) to  $9950 \mu\text{l}$  of phosphate buffered saline-Tween 20 (PBS-T) (1:200). The vessel containing that mixture was wrapped with aluminum foil and mixed for 30 seconds. The PBS-T was prepared by dissolving one tablet of PBS in 199 ml deionised water. One gram of Tween 20 was diluted in 10 ml of deionized water. Afterwards, 1 ml of the prepared Tween 20 solution was added to 199 ml of PBS to prepare (1:200) PBS-T.

The syringe attached to the syringe pump was filled with the prepared fluorescent particle suspension which was pumped through the open microfluidic chip as described in section 2.3.1.2.

## 5.3 Results and discussion

### 5.3.1 Preparation of ITO electrodes with superhydrophobic surfaces

The ITO electrode surface was made superhydrophobic by a two-step process. First, the electrode surface was made hydrophobic by chemical modification using DCDMS in a vapour phase. Then, a thin layer of hydrophobic fumed silica particles was deposited on the hydrophobic electrode surface by a dip coating process to impart superhydrophobicity. The first step was needed to improve the adhesion of fumed silica coating to the substrate by van der Waals forces.

#### 5.3.1.1 Hydrophobisation of the ITO electrode by DCDMS and fumed silica coverage

The wetting properties of the ITO electrode before hydrophobisation were investigated by measuring the contact angle of water drops sitting on the electrode in the air (figure 5.2).

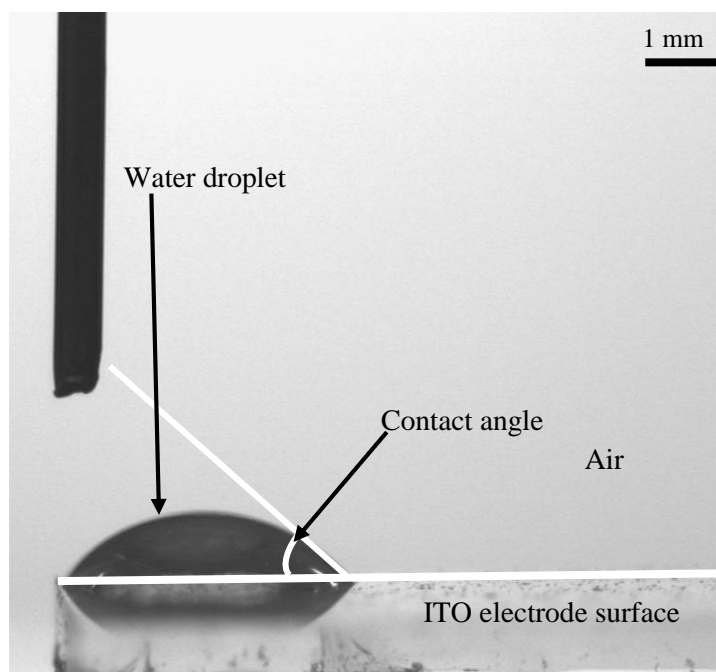


**Figure 5.2.** Side image of a water droplet on an ITO electrode surface in air. The average contact angle  $\theta$ , was found to be  $42.0 \pm 0.7^\circ$ . The scale bar is 1 mm.

The ITO electrodes were hydrophobised using DCDMS in a vapour phase, as described in section 2.2.3.1.

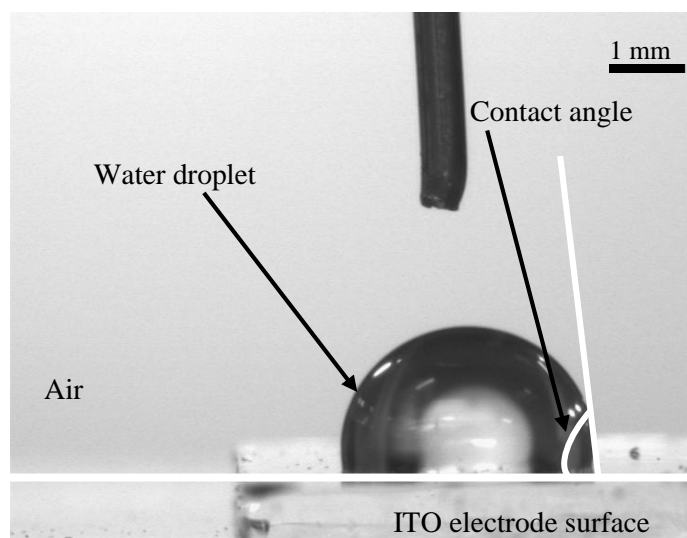


**Figure 5.3.** Side image of a water drop on the ITO electrode surface after its hydrophobisation with DCDMS. The average contact angle of  $101.4 \pm 0.5^\circ$  confirms the hydrophobicity of the surface has increased after treating it with DCDMS. The scale bar is 1 mm.

The contact angle of the unhydrophobised and hydrophobised ITO electrode substrate was measured using the DSA 10, Krüss. It was found that the DCDMS was able to hydrophobise the ITO electrode surface and increase the contact angle from  $42.0 \pm 0.7^\circ$  to a much higher contact angle of  $101.4 \pm 0.5^\circ$ , as can be seen in figures 5.3.

The increase in the contact angle can be explained according to the scheme illustrated in figure 5.1. The surface of an ITO electrode contains hydroxyl groups, while the DCDMS contains hydrolysable reactive  $-Cl$  and non-polar  $-CH_3$  groups. The hydrolysable  $-Cl$  reacts with the hydroxyl group thus replacing the hydroxyl group available on the ITO glass surface with a non-polar methyl group responsible for hydrophobisation. The increase in the concentration of DCDMS leads to the

replacement of the more (-OH) groups by non-polar groups. The effect of hydrophobisation gradually levels off at higher concentrations due to the steric hindrance between the alkoxy groups already grafted to the surface<sup>206</sup>.

The final step in the ITO electrode modification process was to make its surface superhydrophobic (the contact angle is greater than 150°). This was carried out by depositing hydrophobic fumed silica particle layer on the ITO electrode surface by a dip coating process<sup>241</sup> explained in section 2.2.3.2. The hydrophobic fumed silica coating leads to superhydrophobicity of the electrode surface due to its roughness thus causing water repellence similar to the so-called Lotus effect<sup>211</sup>. Indeed, it can be seen from the SEM image of the fumed silica coating (shown in figure 5.4) that the actual surface is rough and consist of many peaks and valleys at microscopic and nanoscopic level. It is expected that a water droplet would sit at the top of the surface protrusions while air is trapped underneath the droplet corresponding to the Cassie-Baxter (CB) model of wetting described in the introduction (section 1.5.2.1).

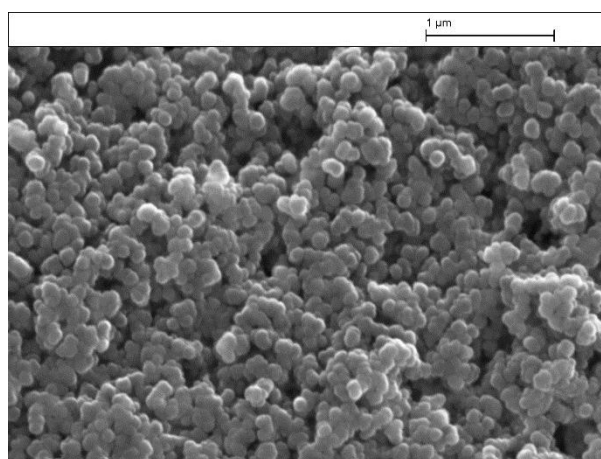


**Figure 5.4.** A SEM image of a fumed silica coating showing that its surface is rough at micro-and nanoscopic level. Scale bar is 1 μm.

To confirm the ITO electrode superhydrophobicity, a small water droplet was placed on the ITO electrode surface in air. As can be seen from figure 5.5 that the water droplet rolls off the surface so the actual contact angle could not determine by the DSA 10, Krüss. Therefore, videos were recorded to capture images of this process and it is expected the contact angle was bigger than  $150^\circ$ .

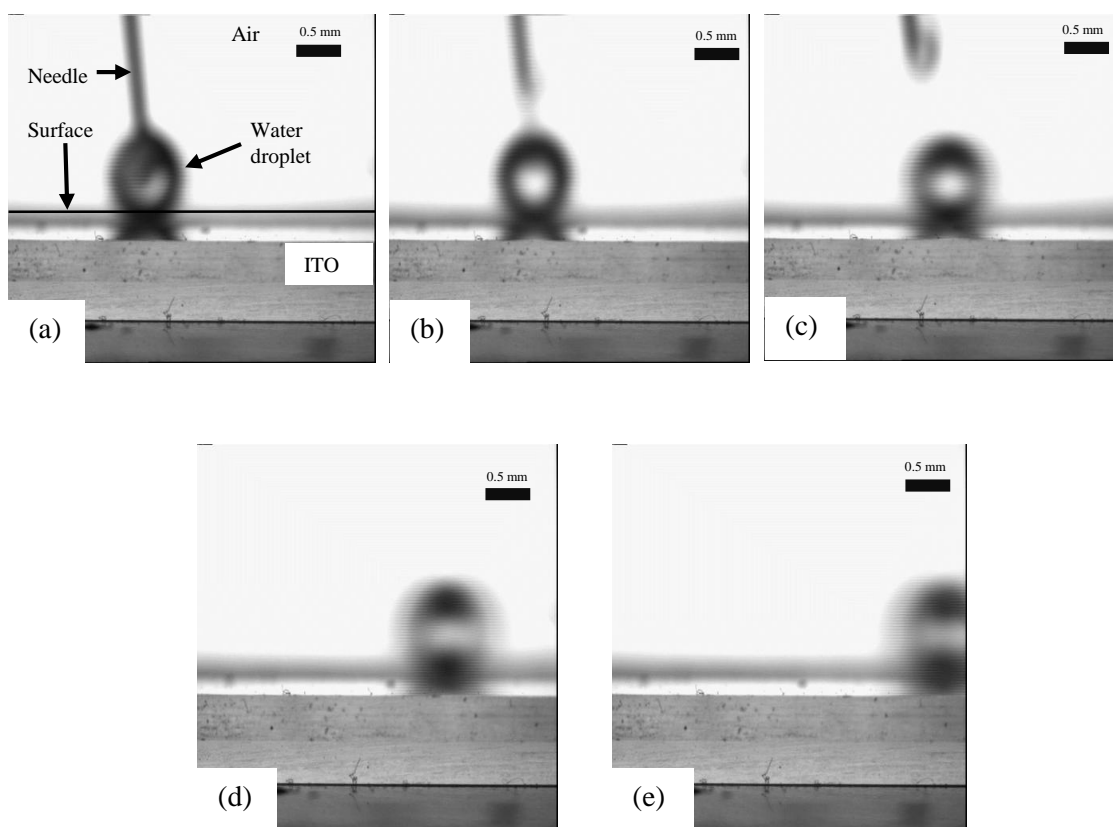


**Figure 5.5.** Images (a-e) show the process of a water droplet rolling over a superhydrophobic surface which is coated with fumed silica. The water droplet easily rolls off the surface even on a horizontal substrate thus confirming its superhydrophobicity. The scale bar is 0.5 mm for all images.

Images that were taken from the videos confirm the effectiveness of fumed silica layer in creating water repellency and the results indicate clearly that after deposition of fumed silica layer the surface becomes superhydrophobic.

### ***5.3.2 Factors affecting the preparation of superhydrophobic ITO electrode surfaces using the dip coating method***

Various factors which may affect the stability and quality of the superhydrophobic coating were investigated. Those included the sonication time for dispersing the fumed silica when making the suspensions, the withdrawal speed of the substrate from the particle suspension in the dip coating process as well as the fumed silica particle concentration. It was found that a sonication time of 10 minutes and withdrawal velocity of  $3.18 \text{ cm min}^{-1}$  gave the best results. The particle concentration of the suspensions was further investigated and optimised as described below.

#### ***5.3.2.1 Coating morphology affected by fumed silica suspension concentration***

Fumed silica suspension at different concentrations (2, 4 and 5 wt.%) were prepared as described in section 5.2.1. Figure 5.6 shows images of the coating taken by optical microscopy at approximately the same location on all the ITO electrode substrates to compare the coating quality. It can be seen that the substrate was only partially coated at 2% silica concentration because of insufficient silica particles in the suspension which led to the limited continuous formation of silica layer. While that produced at 5% silica concentration suffered from defects and cracks due to high silica particles loading (thicker coating) which resulted in cracks due to stresses induced by the drying. The best surfaces were produced at a concentration of 4% fumed silica suspension<sup>242</sup>.

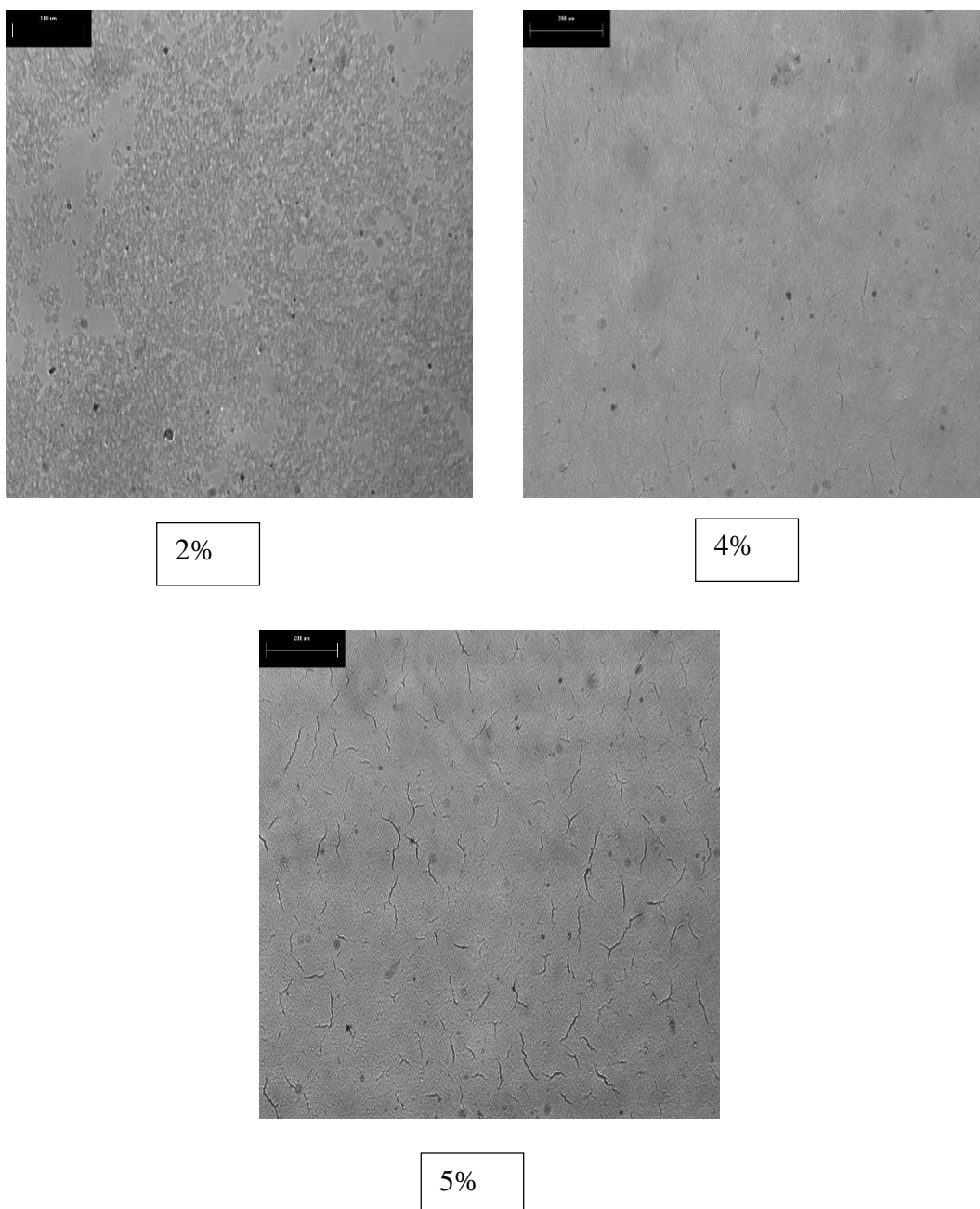


**Figure 5.6.** Optical microscopy images of fumed silica coatings produced by dip coating at a withdrawal speed of  $3.18 \text{ cm min}^{-1}$ . At three different concentrations of fumed silica suspensions (2, 4, and 5 wt.%) in ethanol prepared at 10 minutes sonication time. Cracks and defects are seen on the coating obtained at 5% silica suspension. The decrease of the silica concentration to 4% improves the coating quality by reducing the size and number of cracks. Partial inhomogeneous coatings are obtained at an even lower concentration of 2%. The scale bar on all images is  $200 \mu\text{m}$ .



### 5.3.3 Stability of superhydrophobic surface coating

Having determined the optimum condition for a homogenous coating, experiments were performed to investigate the surface coating stability using the procedure described in section 2.2.5. Images of the superhydrophobic coating before and after being stirred in water are shown in figure 5.7. It can be concluded from the images taken by both the optical microscope and a digital camera, that the coating has not been affected by the washing which makes it suitable for microfluidic applications.

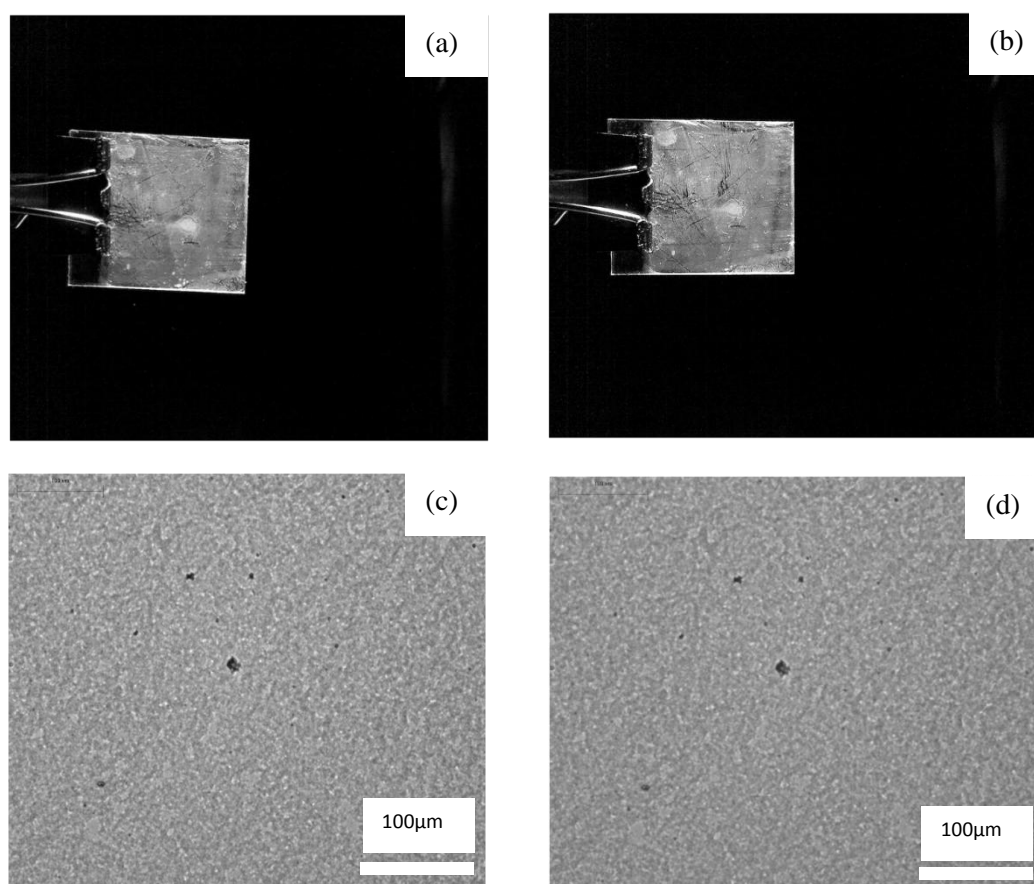


**Figure 5.7.** Images of a superhydrophobic coating deposited on an ITO electrode surface from 4 wt% fumed silica suspension by dip coating at a withdrawal speed of  $3.18 \text{ cm min}^{-1}$  and sonication time 10 minutes, taken by a digital camera (a, b) and an optical microscope (c, d) before (a, c) and after (b, d) stirring in water for 5 min (see section 2.2.5). The coating was stable and not damaged by the water flow during the stirring.

## 5.4 Fabrication of superhydrophilic patterns on superhydrophobic substrates by UV/ozone burning

Having proved the stability of the surface coating, an important investigation was performed to fabricate patterns on the coated surface. Superhydrophilic patterns were obtained by exposing the superhydrophobic coating to UV/ozone light irradiation from a UV/ozone lamp through a photo-mask for a certain period of time (as described in section 2.2.6). Three different masks were used including a microscope coverslip mask fabricated by a laser ablation technique in the Physics section (Hull University), 1 mm thick glass and plastic masks were fabricated using a CNC instrument in the Chemistry section (Hull University). The superhydrophilic patterns were made visible by wetting them with water and images were taken using a digital camera and an optical microscope.

### ❖ *Microscope coverslip masks*

These masks were made by laser ablation and their shape and dimensions are shown in figure 5.8. They were successfully used to fabricate superhydrophilic patterns (figure 5.9) but their main disadvantages were they could easily break and their small sizes made them unsuitable for fabrication of large and more complex patterns.

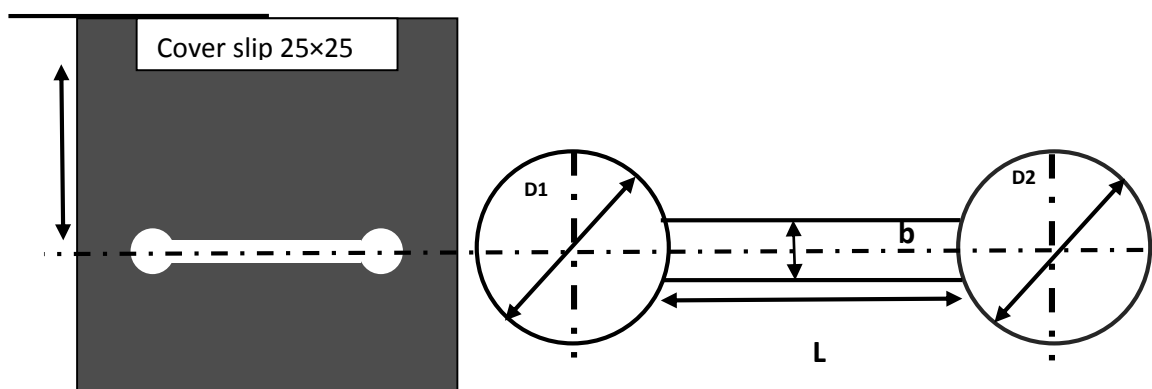


**Figure 5.8.** Left sketch of a mask prepared by laser ablation with a channel in the middle of the coverslip. The right sketch is the shape and size of this laser prepared channel with a dimension of 1mm for  $D_1$  and  $D_2$ , 0.5 mm for  $b$  and 7 mm of  $L$ .

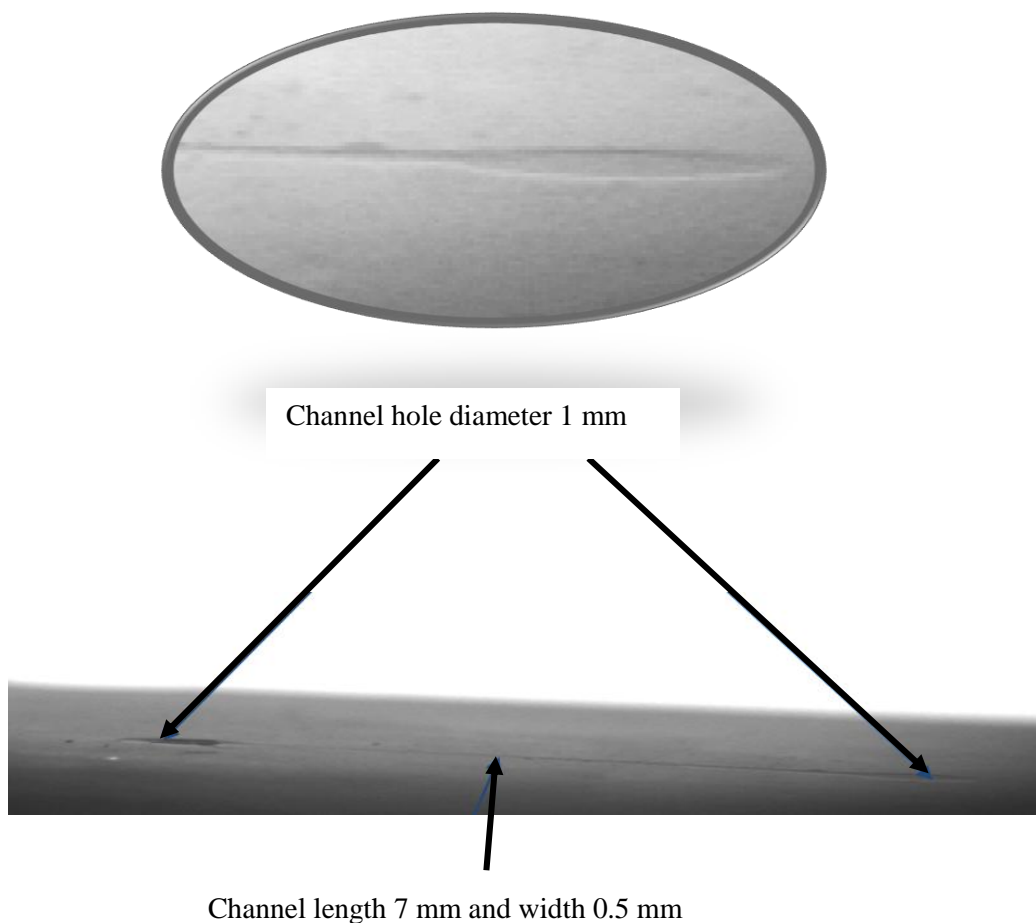


**Figure 5.9.** Images of superhydrophilic patterns fabricated using a UV/ozone light irradiation through a coverslip mask with the following specifications: a dimension of 1 mm diameter for sides, 7 mm length and 0.5 mm width (see Figure 5.8) on the superhydrophobic substrate obtained by dip coating method from a 4 wt% fumed silica suspension, withdrawal speed  $3.18 \text{ cm min}^{-1}$  and sonication time 10 minutes.

❖ *Thick glass and plastic masks*

To overcome the small size of the cover slide masks, 1 mm thick microscope glass slides were used to fabricate the superhydrophilic patterns. It was found that the masks with different shapes could be made and used for the preparation of superhydrophilic patterns (as seen in figure 5.10), but their fabrication was difficult because the glass is a hard and fragile material.

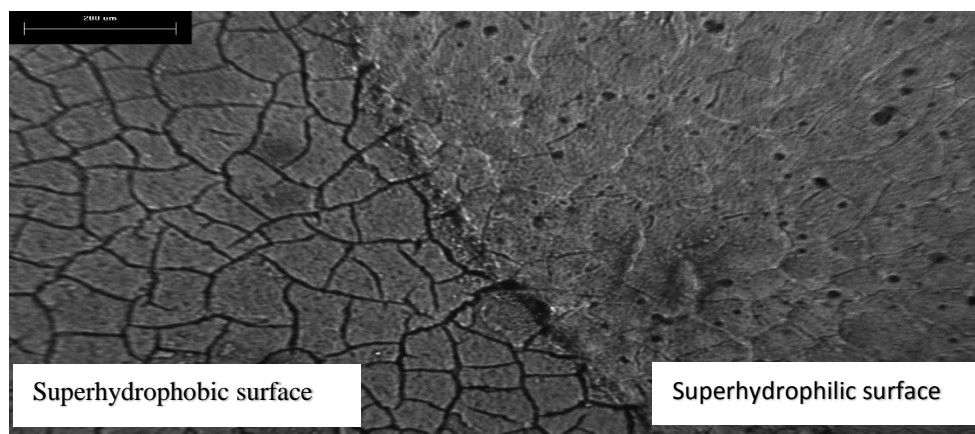


**Figure 5.10.** Shows the fabrication of superhydrophilic patterns on a glass substrate covered with fumed silica 4% wt, withdrawal speed  $3.18 \text{ cm min}^{-1}$ , and sonication time 10 minutes using dip coating method and using UV/ozone lamp. The channel fabrication can be seen as the edges would appear in microscope images at the cross point of superhydrophilic and superhydrophobic layers. Scale bar is  $200\mu\text{m}$ .

An alternative choice to coverslip and 1 mm thick glass slide masks were to make plastic slide masks. Polymethylmethacrylate (PMMA) slides were used for that purpose. PMMA is cheap and available material on the market. It is less fragile material than glass and large plastic slides can be obtained which does not restrict the mask size. Preliminary experiments were carried out to test the plastic slide resistance to the heat produced by the UV/ozone lamp using the setup described in section 2.2.6.1. The temperature on the plastic mask surface under the UV/ozone lamp was measured over a period of time as shown in Figure 5.11. It was seen that the plastic slide was able to sustain the heat for 2000 seconds since the temperature did not exceed  $65^{\circ}\text{C}$ . This makes the PMMA masks suitable for the purpose of creating the superhydrophilic patterns needed for the open microfluidic system. Therefore, PMMA plastic masks were chosen to carry on all further experiments.

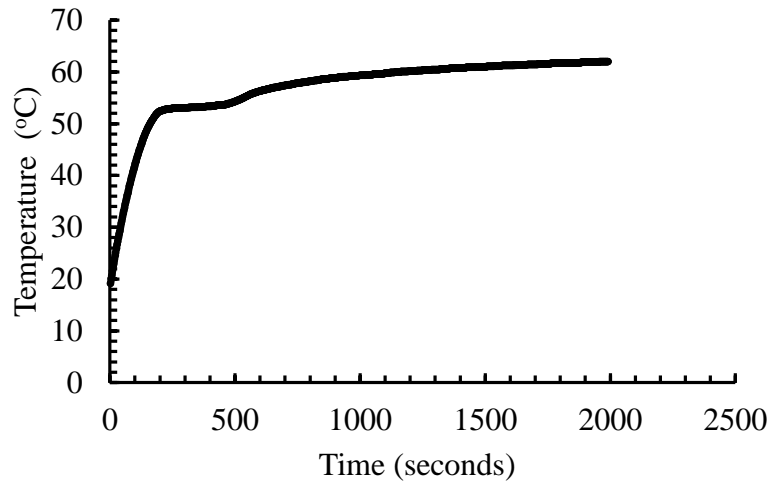


**Figure 5.11.** The temperature of the PMMA mask surface subjected to continuous irradiation from the UV/ozone lamp versus time.

The complete process of fabrication of an open microfluidic pattern is illustrated in figure 5.12 where image (a) represents the bare ITO electrode before hydrophobisation process, (b) represents the plastic masks used for the fabrication of superhydrophilic patterns, and (c) shows the pattern produced after irradiation using a UV/ozone lamp.

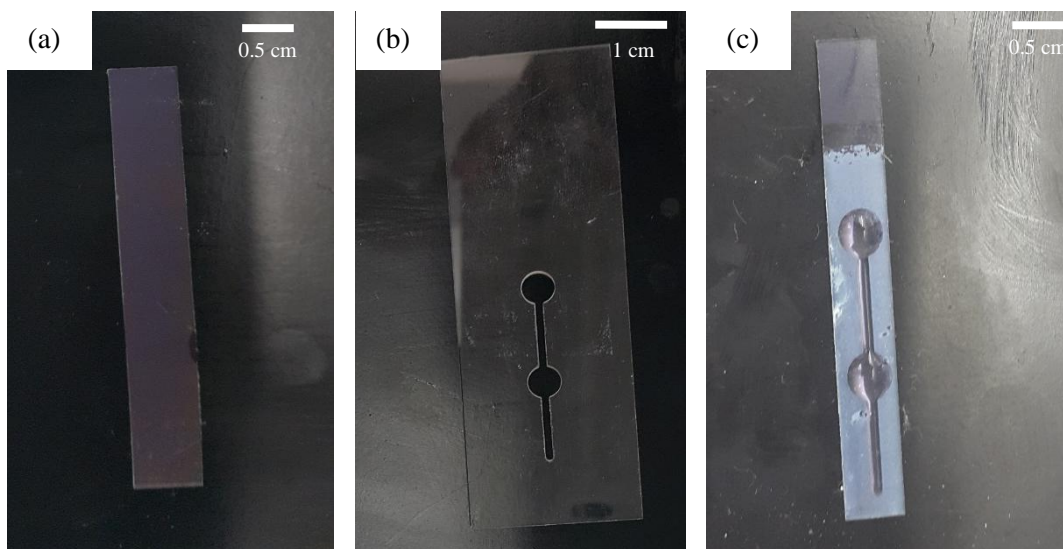


**Figure 5.12.** Shows the hydrophobisation process: image (a) shows the ITO electrode before coating. Image (b) shows the plastic mask that is used for the fabrication of a superhydrophilic channel. Image (c) shows ITO electrode covered with 4% wt concentration of fumed silica suspension withdrawal speed  $3.18 \text{ cm min}^{-1}$  and sonication time of 10 minutes after the fabrication of a superhydrophilic channel using UV/ozone lamp. Scale bar for image 1 and 3 are 0.5 cm. The scale bar for image (a) and (c) are 0.5 cm, and for image (b) is 1 cm.

#### **5.4.1 Investigation of the fluid flow over superhydrophilic patterns**

After preparing the superhydrophilic pattern on superhydrophobic surfaces, experiments were carried out to demonstrate the possibility of fluid flow over the patterns surrounded by the superhydrophobic fumed silica layer. The patterns should act as “wall-less channels” in which the flow should occur. The water was spotted onto these patterns using an Eppendorf micropipette. It was observed that the water rapidly spread over and took the shape of the pattern. This is illustrated in figure 5.13 which confirms the possibility of fluid flow through these “wall-less channels”.

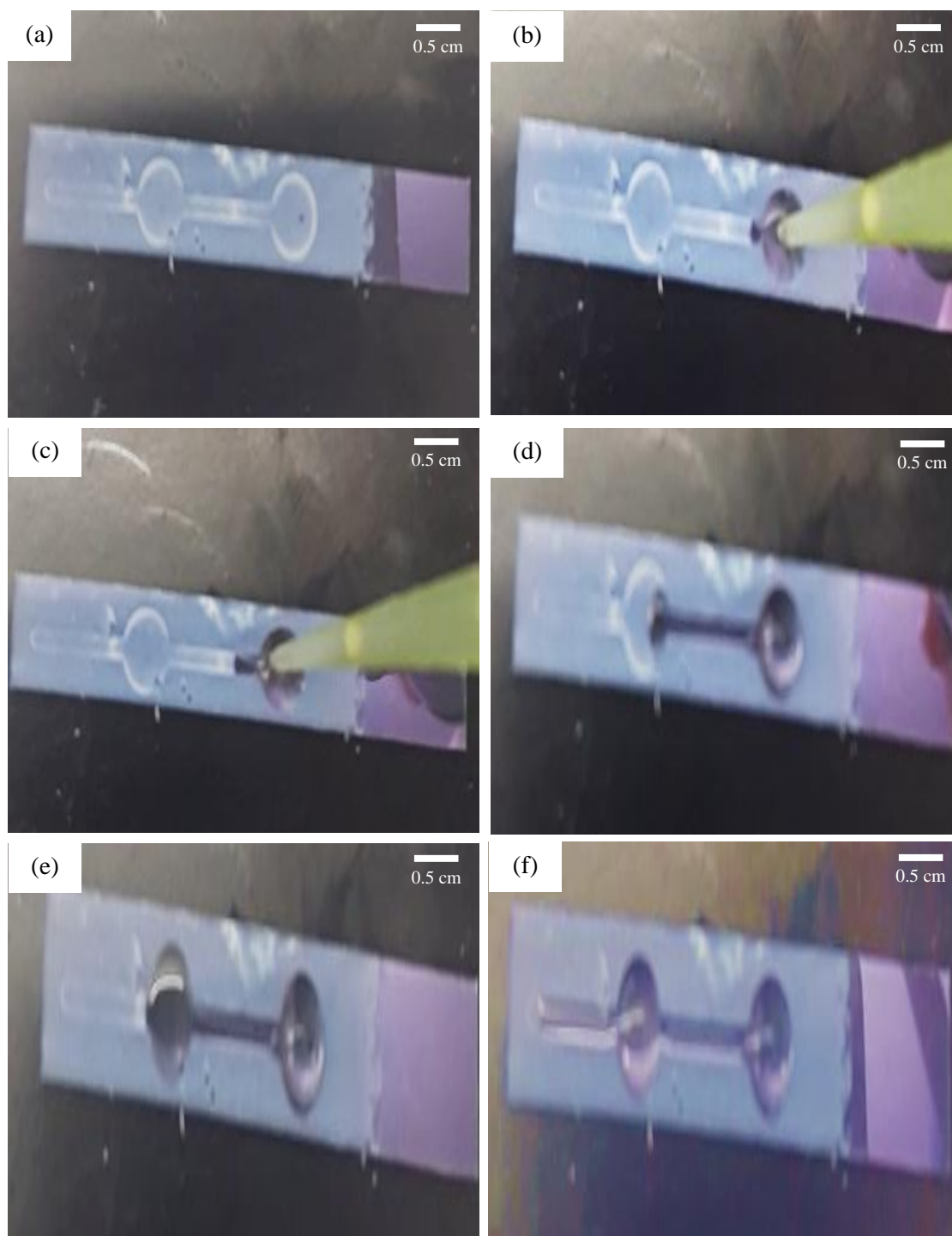


**Figure 5.13.** Series of images (a - f) showing the possibility of fluid flow through the superhydrophilic open microfluidic ‘channels’ fabricated onto an ITO electrode with superhydrophobic fumed silica coating. The scale bar for all images is 0.5 cm.

## ***5.4.2 Construction of a lab-on-a-chip device***

After the successful experiments to make fluid flow off-chip through the patterned channels, a method was designed to pump fluid through the channels using a syringe pump as described in section 2.3.1 and using two different chip design that differs in the introduction of the fluid to the chip as it will be detailed in the next sections.

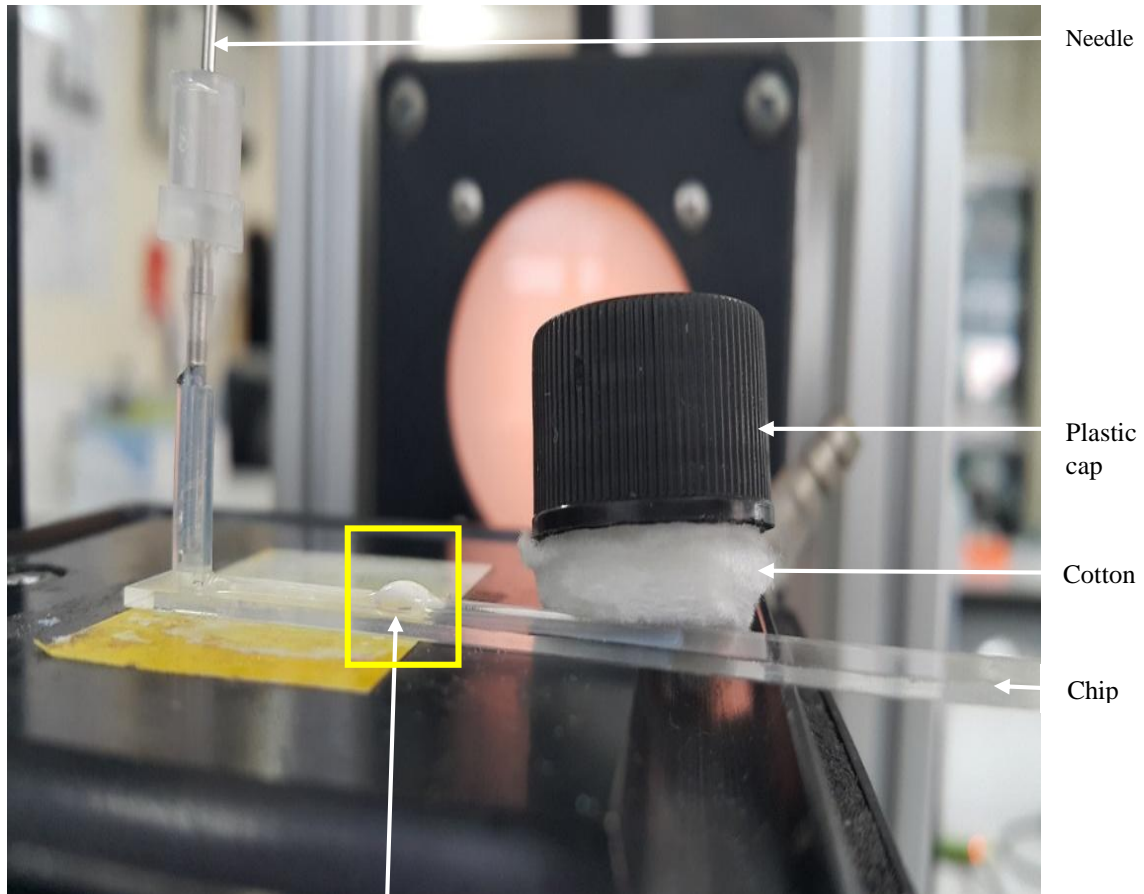
### ***5.4.2.1 Pumping water through open microfluidic channels***

After preparing the superhydrophilic pattern on the superhydrophobic surface and proving the possibility of fluid flow on-chip using only a micropipette, methods to allow automation of this procedure were investigated to eliminate the errors and improve reproducibility. A microfluidic chip was designed where the tube which delivers the fluid was attached from the bottom to a drilled hole in a glass slide to ensure a fixed delivery of fluid and to allow replacement of the desired chip on the top of as detailed in section 2.3.1 and shown in figure 2.9. It was found that this design had several drawbacks including the lack of flow over the superhydrophilic pattern with overspill over the surrounding superhydrophobic surface. Drilling circle and attaching ports to the substrate were additional difficulties associated with this design.

A modification to the original setup was carried out (design 2) by altering the tube position that delivers the fluid and this was achieved by building a plastic stand that was attached from one end of the tube which was attached to the syringe pump located above the inlet of the ITO electrode. While the other end represented the exit of fluid out of the pattern as described in section 2.3.1 and illustrated in figure 2.10. To collect the waste, a plastic cap containing cotton was placed at the exit of the superhydrophilic pattern. The new design effectively delivered fluid and overcame the problems associated with the previous design by omitting the drill circle and attached tubes to the



inlet and outlet. Figure 5.14 illustrates the improved design of the open microfluidic chip setup.



Water droplet

**Figure 5.14.** Shows the image of the design 2 of the set up where the fluid is delivered from a plastic tube attached to the syringe. While the exit is covered with cotton placed in a plastic cap as a waste container.

### **5.4.3 Absorption capacity of the cotton waste water collector**

To simplify the design and operation of the open microfluidic chip, it was decided to use cotton as a waste collector placed on the outlet of the superhydrophilic pattern instead of drilling circle and tubes to remove the waste. The absorption capacity of the cotton collector was measured when water was pumped at different flow rates. The data obtained using the setup described in section 2.3.1.1 are summarized in table 5.1.

**Table 5.1.** The measured and expected mass of water absorbed by the cotton collector attached to the outlet of the open microfluidic system after continuous pumping of water at different flow rates for 900 seconds.

Flow rate $\mu\text{l min}^{-1}$	Cotton mass / g		Absorbed water mass /g	
	Initial	after pumping	measured	Expected
10	1.57	1.70	0.13	0.15
30	1.46	1.83	0.37	0.45
60	1.54	2.32	0.78	0.90
90	1.45	2.80	1.35	1.35

Table 5.1 shows the measured and expected mass of water absorbed by the cotton collector attached to the outlet of the open microfluidic system. The expected mass,  $m$ , was calculated using the following equation

$$m = d \times FR \times t \dots\dots\dots \text{Equation 5.1}$$

Where  $d$  is the density of water ( $\text{g cm}^{-3}$ ),  $FR$  is the flow rate ( $\mu\text{l min}^{-1}$ ),  $t$  is the time (minutes). It can be concluded from the above results that as a waste outlet the used cotton can absorb approximately 0.15 g of sample to be pumped by using  $10 \mu\text{l min}^{-1}$ , 0.45 g when using  $30 \mu\text{l min}^{-1}$ , 0.90 g at flow rate of  $60 \mu\text{l min}^{-1}$  and 1.35 g at  $90 \mu\text{l min}^{-1}$ . The  $30 \mu\text{l min}^{-1}$  seems to be the optimum flow rate with respect to the sample volume and pumping time.

**5.4.4 Investigation of steady state times for water flowing at different rates**

The accurate and stable fluid flow in the lab-on-a-chip system is a crucial factor allowing samples to be manipulated precisely and reproducibly. The steady state in our open microfluidic system can be defined as the state in which the fluid amount that is pumped is equal to that absorbed by the cotton waste water collector. Once the steady

state is reached the amount of fluid and its distribution over the superhydrophilic pattern should remain the same with time. This was studied by taking side images of the pattern and measuring the droplet height over time. Different flow rates including 10, 20, 30, 40 and 50  $\mu\text{l min}^{-1}$  were tested. Figure 5.15 shows a sequence of images taken by the DSA 10, Krüss instrument. The change of the droplet height with time until it reaches the steady state is seen. Figure 5.16 shows different steady state times for different flow rates. For 10, 20, 30, 40 and 50  $\mu\text{l min}^{-1}$  flow rate, the pattern was approximately similar where the fluid droplet grows with time until it plateaus which means the accomplishment of the steady state with different time to reach it.

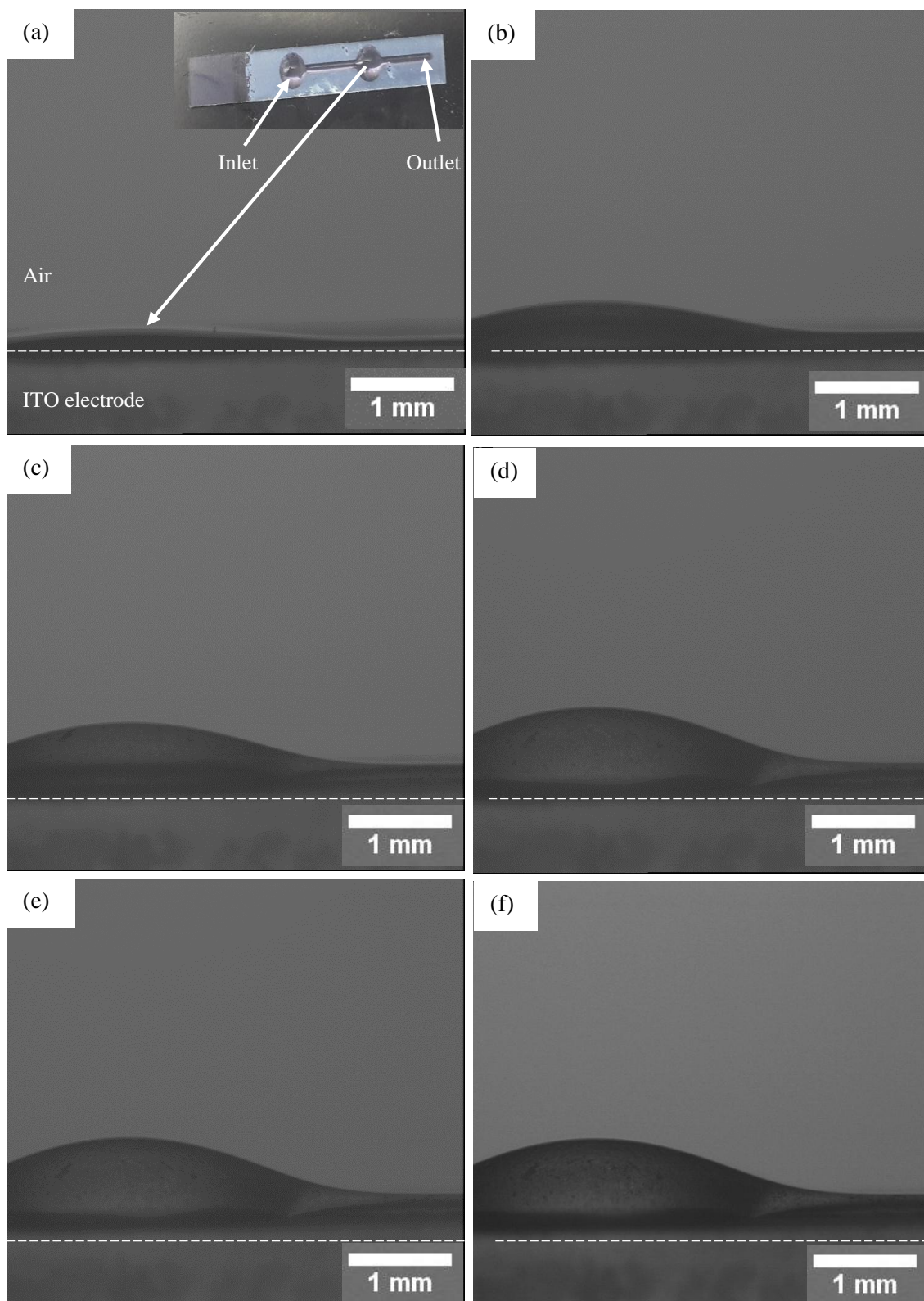


**Figure 5.15.** Consecutive images showing the growth of water droplet at different times (a) 0 seconds insert in (a) a top view of the ITO electrode width of (0.5 cm) with a superhydrophilic pattern, (b) 20 seconds, (c) 60 seconds, (d) 120 seconds, (e) 240 seconds and (f) 300 seconds during pumping at a flow rate of  $30 \mu\text{l min}^{-1}$ . The scale bar is 1mm.

The droplet height started increasing as the pumping continued (Figure 5.15 a-c). After around 60 seconds, the droplet height reached a constant value as illustrated in Figure 5.15 (d - f). The measurements with the same pattern were repeated at different flow rates and the results are shown in figure 5.16 where the height of the droplet is plotted against time. The time required to reach steady state (tss) at flow rate  $10 \mu\text{l min}^{-1}$  was 40 seconds where the droplet height started to plateau at a height of  $800\mu\text{m}$ . At  $20 \mu\text{l min}^{-1}$  time slightly reduced to 35 seconds with an increase of droplet height to  $1100 \mu\text{m}$ . The flow rate at  $30 \mu\text{l min}^{-1}$  showed a similar pattern where the droplet height was stable at 25 seconds and the height was  $1201\mu\text{m}$ . moving to flow rate of  $40 \mu\text{l min}^{-1}$  and as expected the time reduced to 20 seconds and the height increased to  $1520\mu\text{m}$ . For  $50 \mu\text{l min}^{-1}$  flow rate the time required to reach steady state was 15 seconds and the height was  $2120 \mu\text{m}$ . With higher flow rate, the boundary between hydrophilic and hydrophobic surface, virtual wall, cannot withstand leading to water to leave the channel. Steady state time was determined by drawing a line that crosses initial linear region and another line crosses the plateau region. The intersection point represents the time required to reach the steady state (tss).

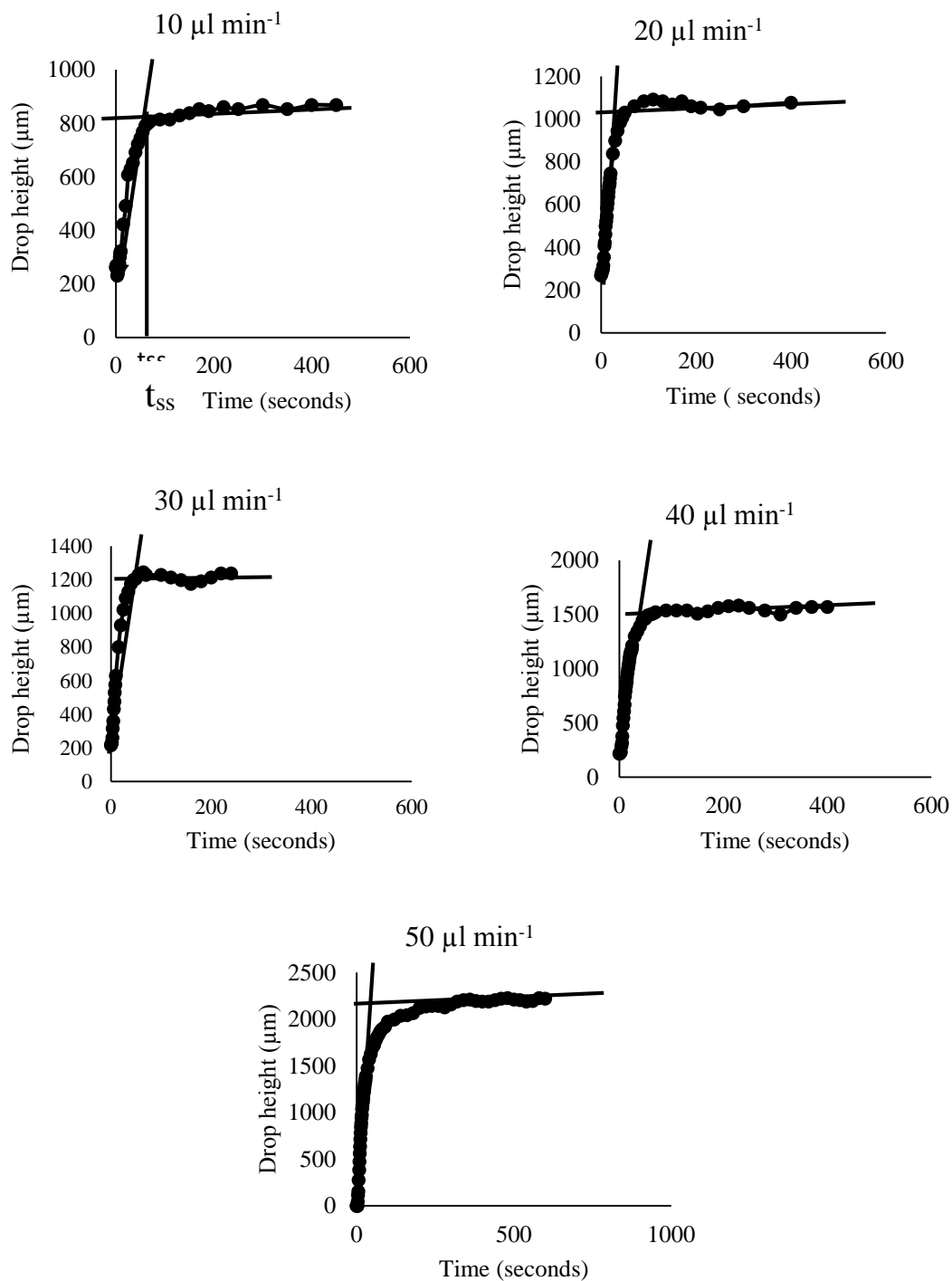


**Figure 5.16.** Droplet height versus time during pumping water in an open microfluidic channel at flow rates of (10, 20, 30, 40 and 50  $\mu\text{l min}^{-1}$ ).

#### ***5.4.5 Investigation of fluorescence particle movement along a hydrophilic channel***

In order to investigate the movement of fluid along the superhydrophilic patterns surrounded by the superhydrophobic surfaces, a fluorescence particle suspension was pumped at different flow rates as explained in section 2.3.1.2. As can be seen from figure 5.17 that the particles move through the whole area of the circle suggesting the reagents will also fill the reaction circle in the immunoassay experiments. This is important for precision and reproducible data.

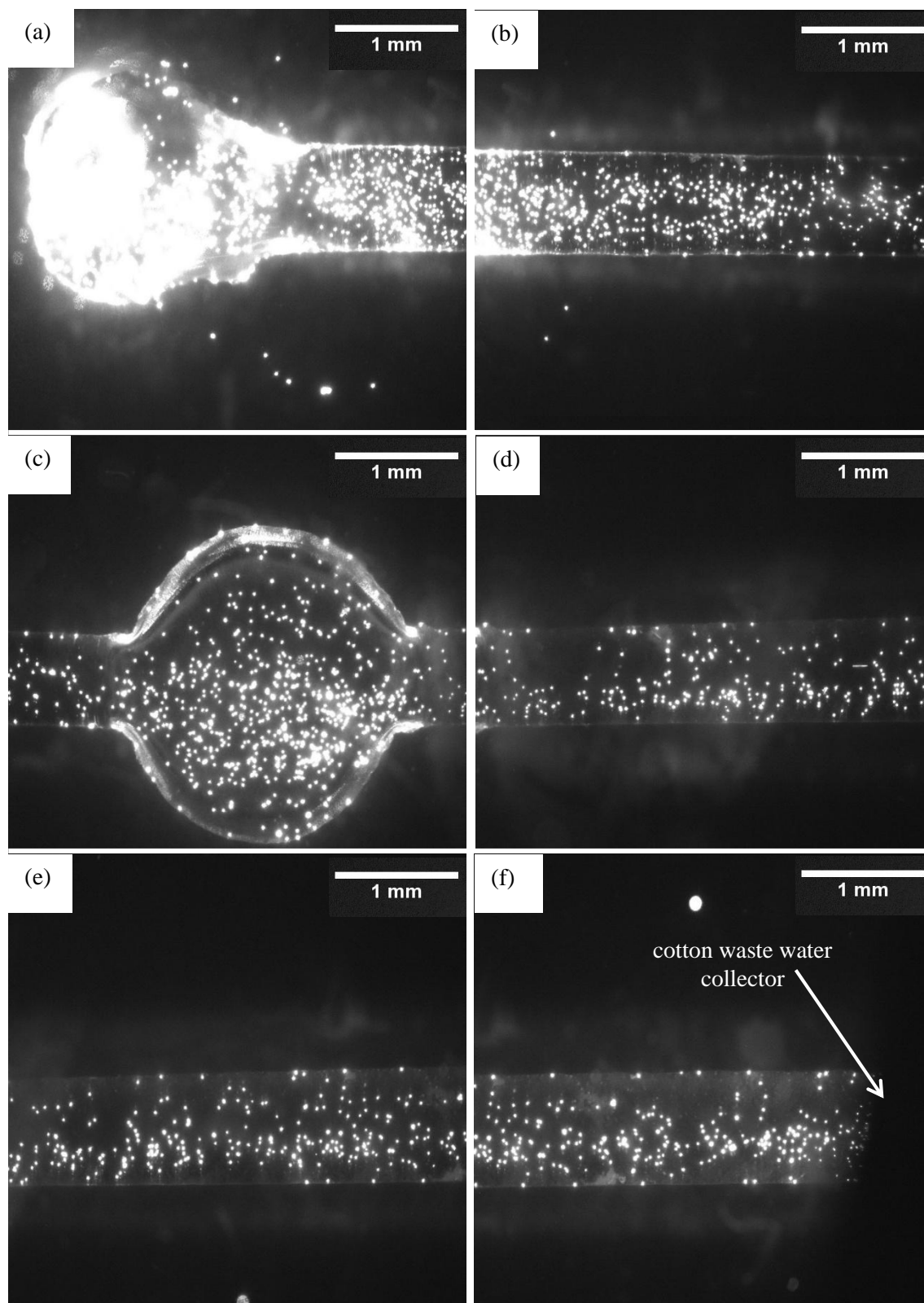


**Figure 5.17.** Consecutive microscope images showing the movement of fluorescence particles starting from the inlet (a), moving through the ‘channel’ (b) to the reaction circle (c) towards the outlet with the cotton waste water collector (f). (b), (d) and (e) represents the path between the inlet, reaction circle, and outlet. This was done using a syringe pump at  $30 \mu\text{l min}^{-1}$  flow rate. The scale bar is 1 mm.



#### 5.4.6 Effect of evaporation

Evaporation can cause problems in open microfluidic systems as it reduces the total volume of fluid reaching the reaction zone through the open channels. As a result, a decrease in the sample reliability and reproducibility is obtained. Therefore, experiments were done using a superhydrophilic circle surrounded by superhydrophobic surface (ITO electrode) which was fabricated using the method outlined in section 5.2.2 and was put inside the box attached to DSA 10, Krüss system to test the effect of the box presence to reduce or prevent fluid evaporation. As demonstrated in figure 5.18 the effect of evaporation was reduced as the contact angle values of the superhydrophilic circle over a period of time reaching 60 minutes gives slightly decrease in the contact angle. This can improve the setup for the open microfluidic system. Other traditional methods used to solve the evaporation issue include the use of superabsorbent such as sodium alginate<sup>243</sup> or Peltier element<sup>244</sup> but these solutions consider an additional step that raises the cost and time consumed; in addition, there may be an effect of interference.

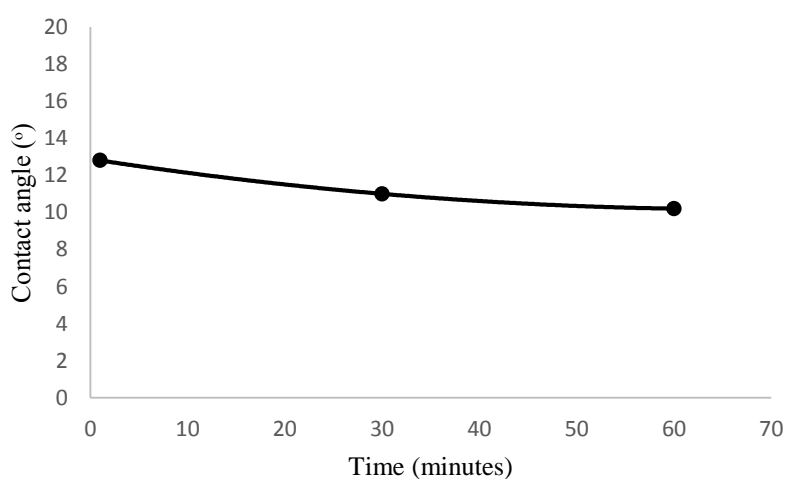


**Figure 5.18.** Shows the contact angle measured using DSA 10, Krüss instrument for superhydrophilic circle surrounded by a superhydrophobic surface after the coverage of the box attached to the DSA 10, Krüss instrument to reduce or prevent evaporation of the solvent and the there was a slight decrease in the contact angle after the immediate addition of solvent until one hour after the addition of the solvent.

## 5.5 Conclusions

In this chapter, a new open microfluidic device had been developed for fluid transport. A robust method of making superhydrophilic patterns on a superhydrophobic substrate was successfully developed that opens up possibilities towards the construction of a lab-on-a-chip device for cortisol and cortisone determination. This was achieved by hydrophobisation of an ITO electrode using DCDMS and coating the electrode with hydrophobic fumed silica particles using a simple and cost effective dip coating technique followed by UV/ozone exposure of the superhydrophobic coating through appropriate photo-masks.

The ability of superhydrophilic patterns to a guide water flow thus acting as a ‘wall-less channel’ was investigated by visual and fluorescent microscopy observations. It was revealed that fluorescence particles moved across the ‘channel’ in a laminar type flow generated by an external syringe pump. These results suggest that the adopted approach is viable and could be used in open microfluidic devices.

A new open microfluidic chip in which the aqueous solution was delivered from above at one end of a superhydrophilic pattern using a needle connected to a syringe pump while the fluid flowing out of the system was absorbed by a cotton waste collector mounted at the other end of the pattern was designed. It was found that the flow reached a steady-state regime for less than a minute and the flow could be continuously maintained at a constant flow rate in the range (10 – 90  $\mu\text{l}/\text{min}$ ) for more than 15 minutes. Our results suggest that such design of an open microfluidic device could be used in a lab-on-chip platform for stress hormone determination or other analytical applications exploiting the continuous open microfluidic principles.

## **Chapter 6 Open microfluidic applications in quantitative measurement system for stress hormones**

In this chapter proof-of-principle experiments were carried out in which the immunoassay that had been developed was performed on the new open microfluidic platform. The aim was to build a device that combines the immunoassay procedure with an open microfluidic platform to determine stress hormones using chemiluminescence procedure.

### **6.1 Introduction**

Earlier this century, stress become a major threatening to health according to the world health organization (WHO) and because it follows a circadian rhythm which makes it difficult to follow its changes<sup>245</sup>. Therefore, attempts to construct different devices designs for LOC, POC,  $\mu$ TAS, etc. for stress hormone determination that are incorporated into the microfluidic system to be in consistency with the ASSURED term<sup>246-248</sup>. Recently, open microfluidic gives the advantage upon closed microfluidic to build such devices as the open systems allows simpler sample and reagent delivery using either a micropipette or more automated instrument such as syringe pump with additional control due to visual observation. The used open microfluidic in chapter 5 provides a simple and inexpensive automated microfluidic system. The developed immunoassay introduced in this thesis (chapter 3 and 4) offers another addition to stress hormones detection making benefit from its selectivity and specify, which was achieved by the lock and a key mechanism.

## **6.2 Experimental**

### **6.2.1 *Ab –Fc immobilization procedures***

To immobilize the Ab-Fc onto the newly designed open microfluidic chip two procedures were followed;

- ❖ The first procedure used the ITO electrode treated initially with DCDMS and dip coated with fumed silica suspension to enable the fabrication of the superhydrophilic patterns using UV/ozone lamp and plastic masks mentioned in section 2.2.3. Then the electrochemical procedure was used to immobilize the Ab-Fc onto the ITO electrode following the procedure in section 3.2.1.1. The cyclic voltammetry measurements were taken according to section 3.2.1.4.
- ❖ In the second procedure, the immobilization of the Ab-Fc onto the ITO electrode was carried out first as described in section 3.2.1.1. The immobilized antibody was then covered with a small circle of adhesive tape (0.5 cm) to protect it and then it was put into an airtight vessel in order to deposit DCDMS. The ITO electrode was then immersed into fumed silica suspension as prepared in section 2.2.3.

### **6.2.2 *Determination of cortisol by chemiluminescence detection integrated on an open microfluidic system***

Preliminary experiments were carried out using the open microfluidic chip as shown in figure 2.12. The Ab-Fc was immobilized and open microfluidic channel was fabricated using the procedure in section 6.2.1 (second procedure), then 20 mM luminol and 10 mM hydrogen peroxide mixture was initially pipetted into the reaction circle, then the next step was to pump the mixture through the channel. The chemiluminescence signal was measured after 200 seconds at a flow rate of 30  $\mu\text{l min}^{-1}$  (as cited in chapter 5 for best flow rate that gives less time to reach steady state with a reduced volume of reagent for the new design).

## 6.3 Results and discussion

### 6.3.1 Immobilization of Ab-Fc onto the open microfluidic chip

In the first procedure, the Ab-Fc was immobilised onto the ITO electrode after it had been treated to prepare the open channels. This initial procedure was not successful as the superhydrophobic surface was damaged after the addition of deposition solution consisting of 0.1 M tetrabutylammonium perchloride (TBAP) and 2mM 4-nitrobenzene diazonium tetrafluoroborate in acetonitrile which can be attributed to the fact that the superhydrophobic surface contains the organic group (methyl groups) which interrupted with the organic groups in the acetonitrile ( $\text{CH}_3\text{CN}$ ) “like dissolves like”, as can be seen in figure 6.1.

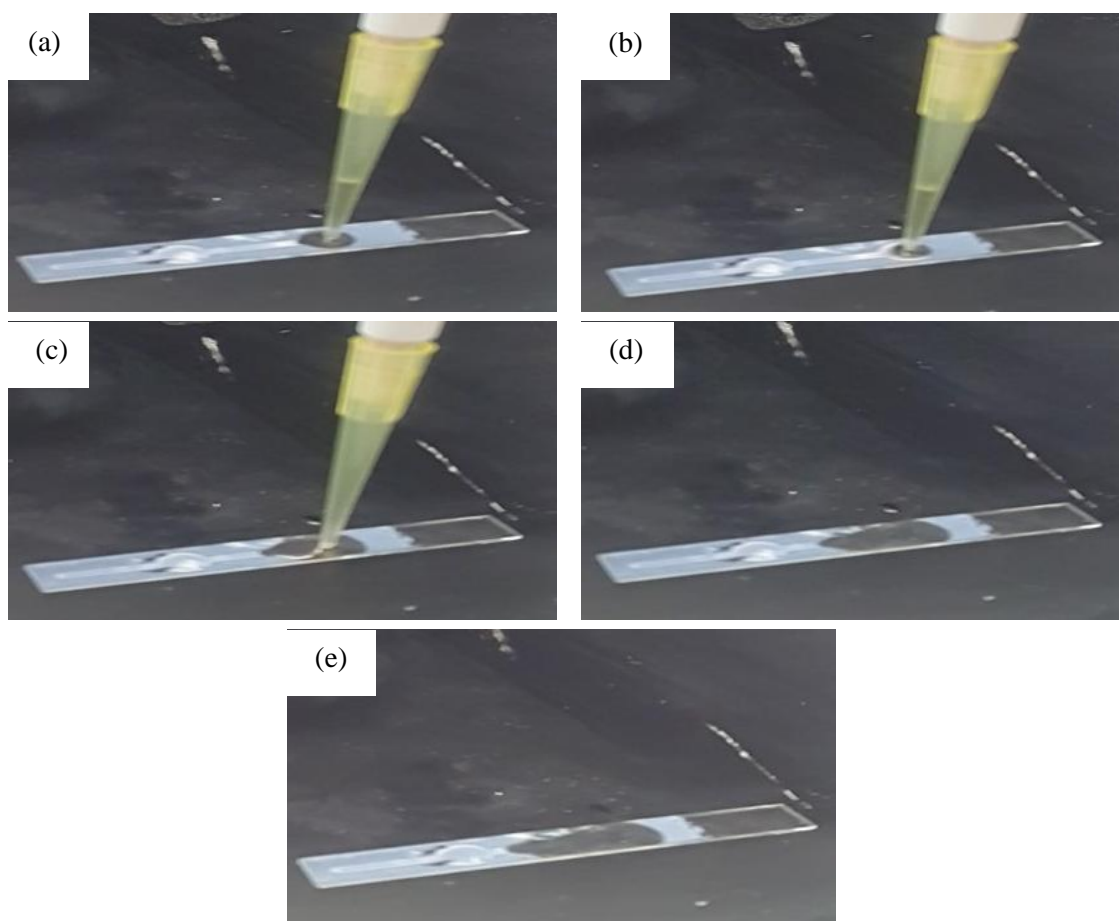


**Figure 6.1.** A serial addition (a-e) of deposition solution (0.1 M tetrabutylammonium perchloride (TBAP) and 2mM 4-nitrobenzene diazonium tetrafluoroborate) dissolved in acetonitrile onto the superhydrophobic surface showing fumed silica surface damage.

Different factors were therefore investigated to reach the best results without damaging the fumed silica texture including:

1. Solvent change. Although different non-polar solvents can be used to dissolve the deposition solution among these solvents methanol, ethanol, acetone, and DMF which were tried, although these solvents solubilized the deposition reagents, they still damaged the fumed silica texture. Polar solvents such as deionized water could not be used as it did not solubilize the deposition solution reagents.

2. Reducing the acetonitrile content of the solvent solution (deposition solution). Another approach to solving the problem was to change the deposition solution ratio, instead of using pure acetonitrile to dissolve tetrabutylammonium perchloride and 4-nitrobenzene diazonium tetrafluoroborate, a compensation of acetonitrile (ACN) and deionized water (DI) were used in different ratio. Varying the ratio of acetonitrile in deionized water were investigated as can be seen in figure 6.2, the use of 50:50 % gives better results by minimizing the surface damage.

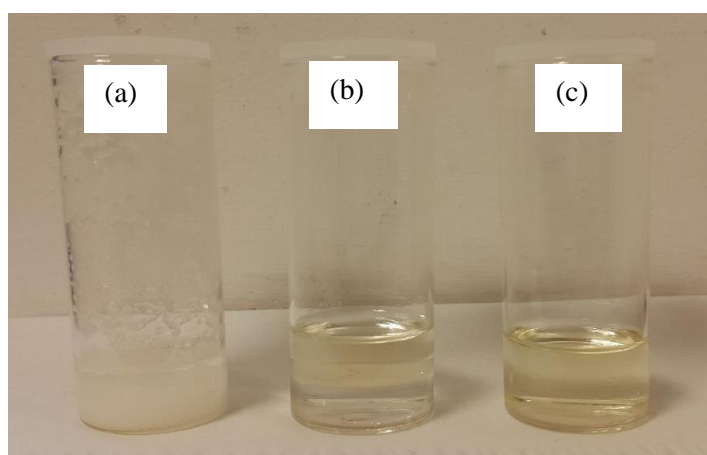


**Figure 6.2.** Shows the change in the acetonitrile ratio to dissolve the deposition chemical components (tetrabutylammonium perchloride (TBAP) and 4-nitrobenzene diazonium tetrafluoroborate) where (a) represent 0.5 ACN: 4.5 DI, (b) 1.5 ACN: 3.5 DI, and (c) 2.5 ACN: 2.5 DI.

The use of 0.5: 4.5 ratio of acetonitrile: deionized water yields a white emulsion (figure 6.2 (a)), with increasing volume of acetonitrile to 1.5 ml two separated layers are produced; the organic acetonitrile sited above the inorganic layer which is deionized water (figure 6.2 (b)). The 2.5: 2.5 ratio of acetonitrile and deionized water (figure 6.2 (c)) gives the best ratio to dissolve the deposition reagents at the same time it minimizes the superhydrophobic surface damage. Further, increase up from 2.5 ml will dissolve the deposition chemical components alongside the superhydrophobic surface damage.

### **6.3.2 Cyclic voltammetry measurement**

Electrochemical measurements were then carried out using the new deposition solution consisting of 0.1 M tetrabutylammonium perchloride and 2mM 4-nitrobenzene diazonium tetrafluoroborate dissolved in 50:50 acetonitrile to deionized water, following the procedure in section 3.2.1.1. Figure 6.3 shows the cyclic voltammogram obtained, where the reduction peak appears at - 0.17 V compared with the ITO electrode prepared in section 3.2.1.1 with a reduction peak at + 0.19 V (figure 3.5). Consequently, the shift in the deposition cycle voltammogram leads to the disappearance of the reduction peak seen at - 0.87 V for the original procedure (figure 3.8) using voltammetric reduction in aqueous ethanol containing potassium chloride and this is seen from the figure 6.4. The peak shift can be attributed to the partially blocked electrodes (PBEs), which can explain; due to the partial coverage of the electrode surface by fumed silica particles. A partial blocking of the electron transfer between the solution-phase redox species and the electrode occurs, and this causes a decrease in

current peak and a modification of the voltammetry wave shape<sup>249</sup>. As illustrated in figures 6.3 and 6.4.

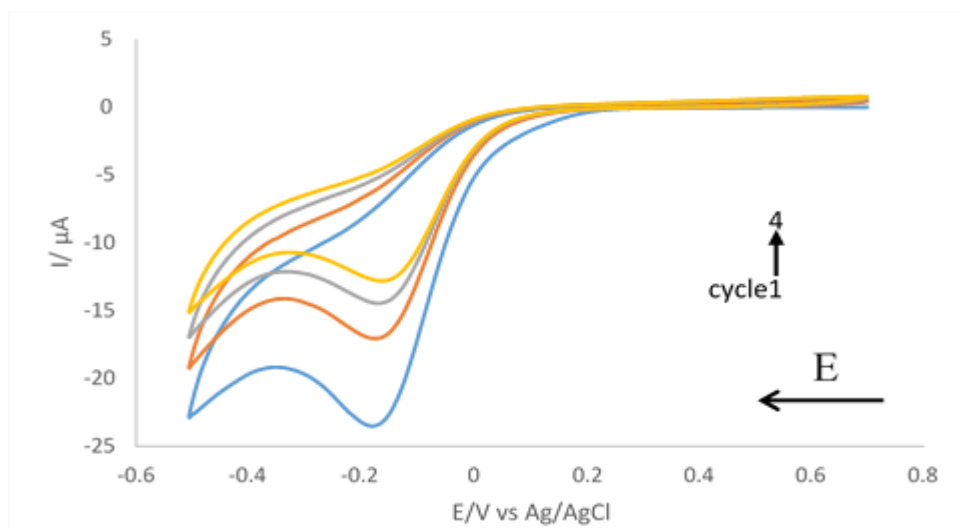


**Figure 6.3.** Voltammogram of the deposition of nitrobenzene on the ITO electrode using a solution of 0.1 M tetrabutylammonium perchlorate and 2 mM 4-nitrobenzene diazonium tetrafluoroborate in 50:50% acetonitrile and deionized water. The cyclic voltammetry was run starting at + 0.7 V scanning down to - 0.6 V and with a return sweep to + 0.7 V performed over four scans with a scan rate of 0.1 V s<sup>-1</sup> at room temperature. The reduction peak of - 0.17 V refers to partially blocked electrodes because the electrode is covered with fumed silica layer<sup>249</sup>.



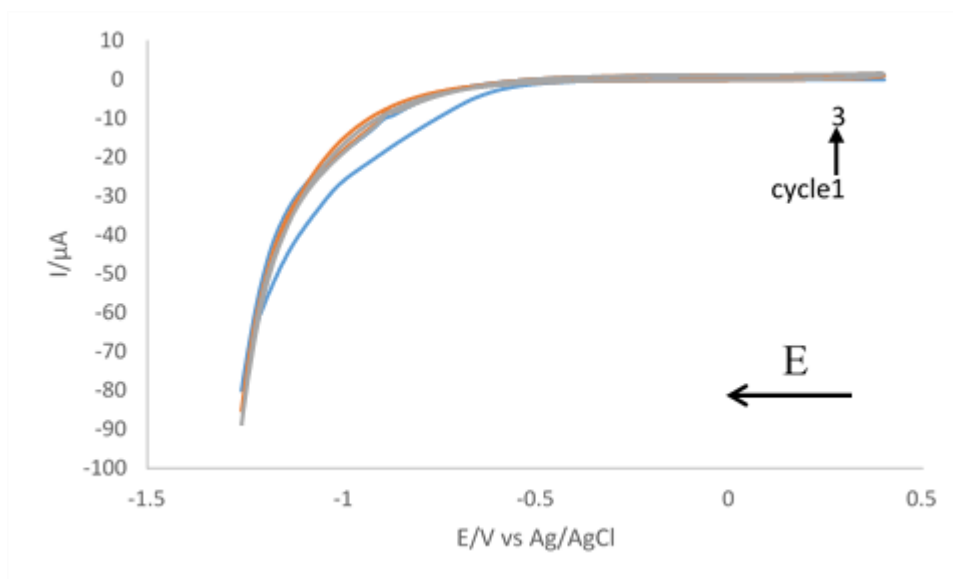


**Figure 6.4.** Cyclic voltammetry of deposition solution dissolved by 50:50 ratio of acetonitrile and deionized water on the ITO electrode using 0.1 M KCl in aqueous ethanol solution (90:10, v: v) as a reduction solution. Scan rate  $0.1 \text{ V s}^{-1}$ .

### 6.3.3 Chemiluminescence detection of Stress hormones

A substitute procedure for the integration of the immunoassay procedure on the superhydrophobic ITO electrode surface was done taking advantage of the rigid structure formed from the amide linkage between the amine (exist on the ITO electrode surface from the modification process mentioned in chapter 3) and the carboxyl group (exist on the antibody). This was explained in details in chapter three. As described in section 6.2.1 second procedure the immobilized Ab-Fc was covered with an adhesive tape and then a superhydrophilic channels were fabricated. Afterwards, a mixture of 20 mM luminol and 10 mM hydrogen peroxide was introduced to the reaction circle by the use of:

1. Eppendorf micropipette: chemiluminescence reagents were pipetted into the reaction circle and images were taken using CCD camera, figure 6.5 shows the obtained results.

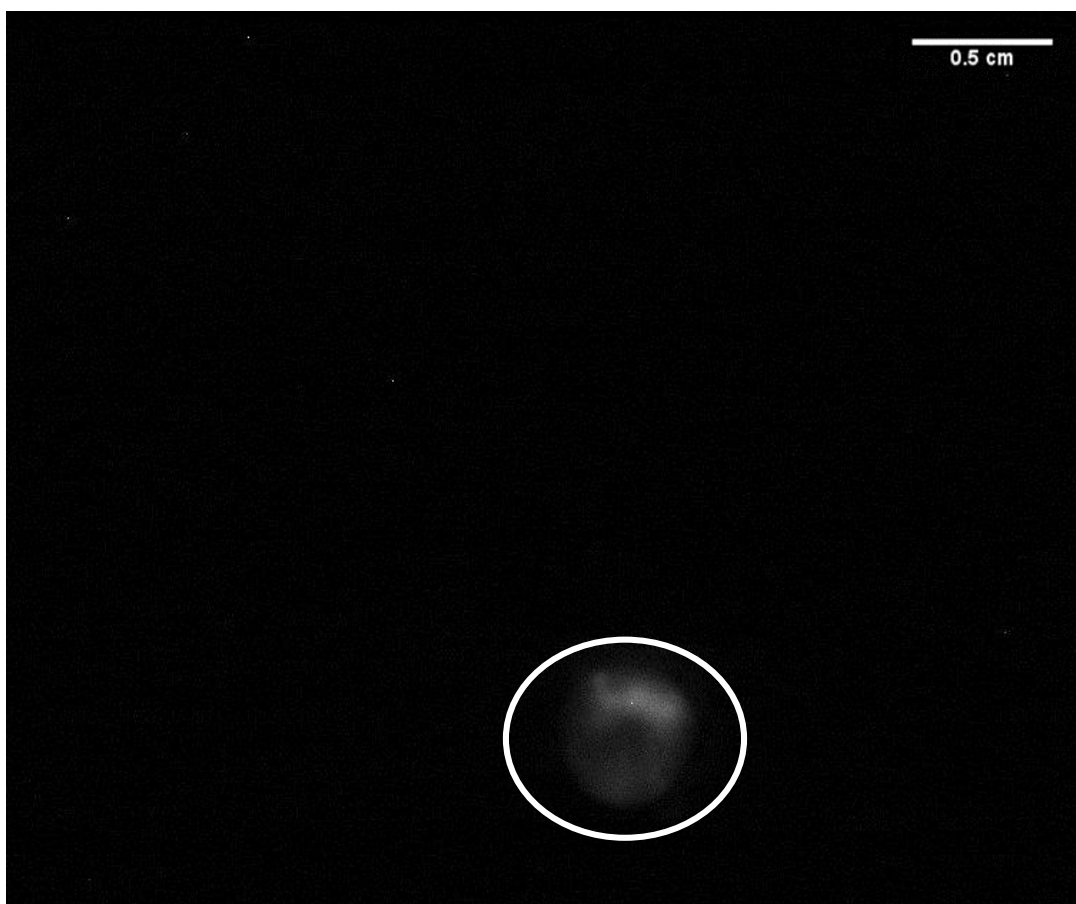


**Figure 6.5.** Shows the chemiluminescence signal of anti-cortisol antibody immobilized onto an ITO electrode, where the immobilization of the Ab-Fc onto the reaction circle was done and afterwards the circle was covered. The fabrication of the open microfluidic was done by depositing DCDMS on it and then the electrode was immersed in fumed silica suspension to fabricate superhydrophobic surface. Then superhydrophilic channel was made using UV/ozone lamp. The chip was placed in the chemiluminescence box under the CCD camera, and the mixture of luminol and hydrogen peroxide was pipetted using Eppendorf micropipette. The scale bar is 0.5 cm.

The initial chemiluminescence signal (figure 6.5) after the use of new procedure gave a well-thought-of the chemiluminescence signal by observing a light of 42.15 RLU value (on chip). Although the chemiluminescence signal observed from the original procedure gave a higher RLU value of 227.3 compared to the developed method, the latter procedure was promising for building an LOC system with further optimization. The

reduced signal could be explained by the fact of using an adhesive tape which may peel off the immobilized antibody.

2. Syringe pump: The second technique involved pumping the mixture of luminol and hydrogen peroxide to automate the procedure which is the aim of this thesis. Initially, the mixture was placed into a syringe attached to a syringe pump and this was pumped for 200 seconds at flow rate  $30 \mu\text{l min}^{-1}$  using the setup in figure 2.12. Figure 6.6 shows the chemiluminescence RLU after pumping the chemiluminescence reagents.

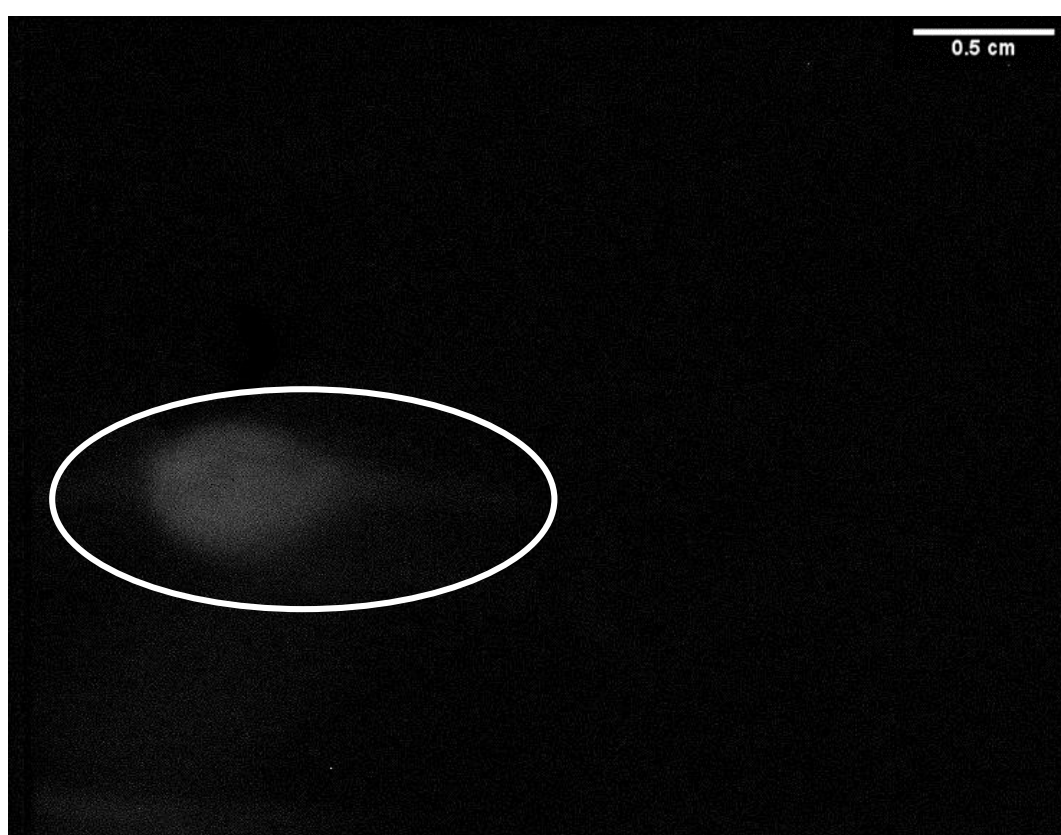


**Figure 6.6.** Shows the chemiluminescence signal of anti-cortisol antibody immobilized onto an ITO electrode, where a mixture of luminol and hydrogen peroxide is pumped for 200 seconds at flow rate of  $30 \mu\text{l min}^{-1}$  using a hydrodynamic syringe pump to fill the reaction circle that had been done by immobilizing the Ab-Fc and then it was covered by an adhesive tape to be immersed into fumed silica, this was done after depositing DCDMS and fumed silica suspension to yield a superhydrophobic surface. The chemiluminescence signal was captured using CCD camera. The scale bar is 0.5 cm.

As can be seen from figure 6.6 the signal chemiluminescence was approximately as same as for pipetting (figure 6.5) with an RLU value of 48.85 compared with 42.15 RLU value for a static procedure which gave an advantage for the microfluidics pumping procedure as it provides the automation over the pipetting.

To determine the reproducibility of chemiluminescence signal using both pipetting and pumping procedures, the previous step was further studied with four electrodes, and the results are cited in table 6.1.

**Table 6.1.** Shows the reproducibility of the chemiluminescence signal using pipetting and pumping procedures of luminol and hydrogen peroxide mixture.

Between electrode	Pipetting RLU signal	Pumping RLU signal
Electrode 1	37.15	35.22
Electrode 2	32.86	37.01
Electrode 3	42.15	48.85
Electrode 4	44.06	43.01
Average $\pm$ STD	39.05 $\pm$ 5.05	41.02 $\pm$ 6.19
RSD %	12.94	15.09

The data obtained from table 6.1 indicates that the use of pipetting or pumping shows good reproducibility using four different electrodes, the RSD % for the pipetting was 12.94 % while the RSD % for pumping procedure was 15.09 %. There was no significant difference in the intensity of light. Having succeeded in automation the newly method combing the immunoassay method with the open microfluidic system.

This needs more optimizations of the parameters to reach the optimum chemiluminescence signal, to improve the precision and enable the detection of the real sample using chemiluminescence reaction but time ran out before this could be completed.

## **6.4 Conclusion**

Due to the selectivity and sensitivity of the immunoassay procedure developed in chapters 3 and 4 and the simplicity of the open microfluidic described in chapter 5, it was decided to try and combine the two procedures. The aim was to use the ITO electrode both as an electrode and also as the substrate for the open microfluidic channels. Two approaches were taken to enable the integration of the different steps. Initially, the electrochemical immobilization of the Ab-Fc was carried out on the ITO electrode after the deposition of the DCDMS for open microfluidic patterning.

In order that an antibody can be immobilized on the ITO electrode, the ITO electrode must be modified electrochemically by the existence of an amine group onto the surface of the electrode using deposition solution. However, the immobilization procedure required the addition of a deposition solution dissolved in acetonitrile which caused damage to the prepared surface.

Different factors were investigated to reduce or prevent the damage to the surface treatment, this included changing the deposition solvent, and the ratio of the deposition solution (0.1 M tetrabutylammonium perchloride and 2mM 4-nitrobenzene diazonium tetrafluoroborate dissolved in acetonitrile) to deionized water. However, most of these factors did not succeed in Ab-Fc immobilization.

An alternative procedure was then tried in which the Ab-Fc was immobilized on the untreated ITO electrode and then this was covered by a self-adhesive tape. The next

step was the deposition of fumed silica layer and fabrication of superhydrophilic patterns. Experiments were performed using chemiluminescence reaction. Promising results were obtained from pipetting the chemiluminescence reagent that gives an RLU average value of  $39.05 \pm 5.05$  and RSD of 12.94 %, while pumping the chemiluminescence gives an RLU average value of  $41.02 \pm 6.19$  and RSD of 15.09 % which shows a close results from both methods, this would upgrade the new immunoassay integrated with open microfluidic system developed in this thesis to automation leading to improvement of stress hormone detection and high throughput results. Lack of time did not permit further investigation and optimization for the new method.

## **Chapter 7 Conclusion**

Lab-on-a-chip devices have had significantly increased attention due to their ability to provide accurate, and rapid information, which allows clinicians and scientist to achieve better outcomes. This thesis focused on the development of an analysis device that integrates a chemiluminescence heterogeneous immunoassay onto an open microfluidic platform as a route to detect stress hormone biomarkers including cortisol and cortisone in biological samples covering Zebrafish whole-body and artificial saliva samples. To achieve this target, the research work was subdivided into the following sections:

- ❖ Development of a robust immunoassay for the quantitative determination of stress hormones using electrochemical antibody immobilisation.
- ❖ Application of the immunoassay developed to the analysis of stress hormones in Zebrafish and artificial saliva using both square wave voltammetry and chemiluminescence as detectors.
- ❖ Development of an open microfluidic system based on the wetting properties of the substrate.
- ❖ The combination of the immunoassay methodology with the open microfluidic chip to detect the stress hormones. The results of these chapters are summarized in the next sections.

### **7.1 Stress hormones antibodies electrochemical immobilization**

The selectivity and sensitivity offered by the immunoassay technique due to the antibody/antigen interaction were the reason for choosing this approach. The inherited problems associated with antibody immobilization represented by reproducibility and orientation were overcome by the application of an electrochemical immobilization protocol.

An ITO electrode was chosen as a solid support surface due to its transparency and the intention to use chemiluminescence detection. The immobilization of the cortisol and cortisone antibodies was achieved by modification of the electrode surface utilising cyclic voltammetry. This was achieved by deposition of a nitrobenzene moieties on the substrate which was subsequently converted to phenylamine by electrochemical reduction to introduce the  $\text{NH}_2$  group needed to form the amide linkage with the antibody. The latter was modified to contain ferrocene tags and the activation buffer (EDC and sulfo-NHS) was used to immobilize the Ab-Fc onto the ITO modified electrode.

Characterization of the immobilisation procedure was carried using CV with different scan rates. Cyclic voltammograms with and without the antibody demonstrated the effective immobilization of the antibodies. A constant current was seen without the addition of the antibody while a peak at + 0.19 V appeared after the immobilization of the antibody.

The stability of the Ab-Fc tagged ITO modified electrode was tested and it was shown that the electrode could be used after the oxidation of the Fc tag for up to one week. A PBS solution was used to preserve the electrodes.

## **7.2 Detection of stress hormones in real sample and off-chip**

To determine the stress hormones in real samples, initially, square wave voltammetry was chosen and was followed by chemiluminescence techniques due to the latter simplicity and sensitivity.

### **❖ *Square wave voltammetry (SWV) detection***

After the successful development of Ab-Fc immobilization onto a solid surface, the application of this protocol to real sample required an optimum incubation time.



Therefore, various incubation time (15, 30, 45 and 60 minutes) were tested and 30 minutes was the optimum time. An electrochemical technique (square wave voltammetry) was first used to analysis the target hormones due to the rapid analysis, simple instrument and high sensitivity. The resulting calibration curve between current and log concentration of cortisol and cortisone respectively were in the required range of stress hormones in Zebrafish and saliva samples which were (0 - 50 ng ml<sup>-1</sup>). The LOD obtained for cortisol was 1.03 pg ml<sup>-1</sup>, while for cortisone the LOD was 0.68 pg ml<sup>-1</sup>.

An investigation was done to compare the use of the traditional method for Zebrafish whole-body sample detection using a time consuming procedure and an alternative method which uses the sample without an extraction procedure and because of the used protocol which is selective, the sample was determined using the sample only without the extraction which reduces time and cost.

However, the target of the work was to combine the sensitivity and selectivity of immunoassay within the microfluidic system. This was difficult to achieve using electrochemical instrument because of the need of reference electrode and the counter electrode and a potentiostat. Nevertheless, this protocol can be used to determine stress hormones in static experiments.

#### ❖ *Chemiluminescence(CL) detection*

The presence of Fc on the antibody allows for chemiluminescence detection as in the oxidised format it can catalyse the chemiluminescence reagents (luminol and hydrogen peroxide) to give the chemiluminescence signal. A simple detection system was then required with a dark environment and camera and gives the possibility for the construction of a portable or automated device that could be used in different fields.

The optimum condition for the chemiluminescence reaction was found to be a luminol concentration of 20 mM, hydrogen peroxide concentration of 10 mM, and exposure time for detection of 200 seconds and incubation time of 30 minutes. Interference studies were conducted and showed the minor effect on the analyte.

A comparison between the developed procedure with standard ELISA procedure gave approximately the same  $R^2$  where developed procedure gave  $R^2 = 0.9912$  for cortisol while ELISA procedure gave  $R^2 = 0.9956$ .

Initially, off-chip stress hormones detection were done giving a better LOD (cortisol was  $0.47 \text{ pg ml}^{-1}$  and cortisone was  $0.34 \text{ pg ml}^{-1}$ ) compared to the electrochemical method. For biological samples, Zebrafish whole-body sample was of recovery (91.0 % and 90.0 %) and artificial saliva was (92.59 % and 90.73 %) for cortisol and cortisone respectively.

### **7.3 Wetting properties investigations towards open microfluidic platform**

In order to build a microfluidic platform, a continuous open microfluidic system was developed making use of the wetting properties. Initially, the contact angle for the bare deposited and coated ITO electrode was measured giving increased contact angles to reach the superhydrophobicity that mimics the lotus superhydrophobicity where originally scientist have the idea of fabrication superhydrophobic surfaces.

The ITO electrode surface was first treated with DCDMS to form a hydrophobic layer deposited onto the surface, then the surface was coated with 4% fumed silica suspension using an optimised dip coating method to obtain a homogenous superhydrophobic surface. Also, the optimization included sonication time which was 10 minutes and withdrawal speed that showed optimum coating at  $3.18 \text{ cm min}^{-1}$ . The next step was to

fabricate superhydrophilic patterns onto the superhydrophobic surface and this was achieved using different masks made from the cover slide, glass slide, and plastic slides. Plastic slides were found to be the cheapest and easiest to use. A UV/ozone lamp was used to irradiate the desired pattern to fabricate the open microfluidic channel.

To investigate the movement of fluid inside the pattern, a solution with fluorescent particles was pumped over the device showing that the fluid flowed in the patterned area towards the outlet port, this would allow reagents and samples to be manipulated. The outlet port has a different design from the traditional outlet port where a hole is drilled and tubes are attached to remove fluid. The design was to put a cotton on the end of the outlet port and the latter worked as a waste container reducing any additional steps of drilling and gluing tubes. Therefore experiments were done to investigate the steady state showing an inversely proportional relationship between flow rate and time whenever the flow rate increases the steady state reached faster and visa verse.

#### **7.4 Combination of immunoassay methodology with open microfluidic system**

The combination of biosensing protocols with microfluidics could provide great opportunities for wider applications of the methods. Experiments were therefore carried out to incorporate the chemiluminescence immunoassay with the open microfluidics. The pre-prepared slide with the immobilised antibody could be inserted into the device for insitu analysis for use by clinicians and scientists.

Combining the two systems has proved challenging. Chemical compatibility was a major issue and a crucial point in the immunoassay immobilisation procedure requires the addition of tetrabutylammonium perchloride and 4-nitrobenzene diazonium

tetrafluoroborate dissolved in acetonitrile. The acetonitrile which is an organic solution interfere with the fumed silica resulting in the damage of the superhydrophobic layer.

Experiments were carried out to ensure the Ab-Fc immobilization onto the superhydrophobic surface including changing the ratio of the deposition solution but weak results were obtained. A promising approach to overcome the problems involved covering the electrode surface with an adhesive tape before the deposition of DCDMS and fumed silica suspension. The adhesive tape was removed and the electrode was slotted inside a fixed holder and the mixture of luminol and hydrogen peroxide was pumped over. The results obtained was promising but due to time restraints, further experiments were not possible.

To our knowledge, there are no previous reports on an open microfluidic immunosensor for stress hormones (cortisol and cortisone) quantification in Zebrafish whole-body and saliva samples that integrates the immunoassay on an ITO electrode surface and chemiluminescence as the detection technique. The immunoassay is based on a competitive assay, and the data obtained is proportional to the stress hormones concentrations. The newly designed open microfluidic chip is based on the chemical reaction with DCDMS and deposition of fumed silica suspension to increase the hydrophobicity, the used mask was from PMMA while other researchers use glass or metal masks which add advantages to the proposed procedure. The combination between the immunoassay and open microfluidic chip renders this immunosensor an actual device for cortisol and cortisone concentrations measurements in both Zebrafish whole-body and saliva samples.

## 7.5 Future work

Future work will consist of improving the biosensor incorporated with an open microfluidic device that enables optimum chemiluminescence signal. This can be done by punching a plastic plaster that contains the pad (0.5 cm) and then to punch the sticky antibody plaster (0.6 cm). Towards the end of designing this cover, the two parts adhered together (as seen in figure 7.1) to prevent the removal of the antibodies that may cause by the addition of adhesive tape as this new design was tested with old antibody and improve the chemiluminescence intensity but due to the lack of materials and time, further experiments were not possible.

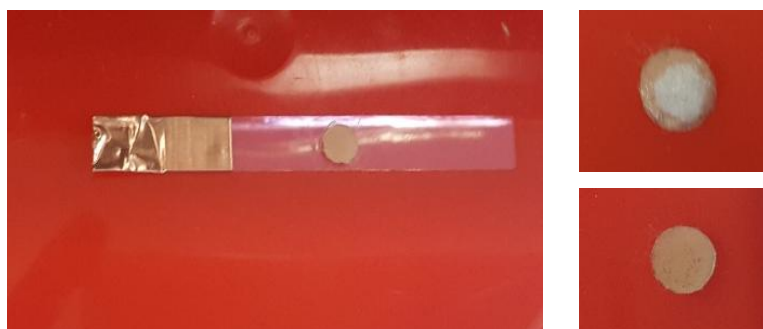


**Figure 7.1.** An actual image for the improved cover that omitted the use of adhesive tap

Optimization of fluid flow for the luminol and hydrogen peroxide mixture, optimization of luminol and hydrogen peroxide concentration, exposure time and incubation time using the syringe pump with immobilized Ab-Fc on the ITO electrode with the new cover.

Also investigations on designing masks that contain more complex designs by making two parallel circles with superhydrophilic channels connecting them rather than the perpendicular circle which could lead to circle contamination with chemiluminescence mixture, this facile the measurement of cortisol and cortisone possible on the same platform, see figure 7.2.

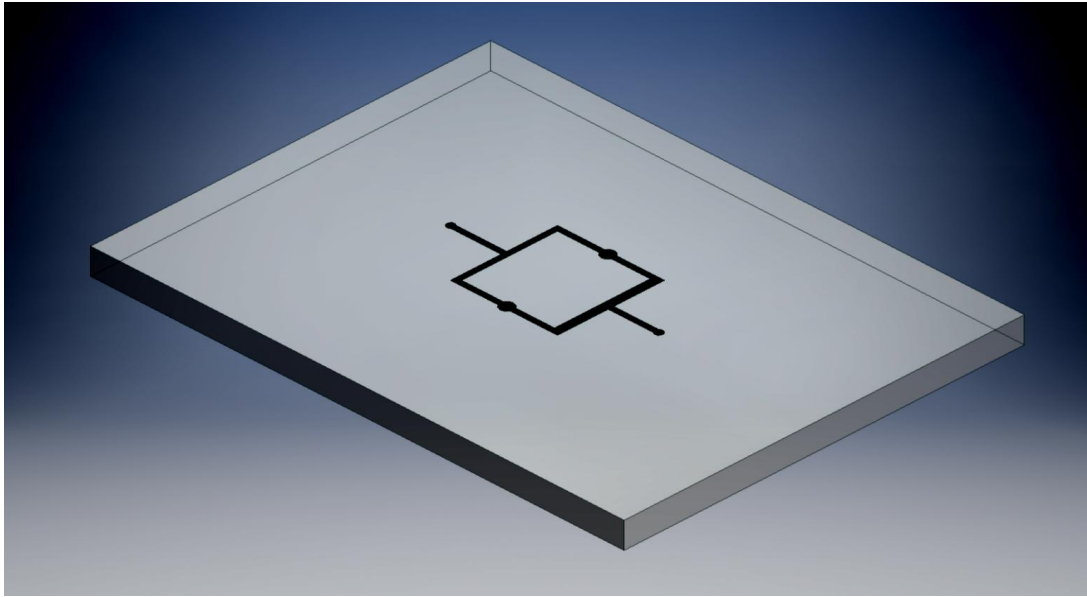


**Figure 7.2.** Preliminary design that enables multi-determination of stress hormones on the same chip.

Another approach to improve the immunoassay integrated open microfluidic system is the waste collector as cotton was used in the preliminary design. A fixed holder containing the disposable cotton collector attached to the end of the system is an attempt for a rigid collection of the solution to be commercially in use.

## References

1. D. Corbalán-Tutau, J. A. Madrid, F. Nicolás and M. Garaulet, *Physiology & behavior*, 2014, **123**, 231-235.
2. A. Kaushik, A. Vasudev, S. K. Arya, S. K. Pasha and S. Bhansali, *Biosensors and Bioelectronics*, 2014, **53**, 499-512.
3. U. Yogeswaran and S.-M. Chen, *Sensors*, 2008, **8**, 290-313.
4. B. W. Davis, PhD, University of California, 2011.
5. J. Bueno, *J. Microb. Biochem. Technol. S*, 2014, **10**.
6. D. Choi, *International Journal of Sensor Networks and Data Communications*, 2016.
7. K.-T. Lin and L.-H. Wang, *Steroids*, 2016, **111**, 84-88.
8. S. Liou, Inflammation, ([http://web.stanford.edu/group/hopes/cgi-bin/hopes\\_test/glucocorticoids/](http://web.stanford.edu/group/hopes/cgi-bin/hopes_test/glucocorticoids/)), (accessed 2016).
9. D. Liu, A. Ahmet, L. Ward, P. Krishnamoorthy, E. D. Mandelcorn, R. Leigh, J. P. Brown, A. Cohen and H. Kim, *Allergy, asthma & clinical immunology*, 2013, **9**, 1.
10. A. E. Coutinho and K. E. Chapman, *Molecular and cellular endocrinology*, 2011, **335**, 2-13.
11. P. J. Barnes, *The Journal of steroid biochemistry and molecular biology*, 2010, **120**, 76-85.
12. T. G. Guilliams and L. Edwards, *The Standard (2)*, 2010, 1-12.
13. C. D. Conrad, *Reviews in the Neurosciences*, 2008, **19**, 395-412.
14. A. Protopopova, *Physiology & behavior*, 2016, **159**, 95-103.
15. A. S. Zainol Abidin, R. A. Rahim, M. K. Md Arshad, M. F. Fatin Nabilah, C. H. Voon, T.-H. Tang and M. Citartan, *Sensors*, 2017, **17**, 1180.
16. N. M. Pires and T. Dong, 35<sup>th</sup> annual international conference of the IEEE engineering in medicine and biology society (EMBC), 2013.
17. N. Pires and T. Dong, *Bio-medical materials and engineering*, 2014, **24**, 15-20.
18. K. Chapman, M. Holmes and J. Seckl, *Physiological reviews*, 2013, **93**, 1139-1206.
19. M. Häggström, *Medicine*, 2014, **1**.

20. T. Andersson, K. Simonyte, R. Andrew, M. Strand, J. Buren, B. R. Walker, C. Mattsson and T. Olsson, *PloS one*, 2009, **4**, e8475.
21. R. Chen, R. L. Muetzel, H. El Marroun, G. Noppe, E. F. van Rossum, V. W. Jaddoe, F. C. Verhulst, T. White, F. Fang and H. Tiemeier, *Psychoneuroendocrinology*, 2016, **74**, 101-110.
22. J. Westermann, A. Demir and V. Herbst, *Clinical laboratory*, 2004, **50**, 11-24.
23. C. Le Roux, G. Chapman, W. Kong, W. Dhillon, J. Jones and J. Alaghband-Zadeh, *The Journal of Clinical Endocrinology & Metabolism*, 2003, **88**, 2045-2048.
24. A. Levine, O. Zagoory-Sharon, R. Feldman, J. G. Lewis and A. Weller, *Physiology & behavior*, 2007, **90**, 43-53.
25. R. L. Taylor, D. Machacek and R. J. Singh, *Clinical chemistry*, 2002, **48**, 1511-1519.
26. R. Gatti, G. Antonelli, M. Prearo, P. Spinella, E. Cappellin and F. Elio, *Clinical biochemistry*, 2009, **42**, 1205-1217.
27. C. Kirschbaum, A. Tietze, N. Skoluda and L. Dettenborn, *Psychoneuroendocrinology*, 2009, **34**, 32-37.
28. R. Gow, S. Thomson, M. Rieder, S. Van Uum and G. Koren, *Forensic science international*, 2010, **196**, 32-37.
29. J.-S. Raul, V. Cirimele, B. Ludes and P. Kintz, *Clinical Biochemistry*, 2004, **37**, 1105-1111.
30. E. Russell, G. Koren, M. Rieder and S. Van Uum, *Psychoneuroendocrinology*, 2012, **37**, 589-601.
31. W. Gao, T. Stalder, P. Foley, M. Rauh, H. Deng and C. Kirschbaum, *Journal of Chromatography B*, 2013, **928**, 1-8.
32. M. Venugopal, K. E. Feuvrel, D. Mongin, S. Bambot, M. Faupel, A. Panangadan, A. Talukder and R. Pidva, *IEEE Sensors Journal*, 2008, **8**, 71-80.
33. E. P. Widmaier, Hershel Raff, Kevin T. Strang, and Arthur J. Vander., "*Body Fluid Compartments.*" *Vander's Human Physiology: The Mechanisms of Body Function*, New York: McGraw-Hill, 2016.
34. S. K. Arya, G. Chornokur, M. Venugopal and S. Bhansali, *Procedia Engineering*, 2010, **5**, 804-807.
35. I. Perogamvros, L. J. Owen, J. Newell-Price, D. W. Ray, P. J. Trainer and B. G. Keevil, *Journal of Chromatography B*, 2009, **877**, 3771-3775.
36. R. L. Jones, L. J. Owen, J. E. Adaway and B. G. Keevil, *Journal of Chromatography B*, 2012, **881**, 42-48.



37. M. Yamaguchi, H. Katagata, Y. Tezuka, D. Niwa and V. Shetty, *Sensing and Bio-Sensing Research*, 2014, **1**, 15-20.
38. J. Tokarz, G. Möller, M. H. de Angelis and J. Adamski, *The Journal of steroid biochemistry and molecular biology*, 2013, **137**, 165-173.
39. L. Ribas and F. Piferrer, *Reviews in Aquaculture*, 2014, **6**, 209-240.
40. (<http://tutorialehd.info/key/z/words-zebra-danio.asp>), (accessed 2016).
41. R. J. Egan, C. L. Bergner, P. C. Hart, J. M. Cachat, P. R. Canavello, M. F. Elegante, S. I. Elkhayat, B. K. Bartels, A. K. Tien and D. H. Tien, *Behavioural brain research*, 2009, **205**, 38-44.
42. P. R. Canavello, J. M. Cachat, E. C. Beeson, A. L. Laffoon, C. Grimes, W. A. Haymore, M. F. Elegante, B. K. Bartels, P. C. Hart and S. I. Elkhayat, *Zebrafish neurobehavioral protocols*, 2011, 135-142.
43. K. Eto, J. K. Mazilu-Brown, N. Henderson-MacLennan, K. M. Dipple and E. R. McCabe, *Molecular Genetics and Metabolism Reports*, 2014, **1**, 373-377.
44. J. M. Ramsay, G. W. Feist, Z. M. Varga, M. Westerfield, M. L. Kent and C. B. Schreck, *Aquaculture*, 2009, **297**, 157-162.
45. F. Benato, E. Colletti, T. Skobo, E. Moro, L. Colombo, F. Argenton and L. Dalla Valle, *Molecular and cellular endocrinology*, 2014, **392**, 60-72.
46. A. S. Félix, A. I. Faustino, E. M. Cabral and R. F. Oliveira, *Zebrafish*, 2013, **10**, 110-115.
47. C.-M. Yeh, M. Glöck and S. Ryu, *PloS one*, 2013, **8**, e79406.
48. L. J. G. Barcellos, F. Ritter, L. C. Kreutz, R. M. Quevedo, L. B. da Silva, A. C. Bedin, J. Finco and L. Cericato, *Aquaculture*, 2007, **272**, 774-778.
49. J. M. Ramsay, G. W. Feist, Z. M. Varga, M. Westerfield, M. L. Kent and C. B. Schreck, *Aquaculture*, 2006, **258**, 565-574.
50. M. B. Khelil, M. Tegethoff, G. Meinlschmidt, C. Jamey, B. Ludes and J.-S. Raul, *Analytical and bioanalytical chemistry*, 2011, **401**, 1153-1162.
51. S. Izawa, K. Miki, M. Tsuchiya, T. Mitani, T. Midorikawa, T. Fuchu, T. Komatsu and F. Togo, *Psychoneuroendocrinology*, 2015, **54**, 24-30.
52. P. A. Accorsi, E. Carloni, P. Valsecchi, R. Viggiani, M. Gamberoni, C. Tamanini and E. Seren, *General and comparative endocrinology*, 2008, **155**, 398-402.
53. S. J. Lupica and J. W. Turner, *Aquaculture Research*, 2009, **40**, 437-441.
54. N. Ashley, P. Barboza, B. Macbeth, D. Janz, M. Cattet, R. Booth and S. Wasser, *General and comparative endocrinology*, 2011, **172**, 382-391.

55. A. Weltring, F. S. Schaebs, S. E. Perry and T. Deschner, *Physiology & behavior*, 2012, **105**, 510-521.
56. E. Russell, G. Koren, M. Rieder and S. H. Van Uum, *Therapeutic drug monitoring*, 2014, **36**, 30-34.
57. S. Liu, G.-G. Ying, J.-L. Zhao, F. Chen, B. Yang, L.-J. Zhou and H.-j. Lai, *Journal of Chromatography A*, 2011, **1218**, 1367-1378.
58. A. A. Ammann, P. Macikova, K. J. Groh, K. Schirmer and M. J. Suter, *Analytical and bioanalytical chemistry*, 2014, **406**, 7653-7665.
59. M. d. C. Lozano, PhD, University of Texas at el Paso, 2013.
60. F. Arioli, M. Fidani, A. Casati, M. L. Fracchiolla and G. Pompa, *Steroids*, 2010, **75**, 350-354.
61. D. Erickson, R. J. Singh, A. Sathananthan, A. Vella and S. C. Bryant, *Clinical endocrinology*, 2012, **76**, 467-472.
62. J. J. Pitt, *Clin Biochem Rev*, 2009, **30**, 19-34.
63. J. Tokarz, W. Norton, G. Möller, M. H. De Angelis and J. Adamski, *PloS one*, 2013, **8**, e54851.
64. M. Rauh, *Molecular and cellular endocrinology*, 2009, **301**, 272-281.
65. S. Fustinoni, E. Polledri and R. Mercadante, *Rapid Communications in Mass Spectrometry*, 2013, **27**, 1450-1460.
66. J. Abdel-Khalik, E. Björklund and M. Hansen, *Journal of Chromatography B*, 2013, **928**, 58-77.
67. L. Kartsova and E. Strel'nikova, *Journal of Analytical Chemistry*, 2007, **62**, 872-874.
68. J. Sherma, in *Encyclopedia of Analytical Chemistry*, John Wiley & Sons, Ltd, 2006, DOI: 10.1002/9780470027318.a5918.
69. H. Shibasaki, H. Nakayama, T. Furuta, Y. Kasuya, M. Tsuchiya, A. Soejima, A. Yamada and T. Nagasawa, *Journal of Chromatography B*, 2008, **870**, 164-169.
70. L. Wood, D. H. Ducroq, H. L. Fraser, S. Gillingwater, C. Evans, A. J. Pickett, D. W. Rees, R. John and A. Turkes, *Annals of clinical biochemistry*, 2008, **45**, 380-388.
71. I. A. Ionita, D. M. Fast and F. Akhlaghi, *Journal of Chromatography B*, 2009, **877**, 765-772.
72. O. A. Sharef, J. Feely, P. Kavanagh, K. Scott and S. Sharma, *Biomedical Chromatography*, 2007, **21**, 1201-1206.

73. N. Krone, B. A. Hughes, G. G. Lavery, P. M. Stewart, W. Arlt and C. H. Shackleton, *The Journal of steroid biochemistry and molecular biology*, 2010, **121**, 496-504.
74. W. Gao, T. Stalder and C. Kirschbaum, *Talanta*, 2015, **143**, 353-358.
75. F. Ceccato, G. Antonelli, M. Barbot, M. Zilio, L. Mazzai, R. Gatti, M. Zaninotto, F. Mantero, M. Boscaro and M. Plebani, *European Journal of Endocrinology*, 2014, **171**, 1-7.
76. M. M. Kushnir, A. L. Rockwood, W. L. Roberts, B. Yue, J. Bergquist and A. W. Meikle, *Clinical biochemistry*, 2011, **44**, 77-88.
77. Z. Chen, J. Li, J. Zhang, X. Xing, W. Gao, Z. Lu and H. Deng, *Journal of Chromatography B*, 2013, **929**, 187-194.
78. S. Wu, W. Li, T. Mujamdar, T. Smith, M. Bryant and F. L. Tse, *Biomedical Chromatography*, 2010, **24**, 632-638.
79. F. B. Fahlbusch, M. Ruebner, W. Rascher and M. Rauh, *Steroids*, 2013, **78**, 888-895.
80. M. A. Saracino, C. Iacono, L. Somaini, G. Gerra, N. Ghedini and M. A. Raggi, *Journal of pharmaceutical and biomedical analysis*, 2014, **88**, 643-648.
81. A. Sánchez-Guijo, M. F. Hartmann, L. Shi, T. Remer and S. A. Wudy, *Analytical and bioanalytical chemistry*, 2014, **406**, 793-801.
82. B. C. McWhinney, S. E. Briscoe, J. P. Ungerer and C. J. Pretorius, *Journal of Chromatography B*, 2010, **878**, 2863-2869.
83. I. A. Darwish, *Int J Biomed Sci*, 2006, **2**, 217-235.
84. C.-C. Lin, J.-H. Wang, H.-W. Wu and G.-B. Lee, *Journal of the Association for Laboratory Automation*, 2010, **15**, 253-274.
85. Z. O. Oiaidha, PhD, University of Hull, 2016.
86. A. N. Barclay, *Seminars in immunology*, 2003, **15**(4), 215-223.
87. W. Wang, S. Singh, D. L. Zeng, K. King and S. Nema, *Journal of pharmaceutical sciences*, 2007, **96**, 1-26.
88. T. Scientific, Antibody Labeling and Immobilization Sites, Available from: (<https://www.thermofisher.com/uk/en/home/life-science/protein-biology/protein-biology-learning-center/protein-biology-resource-library/pierce-protein-methods/antibody-labeling-immobilization-sites.html>), (accessed 2016).
89. D. N. Forthal, *Microbiology spectrum*, 2014, **2**, 1.

90. L. Zhao, L. Sun and X. Chu, *TrAC Trends in Analytical Chemistry*, 2009, **28**, 404-415.
91. L. Rowe, S. Deo, J. Shofner, M. Ensor and S. Daunert, *Bioconjugate chemistry*, 2007, **18**, 1772-1777.
92. Y. Wang, L.-J. Tang and J.-H. Jiang, *Analytical chemistry*, 2013, **85**, 9213-9220.
93. A. C. Moser, C. W. Willicott and D. S. Hage, *Electrophoresis*, 2014, **35**, 937-955.
94. M. Ihara, T. Suzuki, N. Kobayashi, J. Goto and H. Ueda, *Analytical chemistry*, 2009, **81**, 8298-8304.
95. S. D. Gan and K. R. Patel, *Journal of Investigative Dermatology*, 2013, **133**, 1-3.
96. B. W. Smith, J. Strakova, J. L. King, J. W. Erdman Jr and W. D O'Brien Jr, *Biomarker insights*, 2010, **5**, 119.
97. A. M. Sesay, L. Micheli, P. Tervo, G. Palleschi and V. Virtanen, *Analytical biochemistry*, 2013, **434**, 308-314.
98. D. Kyprianou, PhD, University of Cranfield, 2010.
99. B. A. Rodriguez, E. K. Trindade, D. G. Cabral, E. C. Soares, C. E. Menezes, D. C. Ferreira, R. K. Mendes and R. F. Dutra, in *Biosensors-Micro and Nanoscale Applications*, InTech, 2015.
100. A. Basu, K. Rangari and T. Shrivastav, *Health Popul*, 2005, **28**, 205-214.
101. J. Conde, J. T. Dias, V. Grazú, M. Moros, P. V. Baptista and J. M. de la Fuente, *Frontiers in chemistry*, 2014, **2**.
102. M. Yamaguchi, Y. Tahara, S. Kosaka and V. Shetty, international conference on electrical engineering, 2008.
103. S. Sharma, H. Byrne and R. J. O'Kennedy, *Essays in biochemistry*, 2016, **60**, 9-18.
104. F. Rusmini, Z. Zhong and J. Feijen, *Biomacromolecules*, 2007, **8**, 1775-1789.
105. S. Auer, PhD, University of Tampere technology, 2013.
106. J. Fang, J. C. Zhou, E. H. Lan, B. Dunn and J. I. Zink, *Journal of sol-gel science and technology*, 2009, **50**, 176-183.
107. T. G. Shrivastav, *Journal of Immunoassay and Immunochemistry*, 2004, **25**, 215-225.
108. D. Kim and A. E. Herr, *Biomicrofluidics*, 2013, **7**, 041501.

109. W. Leung, P. Chan, F. Bosgoed, K. Lehmann, I. Renneberg, M. Lehmann and R. Renneberg, *Journal of immunological methods*, 2003, **281**, 109-118.
110. S. Renshaw, *Immunohistochemistry and Immunocytochemistry: Essential Methods*, John Wiley & Sons, 2017.
111. N. M. M. Pires, T. Dong, U. Hanke and N. Hoivik, *Sensors*, 2014, **14**, 15458-15479.
112. N. Ibrahim, PhD, University of Bath, 2012.
113. O. Lazcka, F. J. Del Campo and F. X. Munoz, *Biosensors and bioelectronics*, 2007, **22**, 1205-1217.
114. F. Scholz, *Electroanalytical Methods Guide to Experiments and Applications*, Springer Heidelberg Dordrecht London New York, Second, Revised and Extended Edition edn., 2010.
115. F. Zhao, R. C. Slade and J. R. Varcoe, *Chemical Society Reviews*, 2009, **38**, 1926-1939.
116. V. Mirceski, S. Komorsky-Lovric and M. Lovric, *Square-wave voltammetry: theory and application*, Springer Science & Business Media, 2007.
117. K. J. Wright, PhD, University of Hull, 2015.
118. Ton100ya, Wave form of square-wave voltammetry, ([https://commons.wikimedia.org/wiki/File:Square-wave\\_voltammetry.png](https://commons.wikimedia.org/wiki/File:Square-wave_voltammetry.png)), (accessed 2017).
119. H. Duan, L. Wang, L. Zhang, J. Liu, K. Zhang and J. Wu, *PloS one*, 2015, **10**, e0144315.
120. M. Moreno-Guzman, L. Agüí, A. Gonzalez-Cortes, P. Yanez-Sedeno and J. Pingarron, *Journal of Solid State Electrochemistry*, 2013, **17**, 1591-1599.
121. M. Moreno-Guzmán, A. González-Cortés, P. Yáñez-Sedeño and J. M. Pingarrón, *Electroanalysis*, 2012, **24**, 1100-1108.
122. X. Liu, R. Zhao, W. Mao, H. Feng, X. Liu and D. K. Wong, *Analyst*, 2011, **136**, 5204-5210.
123. S. K. Arya, G. Chornokur, M. Venugopal and S. Bhansali, *Analyst*, 2010, **135**, 1941-1946.
124. D. Hauer, F. Weis, T. Krauseneck, M. Vogeser, G. Schelling and B. Roozendaal, *Brain research*, 2009, **1293**, 114-120.
125. J. Smajdor, R. Piech, M. Rumin and B. P. Bator, *Electrochimica Acta*, 2015, **182**, 67-72.

126. K. S. Kim, S. R. Lim, S.-E. Kim, J. Y. Lee, C.-H. Chung, W.-S. Choe and P. J. Yoo, *Sensors and Actuators B: Chemical*, 2016.
127. P. K. Vabbina, A. Kaushik, K. Tracy, S. Bhansali and N. Pala, SPIE sensing technology and application, 2014.
128. P. K. Vabbina, A. Kaushik, N. Pokhrel, S. Bhansali and N. Pala, *Biosensors and Bioelectronics*, 2015, **63**, 124-130.
129. Y. Ueno, K. Furukawa, K. Hayashi, M. Takamura, H. Hibino and E. Tamechika, *Analytical Sciences*, 2013, **29**, 55-60.
130. A. Singh, A. Kaushik, R. Kumar, M. Nair and S. Bhansali, *Applied biochemistry and biotechnology*, 2014, **174**, 1115-1126.
131. M. Hervás, M. A. López and A. Escarpa, *TrAC Trends in Analytical Chemistry*, 2012, **31**, 109-128.
132. E. Helmerhorst, D. J. Chandler, M. Nussio and C. D. Mamotte, *The Clinical Biochemist Reviews*, 2012, **33**, 161.
133. R. C. Stevens, S. D. Soelberg, S. Near and C. E. Furlong, *Analytical chemistry*, 2008, **80**, 6747-6751.
134. T. Kitamori, M. Tokeshi, A. Hibara and K. Sato, *analytical chemistry*, 2004.
135. A. Grumezescu, *Nanobiosensors*, Academic Press, 2016.
136. R. Izquierdo-Hornillos, R. Gonzalo-Lumbreras and A. Santos-Montes, *Journal of chromatographic science*, 2005, **43**, 235-240.
137. T. Bączek, I. Olędzka, L. Konieczna, P. Kowalski and A. Plenis, *The Scientific World Journal*, 2012, **2012**.
138. H. Pääkilä and T. Soukka, *Bioanalytical Reviews*, 2011, **3**, 27-40.
139. W. K. Jerjes, T. J. Peters, N. F. Taylor, P. J. Wood, S. Wessely and A. J. Cleare, *Journal of psychosomatic research*, 2006, **60**, 145-153.
140. A. J. Tomarken, G. T. Han and B. A. Corbett, *Psychoneuroendocrinology*, 2015, **62**, 217-226.
141. J. Stanley, *Essentials of immunology & serology*, Cengage Learning, 2002.
142. S. T. Kochuveedu and D. H. Kim, *Nanoscale*, 2014, **6**, 4966-4984.
143. L. Riegger, M. Grumann, T. Nann, J. Riegler, O. Ehlert, W. Bessler, K. Mittenbuehler, G. Urban, L. Pastewka and T. Brenner, *Sensors and Actuators A: Physical*, 2006, **126**, 455-462.
144. S. A. Van Lenten and L. D. Doane, *Psychoneuroendocrinology*, 2016, **68**, 100-110.

145. M. Monici, *Biotechnology annual review*, 2005, **11**, 227-256.
146. M. Iranifam, *Luminescence*, 2013, **28**, 798-820.
147. J.-H. An, K.-J. Shin, W.-I. Yang and H.-Y. Lee, *BMB reports*, 2012, **45**, 545-553.
148. S. R. Raz and W. Haasnoot, *TrAC Trends in Analytical Chemistry*, 2011, **30**, 1526-1537.
149. M. Liu, Z. Lin and J.-M. Lin, *Analytica Chimica Acta*, 2010, **670**, 1-10.
150. L. Ge, S. Wang, X. Song, S. Ge and J. Yu, *Lab on a Chip*, 2012, **12**, 3150-3158.
151. C. Dodeigne, L. Thunus and R. Lejeune, *Talanta*, 2000, **51**, 415-439.
152. A. Roda, *Chemiluminescence and bioluminescence: past, present and future*, Royal Society of Chemistry, 2011.
153. P. Khan, D. Idrees, M. A. Moxley, J. A. Corbett, F. Ahmad, G. von Figura, W. S. Sly, A. Waheed and M. I. Hassan, *Applied biochemistry and biotechnology*, 2014, **173**, 333-355.
154. K.A.Boudreaux, (<https://www.angelo.edu/faculty/kboudrea/demos/luminol/luminol.htm>), (accessed 2017).
155. A. L. Rose and T. D. Waite, *Analytical chemistry*, 2001, **73**, 5909-5920.
156. J.-X. Dong, Z.-F. Li, H.-T. Lei, Y.-M. Sun, F. Ducancel, Z.-L. Xu, J.-C. Boulain, J.-Y. Yang, Y.-D. Shen and H. Wang, *Analytica chimica acta*, 2012, **736**, 85-91.
157. F. P. Mathew and E. C. Alocilja, *Biosensors and bioelectronics*, 2005, **20**, 1656-1661.
158. M. Luo, X. Chen, G. Zhou, X. Xiang, L. Chen, X. Ji and Z. He, *Chemical Communications*, 2012, **48**, 1126-1128.
159. J. Shi, C. Lu, D. Yan and L. Ma, *Biosensors and Bioelectronics*, 2013, **45**, 58-64.
160. B. Li, D. Wang, J. Lv and Z. Zhang, *Talanta*, 2006, **69**, 160-165.
161. A. R. Bowie, E. P. Achterberg, P. N. Sedwick, S. Ussher and P. J. Worsfold, *Environmental science & technology*, 2002, **36**, 4600-4607.
162. S. Xu, W. Liu, B. Hu, W. Cao and Z. Liu, *Journal of Photochemistry and Photobiology A: Chemistry*, 2012, **227**, 32-37.
163. A. Ilyina, B. Mauricio, S. Sifuentes, H. Martinez, E. Bogatcheva, G. Romero and M. Rodriguez, *Biocatalysis*, 2000, **109**, 113.

164. M. W. Davidson, Concepts in Digital Imaging Technology Photomultiplier Tubes, (<https://micro.magnet.fsu.edu/primer/digitalimaging/concepts/photomultipliers.html>), (accessed 2017).
165. G. M. Whitesides, *Nature*, 2006, **442**, 368-373.
166. S. Marre and K. F. Jensen, *Chemical Society Reviews*, 2010, **39**, 1183-1202.
167. M. J. Jebrail, M. S. Bartsch and K. D. Patel, *Lab on a Chip*, 2012, **12**, 2452-2463.
168. P. Abgrall and A. Gue, *Journal of Micromechanics and Microengineering*, 2007, **17**, R15.
169. A. J. Hopwood, C. Hurth, J. Yang, Z. Cai, N. Moran, J. G. Lee-Edghill, A. Nordquist, R. Lenigk, M. D. Estes and J. P. Haley, *Analytical chemistry*, 2010, **82**, 6991-6999.
170. Y. Xu, K. Jang, T. Yamashita, Y. Tanaka, K. Mawatari and T. Kitamori, *Analytical and bioanalytical chemistry*, 2012, **402**, 99-107.
171. C. J. Easley, J. M. Karlinsey, J. M. Bienvenue, L. A. Legendre, M. G. Roper, S. H. Feldman, M. A. Hughes, E. L. Hewlett, T. J. Merkel and J. P. Ferrance, *Proceedings of the National Academy of Sciences*, 2006, **103**, 19272-19277.
172. D. R. Gossett, W. M. Weaver, A. J. Mach, S. C. Hur, H. T. K. Tse, W. Lee, H. Amini and D. Di Carlo, *Analytical and bioanalytical chemistry*, 2010, **397**, 3249-3267.
173. I. K. Glasgow, H. C. Zeringue, D. J. Beebe, S.-J. Choi, J. T. Lyman, N. G. Chan and M. B. Wheeler, *IEEE transactions on biomedical engineering*, 2001, **48**, 570-578.
174. M.-P. N. Bui, C. A. Li, K. N. Han, J. Choo, E. K. Lee and G. H. Seong, *Analytical chemistry*, 2011, **83**, 1603-1608.
175. A. Hickey, L. Marle, T. McCreeedy, P. Watts, G. Greenway and J. Littlechild, *Biochemical Society Transactions*, 2007, **35**, 1621-1623.
176. H. Jiang, X. Weng and D. Li, *Microfluidics and nanofluidics*, 2011, **10**, 941-964.
177. E. K. Sackmann, A. L. Fulton and D. J. Beebe, *Nature*, 2014, **507**, 181-189.
178. L. Kashkary, C. Kemp, K. J. Shaw, G. M. Greenway and S. J. Haswell, *Analytica chimica acta*, 2012, **750**, 127-131.
179. B. Li, L. Li, A. Guan, Q. Dong, K. Ruan, R. Hu and Z. Li, *Lab on a Chip*, 2014, **14**, 4085-4092.
180. J. Yakovleva, R. Davidsson, A. Lobanova, M. Bengtsson, S. Eremin, T. Laurell and J. Emnéus, *Analytical chemistry*, 2002, **74**, 2994-3004.



181. C.-H. Lin, G.-B. Lee, Y.-H. Lin and G.-L. Chang, *Journal of Micromechanics and Microengineering*, 2001, **11**, 726.
182. Y. Bai, C. G. Koh, M. Boreman, Y.-J. Juang, I.-C. Tang, L. J. Lee and S.-T. Yang, *Langmuir*, 2006, **22**, 9458-9467.
183. T. G. Henares, F. Mizutani and H. Hisamoto, *Analytica Chimica Acta*, 2008, **611**, 17-30.
184. H. Wang, S. Meng, K. Guo, Y. Liu, P. Yang, W. Zhong and B. Liu, *Electrochemistry Communications*, 2008, **10**, 447-450.
185. P. Novo, D. M. F. Prazeres, V. Chu and J. P. Conde, *Lab on a Chip*, 2011, **11**, 4063-4071.
186. F. Darain, K. L. Gan and S. C. Tjin, *Biomedical microdevices*, 2009, **11**, 653-661.
187. R. O. Rodrigues, R. Lima, H. T. Gomes and A. M. Silva, *U. Porto Journal of Engineering*, 2015, **1**, 67-79.
188. T. M. Squires and S. R. Quake, *Reviews of modern physics*, 2005, **77**, 977.
189. D. Mark, S. Haeberle, G. Roth, F. von Stetten and R. Zengerle, *Chemical Society Reviews*, 2010, **39**, 1153-1182.
190. H. A. Stone, A. D. Stroock and A. Ajdari, *Annu. Rev. Fluid Mech.*, 2004, **36**, 381-411.
191. V. Pinto, P. Sousa, S. Catarino, M. Correia-Neves and G. Minas, *Biosensors and Bioelectronics*, 2017, **90**, 308-313.
192. R. M. van Dam, PhD, California Institute of Technology, 2006.
193. K. Khoshmanesh, A. Almansouri, H. Albloushi, P. Yi, R. Soffe and K. Kalantar-Zadeh, *Scientific reports*, 2015, **5**.
194. D. Mark, S. Haeberle, G. Roth, F. Von Stetten and R. Zengerle, in *Microfluidics Based Microsystems*, Springer, 2010, pp. 305-376.
195. J. Berthier, K. A. Brakke and E. Berthier, *Open Microfluidics*, John Wiley & Sons, 2016.
196. M. P. Sousa and J. F. Mano, *Cellulose*, 2013, **20**, 2185-2190.
197. B. P. Casavant, E. Berthier, A. B. Theberge, J. Berthier, S. I. Montanez-Sauri, L. L. Bischel, K. Brakke, C. J. Hedman, W. Bushman and N. P. Keller, *Proceedings of the National Academy of Sciences*, 2013, **110**, 10111-10116.
198. W.-L. Chou, P.-Y. Lee, C.-L. Yang, W.-Y. Huang and Y.-S. Lin, *Micromachines*, 2015, **6**, 1249-1271.

199. T. Schneider, J. Kreutz and D. T. Chiu, *Analytical chemistry*, 2013, **85**, 3476-3482.
200. P. Lam, K. J. Wynne and G. E. Wnek, *Langmuir*, 2002, **18**, 948-951.
201. B. Zhao, J. S. Moore and D. J. Beebe, *Analytical chemistry*, 2002, **74**, 4259-4268.
202. X. Li, J. Tian, G. Garnier and W. Shen, *Colloids and Surfaces B: Biointerfaces*, 2010, **76**, 564-570.
203. X. Li, D. R. Ballerini and W. Shen, *Biomicrofluidics*, 2012, **6**, 011301.
204. C. González-Obeso, W. L. Song, M. A. Rodríguez-Pérez and J. F. Mano, 2013.
205. A. A. Tracton, *Coatings technology handbook*, CRC press, 2005.
206. E. E. Ubuo, PhD, University of Hull, 2016.
207. N. J. Shirtcliffe, G. McHale, S. Atherton and M. I. Newton, *Advances in colloid and interface science*, 2010, **161**, 124-138.
208. H.-J. Butt, D. S. Golovko and E. Bonaccorso, *The Journal of Physical Chemistry B*, 2007, **111**, 5277-5283.
209. X. Xu and X. Wang, *SIAM journal on applied mathematics*, 2010, **70**, 2929-2941.
210. R. Fürstner, W. Barthlott, C. Neinhuis and P. Walzel, *Langmuir*, 2005, **21**, 956-961.
211. X.-M. Li, D. Reinhoudt and M. Crego-Calama, *Chemical Society Reviews*, 2007, **36**, 1350-1368.
212. Y. Yan, N. Gao and W. Barthlott, *Advances in colloid and interface science*, 2011, **169**, 80-105.
213. Y.-L. Zhang, H. Xia, E. Kim and H.-B. Sun, *Soft Matter*, 2012, **8**, 11217-11231.
214. J. West, A. Michels, S. Kittel, P. Jacob and J. Franzke, *Lab on a Chip*, 2007, **7**, 981-983.
215. N. M. Oliveira, A. I. Neto, W. Song and J. F. Mano, *Applied physics express*, 2010, **3**, 085205.
216. A. Ghosh, R. Ganguly, T. M. Schutzius and C. M. Megaridis, *Lab on a Chip*, 2014, **14**, 1538-1550.
217. A. Vasudev, A. Kaushik, Y. Tomizawa, N. Norena and S. Bhansali, *Sensors and Actuators B: Chemical*, 2013, **182**, 139-146.

218. M. Zangheri, L. Cevenini, L. Anfossi, C. Baggiani, P. Simoni, F. Di Nardo and A. Roda, *Biosensors and Bioelectronics*, 2015, **64**, 63-68.
219. R. Ashiri, A. Nemati and M. S. Ghamsari, *Ceramics International*, 2014, **40**, 8613-8619.
220. Y. H. Dou, S. J. Haswell, J. Greenman and J. Wadhawan, *Electroanalysis*, 2012, **24**, 264-272.
221. J. M. Hicks, Z. Y. Wong, D. J. Scurr, N. Silman, S. K. Jackson, P. M. Mendes, J. W. Aylott and F. J. Rawson, *Langmuir*, 2017, **33**, 4924-4933.
222. S. Chen, L. Liu, J. Zhou and S. Jiang, *Langmuir*, 2003, **19**, 2859-2864.
223. J. E. Lee, J. H. Seo, C. S. Kim, Y. Kwon, J. H. Ha, S. S. Choi and H. J. Cha, *Korean J. Chem. Eng.*, 2013, **30**, 1934-1938.
224. C. E. West, J. L. Hardcastle and R. G. Compton, *Electroanalysis*, 2002, **14**, 1470-1478.
225. M. Thirumoorthi and J. Thomas Joseph Prakash, *Journal of Asian Ceramic Societies*, 2016, **4**, 124-132.
226. N. Nadaud, N. Lequeux, M. Nanot, J. Jove and T. Roisnel, *Journal of Solid State Chemistry*, 1998, **135**, 140-148.
227. A. Benedetto, M. Balog, P. Viel, F. Le Derf, M. Sallé and S. Palacin, *Electrochimica Acta*, 2008, **53**, 7117-7122.
228. A. L. Gui, G. Liu, M. Chockalingam, G. Le Saux, E. Luais, J. B. Harper and J. J. Gooding, *Electroanalysis*, 2010, **22**, 1824-1830.
229. M. Okochi, H. Ohta, T. Tanaka and T. Matsunaga, *Biotechnology and bioengineering*, 2005, **90**, 14-19.
230. P. Wood, *Annals of clinical biochemistry*, 2009, **46**, 183-196.
231. M. Khan, S. K. Misra, Z. Wang, E. A. Daza, A. Schwartz-Duval, J. Kus, D. Pan and D. Pan, *Analytical Chemistry*, 2017.
232. F. Liu and C. Zhang, *Sensors and Actuators B: Chemical*, 2015, **209**, 399-406.
233. C. E. Taylor and S. E. Creager, *Journal of Electroanalytical Chemistry*, 2000, **485**, 114-120.
234. R. Wilson and D. J. Schiffrin, *Journal of Electroanalytical Chemistry*, 1998, **448**, 125-130.
235. V. Jain, *Asian Journal of Pharmaceutical Analysis*, 2013, **3**, 138-140.
236. W. Chen, L. Hong, A.-L. Liu, J.-Q. Liu, X.-H. Lin and X.-H. Xia, *Talanta*, 2012, **99**, 643-648.

237. A. Shimoni, S. Azoubel and S. Magdassi, *Nanoscale*, 2014, **6**, 11084-11089.
238. V. T. Nyakubaya, B. C. Durney, M. C. Ellington, A. D. Kantes, P. A. Reed, S. E. Walter, J. R. Stueckle and L. A. Holland, *Analytical and bioanalytical chemistry*, 2015, **407**, 6985-6993.
239. O. W. Flörke, H. A. Graetsch, F. Brunk, L. Benda, S. Paschen, H. E. Bergna, W. O. Roberts, W. A. Welsh, C. Libanati, M. Ettlinger, D. Kerner, M. Maier, W. Meon, R. Schmoll, H. Gies and D. Schiffmann, in *Ullmann's Encyclopedia of Industrial Chemistry*, Wiley-VCH Verlag GmbH & Co. KGaA, 2000, DOI: 10.1002/14356007.a23\_583.pub3.
240. F. Iskandar, M. Abdullah, H. Yoden and K. Okuyama, *Journal of sol-gel science and technology*, 2004, **29**, 41-47.
241. F. R. Michele Ferrara, and Libero Liggieri, *Appl. Phys. Lett.* , 2006, **88** , 203125.
242. B. Hatton, L. Mishchenko, S. Davis, K. H. Sandhage and J. Aizenberg, *Proceedings of the National Academy of Sciences*, 2010, **107**, 10354-10359.
243. S. Hua and A. Wang, *Carbohydrate Polymers*, 2009, **75**, 79-84.
244. M. Zimmermann, S. Bentley, H. Schmid, P. Hunziker and E. Delamarche, *Lab on a Chip*, 2005, **5**, 1355-1359.
245. C. Noeh, C. Fonseca, J. Mollenhauer, S. Hofmann, L. Steinbrecher, A. Haller, M. Scholtes, F. Schudt, K. Sohrabi and V. Gross, *Current Directions in Biomedical Engineering*, 2016, **2**, 337-340.
246. A. F. D. Cruz, N. Norena, A. Kaushik and S. Bhansali, *Biosensors and Bioelectronics*, 2014, **62**, 249-254.
247. A. Kaushik, A. Yndart, R. D. Jayant, V. Sagar, V. Atluri, S. Bhansali and M. Nair, *International journal of nanomedicine*, 2015, **10**, 677.
248. V. Pinto, G. Minas and M. Correia-Neves, IEEE 4<sup>th</sup> Portuguese meeting on Bioengineering (ENBENG), 2015.
249. T. J. Davies, B. A. Brookes, A. C. Fisher, K. Yunus, S. J. Wilkins, P. R. Greene, J. D. Wadhawan and R. G. Compton, *The Journal of Physical Chemistry B*, 2003, **107**, 6431-6444.

## **Presentations**

J. Abdulsattar, G. Greenway, T. Horozov," Cortisol Determination using immunoassay", Regional Chemistry Conference 2015, Nottingham Trent University, Nottingham, UK.

J. Abdulsattar, G. Greenway, T. Horozov, "Wetting properties of an open microfluidic chip", Chemistry Colloquium 2015, University of Hull, Hull, UK.

J. Abdulsattar, G. Greenway, T. Horozov," Fabrication of superhydrophilic patterns on a superhydrophobic substrate: towards open microfluidic applications in a quantitative measurement system for stress hormones ", Ph.D. Experience Conference 2016, University of Hull, Hull, UK.

J. Abdulsattar, G. Greenway, T. Horozov, "Development of an *in situ* quantitative measurement system for stress hormones ", Lab-on-a-chip & Microfluidics 2016, Madrid, Spain.

J. Abdulsattar, G. Greenway, T. Horozov, "Lab-on-chip platform for Zebrafish whole- body sample stress hormone analysis", International Women's Day Chemistry Career Symposium, University of Hull 2016, Hull, UK.

J. Abdulsattar, G. Greenway, T. Horozov, "Development of a point-of-care system for stress hormones; towards open microfluidic system", Chemistry Colloquium 2016, University of Hull, Hull, UK.

J.Abdulsattar, G. Greenway, T. Horozov, "Wetting properties investigations towards constructing open microfluidic system", Ph.D. Experience Conference 2017, University of Hull, Hull, UK.